Investigating the role of homologous recombination in the maintenance of chromosome stability

Emily Graham

Lincoln College, University of Oxford

DPhil in Molecular Cell Biology in Health and Disease

Sir William Dunn School of Pathology

Trinity Term 2023

Declaration

The work in this thesis is my own unless stated otherwise in the text and figure legends.

I collaborated with Isabel Wassing, a DPhil and PostDoc in the Esashi lab, on the work discussed in Chapter 3 of my thesis. Experiments presented in figures 3.5, 3.6, and 3.8 were conducted by Isabel Wassing and are published in (Wassing et al., 2021). The material was reproduced for the purpose of this thesis and permission obtained from Isabel Wassing. I conducted experiments displayed in figures 3.2, 3.3 and 3.4 which are now published in (Wassing et al., 2021).

Data I produced, displayed in figures 4.1A and D, 4.3A, and 5.13A and D, are now published in (Saayman et al., 2023).

Validation experiments in chapter 5 (figures 5.3B and D, and 5.5B, E, H, and K) were conducted by Jacob Wall, at that time a provisional DPhil student, under my direction and supervision.

Acknowledgements

Firstly, I would like to thank my supervisor Prof. Fumiko Esashi for allowing me into her lab and for her support and helpful discussions throughout my DPhil. I would also like to thank Dr Dragana Ahel, for giving me the opportunity to begin my DPhil in Oxford, and Prof. Jordan Raff for their support and advice over my time here. I want to thank my past and present lab members: Jacob, Brian, Santosh, Xanita, Lucia, Grace, Marjorie, and Isabel, for their immense help, support, and friendship throughout this journey.

I am very grateful that the Dunn school has been an amazing place to work. I would like to acknowledge current and past members of OMPI1 and OMPI3, particularly Lucy, Adam, and Xiaomeng, for making my time here such a positive experience.

To my dearest Clementines; old, new, and associate members: Emile, Lucrezia, Violaine, Bertie, Arnau, Will, and Ricky. I'm not sure what I would have done without you all. Thank you for your friendship and showing me that there is more to life than the lab. And finally, to Mum, Dad, and Holly, thank you for dealing with my stress and providing much-needed motivational speeches, I wouldn't be where I am now without you.

Abstract

Homologous recombination (HR) is an essential DNA break repair pathway that maintains genome stability. BRCA2, PALB2, and RAD51 are key modulators of this pathway, mutations within which are associated with tumourigenesis. Centromeres are large repetitive DNA regions in the genome, defined through the presence of CENP-A. There is increasing evidence that centromeres experience instability across the cell cycle, impeding their function.

In this thesis, I first demonstrate a role for *de novo* RAD51 loading in mitosis after mild replication stress to promote mitotic DNA synthesis (MiDAS). Utilising RAD51 separation-of-function mutant cell lines, I present evidence suggesting that RAD51's single stranded DNA binding activity is important to promote MiDAS at undamaged loci. Failure to complete MiDAS in RAD51 deficient cells leads to mitotic defects and increased aberrant centromere recombination and fragility. I next explored the role of HR factors: BRCA2, PALB2, and RAD51 at centromeres RPE1 cells. Here, I show evidence of a role for BRCA2 and RAD51, but not PALB2, in maintaining centromeric CENP-A levels and, using Exo-FISH, show that BRCA2 may have a distinct role in minimising centromeric single stranded DNA accumulation in a cell cycle-dependent manner. Finally, I generated and validated an auxin-inducible degron system to rapidly degrade BRCA2 and PALB2 in the mismatch repair defective, colorectal cancer cell line, HCT116. Using these tools, I highlight the impact of short-term and long-term BRCA2 and PALB2 depletion on chromosome stability, providing an insight into a potential mechanism for tumourigenesis. Investigations into the role of BRCA2 and PALB2 in centromere identity and stability further identified BRCA2 as important for maintaining centromere stability, different from RPE1 cells, highlighting their different genetic backgrounds. Hence, I propose a role for BRCA2 and RAD51 in preserving centromere stability and function, collectively increasing our comprehension of the importance of HR factors at centromeres and how different cellular and chromatin contexts may influence repair at this region to limit tumourigenesis.

Table of Contents

Chapter 1 – Introduction **9**
1.1 Sources of DNA damage **9**
1.2 Early DDR signalling **9**
1.3 Single strand break (SSB) repair **10**
1.4 Double strand break (DSB) repair **10**
1.4.1 Non-Homologous End Joining (NHEJ) 11
1.4.2 Homologous Recombination (HR) 11
1.4.3 Alternative End Joining (alt-EJ) 12
1.4.4 Single Strand Annealing (SSA) 14
1.5 Replication stress **14**
1.5.1 Translesion synthesis (TLS), repriming, and template switching 15
1.5.2 Replication fork reversal 16
1.5.3 Break-induced replication (BIR) 17
1.5.3.1 Mitotic DNA synthesis (MiDAS) 18
1.5.4 Mismatch repair (MMR) 18
1.6 Canonical PALB2-BRCA2-RAD51 complex to maintain genome stability **21**
1.6.1 PALB2 21
1.6.1.1 PALB2 structure 22
1.6.1.2 PALB2 function 22
1.6.1.2.1 Homologous recombination 22
1.6.1.2.2 Replication fork recovery 23
1.6.1.2.3 Chromatin association at transcriptionally active genes 23
1.6.1.2.4 Cell cycle checkpoint control 24
1.6.2 BRCA2 25
1.6.2.1 BRCA2 structure 25
1.6.2.2 BRCA2 binding to RAD51 26
1.6.2.3 BRCA2 function 27
1.6.2.3.1 Homologous Recombination 27
1.6.2.3.2 Interstrand crosslink (ICL) repair 27
1.6.2.3.3 Stalled replication fork protection 28
1.6.2.3.4 R-loops 29
1.6.2.3.5 Faithful chromosome segregation 30
1.6.3 RAD51 31
1.6.3.1 RAD51 structure 31
1.6.3.2 RAD51 recruitment to chromatin 32

1.6.3.3 RAD51 function ... 32
1.6.3.3.1 RAD51-dependent replication stress response ... 32
1.7 Centromeres ... 33
1.7.1 Centromere structure and function ... 33
1.7.2 The Spindle Assembly Checkpoint (SAC) ... 35
1.7.3 CENP-A deposition into centromeric chromatin ... 36
1.7.3.1 Transcription and CENP-A deposition ... 38
1.7.4 Centromere integrity throughout the cell cycle ... 40
1.7.4.1 G1 Phase ... 40
1.7.4.2 S phase ... 41
1.7.4.2.1 Centromeric DNA loops ... 42
1.7.4.2.2 Transcription-replication conflicts (TRCs) ... 44
1.7.4.2.3 Centromere recombination ... 45
1.7.4.3 Mitosis ... 49
1.7.4.3.1 Centromeric Ultrafine Anaphase Bridges ... 49
1.7.4.3.2 Transcription and kinetochore function ... 50
1.7.4.3.3 Centromere compaction and flexibility ... 51
1.7.4.4 Quiescence ... 51
1.8 Research Aims ... 52
Chapter 2 - Materials and Methods ... 54
2.1 Tables of Materials ... 54
2.2 Bacterial cell culture ... 59
2.2.1 Plasmid amplification ... 59
2.2.2 Glycerol stocks ... 60
2.3 DNA analysis techniques ... 60
2.3.1 Genomic DNA extraction ... 60
2.3.2 PCR ... 61
2.3.3 Gel electrophoresis ... 61
2.4 DNA plasmid cloning ... 62
2.4.1 Insert preparation ... 62
2.4.2 Restriction enzyme digestion ... 62
2.4.3 Vector preparation ... 62
2.4.4 Ligation ... 62
2.4.5 Site-directed mutagenesis ... 63
2.4.6 Gibson assembly ... 63
2.4.7 Sanger sequencing ... 64
2.5 Mammalian cell culture ... 64

2.5.1 General cell culture 64
2.5.2 Drug treatments 64
2.5.3 siRNA transfection 64
2.5.4 Generation of U2OS Flp-In T-REx RAD51 separation-of-function variant cell lines 65
2.5.5 Generation of CRISPR-tagged HCT116 OsTIR1 PALB2-mAID-Halo and mAID-Halo-BRCA2 cell lines 65
2.5.6 Generation of stable U2OS cell lines expressing GFP-Lamin B1 and mCherry-Histone H2B 66
2.5.7 Cell synchronisation 66
2.5.7.1 Enriching mitotic cells to observe mitotic DNA synthesis (MiDAS) 66
2.5.7.2 Enriching mitotic cells to generate metaphase spreads 67
2.5.7.3 Serum-starvation 67
2.6 Microscopy techniques 67
2.6.1 Immunofluorescence (IF) 67
2.6.2 Click-IT reaction for EdU labelling 68
2.6.3 Exo-FISH 68
2.6.4 Chromosome-Orientation Fluorescence *In Situ* Hybridisation (CO-FISH) 70
2.6.5 Chromosome 17 FISH staining 71
2.6.6 Live Cell Imaging 72
2.7 Molecular biology techniques 72
2.7.1 Western blotting (WB) 72
2.7.2 Immunoprecipitation (IP) 73
2.7.3 Pulsed-Field Gel Electrophoresis (PFGE) 74
2.7.4 Flow cytometry 75
2.7.5 WST-1 cell proliferation assay 76
2.7.6 Clonogenic cell survival assay 76
2.8 Data analysis 77
2.8.1 Statistics 77
2.8.2 IF quantification in Chapter 3 using FindFoci in ImageJ 77
2.8.3 Exo-FISH and IF quantification in Chapter's 4 and 5 78
Chapter 3 - Investigating RAD51 function in mitotic DNA synthesis 79
3.1 Introduction 79
3.2 Results 79
3.2.1 RAD51 is required for MiDAS 79
3.2.2 Utilising RAD51 separation-of-function mutants to identify its mitotic function 81
3.2.3 RAD51 promotes non-DDR associated MiDAS 83

3.2.4 RAD51 depletion in early mitosis leads to increased mitotic DNA damage 85
3.2.5 Inhibiting RAD51's role in MiDAS promotes mitotic defects 86
3.2.6 RAD51 inhibition in mitosis impacts centromere integrity 88
3.3 Discussion **92**
3.3.1 A role for RAD51 in MiDAS 92
3.3.2 DDR vs non-DDR associated MiDAS 93
3.3.3 MiDAS at centromeres and centromere fragility 96
Chapter 4 – Investigating the role of homologous recombination in centromere stability in RPE1 cells **102**
4.1 Introduction **102**
4.2 Results **103**
4.2.1 Depleting the canonical HR factors in RPE1 cells 103
4.2.2 RAD51 and BRCA2, but not PALB2, impact centromere identity 104
4.2.3 Impact of BRCA2 on centromere identity in non-cycling cells 107
4.2.4 BRCA2 impacts centromeric ssDNA gaps but not DNA breaks 110
4.2.5 BRCA2-dependent centromeric ssDNA exposure is cell cycle-dependent 115
4.3 Discussion **117**
4.3.1 Understanding the role of HR factors in centromere identity 117
4.3.2 Understanding the role HR factors in centromere stability 120
4.3.3 A requirement for DNA breaks in CENP-A deposition at centromeres? 128
Chapter 5 – Exploring the impact of BRCA2 and PALB2 on chromosome stability in HCT116 cells **130**
5.1 Introduction **130**
5.1.1 Gross chromosomal rearrangements (GCRs) drive tumourigenesis 130
5.1.2 Centromere research in RPE1 and HCT116 cells 130
5.2 Results **131**
5.2.1 Generation and validation of an auxin-inducible degron (AID)-tagged BRCA2/PALB2 system in HCT116 cells 131
..... **Error! Bookmark not defined.**
5.2.2 Short-term BRCA2/PALB2 depletion impacts cellular functions 134
5.2.3 Long-term BRCA2/PALB2 depletion reveals distinct chromosome phenotypes 139
5.2.4 Impact of BRCA2 and PALB2 depletion on centromere identity in HCT116 cells 146
5.2.5 Impact of BRCA2/PALB2/RAD51 on centromere integrity in HCT116 cells 152
5.3 Discussion **157**

5.3.1 Using the AID system to study BRCA2 and PALB2 function in HCT116 cells 157
5.3.2 Long-term depletion of BRCA2 and PALB2 reveals distinct chromosomal aberrations 159
5.3.3 A potential role for BRCA2 in centromere identity in HCT116 cells? 164
5.3.4 The role of HR factors in centromere stability in HCT116 cells 166
5.3.5 Variation between AID and siRNA studies 169
Chapter 6 – Discussion 172
6.1 Summary of thesis 172
6.1.1 RAD51 maintains genome stability in mitosis 172
6.1.2 Distinct roles for BRCA2, PALB2, and RAD51 at centromeres 174
6.1.3 Detecting centromeric DNA breaks 179
6.1.4 Chromosome instability after BRCA2 and PALB2 depletion 181
6.2 Concluding remarks 182
Bibliography 183
Appendices 223
1. Automated foci counting and colocalisation analysis (FIJI macro) 223
2. Automated microscopy analysis (FIJI macro) 229
3. Downstream processing of microscopy data (Python) 233

Chapter 1 – Introduction

1.1 Sources of DNA damage

It is estimated that cells experience approximately 70,000 DNA lesions per day (Lindahl & Barnes, 2000). DNA lesions can arise from numerous endogenous sources such as replication and transcription stress, topoisomerases, dNTP misincorporation, and DNA metabolic damage from reactive oxygen species (ROS). Alternatively, exogenous sources of damage include chemotherapeutic agents, ionising radiation (IR), and ultraviolet (UV) light (Ciccia & Elledge, 2010).

It is generally accepted that a majority of DNA lesions are single strand DNA breaks (SSBs) (Tubbs & Nussenzweig, 2017). SSBs can include DNA nicks from lagging strand DNA replication and Okazaki fragment generation, as well as DNA repair pathway intermediates e.g. mismatch repair (MMR), nucleotide excision repair (NER), and ribonucleotide excision repair (RER) (Tubbs & Nussenzweig, 2017). SSBs can also represent single stranded DNA (ssDNA) gaps that can arise during replication-associated damage and replication fork processing (**section 1.5**).

Endogenous DNA double strand breaks (DSBs) occur significantly less frequently than SSBs (Tounekti et al., 2001; Vilenchik & Knudson, 2003). Unrepaired DSBs are particularly genotoxic to cells, therefore several signalling and repair mechanisms, termed the DNA damage response (DDR), have evolved to counter this.

1.2 Early DDR signalling

At DSBs, members of the phosphatidylinositol 3-OH-kinase-related kinase (PI3KK) family, ataxia-telangiectasia-mutated (ATM), ataxia telangiectasia and Rad3-related (ATR), and DNA-dependent protein kinase (DNA-PK) coordinate the DDR (Jackson & Bartek, 2009).All three kinases can redundantly phosphorylate histone H2AX at serine 139 to form ɣH2AX (Burma et al., 2001; Stiff et al., 2004; Ward & Chen, 2001) which can extend for megabases surrounding the DNA break site to initiate signalling and recruitment of repair factors (Mah

et al., 2010). ATM also promotes activation of the DNA damage checkpoint which can trigger cell cycle arrest through phosphorylation and activation of CHK2 and its downstream effectors (Jackson & Bartek, 2009).

SSBs are primarily recognised by PARP1, which binds and signals the DDR through modification of itself and surrounding proteins with branched poly(ADP-ribose) chains. This subsequently promotes recruitment of ssDNA binding repair factors (Caldecott, 2008). Furthermore, ssDNA at stalled replication forks or DSBs are coated with replication protein A (RPA) (Cimprich & Cortez, 2008). ATRIP recognises RPA to recruit and activate ATR which phosphorylates CHK1 and various proteins to direct downstream repair pathways (Zou & Elledge, 2003).

1.3 Single strand break (SSB) repair

PARP1 recognises SSBs and recruits repair factors through PARylation of downstream proteins (**section 1.2**). SSBs can display damaged terminal nucleotides that first need to be processed to restore their ligation chemistry to 3'-hydroxyl and 5'-phosphate groups. Several different enzymes can facilitate this depending on the damage source and type of nucleotide modification, including PNKP, APE1, TDP1, APTX, and Polymerase β (Pol β) (Caldecott, 2008). X-ray repair cross-complementing protein 1 (XRCC1) is a molecular scaffold protein that interacts with, stabilises, and stimulates the SSB repair process where Pol β promotes ssDNA gap filling and DNA ligation is facilitated by ligase 1 (LIG1), ligase 3 (LIG3), and ligase 4 (LIG4) (Caldecott, 2008).

SSBs and ssDNA gaps can also be resolved via translesion synthesis (TLS) and template switching (**section 1.5.1**).

1.4 Double strand break (DSB) repair

There are several DSB repair pathways including non-homologous end joining (NHEJ), homologous recombination (HR), alternative-end joining (alt-EJ), and single strand annealing (SSA), all of which display varying degrees of accuracy. Cell cycle stage and

DNA break end processing are major factors determining DSB repair pathway choice (Ceccaldi et al., 2016).

1.4.1 Non-Homologous End Joining (NHEJ)

NHEJ is active throughout the cell cycle, with activity lowest in G1 and highest in G2/M phase. Hence, it is regarded as the major DSB repair pathway across all cell cycle stages (Mao et al., 2008). NHEJ involves the direct ligation of DSB ends without significant resection. At DSBs, the Ku70-Ku80 heterodimer is loaded onto DNA ends, recruiting DNA-PK_{cs}, to form the active kinase. DNA-PK phosphorylates histone H2AX (**section 1.2**) and other repair proteins including XRCC4, stimulatory factor XLF, and LIG4, to religate the DNA ends.

In some cases, terminal nucleotides at the break site are removed or modified by ARTEMIS, APLF, and PNK kinase/phosphatase, to facilitate the ligation reaction. However, ARTEMIS-dependent processing of DNA ends can lead to small deletions, thus NHEJ is considered an error-prone repair process. It can also promote large translocations if break ends from different genomic loci are fused (Ceccaldi et al., 2016).

1.4.2 Homologous Recombination (HR)

HR-mediated repair is considered an accurate repair pathway as it utilises the homologous sister chromatid as a template for repair so that no sequence information is lost (**figure 1.1A**). Due to this, HR is generally restricted to S and G2 phase, after DNA replication. HR can repair both SSBs (nick-induced HR) and DSBs (Davis & Maizels, 2014; Vriend & Krawczyk, 2017).

Firstly, the MRN complex (MRE11-RAD50-NBS1) is recruited to lesions and promotes ATM activation (Uziel et al., 2003). MRE11 possess endonuclease and 3'-5' exonuclease activity to promote extensive break end resection along with CtIP, BRCA1, EXO1, DNA2, and BLM (Garcia et al., 2011; Gravel et al., 2008; Mimitou & Symington, 2008; Nimonkar et al., 2008; Zhu et al., 2008). This produces 3' ssDNA overhangs and commits the cell to HR-mediated

repair. RPA binds ssDNA to protect it from nucleolytic damage and prevent secondary DNA structure formation (Symington, 2002). It is subsequently replaced with RAD51 by the BRCA1-PALB2-BRCA2 complex (Chen et al., 1998b; Sy et al., 2009b; Zhang et al., 2009a; Zhang et al., 2009b). The RAD51 nucleoprotein filament mediates strand invasion into the sister chromatid to search for homologous sequences. This invasion forms a displacement loop (D-loop) and is extended by DNA polymerase, using the invading DNA strand as a primer for DNA synthesis.

The D-loop structure can be resolved through several mechanisms. Synthesis-dependent strand annealing (SDSA) involves direct displacement of the 3' strand from the homologous template and reannealing at the DNA break to produce non-crossover products. Second-end capture entails invasion of the extended break end into the homologous template, forming a double Holliday junction (HJ). HJs can be dissolved by BLM and topoisomerase IIIα (TOP3A) without cleavage to produce non-crossover products, or processed by structure-specific endonucleases including GEN1, MUS81/EME1, and SLX1/SLX4 to produce crossover or non-crossover products, depending on the site of cleavage (**figure 1.1A**) (Ceccaldi et al., 2016).

Crossover recombination is a relatively uncommon event however it is detrimental and can contribute towards loss of heterozygosity and large structural rearrangements (Richardson & Jasin, 2000; Stark & Jasin, 2003). HR between non-allelic repeats (NAHR) results in disease-associated rearrangements (Gu et al., 2008; Liu et al., 2012), thus HR is a tightly regulated process.

1.4.3 Alternative End Joining (alt-EJ)

Alt-EJ, also known as microhomology-mediated end joining (MMEJ), functions in S phase as a mutagenic backup DSB repair pathway to HR and requires limited resection of DSB ends (5-25bp).

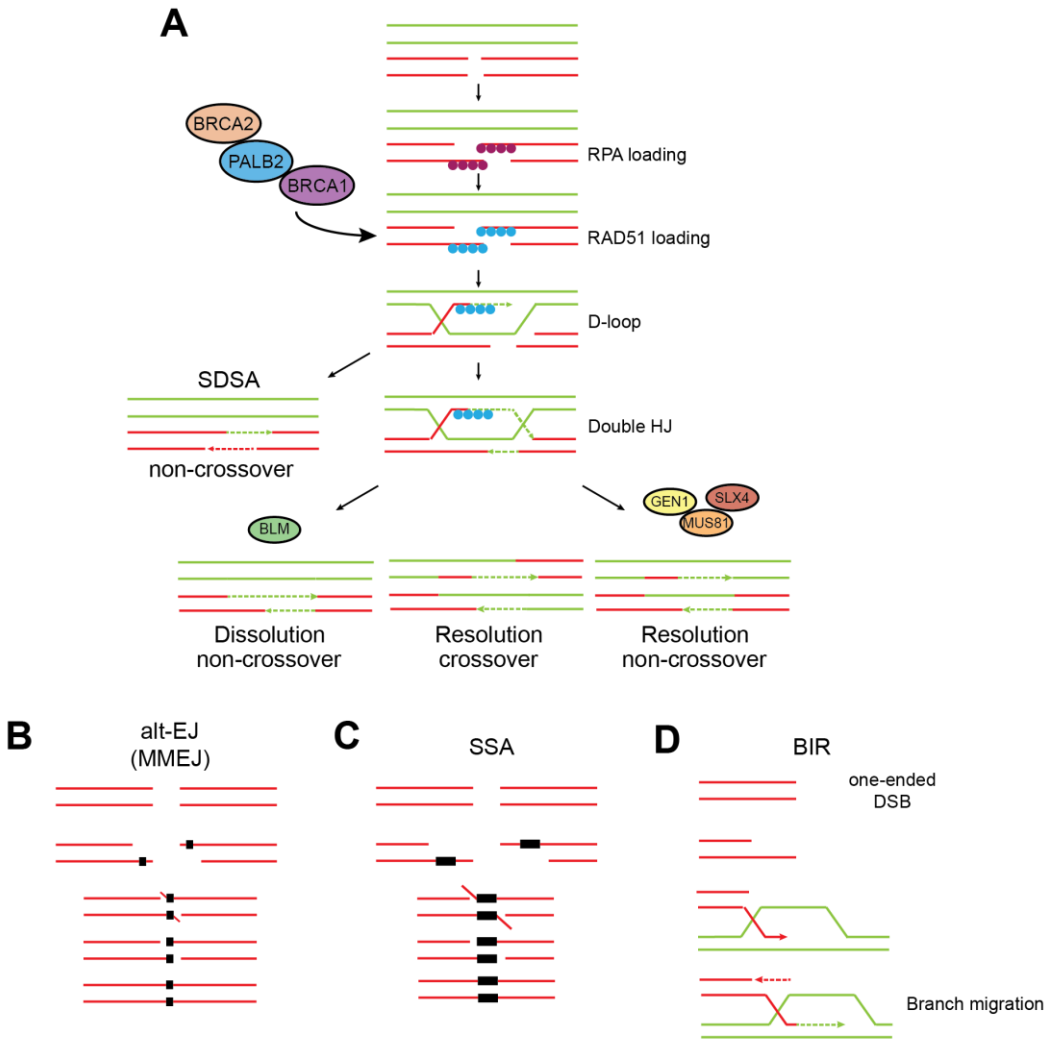


Figure 1.1 Resection-dependent DSB repair pathways.
A Homologous recombination (HR) involves resection of a DNA break to give 3' ssDNA overhangs. RPA binds the exposed ssDNA which is exchanged for RAD51 by the BRCA1-PALB2-BRCA2 complex. RAD51 facilitates strand invasion and D-loop formation. This can be resolved through a non-crossover mechanism involving synthesis-dependent strand annealing (SDSA). Alternatively, a double HJ can form. The repaired DNA strands can undergo BLM-dependent dissolution to give non-crossover repair products or structure-specific nuclease dependent resolution which can produce non-crossover and crossover repair products. **B** Alternative end joining (Alt-EJ, also known as MMEJ) involves resection of DSBs and annealing of short homology regions (~10bp), cleavage of unpaired nucleotides, and ligation of the DNA backbone. **C** Single strand annealing (SSA) requires more extensive resection at the DSB and annealing of longer homology regions (~30bp). The unpaired DNA ends are removed by nucleases and the DNA backbone ligated. **D** Break-induced replication (BIR) repairs one-ended DSBs and can facilitate replication restart. The exposed ssDNA end invades into the homologous template and facilitates branch migration with DNA polymerases to complete DNA replication.

In this pathway, PARP1 mediates annealing of microhomology regions (~10bp) (Ceccaldi et al., 2016) and recruits Polymerase θ (Pol θ), a TLS polymerase, that inhibits HR by binding RAD51 and preventing nucleofilament formation. Pol θ promotes error-prone fill-in

DNA synthesis surrounding the annealed region by extending 3' ssDNA ends. FEN1, LIG1, and LIG3 cleave the DNA flaps and facilitate strand ligation (Belan et al., 2022; Ceccaldi et al., 2016) (**figure 1.1B**).

Due to annealing of short homology regions, alt-EJ can produce short deletions or insertions, chromosomal translocations, and mutagenic rearrangements when combining DSBs from different chromosomes (Ceccaldi et al., 2016).

1.4.4 Single Strand Annealing (SSA)

Like alt-EJ, SSA is another mutagenic backup repair pathway but requires extensive DSB resection and anneals long stretches of homology (~30bp). Consequently, SSA can result in large deletions (Ceccaldi et al., 2016).

RPA protects extensive 3' ssDNA overhangs before RAD52 binds the exposed DNA at the DSBs and promotes annealing of homologous repeats. ERCC4-ERCC1 cleave the non-homologous 3' DNA flaps and the DNA backbone is ligated by LIG1 (Bennardo et al., 2008; Ceccaldi et al., 2016) (**figure 1.1C**).

1.5 Replication stress

Replication stress refers to the slowing or stalling of DNA replication forks in response to challenges blocking fork progression (Berti & Vindigni, 2016). DNA lesions, secondary DNA structures, and DNA-protein complexes can all impede fork progression (Magdalou et al., 2014). Replication fork stalling can promote separation of the replicative MCM helicase and polymerase, leading to an accumulation of ssDNA and RPA binding (Berti & Vindigni, 2016; Magdalou et al., 2014). Stalled forks display ɣH2AX signalling, even in the absence of DSBs, to activate the DDR (Petermann et al., 2010).

Several mechanisms mitigate the consequences of replication stress (**figure 1.2**). Dormant origins can be activated upon fork stalling to complete replication in a timely manner (Ge et al., 2007). Some regions of the genome contain a low frequency of dormant origins so replication fork restart after lesion removal is vital. DNA lesions can also be bypassed

through error-prone mechanisms to continue replication (**section 1.5.1**), or else replication forks can be remodelled to protect nascent DNA (**section 1.5.2**) while the DNA lesion is removed.

Collision with an unrepaired DNA break or MUS81-dependent cleavage of stalled replication forks results in fork collapse and breakage, producing a one-ended DSB. One-ended DSBs must be repaired using break-induced replication (BIR) (**section 1.5.3**). Therefore, timely resolution of replication stress and replication completion is essential for genome stability.

1.5.1 Translesion synthesis (TLS), repriming, and template switching

Translesion synthesis (TLS), PRIMPOL-dependent repriming, and HR-mediated template switching are DNA damage tolerance pathways to circumvent DNA lesions during replication (**figure 1.2**). Some lesions can be bypassed using low fidelity translesion synthesis (TLS) polymerases such as Pol κ, Pol ι, Pol η, REV1, and Pol ζ which can directly synthesise past the DNA lesion (Bainbridge et al., 2021).

Alternatively, lesions can also be bypassed using PRIMPOL-mediated repriming. This allows replication to continue, producing a ssDNA gap. Identified in bacteria, yeast, and mammalian cells (Callegari et al., 2010; Elvers et al., 2011; Heller & Marians, 2006; Lopes et al., 2006), PRIMPOL is a DNA/RNA primase and TLS polymerase that can facilitate fork progression in unperturbed S phase and fork restart after UV-induced DNA damage (Bianchi et al., 2013; García-Gómez et al., 2013; Keen et al., 2014; Mourón et al., 2013). Loss of PRIMPOL results in defective fork progression and mitotic DNA breaks (Bianchi et al., 2013) The resulting ssDNA gap requires RAD51-mediated HR for repair through a template switching mechanism (Piberger et al., 2020).

Template switching involves RAD51-dependent strand invasion of the nascent DNA strand into the undamaged sister chromatid, forming a double HJ and enabling DNA synthesis and

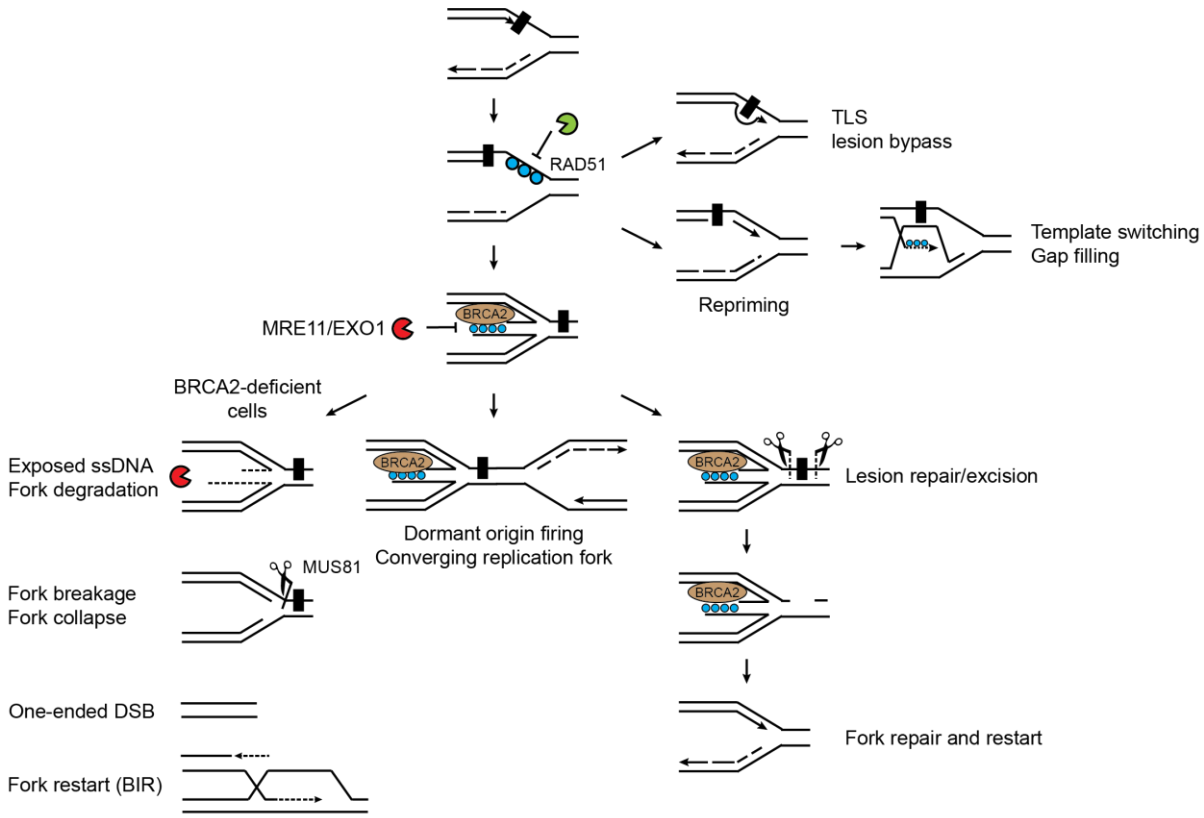


Figure 1.2 Replication stalling and restart mechanisms.
DNA lesions or topological stress can block fork progression, leading to fork stalling. ssDNA is protected by RAD51 binding. Lesions at stalled forks can be bypassed using translesion synthesis (TLS) or repriming past the DNA lesion and subsequent gap filling through a HR-dependent template switching mechanism. Stalled forks can be remodelled into a four-way branched DNA structure. RAD51 and BRCA2 block MRE11/EXO1-mediated degradation of nascent DNA. In BRCA2-deficient cells, nucleases degrade exposed ssDNA, creating a structure that can be cleaved by MUS81, causing fork collapse and a one-ended DSB. The DNA is repaired and replication restarted through a BIR-dependent mechanism. Dormant origins can also be activated upon fork stalling to complete replication. Alternatively, the lesion can be excised and repaired before fork restoration and replication restart.

gap filling (Tirman et al., 2021). The involvement of HR at replication-associated ssDNA is now understood to drive chemosensitivity in HR-deficient cancers, rather than its role in DSB repair (Cong et al., 2021; Panzarino et al., 2021; Tirman et al., 2021).

1.5.2 Replication fork reversal

Low dose (25 nM) camptothecin treatment was found to induce replication fork slowing, largely independent of fork breakage, in mammalian U2OS cells, *S. cerevisiae*, and *Xenopus laevis* egg extracts (Ray Chaudhuri et al., 2012; Zellweger et al., 2015). *In vivo* psoralen crosslinking and electron microscopy later revealed a mechanism for replication

fork reversal as an explanation for this fork slowing phenomenon. Replication fork reversal involves the conversion of a replication fork into a four-way branched (chicken foot) structure where nascent DNA strands anneal to minimise nucleolytic damage upon replication stress (**figure 1.2**). Replication fork reversal minimises DSB formation and chromosome instability upon replication stress (Ray Chaudhuri et al., 2012).

Several translocases have been linked to fork reversal under different contexts including SMARCAL1, ZRANB3, HTLF, PARP1, and RAD51 (Kile et al., 2015; Kolinjivadi et al., 2017b; Ray Chaudhuri et al., 2012; Vujanovic et al., 2017; Zellweger et al., 2015). Once reversed, nascent ssDNA is protected from MRE11-dependent degradation by BRCA2 and RAD51 (**section 1.6.2.3.3**) (Schlacher et al., 2011, 2012). Replication can then either continue, using the nascent strand as a template i.e. replication bypass, or the DNA lesion is resolved, and the reversed fork is restored to its canonical 3-armed structure using RECQ1, to resume replication (Berti et al., 2013).

Overall, it is proposed that replication fork reversal is a mechanism employed by cells to prevent DSB formation and chromosome instability upon replication stress.

1.5.3 Break-induced replication (BIR)

Break-induced replication (BIR) is an error-prone process to resume replication after fork collapse and one-ended DSB generation (Anand et al., 2013) (**figure 1.1D**). In yeast, BIR is mediated by RAD51 or RAD52. In humans, BIR is described to be primarily RAD51-dependent (Costantino et al., 2014; Hashimoto et al., 2011). BIR involves the invasion of the broken DNA end into the homologous template, forming a migrating D-loop which undergoes DNA polymerase POLD3-dependent branch migration, serving as a replication template (Sotiriou et al., 2016). RAD52 strand annealing is also involved in a BIR-like process after replication stress in cancerous U2OS cells (Sotiriou et al., 2016) (**section 1.5.3.1**).

BIR-mediated replication restart can be mutagenic. In fact, BIR within repetitive DNA sequences can contribute to gross chromosomal rearrangements and mutagenesis in fission and budding yeast (Deem et al., 2011; Tinline-Purvis et al., 2009). Hence, BIR is typically restrained to short distances due to endonuclease activity such as MUS81-EME1 (Bhowmick et al., 2016).

1.5.3.1 Mitotic DNA synthesis (MiDAS)

Mild replication stress that does not induce DNA breaks can mean cells enter mitosis with under-replicated DNA. Incomplete replication can be resolved in early mitosis through mitotic DNA synthesis (MiDAS), a DDR-associated, BIR-like mechanism (**figure 1.3**) (**section 1.5.3**) (Minocherhomji et al., 2015). MiDAS has previously been associated with difficult-to-replicate regions such as common fragile sites (CFSs) (Minocherhomji et al., 2015) and telomeres (Dilley et al., 2016; Min et al., 2017).

Unlike BIR (**section 1.5.3**), MiDAS in human cells is RAD52-dependent (Bhowmick et al., 2016). In short, stalled forks are cleaved in early prophase by SLX4-associated MUS81-EME1 to produce a one-ended DSB. RPA bound to ssDNA is subsequently replaced by RAD52 to facilitate strand annealing and invasion into the homologous template, forming a D-loop. DNA polymerase POLD3 facilitates branch migration of this D-loop, thus restarting conservative DNA replication (Bhowmick et al., 2016; Lai et al., 2017; Minocherhomji et al., 2015; Sotiriou et al., 2016). Interestingly, MiDAS has been described as ATR-, BRCA2-, and RAD51-independent (Minocherhomji et al., 2015; Sotiriou et al., 2016).

Completion of DNA replication by MiDAS is essential to prevent mitotic aberrations such as chromosome missegregation and non-disjunction (Minocherhomji et al., 2015).

1.5.4 Mismatch repair (MMR)

Mismatch repair (MMR) functions to correct nucleotide mismatches, chemical/physical base damage, and small DNA loops generated during DNA replication (Pećina-Šlaus et al., 2020;

Spies & Fishel, 2015). Failure to correct these mismatches leads to accumulation of mutations, microsatellite instability, and cancer.

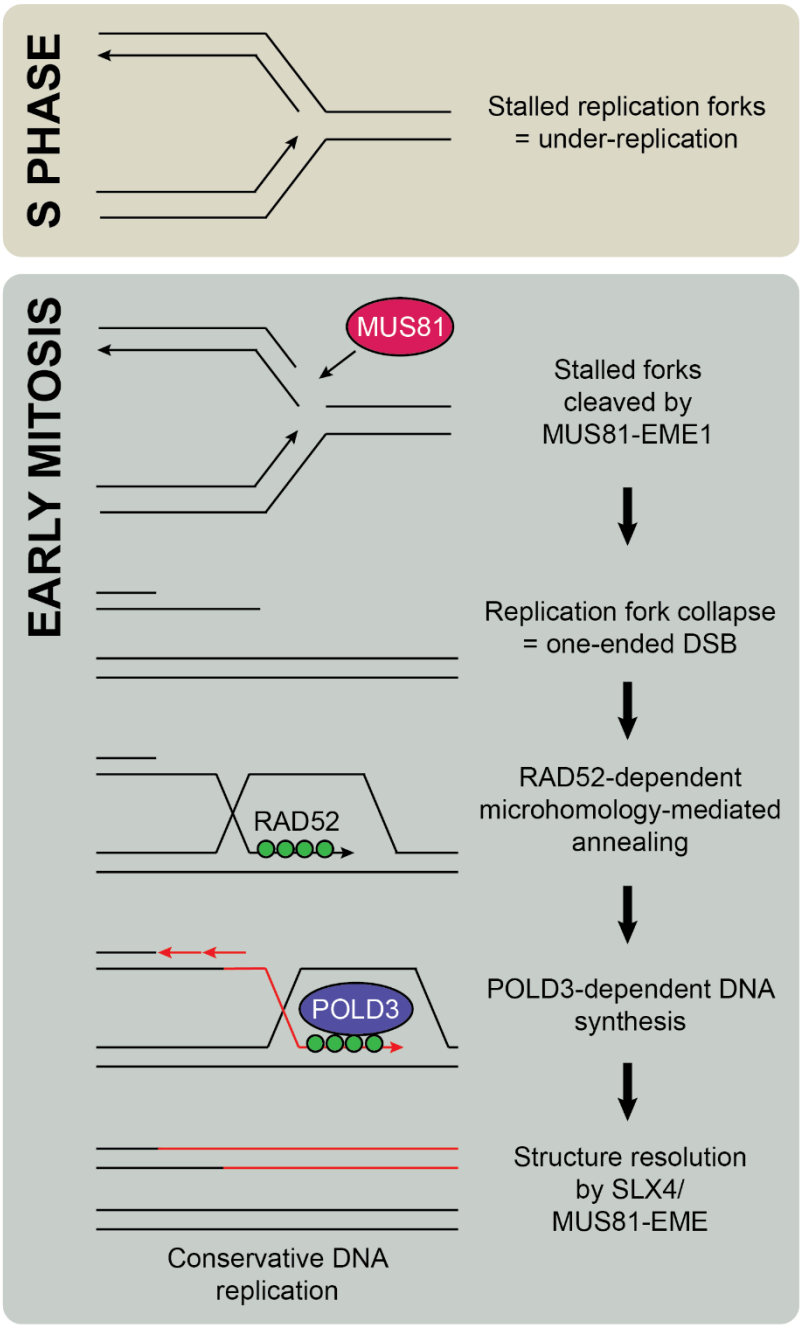


Figure 1.3 Mitotic DNA synthesis (MiDAS)
The current understanding of MiDAS is that replication stress can lead to stalled forks and incomplete replication by the end of S phase. Upon mitotic entry, stalled forks are cleaved by endonuclease MUS81-EME1, producing one-ended DSBs. RAD52 binds ssDNA and promotes microhomology-mediated annealing into the homologous template. Conservative DNA replication is completed in a BIR-like, POLD3-dependent process. The D-loop is resolved by SLX4 and MUS81-EME1.

MMR machinery performs an excision-resynthesis reaction to repair DNA. In humans, heterodimers MSH2-MSH6, which detects single base mismatches and small DNA loops, or MSH2-MSH3, which detects larger DNA loops, recognise the mismatches and initiate MMR. At the mismatch, ADP is exchanged for ATP, inducing a conformational change of the heterodimer into a sliding clamp structure on the DNA. MLH1/PMS2, an endonuclease complex, is subsequently recruited with proliferating cell nuclear antigen (PCNA) to excise the mismatch and generate an SSB. EXO1 degrades the mismatched DNA and Pol δ fills the gap (Chakraborty & Alani, 2016; Pećina-Šlaus et al., 2020; Spies & Fishel, 2015).

MMR has also been described to promote HR by inhibiting homeologous recombination. MMR proteins facilitate this by repairing mismatches within heteroduplex DNA or by completely rejecting heteroduplex formation through an unwinding mechanism (Chakraborty & Alani, 2016; Spies & Fishel, 2015). Hence, defects in MMR increase gene conversion and recombination between divergent sequences (Spies & Fishel, 2015). Furthermore, MLH1 and MSH2 have been linked to Fanconi Anaemia pathway activation and interstrand crosslink (ICL) repair (**section 1.6.2.3.2**) through interactions with FANCD2 and FANCJ, to facilitate DNA unwinding (Williams et al., 2010).

MMR is also important in ribonucleotide excision repair (RER) (Kellner & Luke, 2020). Ribonucleotides can be erroneously incorporated during DNA replication by Pol α, δ, and ε. RER can proceed through two pathways involving RNase H2 or topoisomerase I (TOP1) (Kellner & Luke, 2020). RNase H2 recognises ribonucleotides within the DNA backbone and incises at the site to create an SSB. From the SSB, strand displacement synthesis by Pol δ/ε creates a flap structure containing the ribonucleotide. FEN1/EXO1 cleave the flap and LIG1 ligates the remaining single strand nick. This pathway can provide an entry point for MLH1/PMS2 to target MMR to mismatches on the nascent DNA strand (Ghodgaonkar et al., 2013; Lujan et al., 2013). Furthermore, MLH1/PMS2 can also promote complete excision of ribonucleotides following RNase H2 nicking activity, hence MMR is important to complete RER under some conditions (Williams et al., 2016).

Alternatively, TOP1-mediated ribonucleotide removal occurs in the absence of RNase H2 and MMR (Kellner & Luke, 2020). In budding yeast, TOP1 cleaves at ribonucleotides to form a TOP1 cleavage complex (TOP1cc). This TOP1cc can be broken by nucleophilic attack by the adjacent 2'OH group on the ribose moiety, releasing TOP1 and creating an unligatable 2',3'-cyclic phosphate which requires further processing. Repair can then proceed in several ways: (i) a second TOP1 cleavage event removes the ribonucleotide and the resulting TOP1cc is released by tyrosyl-DNA phosphodiesterase (TDP1). The SSB can then be repaired through an error-free mechanism. (ii) TOP1 may realign the DNA backbone and ligate the nick creating 2-5bp deletions. (iii) A second TOP1 incision on the opposite strand creates a DSB which requires HR for repair. Hence, RNase H2 loss is synthetic lethal with BRCA1/2 deletion in human cells (Zimmermann et al., 2018).

1.6 Canonical PALB2-BRCA2-RAD51 complex to maintain genome stability

PALB2, BRCA2, and RAD51 are vital for maintaining genome stability. Part of canonical HR-mediated DSB repair (**section 1.4.2**), the proteins have additional roles in the replication and transcription stress response, among others.

The sections below will describe the structure and functions of these proteins, and how they relate to one another.

1.6.1 PALB2

Partner and localiser of BRCA2 (PALB2) is a tumour suppressor, first described for its role in bridging BRCA1 and BRCA2 for RAD51 recruitment at sites of DNA damage (Xia et al., 2006).

Mutations in PALB2 are associated with breast, pancreatic, and ovarian cancer (reviewed in (Wu et al., 2020)). Biallelic germline mutations in PALB2 also give rise to Fanconi Anaemia (FA) subtype FA-N (Xia et al., 2007). FA-N patients are hypersensitive to mitomycin C (MMC) treatment, displayed defective RAD51 foci formation, and are predisposed to embryonal cancer development (Tischkowitz & Xia, 2010).

1.6.1.1 PALB2 structure

PALB2 is a large protein of 1186 residues. The N-terminus contains PALB2's DNA binding domains (DBD) (Buisson et al., 2010; Deveryshetty et al., 2019) and a coiled-coil domain which interacts with BRCA1 to facilitate HR (Sy et al., 2009b; Zhang et al., 2009a; Zhang et al., 2009b) (**section 1.6.1.2.1**).

A ChAM domain enables PALB2 binding to nucleosomes and chromatin for rapid recruitment to DNA breaks (Bleuyard et al., 2012; Fournier et al., 2022). PALB2 also contains an MRG15 binding domain (MBD) through which it binds transcriptionally active genes via MRG15 (Bleuyard et al., 2017; Redington et al., 2021; Sy et al., 2009a) (**section 1.6.1.2.3**).

The C-terminal WD40 domain is a WD40-type β-propeller with seven blades (Oliver et al., 2009), important for several protein-protein interactions, including BRCA2 and RAD51 (Park et al., 2014; Xia et al., 2006). A cancer-associated mutation (Y1183X) within this WD40 domain results in PALB2 truncation, disrupting hydrogen bonding between the β-propeller blades and protein folding, leading to protein degradation (Oliver et al., 2009; Reid et al., 2007).

1.6.1.2 PALB2 function

PALB2 has several functions to maintain genome stability in cells, some of these are described below.

1.6.1.2.1 Homologous recombination

PALB2 was identified as a partner of BRCA2 by mass spectrometry analysis (Xia et al., 2006) and subsequently found to promote HR-mediated repair by bridging BRCA1 and BRCA2 at sites of DNA damage to stimulate RAD51-dependent D-loop formation (Zhang et al., 2009a; Zhang et al., 2009b) (**section 1.4.2**).

1.6.1.2.2 Replication fork recovery

ATR-dependent RPA phosphorylation at stalled forks recruits PALB2 and BRCA2 to promote ssDNA gap filling and fork recovery (Murphy et al., 2014). Phosphorylated RPA-ssDNA led to a 4.6-fold increase in PALB2 binding compared to non-phosphorylated RPA-ssDNA *in vitro*. Additionally, PALB2, and BRCA2 to a lesser extent, were demonstrated to stimulate Pol η-mediated DNA synthesis activity after RAD51-dependent D-loop formation *in vitro*, via its WD40 domain (Buisson et al., 2014).

The breast cancer-associated PALB2 Q775X mutant, within the WD40 domain, failed to stimulate Pol η-dependent DNA synthesis (Buisson et al., 2014). Furthermore, the PALB2-phospho-RPA interaction protected against replication fork collapse, DSB induction, and micronuclei formation (Murphy et al., 2014). Collectively highlighting the importance of these pathways in mitigating DNA breakage and genome instability at stalled replication forks.

1.6.1.2.3 Chromatin association at transcriptionally active genes

Genome-wide ChIP-seq revealed PALB2 occupancy at actively transcribed genes through its association with elongating RNA Polymerase II (RNAPII) (Gardini et al., 2014; Zhang et al., 2006). MRG15 (MORF-related gene on chromosome 15) is a component of histone acetyltransferase-deacetylase complexes (Hayakawa et al., 2010) and interacts with transcription elongation markers H3K36me2 and H3K36me3 *in vitro* (Zhang et al., 2006).

MRG15 has an N-terminal chromodomain that binds H3K36me3, catalysed by SETD2 methyltransferase, to promote RNAPII binding and transcription (Bleuyard et al., 2017). PALB2 interacts with MRG15 via a central MBD to promote its rapid recruitment to actively transcribed genes, along with BRCA2 and RAD51, in response transcription-replication conflicts, replication stress, and DNA breaks (Bleuyard et al., 2017; Hayakawa et al., 2010; Martrat et al., 2011; Sy et al., 2009a). MRG15 depletion and MBD mutations significantly impaired PALB2 and BRCA2 association with actively transcribed, but unperturbed genes, and RAD51 foci formation was shown to be dependent on active transcription (Bleuyard et al., 2017).

MRG15-deficient cells have reduced HR efficiency by over 50% and hypersensitivity to MMC (Hayakawa et al., 2010). Furthermore, several cancer-associated PALB2 mutations within the MBD have been identified to reduce binding efficiency (Redington et al., 2021), highlighting the importance of this interaction in maintaining genome stability.

The conserved chromatin-association motif (ChAM) further regulates PALB2's chromatin association in unperturbed and damaged cells (Bleuyard et al., 2012). Mass spectrometry revealed that lysine acetyltransferase 2A and 2B (KAT2A/KAT2B) acetylate a cluster of seven lysine residues within PALB2's ChAM, enhancing PALB2's (and ultimately BRCA2 and RAD51's) interaction with nucleosomes on undamaged chromatin (Fournier et al., 2016, 2022). EUFA1341 cells expressing a PALB2 ChAM deletion failed to localise to DNA upon MMC and IR treatment (Bleuyard et al., 2012). In fact, upon DNA damage, ChAM is deacetylated by lysine deacetylases (KDACs) to increase PALB2 mobility to DNA break sites (Fournier et al., 2022).

ChAM, MRG15, and BRCA1 likely work together closely across different contexts to regulate PALB2 levels on chromatin. In unperturbed cells, ChAM and MRG15 maintain PALB2, BRCA2, and RAD51 on chromatin. Upon DNA damage, this close association allows efficient reassembly of the BRCA complex and additional recruitment, promoting rapid DNA repair (Bleuyard et al., 2012; Fournier et al., 2022).

1.6.1.2.4 Cell cycle checkpoint control

DNA damage can trigger G2/M checkpoint activation, blocking mitotic entry through inhibition of cyclin B-CDK1 activity (Iliakis et al., 2003). An RNA interference screen in p53 dominant-negative U2OS cells identified a role for PALB2 in IR-induced G2/M checkpoint maintenance, independent of RAD51 and HR (Menzel et al., 2011). PALB2 was demonstrated to be important for activation and maintenance of the checkpoint through interactions with BRCA1 and BRCA2, respectively (Simhadri et al., 2019). It was proposed that BRCA2 and PALB2 may function to prevent inappropriate Aurora A-PLK1 (Polo-like kinase 1) activation and checkpoint recovery (Macůrek et al., 2008; Menzel et al., 2011; van

Vugt et al., 2004). Loss of PALB2's involvement in the G2/M checkpoint leads to an accumulation of chromosomal abnormalities and mitotic defects due to both defective HR and checkpoint control. This results in additional DNA damage from chromosome missegregation e.g. radial and dicentric chromosomes, potentially contributing to tumourigenesis (Simhadri et al., 2019).

1.6.2 BRCA2

BRCA2 (breast cancer 2) plays an essential role in the DDR, including HR and the replication stress response, to maintain genome stability. BRCA2 is a breast cancer susceptibility gene on chromosome 13q12-q13 that was first identified due to its link to hereditary breast cancer (Wooster et al., 1995). It has since also been linked to susceptibility to ovarian and prostate cancers, among others (Fradet-Turcotte et al., 2016). Like PALB2, biallelic mutations in BRCA2 are also associated with FA (Howlett et al., 2002).

1.6.2.1 BRCA2 structure

BRCA2 is a large scaffold protein of 3418 amino acids, encoded by a gene composed of 27 exons (Fradet-Turcotte et al., 2016). BRCA2's N-terminus is responsible for its interaction with PALB2 in HR (Oliver et al., 2009; Xia et al., 2006).

BRCA2 contains eight conserved BRC repeats encoded by exon 11 (Bignell et al., 1997; Bork et al., 1996) that are important for various protein-protein interactions including monomeric RAD51 (Brough et al., 2012; Buisson et al., 2014; Chen et al., 1998a; Wong et al., 1997). Furthermore, BRCA2 can act as a dimer to bind ssDNA and promote interactions with RAD51 monomers and loading onto ssDNA (Shahid et al., 2014).

BRCA2 also contains a DNA binding domain (DBD) comprised of a helical domain, three oligonucleotide/oligosaccharide-binding (OB) folds, and a tower domain (Yang et al., 2002). This DBD domain is important for interactions with ssDNA, DSS1, and poly(ADP)-ribose to facilitate its rapid recruitment to DNA damage (Marston et al., 1999; Yang et al., 2002; Zhang et al., 2015).

Finally, BRCA2 contains a C-terminal TR2 domain important for stabilising RAD51 nucleofilaments (Davies & Pellegrini, 2007; Esashi et al., 2007; Sharan et al., 1997). Two nuclear localisation signals (NLS) direct BRCA2 function to the nucleus, mutations within which have been associated with tumourigenesis and hereditary breast cancer (Spain et al., 1999; Yano et al., 2000).

1.6.2.2 BRCA2 binding to RAD51

BRCA2 BRC repeats mediate its interaction with RAD51 required for DNA repair and the replication stress response (Chen et al., 1999; Chen et al., 1998a). Carreira and Kowalczykowski suggest two subgroups of BRC repeats that display different functions: BRC1-4 repeats bind monomeric RAD51 strongly to load RAD51 onto ssDNA and stabilise this complex to promote strand invasion *in vitro* (Carreira & Kowalczykowski, 2011; Davies et al., 2001). Supporting this, BRC4 binding to RAD51 inhibits its ATPase activity and dissociation from ssDNA (Carreira et al., 2009). Upon nucleation, BRC5-8 repeats bind the nascent RAD51 nucleoprotein filament to further stabilise filament extension (Carreira & Kowalczykowski, 2011; Chatterjee et al., 2016). However, BRC4 peptides disrupt RAD51 oligomerisation *in vitro* and *in vivo* (Chen et al., 1999; Davies et al., 2001; Pellegrini et al., 2002) and BRC overexpression can inhibit RAD51 recruitment and foci formation by blocking oligomerisation (Chen et al., 1999; Haas et al., 2018).

Hence, RAD51 nucleoprotein filaments are further stabilised through interaction with the C-terminal TR2 domain of BRCA2 *in vitro* (Esashi et al., 2007). Interestingly, RAD51 binding to the TR2 domain is disrupted by CDK-dependent phosphorylation at S3291 (Esashi et al., 2005). This phosphorylation peaks in G2/M phase and has been proposed to stimulate RAD51 disassembly and inhibit mitotic recombination (Ayoub et al., 2009; Esashi et al., 2005).

BRCA2 truncations correlate with reduced HR activity by GFP-based reporter assays (Moynahan et al., 2001; Tutt et al., 2001) and increased tumour incidence in mice and humans (Donoho et al., 2003; Håkansson et al., 1997; McAllister et al., 2002). Therefore,

BRCA2's C-terminus is essential for HR-mediated DSB repair by extending RAD51 filaments and coordinating the homology search (Haas et al., 2018).

1.6.2.3 BRCA2 function

BRCA2 has numerous functions to maintain chromosome stability throughout the cell cycle, the most relevant of which are described below.

1.6.2.3.1 Homologous Recombination

BRCA2-mediated RAD51 loading is essential for HR (**section 1.6.2.2**). CAPAN-1 cells, containing only one copy of the BRCA2 gene and a 6174delT mutation, showed defective IR-induced RAD51 foci formation but upstream RAD50 foci formation was unaffected (Yuan et al., 1999). Furthermore, I-SceI endonuclease-induced DSBs in BRCA2 mutant cells showed 100-fold reduced HR compared to WT cells (Moynahan et al., 2001).

BRCA2 is localised to sites of DNA damage by PALB2 and BRCA1 to facilitate HR (**sections 1.4.2 and 1.6.1.2.1**). BRCA2 binds DNA through its DBD domain and facilitates RPA exchange for RAD51 on ssDNA via DSS1 (Zhao et al., 2015). DSS1 binds and evicts RPA70 from ssDNA *in vitro* (Zhao et al., 2015) while stabilising monomeric BRCA2 to promote RAD51 loading and ultimately DNA repair (Jensen et al., 2010; Le et al., 2020).

1.6.2.3.2 Interstrand crosslink (ICL) repair

Interstrand crosslinks (ICLs) are detected by two converging replication forks. This recruits members of the FA core complex, consisting of eight FANC proteins (FANCA, FANCB, FANCC, FANCE, FANCF, FANCG, FANCL, and FANCM) and other supplementary factors including BRCA1, PALB2, BRCA2, and RAD51. The FA core complex facilitates monoubiquitylation of FANCI/FANCD2 (ID complex) which then cleaves at the converged forks to release the ICL. A second cleavage event by endonucleases including SLX4, ERCC4-ERCC1, MUS81-EME1, and FAN1, completely removes the ICL, and the resulting DSB is repaired by HR (Deans & West, 2011).

1.6.2.3.3 Stalled replication fork protection

BRCA2-deficient cells show increased DSBs upon hydroxyurea (HU)-induced replication stress *in vivo,* indicating its functional importance in protecting stalled forks (Lomonosov et al., 2003; Schlacher et al., 2011). BRCA2 restrains fork progression by acting with MCM10 to suppress PRIMPOL recruitment and ssDNA gap accumulation, otherwise susceptible to cleavage, in unperturbed cells (Kang et al., 2021).

BRCA2 is also essential to protect stalled replication forks from MRE11-mediated nucleolytic degradation. BRCA2 is dispensable for RAD51-mediated fork reversal (**sections 1.5.2 and 1.6.3.3.1**) but BRCA2's C-terminal RAD51 stabilisation activity on ssDNA protects the nascent DNA of the regressed arm by blocking MRE11- and EXO1-mediated digestion (Mijic et al., 2017; Ray Chaudhuri et al., 2016; Schlacher et al., 2011). Furthermore, depletion of fork remodelling factors decreased nascent DNA degradation and genomic instability in BRCA1/2-deficient cells (Taglialatela et al., 2017). This ssDNA protection activity is independent of BRCA2 and RAD51's HR activity and requires FANCD2 ubiquitylation and BRCA1 *in vivo* (Schlacher et al., 2011, 2012). Separately, BRCA2 can also act with FANCJ, FANCD2, and RAD51 to promote HR-mediated fork restart after stalling (Raghunandan et al., 2015; Zimmer et al., 2016).

Extensive resection in BRCA-deficient cells creates a substrate for MUS81-EME1 cleavage, triggering fork collapse. The resulting one-ended DSBs is subsequently repaired, and replication restarted through a POLD3-dependent, BIR pathway (**figure 1.2**) (**section 1.5.3**) (Lemaçon et al., 2017). Failure to protect ssDNA resulted in chromosome instability and mutagenesis including chromatid breaks, gaps, and triradial/quadriradial chromosomes (Schlacher et al., 2011). Interestingly, increased PRIMPOL expression in BRCA1/2-deficient cancer cells can increase tolerance to replication-stalling chemotherapeutic agents by rescuing degradation of unprotected reversed forks and promoting replication restart through repriming (Quinet et al., 2020; Tirman et al., 2021). Therefore, PRIMPOL-mediated

lesion bypass is likely a tightly regulated process, restricted to certain cellular contexts which are currently unknown (Kang et al., 2021; Quinet et al., 2020; Tirman et al., 2021).

1.6.2.3.4 R-loops

R-loops arise from interactions between nascent RNA with DNA, forming RNA-DNA hybrids and displaced ssDNA. They have been associated with promoter-proximal pausing (PPP) of RNAPII and transcription termination (Bhatia et al., 2014; Shivji et al., 2018). Excessive accumulation of R-loops can be deleterious and have been associated with genome instability, hence several proteins have been identified to promote R-loop removal including RNase H1, RNase H2, and senataxin (Bhatia et al., 2014; García-Rubio et al., 2015; Sessa et al., 2021; Tan et al., 2017). Recently, there has been increasing evidence for a role of BRCA2 in mitigating R-loop formation and promoting their resolution.

DNA-RNA immunoprecipitation (DRIP) at I-PpoI-induced DSBs found RNAPII-dependent long non-coding RNAs (lncRNAs) transcription generates R-loops extending bidirectionally ~1.5-3kb from the break site (D'Alessandro et al., 2018; Michelini et al., 2017). Excessive R-loop accumulation at DSBs can impede HR (Sessa et al., 2021) and BRCA2 depletion increases R-loop accumulation genome wide (Bhatia et al., 2014). As such, BRCA2 promotes R-loop resolution through recruitment of RNase H2 via its BRC1 and 3 repeats *in vitro* (D'Alessandro et al., 2018) and stimulation of DDX5 ATPase activity for R-loop unwinding *in vitro*, facilitating DSB end resection (Sessa et al., 2021). BRCA2 activity on R-loops appears to be largely independent of RAD51 recruitment and HR (Bhatia et al., 2014; Wang et al., 2022) although it has been proposed that BRCA2 may function with BRCA1 and the ICL repair pathway to mitigate R-loop-dependent replication fork stalling, preventing fork collapse, and promoting fork restart (Bhatia et al., 2014; García-Rubio et al., 2015)

BRCA2 also functions to limit R-loop formation. BRCA2 acts with TREX-2 and Krüppel-like zinc finger transcription factor, ZFP281, to limit R-loop formation in replicating cells (Bhatia et al., 2014; Martinez et al., 2015; Wang et al., 2022). Furthermore, BRCA2 recruits RNAPII-associated factor 1 (PAF1) to relieve RNAPII PPP and facilitate transcription elongation

(Shivji et al., 2018). C-terminal BRCA2 truncations associated with breast and ovarian cancer (Rebbeck et al., 2015) fail to recruit PAF1, accumulating R-loops at PPP sites and ERCC4-dependent DSBs, contributing to genome instability at actively transcribed genes (Shivji et al., 2018).

Structural chromosomal aberrations resulting from BRCA2 deficiency e.g. radial chromosomes, are reduced by overexpression of RNase H1, suggesting that these mitotic gross chromosomal rearrangements (GCRs) do not only result from aberrant recombination (Bhatia et al., 2014; Tan et al., 2017). Therefore, failure to maintain BRCA2-dependent R-loop processing significantly contributes to genome instability and tumourigenesis.

1.6.2.3.5 Faithful chromosome segregation

BRCA2 depletion leads to decreased spindle assembly checkpoint (SAC) activation, premature chromosome segregation, and aneuploidy (Choi et al., 2012). BRCA2's N-terminus acts as a scaffold for PCAF acetyltransferase mediated acetylation of BubR1 at K250 to facilitate SAC activation (Choi et al., 2012). BubR1 also phosphorylates BRCA2 *in vitro* although the function of this is currently unknown (Futamura et al., 2000). PLK1 further modulates the BRCA2-PCAF acetyltransferase interaction by hyperphosphorylating BRCA2 across at least three sites in mitosis. This modification disassembles the complex and promotes anaphase entry (Lin et al., 2003). This PLK1-dependent phosphorylation activity is inhibited upon DNA damage to minimise mitotic damage (Lee et al., 2004). PLK1 also phosphorylates BRCA2 at T207 to facilitate binding along with protein phosphatase 2A (PP2A), and pT680-BubR1 at the kinetochore, promoting proper chromosome alignment and segregation (Ehlén et al., 2020).

The role of BRCA2 in cytokinesis is controversial. (Daniels et al., 2004) found that BRCA2 deficient cells displayed binucleation and abnormal myosin II organisation during cytokinesis, while (Lekomtsev et al., 2010) found no evidence for this role. This variation is suspected to arise from differences in cell type or antibody specificity. Regardless, PLK1-dependent S193 phosphorylation and actin-binding protein filamin A localise BRCA2 to the

midbody to recruit nonmuscle myosin IIC to stimulate myosin II contractile ring formation and ESCRT-associated membrane abscission (Mondal et al., 2012; Takaoka et al., 2014).

Overall, BRCA2 appears to have a role in regulating the SAC and abscission, independently of its role in HR.

1.6.3 RAD51

RAD51 is evolutionarily conserved. Its loss leads to embryonic lethality in mice, and G2/M cell cycle arrest and cell death in chicken lymphocyte DT40 cells (Sonoda et al., 1998; Tsuzuki et al., 1996). It is essential to support DNA repair and stability, demonstrated by the link to FA when mutated (Ameziane et al., 2015).

1.6.3.1 RAD51 structure

The crystal structure of the *Saccharomyces cerevisiae* RAD51 filament in the presence of DNA was first elucidated in (Conway et al., 2004), revealing an allosteric relationship between ATPase- and DNA-binding sites of RAD51 on DNA. Since then, cryo-EM analysis of the human RAD51 recombinase identified an α/β ATPase core domain containing a Walker A and Walker B motif for ATP binding and hydrolysis (Xu et al., 2017). Additional N-terminal α-helices and β-strands facilitate RAD51 monomer-monomer interactions while two disordered loops allow DNA binding, joined by a flexible interdomain linker sequence (Xu et al., 2017).

RAD51 catalyses HR through its ATP-dependent DNA binding and recombination activity (Baumann et al., 1996; Benson et al., 1994; Bonilla et al., 2020). Each RAD51 monomer binds 3 nucleotides (Tombline & Fishel, 2002). While RAD51 can bind both ssDNA and double stranded DNA (dsDNA), it binds ssDNA with higher affinity (Subramanyam et al., 2016), forming a right-handed helical nucleoprotein presynaptic filament which can subsequently facilitate strand invasion for DNA repair or related activities (Xu et al., 2017).

1.6.3.2 RAD51 recruitment to chromatin

As discussed previously, a major pathway of RAD51 recruitment to chromatin is via BRCA2 (**section 1.6.2.2**). There are several other mechanisms facilitating RAD51's recruitment to chromatin for DNA repair and the DNA replication stress response (described in (Wassing & Esashi, 2021)). One pathway involves the recruitment of RAD51 via PLK1- and casein kinase 2 (CK2)-dependent phosphorylation. Firstly, PLK1 phosphorylates RAD51 at serine 14 followed by threonine 13 phosphorylation by CK2. PLK1-dependent RAD51 phosphorylation is supported by a direct interaction between PLK1 and BRCA2's N-terminus, mediated through CDK-dependent phosphorylation of T77 on BRCA2 (Yata et al., 2014). These phosphorylation events facilitate an interaction between RAD51 and NBS1, part of the MRN complex (Yata et al., 2012). PLK1 activity, and therefore RAD51 phosphorylation, is cell cycle regulated and highest during late G2 and mitosis.

1.6.3.3 RAD51 function

RAD51 functions to maintain genome stability. Several of these functions have been described previously (**sections 1.4.2, 1.5.2, 1.6.2.3.1, and 1.6.2.3.3**) but further insights are discussed below.

1.6.3.3.1 RAD51-dependent replication stress response

RAD51 promotes replication fork reversal (**section 1.5.2**) after TOP1 inhibitor mediated fork stalling, independent of its strand exchange activity (Mason et al., 2019; Zellweger et al., 2015). The exact role of RAD51 in promoting fork reversal is still unknown, however it has been proposed to involve RAD51 binding and stabilisation of the regressed nascent DNA arm (Zellweger et al., 2015). RAD51 stimulates fork restart after short term HU-mediated fork stalling in a HR-independent mechanism (Petermann et al., 2010). It was proposed that RAD51-dependent fork reversal facilitates XRCC3-dependent invasion into the homologous nascent DNA template, from which RAD51 promotes replication restart. Furthermore, RAD51 facilitates continuous DNA replication through a direct interaction with Pol α primase complex to promote Pol α and Pol β binding to the stalled fork for replication restart. Using

Xenopus laevis egg extract, in BRCA2- and RAD51-deficient conditions, accumulation of ssDNA gaps triggers SMARCAL1-dependent fork remodelling and MRE11-mediated digestion of nascent DNA (Kolinjivadi et al., 2017b). Fork reversal protects against fork collapse and breakage under replication stress (Zellweger et al., 2015). *In vivo* electron microscopy visualisation of replication intermediates in *Xenopus laevis* egg extracts demonstrated RAD51's role in protecting nascent DNA and excessive accumulation of ssDNA at stalled replication forks (Hashimoto et al., 2010) (**section 1.6.2.3.3**).

On the other hand, RAD51-dependent HR is required to repair one-ended DSBs after MUS81-dependent cleavage of stalled replication forks, and restart replication (Groth et al., 2012; Petermann et al., 2010). RAD51 promotes reassembly of replication machinery on collapsed forks for replication completion through a PCNA-dependent, BIR-like process (**section 1.5.3**) (Hashimoto et al., 2011).

These RAD51-dependent DNA protection mechanisms are essential for cell viability and maintain chromosome stability during unperturbed conditions (Kolinjivadi et al., 2017a).

1.7 Centromeres

Centromeres form the site of kinetochore nucleation and microtubule attachment and are essential for accurate chromosome segregation. Errors in centromere specification and integrity and the resulting mitotic defects are common hallmarks of disease and tumourigenesis (Barra & Fachinetti, 2018; Black & Giunta, 2018; McKinley & Cheeseman, 2016).

1.7.1 Centromere structure and function

Human centromeres are comprised of repetitive AT-rich, α-satellite DNA monomers that are 171 bp in length and arranged in a tandem head-to-tail fashion known as higher order repeats (HORs). HORs can extend until 3-5 Mb in length to form the core active centromeres (Barra & Fachinetti, 2018; Niikura et al., 2015). Expanding out from this is pericentromeric heterochromatin containing α-satellite and other satellite DNA stretches of

varying sequences and length (McKinley & Cheeseman, 2016; Ohzeki et al., 2020; Thakur et al., 2021) (**figure 1.4**).

Despite this unique DNA nature, centromeres are defined epigenetically through the presence of histone H3 variant, CENP-A; contained within nucleosomes interspersed between canonical nucleosomes throughout the core α-satellite arrays (Earnshaw & Rothfield, 1985; Fachinetti et al., 2013; Palmer et al., 1987; Sullivan et al., 1994). CENP-A shares 62% homology with histone H3 (McKinley & Cheeseman, 2016; Sullivan et al., 1994) and is essential for survival (Howman et al., 2000). Cryo-EM reconstitution of CENP-A tri-nucleosomes (H3-CENP-A-H3) demonstrate that these nucleosomes adopt an untwisted structure making them more accessible for protein binding (Takizawa et al., 2020).

CENP-B is one of the only sequence-specific proteins at human centromeres (Ohzeki et al., 2015). CENP-B binds 17 bp CENP-B boxes present in every other α-satellite monomer (**figure 1.4**) (Ikeno et al., 1994; Masumoto et al., 1989; Muro et al., 1992) on all chromosomes except the Y chromosome (Masumoto et al., 1989). CENP-B binding is essential for *de novo* centromere formation and chromosome segregation of human artificial chromosomes (HAC) (Hoffmann et al., 2016; Ohzeki et al., 2002). However, CENP-B's exact role remains unclear; although it promotes CENP-A stability at centromeres (**section 1.7.3**), CENP-B knockout mice are viable (Hudson et al., 1998; Kapoor et al., 1998; Perez-Castro et al., 1998).

In centromeric chromatin, CENP-A is essential for the deposition of the 16-subunit constitutive centromere associated network (CCAN) (McKinley & Cheeseman, 2016; Pesenti et al., 2016). The CCAN is comprised of five subgroups: CENP-C, CENP-L/N, CENP-H/I/K/M, CENP-T/W/S/X, and CENP-O/P/Q/U/R, and forms the inner kinetochore which remains associated with the centromere across the cell cycle (Cheeseman & Desai, 2008; Foltz et al., 2006). The CCAN provides a complex scaffold for outer kinetochore KNL1-MIS12-NDC80 (KMN) complex assembly in mitosis (Cheeseman & Desai, 2008; Gascoigne & Cheeseman, 2013). The KMN complex functions to bind microtubules and is

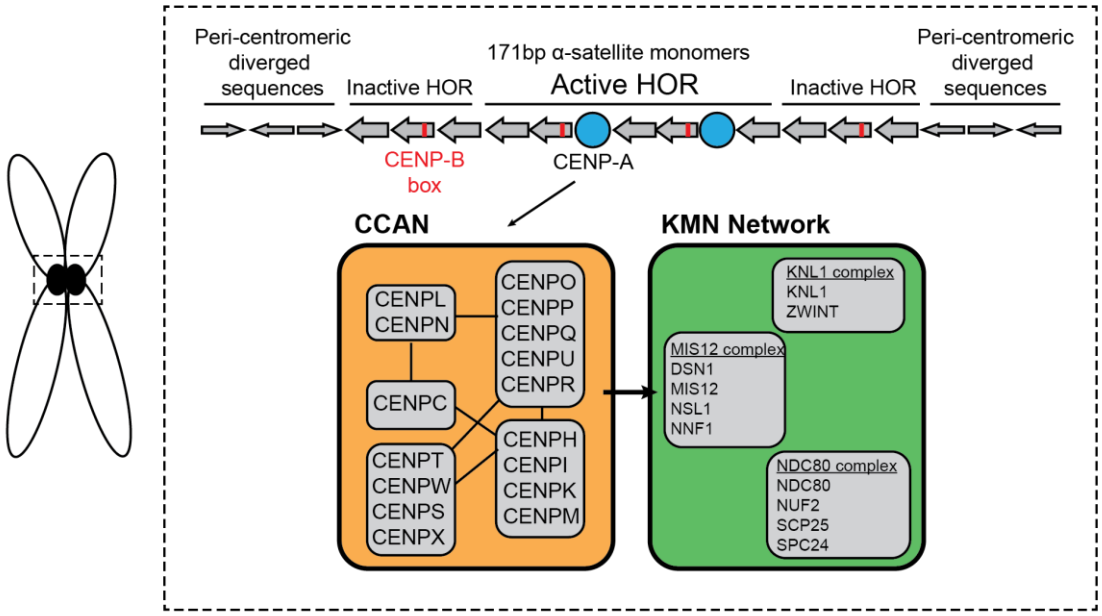


Figure 1.4 Centromere structure.
Centromeres consist of repetitive α-satellite DNA monomers arranged in a tandem head-to-tail fashion, termed higher order repeats (HORs) (large grey arrows). This forms the active centromere (active HOR). Surrounding this, pericentromeric chromatin contains satellite DNA of varying sequence, length, and arrangement (smaller grey arrows). Centromeres are defined epigenetically with CENP-A-containing nucleosomes (blue circles). Alternating monomers also contain a CENP-B binding box (red lines). From CENP-A, the constitutive centromere associated network (CCAN) forms, from which the outer kinetochore machinery (the KMN network) assembles to bind microtubules in mitosis and facilitate chromosome segregation.

the site of the mitotic SAC to ensure accurate chromosome segregation (**figure 1.4**) (McKinley & Cheeseman, 2016; Müller & Almouzni, 2017; Niikura et al., 2015).

Neocentromeres are functional centromeres that form outside of the canonical α-satellite DNA region (Voullaire et al., 1993). They do not require repetitive α-satellite DNA sequences nor CENP-B for their formation (Depinet et al., 1997) but retain CENP-A to assemble centromere and kinetochore machinery and can therefore act as functional centromeres (Barnhart et al., 2011; Heun et al., 2006; Marshall et al., 2008; Mendiburo et al., 2011; Van Hooser et al., 2001).

1.7.2 The Spindle Assembly Checkpoint (SAC)

Accurate and timely chromosome segregation in mitosis is vital for genome stability and cell survival. The spindle assembly checkpoint (SAC) is one mechanism by which accurate

chromosome segregation is regulated by ensuring correct kinetochore-microtubule attachments.

The SAC is maintained from prophase until all kinetochores are correctly attached to microtubule spindles, upon which anaphase onset is triggered and chromosome segregation can occur (Lara-Gonzalez et al., 2021). At unattached kinetochores, MPS1 phosphorylates KNL1 to promote recruitment and assembly of the mitotic checkpoint complex (MCC), comprised of MAD2, CDC20, BUBR1, and BUB3. The MCC subsequently binds APC/C^{Cdc20} and inhibits its ability to interact with E2 ubiquitin conjugating enzymes.

Upon binding of microtubules to the kinetochore and proper chromosome alignment at the metaphase plate, MPS1 is displaced, and the SAC is silenced. APC/C then ubiquitinates securin and cyclin B to promote loss of sister chromatid cohesion and chromosome segregation (Lara-Gonzalez et al., 2021).

Accurate microtubule binding to kinetochores requires time and thus inhibition of the SAC vastly reduces time to anaphase onset in mitosis and leads to chromosome segregation errors due to aberrant attachments. This results in aneuploidy which is strongly linked to tumourigenesis.

1.7.3 CENP-A deposition into centromeric chromatin

CENP-A loading is temporally and spatially regulated across the cell cycle (**figure 1.5**). Unlike canonical histone deposition, CENP-A loading is uncoupled from DNA replication. Pulse labelling CENP-A using SNAP found that new CENP-A is assembled into centromeres upon mitotic exit in G1 (Bodor et al., 2013; Jansen et al., 2007). CENP-A is diluted in S phase as it is distributed between the replicated sister chromatids and replaced by histone H3.3 as a placeholder (Dunleavy et al., 2011; Zasadzińska et al., 2018). Therefore, upon mitotic entry and kinetochore assembly, CENP-A-containing nucleosomes are interspersed among canonical H3-containing nucleosomes across the centromere region (Jansen et al., 2007; McKinley & Cheeseman, 2016).

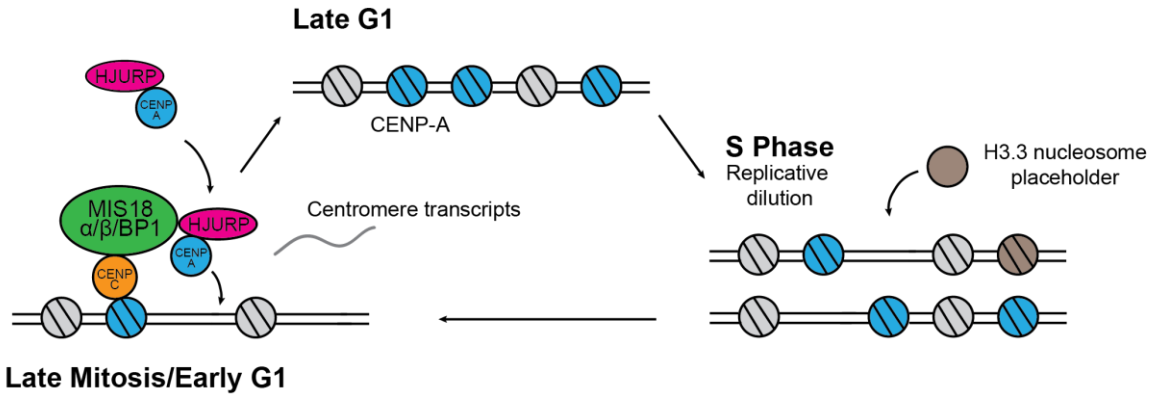


Figure 1.5 CENP-A deposition is spatially and temporally regulated
CENP-A is loaded into chromatin by late G1. CENP-A is diluted between replicated sister chromatids during S phase. Chromatin gaps are filled by histone H3.3 as a placeholder. In late mitosis and early G1 of the following cell cycle, CENP-A is loaded into DNA using the MIS18 complex and HJURP, aided by CENP-C and centromere transcription.

Canonical CENP-A loading requires the involvement of several histone chaperones including the MIS18 complex and Holliday Junction recognition protein, HJURP. In mitosis, MIS18-binding protein 1 (M18BP1) is directed to pre-existing sites of CENP-A incorporation by binding to CENP-C and CENP-I (Dambacher et al., 2012; Fujita et al., 2007; Moree et al., 2011). M18BP1 subsequently recruits other members of the MIS18 complex: MIS18α, MIS18β (Fujita et al., 2007; Hayashi et al., 2004; Maddox et al., 2007; McKinley & Cheeseman, 2016; Moree et al., 2011). In early G1, MIS18α and MIS18β regulate HJURP association at centromeres and CENP-A deposition within the α-satellite arrays (Müller & Almouzni, 2017; Ohzeki et al., 2020). CDK and PLK1 activity limits CENP-A deposition to G1 by regulating MIS18 complex localisation and HJURP recruitment (McKinley & Cheeseman, 2014; Niikura et al., 2015; Silva et al., 2012; Swartz et al., 2019). HJURP directly interacts with CENP-A via its centromere targeting domain (CATD) to facilitate CENP-A loading (Bassett et al., 2012; Bernad et al., 2011; Black et al., 2007; Dunleavy et al., 2009; Foltz et al., 2009; Müller & Almouzni, 2017; Shuaib et al., 2010). Failure to facilitate M18BP1 and HJURP localisation at centromeres reduces CENP-A centromeric deposition (Moree et al., 2011).

Several CCAN components have additionally been demonstrated to be important for CENP-A stability and incorporation into chromatin. CENP-B is essential for *de novo* CENP-A loading on α-satellite DNA in HACs (Ohzeki et al., 2002; Okada et al., 2007) and stabilises CENP-C at pre-existing centromeres to further promote CENP-A deposition and preserve centromere positioning within chromosomes (Fachinetti et al., 2013, 2015; Hoffmann et al., 2020; Suzuki et al., 2004). Subsequently, CENP-B-free and neocentromeric chromosomes are prone to increased missegregation (Fachinetti et al., 2015). Interestingly, utilising bacterial artificial chromosomes (BACs) for ectopic integration of α-satellite DNA into chromosome arms, CENP-B-proficient cells displayed increased H3K9me3 and CpG hypermethylation, indicating that heterochromatin suppresses centromere formation (Okada et al., 2007). Hence, this suggests that CENP-B can function to both facilitate and inhibit CENP-A deposition and centromere formation. Exactly how CENP-B recognises the different chromatin states is still unclear although it is known to recruit various chromatin modifiers e.g. H3K36 methylase ASH1L, H3K9 methylase Suv39h1, and HP1 to regulate the chromatin environment and CENP-A assembly (Otake et al., 2020). Once the epigenetic landscape has been established, and CENP-A incorporated, CENP-B is no longer required for HAC maintenance and inheritance (Okada et al., 2007).

Furthermore, CENP-C binds CENP-A to target it to centromeres and promote localisation of other CCAN factors with CENP-N (Carroll et al., 2009, 2010; Falk et al., 2015; Kato et al., 2013; Logsdon et al., 2015). More recently, CENP-I was demonstrated to directly interact with AT-rich, centromeric DNA, in a sequence-specific manner, to promote CENP-A loading and nucleosome formation *in vitro* (Hu et al., 2023), making it the only sequence-specific CCAN protein other than CENP-B.

1.7.3.1 Transcription and CENP-A deposition

Despite the heterochromatic nature of (peri)centromeric chromatin (Ribeiro et al., 2010), human and *Drosophila melanogaster* centromeres contain transcriptionally permissive markers, H3K4me2 and H3K36me2 (Bergmann et al., 2011; Ribeiro et al., 2010; Sullivan &

Karpen, 2004). Centromeric RNAPII-mediated DNA transcription occurs throughout late mitosis and G1 (Black & Giunta, 2018). In G1, CENP-A is loaded into centromeric nucleosomes along with >10,000 transcriptionally active sites across the chromosome arms (Nechemia-Arbely et al., 2019). This ectopically incorporated CENP-A is subsequently removed during DNA replication through an error correction mechanism to ensure correct CENP-A localisation (Nechemia-Arbely et al., 2019). CENP-B also regulates centromere transcription through ZFAT localisation and KAT2B-dependent, RNAPII-mediated non-coding RNA (ncRNA) transcription to promote accurate chromosome segregation. (Ishikura et al., 2020, 2021).

HJURP recruitment is at least partially dependent on RNAPII-mediated transcription (**figure 1.5**). HJURP and CENP-C were observed to interact with 1.3 kb RNA molecules *in vivo* to promote CENP-A loading (Quénet & Dalal, 2014). LncRNAs from active centromeric α-satellite arrays also facilitate stabilisation of CENP-A and CENP-C (McNulty et al., 2017). Furthermore, depletion of transcriptionally permissive marker, H3K4me2, through tetO-mediated tethering of lysine-specific demethylase 1 (LSD1) at HAC α-satellite DNA sequences failed to recruit HJURP and CENP-A suggesting that CENP-A loading is a transcription-dependent process (Bergmann et al., 2011). Similar relationships were also shown to be the case in Drosophila (Bobkov et al., 2018; Chen et al., 2015) and fission yeast (Choi et al., 2011). In Drosophila, lncRNAs from SATIII sequences on the X chromosome localised to centromeres to bind CENP-C and promote stable localisation of various kinetochore proteins including CENP-A and Spc105, and is therefore important for mitotic progression (Rošić et al., 2014).

Loss of centromeric RNA transcription reduces CENP-A levels (McNulty et al., 2017), highlighting the importance of centromere transcripts in centromere function, kinetochore assembly, and cell cycle progression. Despite this, there is still some debate on how centromere transcription influences CENP-A deposition. Bury et al., utilised single molecule FISH (smFISH) to reveal α-satellite RNA transcripts vary across the cell cycle but do not

remain associated with their centromere of origin (Bury et al., 2020). Thus, they proposed that it is the process of centromere transcription, rather than the presence of α-satellite RNA molecules themselves, which is important for centromere function, perhaps by altering centromere chromatin dynamics and protein binding (Bobkov et al., 2018; Bury et al., 2020).

1.7.4 Centromere integrity throughout the cell cycle

There is increasing evidence that centromeres display innate DNA fragility. Analysis of next generation sequencing (NGS) datasets reveal *de novo* DNA break enrichment within active centromeres of both proliferating and quiescent human cells (Crosetto et al., 2013; Saayman et al., 2023) and in yeast (Bensasson, 2011; Sriramachandran et al., 2020). Centromeric DNA breaks and rearrangements have been strongly linked to tumourigenesis and other developmental diseases (Barra & Fachinetti, 2018; Black & Giunta, 2018).

The following sections will discuss the numerous sources of centromere fragility that have been revealed across the cell cycle and the different protective repair mechanisms described to maintain centromere stability and function.

1.7.4.1 G1 Phase

In G1, cells have undergone cell division and are preparing for the upcoming DNA replication in S phase. Centromere transcription is high in G1 to facilitate CENP-A specification (**section 1.7.3.1**). As such, transcription-dependent torsional stress and R-loops can stabilise secondary DNA structures on the resulting exposed ssDNA, including DNA hairpins, cruciforms, and i-motifs (**figure 1.6A**) (Zhao et al., 2010), all currently associated with centromeres in humans, yeast, and flies (Aze et al., 2016; Garavís, Escaja, et al., 2015; Garavís, Méndez-Lago, et al., 2015; Jonstrup et al., 2008; Kabeche et al., 2018). Intriguingly, analysis of centromere DNA sequences across several species revealed enrichment of dyad symmetries which can adopt these structures (Kasinathan & Henikoff, 2018; Liu et al., 2023). This observation correlates with the absence of CENP-B in these organisms suggesting that they may serve a similar function, such as *de novo* CENP-A deposition. In fact, genome-wide mapping of R-loop distribution in maize found them to be

enriched in (peri)centromeric heterochromatin regions, overlapping with CENP-A binding sites (Liu et al., 2021).

Homologous recombination (HR) has been proposed to repair centromeric DNA breaks in G1 and facilitate CENP-A incorporation (**figure 1.7A**) (Yilmaz et al., 2021). Transcriptionally active chromatin marker, H3K4me2, and R-loops were enriched at sites of Cas9-induced DNA DSBs. Displaced ssDNA from R-loops, susceptible to nucleolytic cleavage, are bound by RPA. While the impact of R-loops in aiding or impeding HR-mediated repair is debated (Marnef & Legube, 2021), Yilmaz et al., find that Ubiquitin Specific Peptidase 11 (USP11) deubiquitylates PALB2 to promote PALB2-BRCA2-RAD51 complex formation and HR-mediated repair. This agrees with previous findings that USP11 can regulate R-loops (Jurga et al., 2021) and deubiquitylates PALB2 to facilitate its interaction with BRCA1 during S and G2 phase, limiting HR activity to these phases (Orthwein et al., 2015). USP11 also deubiquitylates HJURP to facilitate CENP-A recruitment and incorporation into the G1 centromeric chromatin, perhaps indicating a functional connection between centromeric DNA breaks and CENP-A deposition (Yilmaz et al., 2021).

HR is typically associated with S and G2 phases of the cell cycle due to the requirement of the homologous sister chromatid template however the repetitive and compact nature of centromere α-satellite DNA sequences may negate this requirement through intra-strand invasion of centromere repeats on the same chromatid (discussed further in **section 1.7.4.2.3**) (Piazza et al., 2021; Rief & Löbrich, 2002).

1.7.4.2 S phase

Human centromeres are replicated in late S phase (Hagen et al., 1990). Like transcription, DNA replication and unwinding of dsDNA can generate torsional stress and secondary DNA structure formation (**section 1.7.4.1**) (**figure 1.6Ba**). Secondary DNA structures at centromeres are understood to increase susceptibility to replication and transcription stress, predisposing centromeres to DNA instability and rearrangement (Barra & Fachinetti, 2018).

In fact, cruciform structures in AT-rich sequences are correlated with increased genomic rearrangements and mutations (Zhao et al., 2010). Centromere DNA breaks were shown to be initially dependent on active DNA replication (Saayman et al., 2023) and increased upon aphidicolin-induced replication stress (Crosetto et al., 2013). ERCC6L2, a member of the Sucrose Non-Fermenting 2 (SNF2) family of ATPases, was recently linked to replication processivity at centromeres (Carnie et al., 2023). In ERCC6L2 knockout U2OS cells, decreased levels of heterochromatic markers H3K27me2, H3K27me3, and H1 were observed, demonstrating reduced chromatin compaction. Without ERCC6L2, replication was less constrained at centromeric regions implying that centromere compaction and secondary DNA structures impose replication stress in these regions. Despite this, *in vitro* reconstitution of centromere replication in *Xenopus laevis* egg extract found no altered replication kinetics in untreated conditions compared to other chromosome regions (Aze et al., 2016), collectively suggesting that centromere replication is relatively unperturbed under physiological conditions.

1.7.4.2.1 Centromeric DNA loops

Secondary DNA structures can impede replication fork progression leading to the suggestion that centromeres are inherently difficult-to-replicate (Aze et al., 2016; Black & Giunta, 2018; Greenfeder & Newlon, 1992; Nakamura et al., 2008). Electron microscopy on BACs containing α-satellite DNA sequences identified replication- and condensin-dependent positively supercoiled dsDNA loops which accumulate behind the replication fork (Aze et al., 2016). These dsDNA loops limit RPA binding and local ATR activation for timely completion of DNA replication before the end of S phase. Interestingly, a recent study suggests a DNA damage-independent role for ATR in maintaining centromeric CENP-A occupancy (Trier et al., 2023). Combined with the centromeric role of ATR in mitosis (**section 1.7.4.3.2**), this implies a complex role for ATR at centromeres which needs further investigation. Various DNA repair factors including MMR proteins: MSH2 and MSH6, base excision repair factors: XRCC1 and PARP1, and DSB repair proteins: XRCC5 and MRN

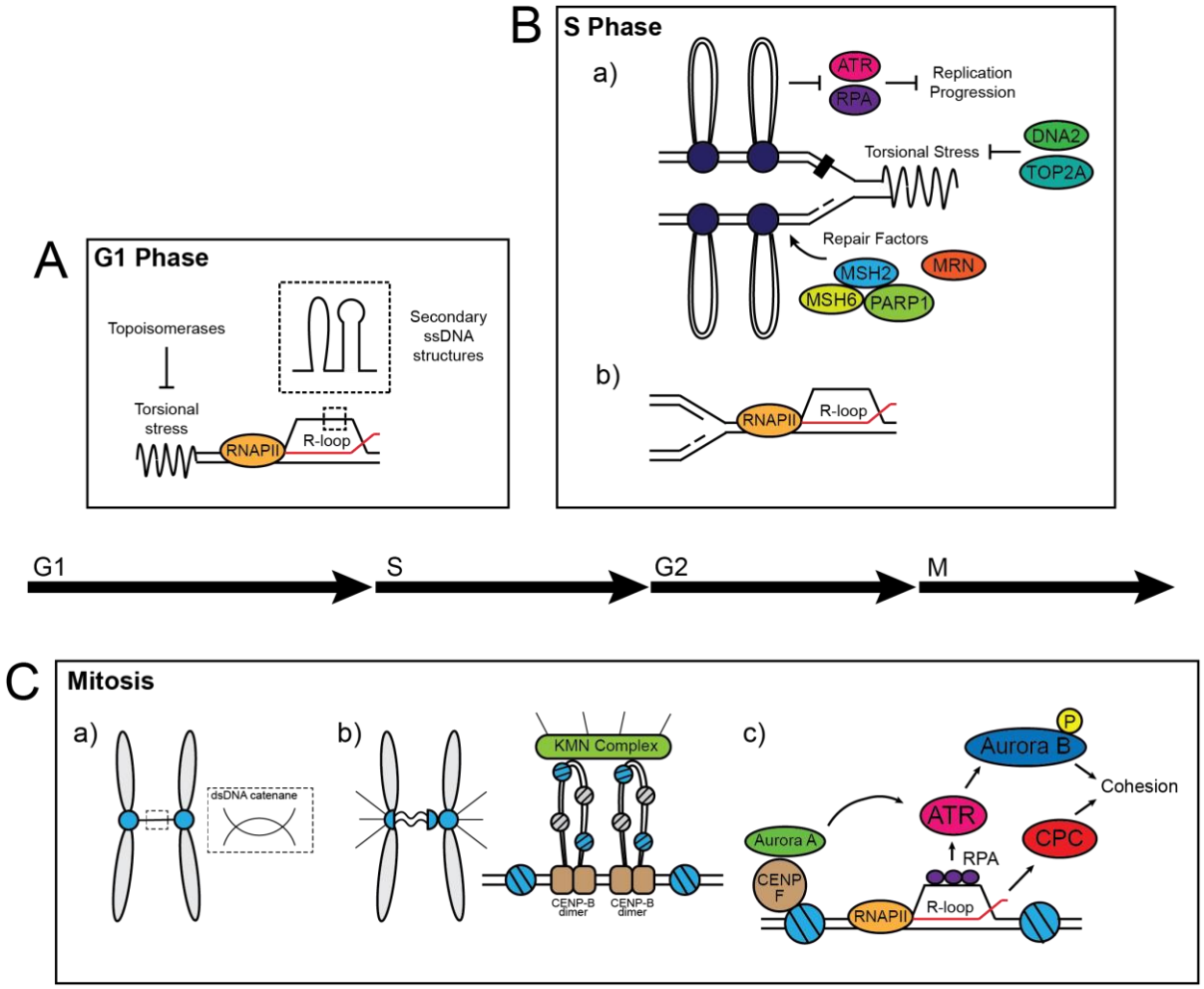


Figure 1.6 Sources of centromere instability across the cell cycle.
A Transcription and R-loops in G1 can stabilise secondary DNA structures in the exposed ssDNA. Topoisomerases resolve transcription-dependent torsional stress. **B a)** Condensin-dependent dsDNA loops in centromeric DNA impede replication progression. These loops, lesions, or torsional stress can impede replication fork progression and recruit various DDR factors to resume replication. **b)** Transcription-replication conflicts block fork progression. **C** Mitotic centromere instability can arise from **a)** dsDNA catenanes and ultrafine anaphase bridges (UFBs), **b)** reduced centromere compaction and flexibility, reducing centromere resistance to mitotic pulling forces, **c)** RNAPII-dependent centromere transcription recruiting Aurora B and the Chromosome Passenger Complex (CPC) to promote chromosome cohesion.

complex, were also enriched at centromeres indicating a special requirement in maintaining centromere stability during DNA replication (**figure 1.6Ba**) (Aze et al., 2016; Gao et al., 2018).

Non-B form DNA structures and R-loops can be resolved by structure-specific nucleases such as type I and type II topoisomerases which induce transient SSBs or DSBs, respectively, to remove torsional stress (Pommier et al., 2022). Hairpin loops in human α-

satellite sequences have been demonstrated to be cleaved by topoisomerase IIα (TOP2A) *in vitro* (Jonstrup et al., 2008), although the exact position of cleavage is still contested (Amir-Aslani et al., 1995, 1996; El Amri et al., 1999; Froelich-Ammon et al., 1994; Jonstrup et al., 2008; Mauffret et al., 1998). TOP2 has previously been associated with condensed active centromeric chromatin in a cell cycle-dependent manner from late S phase to anaphase to regulate centromere cohesion (Andersen et al., 2002; Floridia et al., 2000; Rattner et al., 1996; Sumner, 1996). Additionally, TOP2 can resolve topological and replication stress from SMC5/6 in *S. cerevisiae* which would otherwise induce replicative DNA damage (Minchell et al., 2020).

Further to this, the helicase and endonuclease, DNA2, was found to predominantly localise to centromeric regions to promote efficient centromere replication (Li et al., 2018). It was proposed that DNA2 cleaves hairpin and DNA loop structures *in vitro* to promote efficient replication and similarly prevent ATR accumulation and activation at centromeres. Failure of DNA2 to cleave centromeric DNA leads to impaired centromeric DNA replication and CENP-A deposition, and mitotic defects (Li et al., 2018).

Overall, secondary DNA structures at centromeres may create a special requirement for DDR factors at centromeres to maintain efficient DNA replication and minimise centromere instability.

1.7.4.2.2 Transcription-replication conflicts (TRCs)

Although centromere transcription is largely restricted to G1 and mitosis, some transcripts can persist into S phase and form R-loops. Conversely to the beneficial role of R-loops in G1 (**sections 1.7.3.1 and 1.7.4.1**), unresolved R-loop accumulation in S phase can impede DNA replication, resulting in transcription-replication conflicts (TRCs) and centromere instability (**figure 1.6Bb**) (Castellano-Pozo et al., 2013; Giunta et al., 2021; Hamperl et al., 2017; Racca et al., 2021). In fact, ssDNA at stalled replication forks and R-loops after head-on TRCs activate ATR-CHK1 signalling and is susceptible to cleavage (Hamperl et al., 2017).

CENP-A-enriched centromeric chromatin can suppress R-loop formation in late S phase to facilitate efficient DNA replication (Giunta et al., 2021). Furthermore, DRIP followed by qPCR showed R-loop-dependent BRCA1 occupancy at human centromeres to counteract R-loop accumulation through SETX activity and maintain CENP-A at centromeres (**figure 1.7Bb**) (Racca et al., 2021). Incomplete centromere replication upon increased TRCs can be resolved through mitotic DNA synthesis (MiDAS) (**section 1.5.3.1**) however this can contribute to further centromere fragility due to elevated recombination, loss of heterozygosity, and promote chromosome fusions (Giunta et al., 2021; Racca et al., 2021). BRCA1 depletion increased R-loop-dependent centromeric DNA breaks, as demonstrated by ɣH2AX ChIP data (Racca et al., 2021)

While unresolved centromeric R-loops hamper DNA replication, centromere transcripts have been positively linked to sister chromatid cohesion (Chen et al., 2021). Tethering transcriptional suppressor KOX1 to the centromere, decreased centromeric transcription and cohesion leading to mitotic progression defects. CENP-C itself was also found to suppress centromeric transcription (Bury et al., 2020; Chen et al., 2021). Therefore, centromere transcription is likely a highly regulated process required for centromere function but detrimental for centromere stability if dysregulated.

1.7.4.2.3 Centromere recombination

The presence of DNA breaks at centromeres and their highly repetitive nature makes them susceptible to recombination during S and G2 phase when HR repair is functional (**figure 1.7Ba**). CO-FISH (chromosome orientation fluorescence *in situ* hybridisation) is a methodology to differentially label the two sister chromatid centromeres and visualise sister chromatid exchanges (SCEs). On mitotic mouse centromeres, centromeres were found to be 175-fold more recombinogenic than the rest of the genome (Jaco et al., 2008). Mitotic centromere recombination was previously described in yeast (Liebman et al., 1988). Centromeres are recombination cold spots during eukaryotic meiosis (Jackson et al., 1996; Mahtani & Willard, 1998) due to the potential negative effect on meiotic chromosome

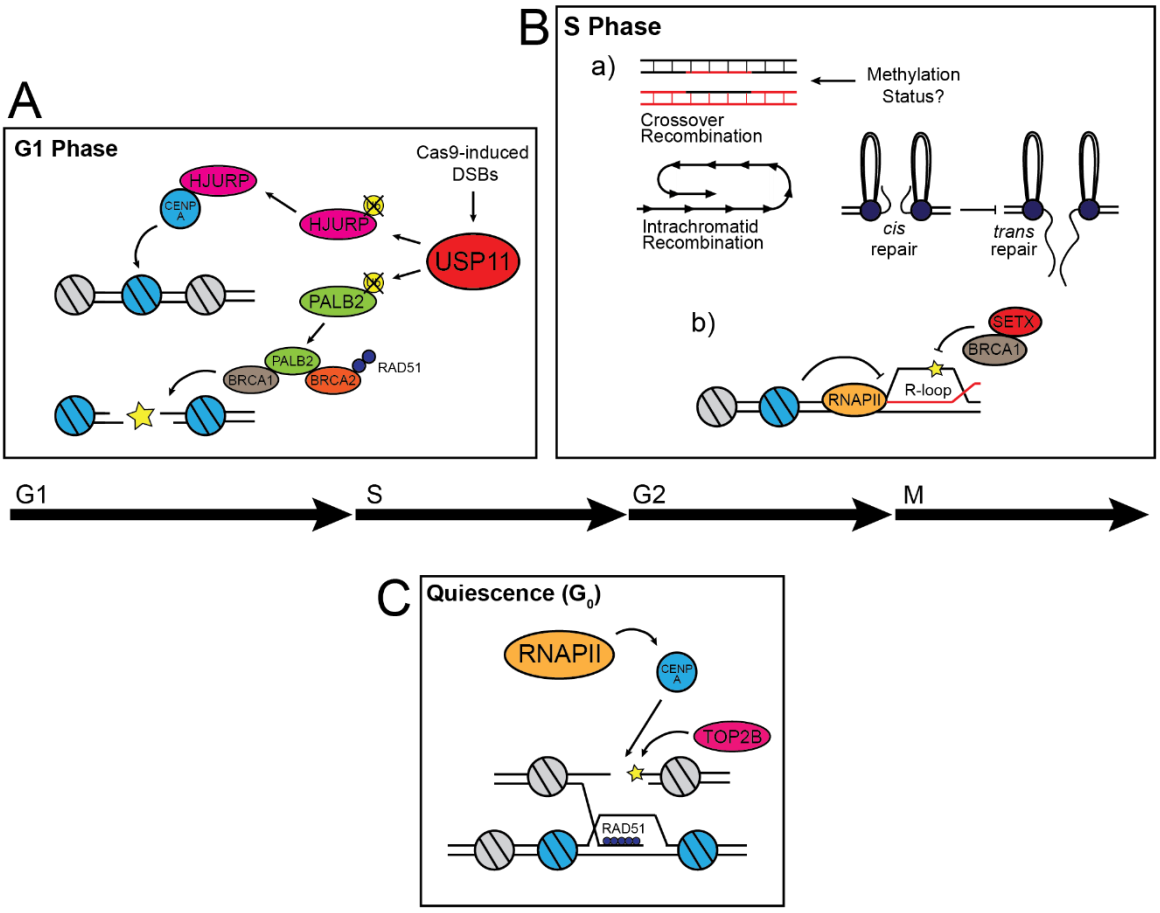


Figure 1.7 Repair of centromere breaks across the cell cycle.
A Cas9-induced DSBs in G1 phase activate deubiquitylase USP11 which deubiquitylates HJURP and PALB2 to promote CENP-A loading and DSB repair, respectively. **B a)** Crossover recombination and repetitive sequences can promote loss of heterozygousity and deletion of arrays. Centromere compaction acts to restrain the homology search after DSBs to limit aberrations. **b)** CENP-A can suppress R-loop formation at transcription-replication conflicts. BRCA1 and SETX function to resolve R-loops and limit DNA breaks. **C** Quiescent cells maintain their proliferative potential by promoting CENP-A deposition at TOP2B-induced DSBs, a process that requires RNAPII-mediated transcription and RAD51-dependent strand exchange activity.

segregation, breakage, and loss (Talbert & Henikoff, 2010; Vincenten et al., 2015). Despite this, there is increasing evidence for the repetitive nature of centromeres making them hot spots for recombination across the mitotic cell cycle, potentially disrupting centromere integrity (Barra & Fachinetti, 2018; Jaco et al., 2008; Onaka et al., 2016).

Centromere recombination occurs frequently in unperturbed cells. Uncontrolled somatic cell recombination is considered to detrimental to cells, for example promoting tumourigenesis. This could suggest that centromere recombination may serve a functional benefit such as

VDJ recombination in immune cell development. CENP-A is recruited to DSBs via its CATD, and this is increased upon active NHEJ (Zeitlin et al., 2009). HJURP itself was first identified to interact with MSH5 and NBS1 as part of the HR repair pathway, forming foci in response to DNA damage in S phase and binding HJs *in vitro* (Kato et al., 2007).

Furthermore, UV laser stripe experiments and I-SceI endonuclease-induced DSBs in human and mouse cells revealed rapid recruitment of CENP-A to sites of damage along with CCAN constituents CENP-N, CENP-T, and CENP-U (Zeitlin et al., 2009). The exact function of CENP-A recruitment at DNA lesions is still unclear but could indicate an important role for DNA breaks in centromere specification and CENP-A deposition, supported by the proposed role of RAD51-dependent recombination for CENP-A turnover in quiescent RPE1 cells (Saayman et al., 2023).

DNA breaks resulting from replication stress can promote SCEs and DNA rearrangements through erroneous repair pathways such as SSA, BIR, and alt-EJ (Gan et al., 2011; Giunta et al., 2021; Promonet et al., 2020; Sollier et al., 2014; Tuduri et al., 2009; Yilmaz et al., 2021). Excessive centromere recombination can be detrimental to centromere stability through loss of HORs and CENP-A binding sites (Jaco et al., 2008). Several cancer cell lines display reduced chromatin-bound CENP-A and ~15% increase in centromeric SCEs compared to non-cancerous RPE1 cells (Bellacosa et al., 2010; Giunta & Funabiki, 2017).

Consequently, recombination appears to be largely suppressed at centromeres. Dnmt3α and Dnmt3β methyltransferase depletion in mouse embryonic stem cells increased centromeric SCEs (Jaco et al., 2008). Conversely, active centromeres were recently identified as hypomethylated DNA regions (Altemose et al., 2023) hence this model cannot fully explain suppressed recombination at centromeres (**figure 1.7Ba**). ERCC6L2 was found to limit DSB resection and promote NHEJ, presumably through its chromatin compaction activity. Loss of ERCC6L2 reduced CENP-A, CENP-B, and CENP-C levels at the centromere which could potentially act to further drive compaction, limit resection and therefore recombination. Supporting this, ERCC6L2 knockout cells displayed increased SCEs by CO-

FISH indicative of centromere recombination and fusions (Carnie et al., 2023). Furthermore, CENP-A, CENP-C, CENP-T, and CENP-W were described to protect centromeres against extensive rearrangements in cycling and senescent human cells (Giunta et al., 2021; Giunta & Funabiki, 2017), however this was at least partially due to DSB suppression in budding yeast (Vincenten et al., 2015).

Centromeric SCEs are indicative of crossover resolution of recombination events. In somatic cells, recombination is primarily resolved through non-crossover mechanisms such as SDSA or dissolution of HJs (Scully et al., 2019) (**section 1.4.2**). Non-crossover recombination cannot be detected using CO-FISH, suggesting that recombination events remain largely undetected at centromeres (Zafar et al., 2017). Chromatin organisation regulates the homology search in HR in *S. cerevisiae* (Piazza et al., 2021). Centromeric DNA hairpin loops maintained by cohesin limit DNA resection during repair and subsequently limit the homology search to promote *in cis* recombination events (**figure 1.7Ba**) (Piazza et al., 2021). Moreover, the heterochromatic nature of centromere DNA restricts the mobility of break ends, thought to limit incorrect DSB repair (Rief & Löbrich, 2002). Centromere HR did not cause chromosomal translocations in G1, further indicating that centromere repeats are repaired *in cis* (Yilmaz et al., 2021). Furthermore, studies utilising a minichromosome containing centromere sequences in *S. pombe* found RAD51 and RAD54 are important to suppress GCRs, including translocations between homologous chromosomes and isochromosomes, by facilitating non-crossover recombination between repeats on the same chromatid, otherwise inhibiting crossover recombination repair pathways such as BIR, SSA, or alt-EJ, which occur with higher prevalence on chromosome arms (Nakamura et al., 2008; Onaka et al., 2016; Zafar et al., 2017). Therefore, non-crossover recombination events likely commonly occur at centromeres to maintain their integrity and limit loss of α-satellite HORs and GCRs resulting from aberration recombination events.

1.7.4.3 Mitosis

Chromosomes undergo extensive changes during mitosis including chromatin compaction. Centromeres remain transcriptionally active during this period and assemble the kinetochore machinery to attach microtubule spindles in early mitosis before chromosome segregation in anaphase. The dynamic nature of DNA during mitosis gives rise to several potential sources of instability.

1.7.4.3.1 Centromeric Ultrafine Anaphase Bridges

Superhelical tension generated during replication termination is resolved by TOP2A, producing dsDNA catenanes (Baxter, 2015). dsDNA catenanes play a role in centromere cohesion and are generally resolved before anaphase onset. Incomplete TOP2A decatenation leads to the maintenance of catenanes into anaphase and formation of centromeric ultrafine anaphase bridges (C-UFBs) (**figure 1.6Ca**). UFBs are uncondensed, dechromatinised topological DNA entanglements between sister chromatids that cannot be detected using typical DNA dyes including DAPI (Sarlos et al., 2017; Wang et al., 2010). C-UFBs arise commonly in unperturbed cells (Broderick & Niedzwiedz, 2015; Wang et al., 2008). C-UFBs are resolved through the action of dsDNA translocase PICH (Baumann et al., 2007), BLM (Chan et al., 2007), and TOP2A (Broderick et al., 2015). In short, PICH localises to stretched DNA in anaphase (Albers et al., 2018; Biebricher et al., 2013; Chan & West, 2018), recruiting BLM and TOP2A to remove distorted DNA structures. After TOP2A-mediated decatenation, the dsDNA forming C-UFBs can be fully disentangled, and chromatid separation and telophase can proceed.

Whether C-UFBs have a physiologically important role during mitosis remains debated. Due to their frequency, it has been suggested that C-UFBs may act to sense tension in anaphase to maintain centromere cohesion or function as part of the SAC (Bizard & Hickson, 2018; King et al., 2016), and that complete centromere decatenation only occurs after anaphase onset (Wang et al., 2008, 2010). Alternatively, their presence could reflect impaired TOP2A decatenation activity at centromeres (Bizard & Hickson, 2018). Nevertheless, timely C-UFB resolution and complete separation of nascent DNA strands prevents centromere instability and cell death

(Ramamoorthy et al., 2012). Indeed, unresolved UFBs increase 53BP1 nuclear bodies and PICH depletion can give rise to mitotic defects such as micronuclei and aneuploidy. In this way, UFB breaks can increase the risk of genome instability such as altered centromere length and translocations which can contribute to changes in gene expression and cancer (Albers et al., 2018; Black & Giunta, 2018; Lukas et al., 2011).

1.7.4.3.2 Transcription and kinetochore function

Active RNAPII-mediated transcription is essential at centromeres in mitosis to influence the kinetochore environment and promote timely and accurate chromosome segregation (**figure 1.6Cc**). Centromere transcripts and lncRNAs localised to centromeres stabilise CENP-C and the chromosome passenger complex (CPC) at the mitotic kinetochore, promoting Aurora B localisation. Inhibition of this process delays anaphase progression and produces lagging chromosomes (Blower, 2016; Chan et al., 2012). Furthermore, R-loop-dependent CPC recruitment to the mitotic centromere maintains centromere cohesion and is ultimately resolved through Aurora B kinase activity (Moran et al., 2021).

ATR activity is reduced on centromeric chromatin in S phase (Aze et al., 2016; Li et al., 2018) however it has a vital role in chromosome segregation in unperturbed mitosis (Kabeche et al., 2018). ssDNA resulting from mitotic centromeric R-loops is bound by RPA promoting recruitment and activation of ATR-ATRIP (Kabeche et al., 2018). ATR localisation is further compounded by Aurora A and CENP-F, before ATR phosphorylates CHK1 at S317, S345, and S296 in prometaphase to promote Aurora B kinase recruitment and activation for chromosome segregation.

Collectively, these papers highlight the importance of centromere transcription and R-loops in unperturbed mitosis by facilitating Aurora B activation, without which, mitotic defects would negatively impact genome stability. This appears to be distinct from the detrimental role of R-loops in S phase (**section 1.7.4.2.2**) and further emphasises that centromeric transcription is a tightly regulated process to maintain centromere and genome stability.

1.7.4.3.3 Centromere compaction and flexibility

Micronuclei containing centromeric DNA sequences resulting from mitotic spindle defects suggest that mechanical forces can result in centromere shearing in mitosis (Guerrero et al., 2010). (Peri)centromeric DNA loops have been proposed to be important for responding to tension generated by spindle pulling forces in mitosis to promote proper chromosome segregation (Lawrimore & Bloom, 2019). Chardon et al., utilised high resolution optical tweezers and atomic force microscopy to identify highly dynamic CENP-B-dependent DNA loops on centromeric chromatin (Chardon et al., 2022), approximately 350-500 bp in size, agreeing with previous electron microscopy observations (Aze et al., 2016). CENP-B-dependent loops facilitate centromere flexibility to withstand DNA tension from microtubule pulling forces in mitosis (**figure 1.6Cb**). In the absence of CENP-B and DNA loops, centromere fragility was increased and 53BP1 nuclear bodies, which mark broken DNA, were enriched in the following G1 (Chardon et al., 2022).

A similar principle was also demonstrated by (Addis Jones et al., 2019). Here, PLK1 functions to inhibit BLM-dependent centromeric DNA unwinding in mitosis to maintain DNA integrity upon chromosome segregation. Spindle pulling forces after PLK1 inactivation and BLM unwinding leads to severe centromere decompaction, rupture, and whole chromosome arm splitting (**figure 1.6Cb**) (Addis Jones et al., 2019). Therefore, non-B form DNA structures are vital for centromere integrity upon anaphase entry and chromosome segregation to prevent GCRs and fragmentation.

1.7.4.4 Quiescence

Quiescence is a state of reversible exit from the cell cycle where cells maintain their capacity to divide. There are many different types of quiescent cells in humans that maintain their proliferative potential, including somatic stem cells, lymphocytes, and oocytes (Marescal & Cheeseman, 2020). This is retained through the gradual turnover of CENP-A at centromeres via RNAPII-dependent destabilisation of pre-existing CENP-A nucleosomes and HJURP-mediated reloading (**figure 1.7C**) (Swartz et al., 2019).

Saayman et al., recently proposed a role for RAD51-mediated DNA repair at topoisomerase IIβ (TOP2B)-induced centromere breaks to facilitate CENP-A deposition in non-cycling RPE1 cells (**figure 1.7D**) (Saayman et al., 2023). This was found to require RAD51's strand exchange activity. CENP-A loading in quiescent cells was accelerated between 4 and 7 days after serum starvation in RPE1 cells (Swartz et al., 2019), which is in line with *de novo* centromeric DNA break induction (Saayman et al., 2023). Therefore, active DNA repair is likely important for CENP-A occupancy in quiescent RPE1 cells. RAD51 and RAD52 were previously shown to directly interact with CENP-A^{CaCse4} *in vivo* in *C. albicans* during DNA replication to load CENP-A onto ssDNA generated upon fork stalling at sites of pre-existing CENP-A (Mitra et al., 2014). It is currently unclear which factors direct CENP-A loading at sites of RAD51-mediated repair specifically, although transcription and centromere chromatin compaction have been proposed (Saayman et al., 2023).

Additionally, topoisomerase I (TOP1)-dependent processing of R-loops in non-cycling cells can drive SSB and DSB induction (Cristini et al., 2019). Removal of TOP1 cleavage complexes (TOP1cc) by TDP1 and R-loop cleavage by endonucleases such as XPF, XPG, and FEN1 can induce staggered SSBs, effectively forming DSBs (Cristini et al., 2019). Although, this was not shown at centromeres specifically, active centromere transcription during quiescence (Swartz et al., 2019) could promote accumulation of centromere breaks through a similar mechanism.

1.8 Research Aims

Centromeres experience instability throughout the cell cycle. However, we are only just beginning to gain insight into how centromere breaks are repaired and impact centromere function. Evidence suggests that RAD51-mediated HR and recombination play a prominent role at centromeres however the exact function and requirements for this pathway, in this context, remains unknown.

I aimed to investigate the function of canonical HR factors: RAD51, BRCA2, and PALB2, in chromosome and centromere stability. Firstly, in **chapter 3**, I discuss my work contributing

to (Wassing et al., 2021), investigating a mitotic role for RAD51 in MiDAS and at centromeres. Expanding on this and (Saayman et al., 2023), in **chapter 4**, I explored the role of other HR factors: BRCA2 and PALB2, in centromere identity and stability in non-cancerous RPE1 cells. Finally, in **chapter 5**, I extended this study to cancerous HCT116 cells to explore the role of BRCA2 and PALB2 in the context of tumourigenesis and centromere stability.

Chapter 2 - Materials and Methods

2.1 Tables of Materials

Table 2.1 Mammalian cell lines

Cell line	Source	Growth Conditions
U2OS Flp-In T-REx	Daniel Durocher	Dulbecco Modified Eagle Medium (DMEM) (Sigma-Aldrich), 10% v/v foetal bovine serum (FBS) (Sigma-Aldrich), 1% v/v penicillin-streptomycin (15140122, Life Technologies, equal to 100 U/mL penicillin and 100 µg/mL streptomycin), 100 µg/mL Zeocin (ant-zn-1, InvivoGen), 10 µg/mL Blasticidin (ant-bl-1, InvivoGen)
U2OS Flp-In T-REx FLAG-RAD51-WT	Isabel Wassing	DMEM, 10% v/v FBS, 1% v/v penicillin-streptomycin, 100 µg/mL Hygromycin B Gold (ant-hg-2, InvivoGen), 10 µg/mL Blasticidin
U2OS Flp-In T-REx FLAG-RAD51-K133R	Isabel Wassing	DMEM, 10% v/v FBS, 1% v/v penicillin-streptomycin, 100 µg/mL Hygromycin B Gold, 10 µg/mL Blasticidin
U2OS Flp-In T-REx FLAG-RAD51-T131P	Isabel Wassing	DMEM, 10% v/v FBS, 1% v/v penicillin-streptomycin, 100 µg/mL Hygromycin B Gold, 10 µg/mL Blasticidin
U2OS GFP-Lamin B1 mCherry-Histone H2B	Isabel Wassing	DMEM, 10% v/v FBS, 1% v/v penicillin-streptomycin
hTERT RPE1	ATCC	1:1 DMEM/F12 (31330-038, Gibco), 10% v/v FBS, 1% v/v penicillin-streptomycin, 0.123% sodium bicarbonate (S8761, Sigma-Aldrich)
HCT116	Robert Fisher	McCoy's 5A (Modified) medium (26600080, Life Technologies), 10% v/v FBS, 1% v/v penicillin-streptomycin
HCT116 CMV-OsTIR1		McCoy's 5A (Modified) medium, 10% v/v FBS, 1% v/v penicillin-streptomycin
HCT116 OsTIR1 PALB2-mAID-Halo	Christine Ralf	McCoy's 5A (Modified) medium, 10% v/v FBS, 1% v/v penicillin-streptomycin
HCT116 OsTIR1 mAID-Halo-BRCA2	Christine Ralf	McCoy's 5A (Modified) medium, 10% v/v FBS, 1% v/v penicillin-streptomycin

Table 2.2 DNA Plasmids

Plasmid/primer	Purpose	Source
pBSKS_PALB2_HR_mAID_Halo_NeoR	CRISPR template for repair containing homology ends against exon 27 and 3'UTR of PALB2 and tags	Christine Ralf
pMK341_NeoR_mAID_Halo_BRCA2	CRISPR template for repair containing homology ends against exon 1 and 5'UTR of BRCA2	Christine Ralf
pcDNA_FRT_TO_FLAG	Starting plasmid for generating Flp-In T-Rex cell lines expressing RAD51 separation-of-function variants	
pcDNA_FRT_TO_FLAG_RAD51 WT	Plasmid for generating Flp-In T-Rex cell lines expressing RAD51 separation-of-function variants	(Wassing et al., 2021)
pcDNA_FRT_TO_FLAG_RAD51 K133R	Plasmid for generating Flp-In T-Rex cell lines expressing RAD51 separation-of-function variants	(Wassing et al., 2021)
pcDNA_FRT_TO_FLAG_RAD51 T131P	Plasmid for generating Flp-In T-Rex cell lines expressing RAD51 separation-of-function variants	(Wassing et al., 2021)
pcDNA3_GFP-Lamin B1	Plasmid to generate cells for live cell imaging	David Vaux
pcDNA3_mCherry-Histone H2B	Plasmid to generate cells for live cell imaging	Addgene 20972
pOG44	Co-transfection into Flp-In T-Rex cell lines for integration of pcDNA_FRT_TO plasmids expressing RAD51 separation-of-function variants	V600520, Invitrogen
pX458_pSpCas9(-BB-)2A-GFP-BRCA2-gRNA	Cas9- and gRNA-expressing plasmid for generating HCT116 OsTIR1 mAID-Halo-BRCA2 cell lines by CRISPR	
pX459_pSpCas9_Puro_GFP_PALB2_gRNA	Cas9- and gRNA-expressing plasmid for generating HCT116 OsTIR1 PALB2-mAID-Halo cell lines by CRISPR	

Table 2.3 DNA oligonucleotides

Name	Sequence (5'-3')	Purpose
BRCA2_CHK_F	TCCCTGGGTCTCCATTTCCC	PCR screening of CRISPR-generated HCT116 OsTIR1 mAID-Halo-BRCA2 cell lines
BRCA2_CHK_R	GCTAGTCAAGGGGCCAGTTT	PCR screening of CRISPR-generated HCT116 OsTIR1 mAID-Halo-BRCA2 cell lines
BRCA2_CHK_R_HaloTag	CAGCCGATTGTCTGTTGTGC	PCR screening of CRISPR-generated HCT116 OsTIR1 mAID-Halo-BRCA2 cell lines
BRCA2_CHK_F_pMK341	AGCGTGACCGCTACACTTG	PCR screening of CRISPR-generated HCT116 OsTIR1 mAID-Halo-BRCA2 cell lines
PALB2_CHK_F	TGCTAAGAGCTGGGGTGAGA	PCR screening of CRISPR-generated HCT116 OsTIR1 PALB2-mAID-Halo cell lines
PALB2_CHK_R	TGCAGCACTGGCATGAAAGA	PCR screening of CRISPR-generated HCT116 OsTIR1 PALB2-mAID-Halo cell lines
PALB2_CHK_R_HaloTag	TACCGATCAGGTCTGGAGCA	PCR screening of CRISPR-generated HCT116 OsTIR1 PALB2-mAID-Halo cell lines
PALB2_CHK_F_pBS	AATTTCCATTCGCCATTCAGGC	PCR screening of CRISPR-generated HCT116 OsTIR1 PALB2-mAID-Halo cell lines

Table 2.4 Drugs

Drug	Concentration(s)	Catalogue Number
DMSO	-	D2650, Sigma-Aldrich
Indole-3-acetic acid (IAA)	5 μM, 500 μM	I5148, Sigma Aldrich
Olaparib (AZD2281)	0.25 - 3 μM	S1060, Selleck Chemicals
Mitomycin C (MMC)	2.5 - 100 nM	Ab120797, Abcam
RAD51 inhibitor (B02)	20 μM, 50 μM	533525, Calbiochem
Aphidicolin (APH)	0.4 μM, 2 mM	sc-201535, Santa Cruz Biotechnology
CDK1 inhibitor (RO3306)	9 μM	270-463-M005, Alexis Biochemicals
Thymidine (Thy)	2 mM	T1895, Sigma-Aldrich
RAD52 inhibitor (AICAR)	20 μM	A9978, Sigma-Aldrich
Neocarzinostatin (NCS)	50 nM	N9162, Sigma-Aldrich
MPS1 inhibitor (AZ3146)	2 μM	Sc-361114, Santa Cruz Biotechnology
Colcemid	0.1 μg/mL	234109, Calbiochem
Doxycycline hyclate (DOX)	1 μg/mL	D9891, Sigma-Aldrich

Table 2.5 siRNAs

Target	Final Concentration	Sequence (5'-3')	Supplier	Reference
CENPA	20 nM	GGACUCUCCAGAGCCAUGAUU	Dharmacon	(Giunta & Funabiki, 2017)
BRCA2 #1	20 nM	CAACAAUUACGAACCAAAC	Invitrogen	(Yata et al., 2012)
BRCA2 #2	20 nM	CUGAGCAAGCCUCAGUCAA	Invitrogen	(Yata et al., 2012)
PALB2 #1	20 nM	GGAAAGAGCCGGUUGUAAAdTdT	Sigma Aldrich	(Zhang et al., 2009b)
PALB2 #2	20 nM	GGAGAAAUUAGCAUUCUUGdTdT	Sigma Aldrich	(Zhang et al., 2009b)
RAD51 #1	20 nM	GACUGCCAGGAUAAAGCUU	Invitrogen	
RAD51 #2	20 nM	GUGCUGCAGCCUAAUGAGA	Invitrogen	

Table 2.6 Primary antibodies

IF = Immunofluorescence, WB = Western blot

Antibody	IF Dilution	WB Dilution	Flow cytometry Dilution	Species	Catalogue number	Source
p53		1:1000		Mouse	ab1101	Abcam
p21		1:1000		Rabbit	2947S	Cell Signaling Technology
ɣH2AX	1:1000			Mouse	05-636	Millipore
CENPA	1:500	1:500		Mouse	GTX13939	GeneTex
CENPB	1:1000	1:1000		Rabbit	IHC-00064	Bethyl Laboratories
BRCA2		1:1000		Mouse	OP95	Millipore
PALB2		1:1000		Rabbit	orb412704	Biorbyt
RAD51		1:5000		Rabbit	7946	Biogenes
RAD51	1:1000			Rabbit	ab176458	Abcam
Lamin A		1:10000		Rabbit	L1293	Sigma-Aldrich
pH3S10			1:100	Rabbit	06-570	Millipore
IgG				Mouse	02-6502	Invitrogen

Table 2.7 Secondary antibodies

IF = Immunofluorescence, WB = Western blot

Antibody	**IF Dilution**	**WB Dilution**	**Flow Cytometry Dilution**	**Catalogue number**	**Source**
Goat anti-Rabbit HRP		1:5000		PO448	Dako
Goat anti-Mouse HRP		1:5000		PO447	Dako
Alexa-Fluor Goat anti-Rabbit 488	1:500		1:100	A11070	Invitrogen
Alexa-Fluor Goat anti-Mouse 488	1:500			A11017	Invitrogen
Alexa-Fluor Goat anti-Rabbit 647	1:500			A27040	Invitrogen

Table 2.8 PNA probes

Target	Catalogue Number	Sequence (5'-3')	Source
CENPB-A488	F3004	ATTCGTTGGAAACGGGA	PNABio
CENPB-RC-Cy3	F3009	TCCCGTTTCCAACGAAT	PNABio
TelC-Cy5	F1003	CCCTAACCCTAACCCTAA	PNABio

2.2 Bacterial cell culture

2.2.1 Plasmid amplification

DH5α or TOP10 competent E. coli cells were thawed on ice and transformed by mixing ~100 ng plasmid with ~30 µL competent cells. The mixture was incubated on ice for 20 minutes before heat shock for 45 seconds at 42°C. The samples were briefly placed back on ice, and 250 µL super optimal broth (SOB) containing 20 mM glucose was added. Transformed cells were allowed to recover for 1 hour at 37°C with gentle agitation. Finally, cells were pelleted at 1200 x g for 3 minutes, and the pellet resuspended in ~100 µL SOB

containing 20 mM glucose. Cells were plated onto LB agar plates containing 100 µg/mL ampicillin and incubated at 37°C overnight.

Single colonies were subsequently inoculated in 3-50 mL LB broth cultures containing 100 µg/mL ampicillin and incubated at 37°C with constant agitation overnight. Plasmids were extracted from these overnight bacterial cultures using the GeneJET Plasmid miniprep kit (K0503, Thermo Fisher Scientific) or Qiagen Plasmid Plus midiprep kit (12943, Qiagen), according to manufacturer's instructions. DNA concentration was measured using a NanoPhotometer N60 (Implen).

2.2.2 Glycerol stocks

Bacterial glycerol stocks were formed by mixing 500 µL bacterial overnight cultures with 500 µL 50% glycerol, inverting to mix, and stored in cryovials at -80°C for long-term storage.

2.3 DNA analysis techniques

2.3.1 Genomic DNA extraction

Genomic DNA was extracted from mammalian cells using Phenol-Chloroform DNA extraction. Cells were harvested by trypsinisation, washed with PBS, counted, and lysed in cell lysis solution (10 mM Tris-Cl pH 8, 100 mM NaCl, 10 mM EDTA, 0.5% v/v SDS), adding 200 µL per $1x10^6$ cells. 20 µg/mL RNase A (R4875, Sigma-Aldrich) was added and samples incubated at room temperature (RT) for 15 minutes. Next, 1 mg/mL proteinase K (03115887001, Roche) was added and the suspension was incubated at 50°C for at least 1 hour. The samples were then cooled to RT and glycogen was added (1:100 dilution) and mixed thoroughly to improve visibility of the DNA pellet. Next, an equivalent volume of 25:24:1 Phenol:Chloroform:Isoamyl alcohol (P3803, Sigma-Aldrich) was added to the samples and vortexed at max speed (3200 rpm) (Vortex-Genie 2 (Model G560E), SI-0266), continuously for 2 minutes. Samples were centrifuged at 16100 x g for 2 minutes and the top aqueous layer was transferred to a new tube. An equivalent volume of chloroform (288306, Sigma-Aldrich) was added, and the samples vortexed and centrifuged again, as

before. The top aqueous layer was again transferred to a new tube and 2X volume of ice-cold 100% ethanol was added and mixed thoroughly before incubating at -20°C for at least 30 minutes. Finally, the samples were spun down at 16100 x g for 30 minutes at 4°C, the DNA pellets washed once with ice-cold 70% ethanol, and centrifuged again for 10 minutes at 16100 x g, 4°C. Any residual ethanol was removed and the pellets allowed to air dry before resuspension in elution buffer (10 mM Tris-Cl pH 8.5, Qiagen) or dH_2O. DNA concentration was determined using a NanoPhotometer N60 (Implen).

2.3.2 PCR

For cloning and cell line validation, PCR was conducted using HiFi polymerase (PB10.41-02, PCR Biosystems) according to manufacturer's recommendations. Per PCR reaction, ~100 ng plasmid DNA or genomic DNA was amplified with 1X PCRBIO reaction buffer, 400 nM forward and reverse primers, and 1 U PCRBIO HiFi polymerase, with the reaction volume topped up to 50 µL with dH_2O. The PCR was performed in a T100 Thermal Cycler (Bio-Rad) using the cycle conditions shown in **Table 2.9**.

Table 2.9 Standard PCR protocol

Cycles	Temperature	Time	Notes
1	95°C	1 minute	Initial denaturation
25-35	95°C	15 seconds	Denaturation
	55-65°C	15 seconds	Primer Annealing
	72°C	30 seconds per kb	Extension
-	4°C	Infinite hold	

2.3.3 Gel electrophoresis

PCR products and digested or purified plasmids were validated using agarose gel electrophoresis based on the presence and size of expected DNA products. Samples were mixed with 1X gel loading dye (B7025S, NEB) and resolved on a 1% agarose (16500-500, Invitrogen) gel containing 0.5 µg/mL ethidium bromide (E1510, Sigma-Aldrich) at 60 V in 1X TBE buffer for ~1 hour. 100 bp (N3231, NEB) and 1 kb (N3232, NEB) DNA ladders were

used to estimate the size of DNA products. DNA bands were visualised using a UV transilluminator (UVP).

2.4 DNA plasmid cloning

2.4.1 Insert preparation

PCR was performed to amplify the required DNA fragment from plasmid DNA using the appropriate set of primers. 5 µL PCR product was run on an agarose gel (as in **section 2.3.3**) to confirm successful amplification of the correct DNA fragment. The remaining PCR product was purified using the QIAquick PCR purification kit (28104, Qiagen), according to manufacturer's instructions, ready for subsequent digestion (**section 2.4.2**) and ligation (**section 2.4.4**).

2.4.2 Restriction enzyme digestion

Digestion of DNA fragments and DNA plasmids with DNA restriction enzymes was performed according to manufacturer's instructions (NEB). In short, 1 µg DNA was mixed with 1X reaction buffer and 20 U restriction enzyme to a final volume of 50 µL. Typically, digestions were performed at 37°C for 1 hour, unless otherwise specified.

2.4.3 Vector preparation

DNA plasmids were digested as above (**section 2.4.2**) before being supplemented with 4 U Calf Intestinal Alkaline Phosphatase (CIP) (M0290, NEB) for 30 minutes at 37°C, to prevent vector re-ligation, where appropriate. The digested vector was run on an agarose gel (**section 2.3.3**) and purified using gel extraction using a QIAquick Gel Extraction kit (28704, Qiagen) according to manufacturer's instructions.

2.4.4 Ligation

Ligations were performed with 1:3 vector:insert molar ratio using a Takara DNA Ligation Kit (6023, Takara Bio) according to manufacturer's instructions. Ligation products were subsequently used for plasmid amplification (**section 2.2.1**).

2.4.5 Site-directed mutagenesis

Site-directed mutagenesis was used to generate RAD51 separation-of-function mutants from pcDNA_FRT_TO_FLAG_RAD51 WT (**Table 2.2**) by Isabel Wassing (Wassing et al., 2021). The QuickChange II Site-Directed Mutagenesis kit (Agilent Technologies) was used to do this, as per manufacturer's instructions. A 50 µL PCR was prepared containing 400 ng each of the relevant forward and reverse primers, 100 ng plasmid DNA template, 0.5 mM dNTPs, and 3.75 U PfuTurbo DNA polymerase in 1X PfuTurbo reaction buffer with $MgSO_4$. The PCR was performed in a T100 Thermal Cycler (Bio-Rad) using the cycle conditions shown in **Table 2.10**.

Table 2.10 Site-directed mutagenesis PCR protocol

Cycles	Temperature	Time	Notes
1	95°C	3 minutes	Initial denaturation
35x	95°C	30 seconds	Denaturation
	60-65°C	1 minute	Primer Annealing
	68°C	1 minute per 0.5kb	Extension
-	4°C	Infinite hold	

After PCR amplification, 20 U DpnI restriction enzyme was added to the reaction mixture and incubated for 2 hours at 37°C to digest parental plasmid DNA. The sample was subsequently transformed into TOP10 competent cells, plated onto LB-agar plates, and DNA purified as in section 2.2.1.

2.4.6 Gibson assembly

Gibson assembly was used to generate pBSKS_PALB2_HR_mAID_Halo_NeoR and pMK341_NeoR_mAID_Halo_BRCA2 (**Table 2.2**) by Christine Ralf. The NEBuilder HiFi DNA Assembly Cloning kit (E5520, NEB) was used according to manufacturer's instructions. In short, the vector was mixed with the insert at a 1:2 molar ratio. Next, 10 µL Gibson Assembly Master Mix was added to the vector:insert mixture with dH_2O, to give a final volume of 20 µL. The reaction mix was subsequently incubated at 50°C for 1 hour

before transformation into NEB 5α competent E. coli cells (C2987, NEB) as described previously (section 2.2.1).

2.4.7 Sanger sequencing

All DNA concentrations were measured using a NanoPhotometer N60 (Implen). If required, the DNA was validated using Sanger sequencing by Source BioScience UK Ltd using their recommended sample requirements.

2.5 Mammalian cell culture

2.5.1 General cell culture

All cell lines were cultured in a humidified environment at 37°C supplemented with 5% CO_2 in the corresponding cell culture media, as described in **Table 2.1**. Cells were passaged every 2-3 days, when approximately 80% confluent, by trypsinisation. For cell line storage, cells were resuspended in FBS containing 10% v/v DMSO and frozen at -80°C in a Mr Frosty Freezing container (Nalgene). For long term storage, cryovials were stored in liquid nitrogen. All centrifugation steps involving live cells were performed at a maximum of 500 x g.

2.5.2 Drug treatments

All drugs were used at the indicated concentrations (**Table 2.4**) and time periods as specified in the text.

2.5.3 siRNA transfection

siRNA transfections were performed using Lipofectamine RNAiMAX (13778150, Thermo Scientific) according to manufacturer's instructions, using a final concentration of 20 nM siRNA. siRNA sequences are listed in **Table 2.5** and MISSION siRNA was used as a universal negative control (SIC001, Sigma-Aldrich). The lipid-siRNA suspension was added dropwise to cells cultured in antibiotic-free media. The transfected cells were incubated for 24 hours before the media was changed to fresh complete media and further incubated for the indicated time period.

2.5.4 Generation of U2OS Flp-In T-REx RAD51 separation-of-function variant cell lines

These cell lines were generated by Isabel Wassing (**Table 2.1**) (Wassing et al., 2021). Stable U2OS Flp-In T-REx cell lines (a kind gift from Daniel Durocher) were seeded into a 6-well plate so that they were approximately 80% confluent at the time of transfection. Cells were transfected with 0.5 µg pcDNA5_FRT_TO plasmid expressing FLAG or RAD51 separation-of-function variants and 1.5 µg pOG44 (**Table 2.2**) using 4 µL jetPRIME transfection reagent and 200 µL jetPRIME buffer (101000027, Polyplus) according to manufacturer's instructions. 24 hours post transfection, the transfection media was replaced with fresh complete media. After a further 24 hours, cells were selected using 200 µg/mL hygromycin and 10 µg/mL blasticidin for 48 hours. After selection, cells were maintained in complete media plus 100 µg/mL hygromycin and 10 µg/mL blasticidin. 1 µg/mL DOX was used to induce RAD51 separation-of-function expression and the cell lines were validated by western blot (**section 2.7.1**).

2.5.5 Generation of CRISPR-tagged HCT116 OsTIR1 PALB2-mAID-Halo and mAID-Halo-BRCA2 cell lines

These cell lines were generated by Christine Ralf (**Table 2.1**). Cells were transfected using Lipofectamine LTX (A12621, Thermo Scientific) according to manufacturer's instructions. 10 µL Lipofectamine LTX and 1677 ng repair template (pMK341_NeoR_mAID_Halo_BRCA2 or pBSKS_PALB2_HR_mAID_Halo_NeoR), and 3333 ng Cas9-gRNA (pX458_pSpCas9(-BB-)2A-GFP-BRCA2-gRNA or pX459_pSpCas9_Puro_GFP_PALB2_gRNA) and 2.5 µL Plus reagent were mixed and incubated for 15 minutes at RT. The lipofectamine-DNA mixture was added to cells cultured in antibiotic-free media. 24 hours post transfection, the transfection media was replaced with fresh complete media. Cells were then maintained in culture under selection with 700 µg/mL G418 (G8168, Sigma-Aldrich) for approximately 1 week.

To generate monoclonal cell lines, single cells were plated into 96-well plates using Fluorescence-activated cell sorting (FACS) (BD FACS Aria III) and were allowed to grow for 2-4 weeks after which growing clones were expanded and screened for successful tagging by western blot (**section 2.7.1**) and PCR (**section 2.3.2, Table 2.3**).

2.5.6 Generation of stable U2OS cell lines expressing GFP-Lamin B1 and mCherry-Histone H2B

These cell lines were generated by Isabel Wassing (**Table 2.1**) (Wassing et al., 2021). Cells were transfected at approximately 80% confluency with 3 µg pcDNA3.1_GFP-Lamin B1 and 3 µg pcDNA3.1_mCherry-Histone H2B (**Table 2.2**) using 9 µL Lipofectamine LTX reagent with 3 µL Plus reagent, according to manufacturer's instructions. Successfully transfected cells were selected using 500 µg/mL G418 for approximately 1 week. GFP- and mCherry-expressing cells were sorted using FACS as in **section 2.5.5** and monoclonal cell lines were maintained in 400 µg/mL G418 and screened by microscopy.

2.5.7 Cell synchronisation

2.5.7.1 Enriching mitotic cells to observe mitotic DNA synthesis (MiDAS)

Cells were synchronised at the G1/S phase boundary using a double thymidine block. 2 mM thymidine (T1895, Sigma-Aldrich) was added to the cells for 18 hours, before washing thoroughly with pre-warmed PBS and released into pre-warmed fresh media for 9 hours. A second thymidine block was applied for an additional 18 hours and subsequently released as before. After 1 hour release into S phase, 0.4 µM Aphidicolin (APH) (sc-201535, Santa Cruz Biotechnology) was added to the cells to induce replication stress. After 18 hours, 9 µM RO3306 (270-463-M005, Alexis Biochemicals) was added to induce G2 phase arrest. At this point, 1 µg/mL doxycycline (DOX) (D9891, Sigma-Aldrich) was added to the relevant samples and time points. After 5 hours, cells were released into fresh media, with or without DOX, to facilitate mitotic entry. 5-ethynyl-2'-deoxyuridine (EdU) (Life Technologies) was also added at this stage to label sites of mitotic DNA synthesis. After 30 minutes, mitotic cells were collected by mitotic shake-off and processed as required.

2.5.7.2 Enriching mitotic cells to generate metaphase spreads

To enrich for mitotic cells, cells were treated with 0.1 µg/mL colcemid (234109, Calbiochem) for the indicated time (3-5 hours). Mitotic cells were observed under the microscope and harvested through mitotic shake-off.

2.5.7.3 Serum-starvation

To induce quiescence, cells were cultured in serum-starved media containing 0.5% FBS instead of the usual 10%. After 24 hours incubation in serum-starved media, cell proliferation is essentially halted. Culture was maintained in the serum-starved media, refreshed every 24 hours, until the indicated time.

Quiescence after serum-starvation was confirmed through EdU incorporation. 10 µM EdU was added to the cells for the indicated time and analysed by flow cytometry.

2.6 Microscopy techniques

2.6.1 Immunofluorescence (IF)

12 mm glass coverslips were treated with poly-L-lysine for 5 minutes before air-drying for at least 15 minutes. Cells were harvested under the relevant conditions, washed with PBS, and counted. ~1x10^5 cells were seeded onto each coverslip and allowed to attach at 4°C for 10-15 minutes. Next, cells were fixed using PTEMF buffer (20 mM PIPES pH 6.5 (P1851, Sigma-Aldrich), 10 mM EGTA, 0.2% v/v Triton X-100 (93443, Sigma-Aldrich), 1 mM MgCl2, 4% v/v paraformaldehyde (28908, Thermo Scientific)) for 20 minutes and then washed three times with PBS. Fixed samples were stored in PBS at 4°C for up to 2 weeks. Cells were incubated with blocking buffer (3% w/v BSA (A7906, Sigma-Aldrich), 0.5% v/v Triton X-100) for at least 30 minutes at RT before incubation with the relevant primary antibodies (**Table 2.6**), diluted in blocking buffer, for 1 hour at RT. Coverslips were washed 3 times with PBS-TX (0.5% v/v Triton X-100, PBS) for 5 minutes and then incubated with the relevant secondary antibodies (**table 2.7**), diluted in blocking buffer, for 1 hour at RT, before washing as before. Cells were stained with 0.1 µg/mL DAPI (564907, BD Biosciences) in PBS for 10

minutes, washed twice with PBS, and once with dH_2O. Coverslips were left to air-dry completely, cell-side up on blotting paper, before mounting using Mowiol mounting media (10% w/v Mowiol 4-88 (475904, Millipore), 25% w/v glycerol, 0.1 M Tris pH 8.5).

Samples were imaged using Olympus FluoView FV1200 using FV10-ASW software (version 4.2). Cells to be imaged and analysed were selected in an unbiased manner based on DAPI staining. Image processing and quantification are described below.

2.6.2 Click-IT reaction for EdU labelling

For immunofluorescence containing EdU staining, samples were incubated with 10 μM EdU for 30 minutes before harvest. Cells were subsequently prepared and fixed as above (**section 2.6.1**). After blocking, cells were incubated with Click-IT reaction buffer (PBS pH 7.2, 2 mM $CuSO_4$ (209198, Sigma-Aldrich), 10 mM sodium L-ascorbate (A4034, Sigma-Aldrich), Alexa Fluor Azide 555 (A20012, Life Technologies)) for 1 hour, RT. Coverslips were next washed thrice with PBS before proceeding with antibody staining as before (**section 2.6.1**).

2.6.3 Exo-FISH

Interphase cells were collected by trypsinisation at the required time points. Cells were washed with PBS, counted, and $1.2x10^5$ cells ($2x10^4$/slide) were collected per 15 mL falcon tube. Cells were gently resuspended in 0.56% KCl (~$2x10^4$ cells/mL) and incubated at RT for 20 minutes on a tilt table. Cells were centrifuged at 300 x g for 3 minutes and all but 100 μL supernatant was removed. The cell pellet was resuspended in this remaining liquid by carefully tapping against the tube. The cells were subsequently fixed in 3:1 Methanol:Acetic acid (~$2x10^4$ cells/mL) for 15 minutes at RT, adding the first 1 mL dropwise with constant gentle cell agitation to minimise cell aggregation. Cells were centrifuged again, as before, and all but 60 μL (~10 μL/slide) supernatant was removed. Fixed cells were spread onto glass slides by dropping 10 μL cell suspension onto a 20 μL water droplet. Cell density can influence FISH signal intensity so cell number per slide was kept consistent across samples

and experiments. Cell spreads were allowed to dry overnight at room temperature in the dark. Homogeneous cell spreading was confirmed via light microscopy.

The next day, slides were rehydrated in PBS for 5 minutes at RT in Coplin jars and treated with 0.5 mg/mL RNase A (R6513, Sigma-Aldrich) for 10 minutes at 37°C in a humidified chamber, before rinsing briefly with PBS. Slides were then treated with or without 100 µg/mL pepsin (10264440, Fisher Scientific) in 0.01 M HCl for 10 minutes, 37°C. Samples were then washed three times with PBS for 5 minutes. Next, slides were incubated with 0-200 mU/µl Exonuclease III (M1811, Promega) in 1X Exonuclease III buffer (50 mM Tris-Cl, 5 mM $MgCl_2$, 5 mM DTT pH 8) for 30 minutes at 37°C in a humidified chamber. Slides were washed with PBS and serially dehydrated in 70%, 95%, and 100% Ethanol, for 5 minutes each before air-drying.

Exo-FISH was validated using restriction enzyme, Nt.BsmAI, to induce SSBs *in vitro*. Cells were treated with 25 mU/µL (5 U total) Nt.BsmAI (R0121S, NEB) in 1X CutSmart buffer (NEB) for 1 hour at 37°C in a humidified chamber, before Exonuclease III treatment. Negative control samples were treated with 1X CutSmart buffer alone.

Slides were hybridised with 200 nM CENPB-RC-Cy3 (F3009, PNABio) and 200 nM TelC-Cy5 (F1003, PNABio) for 1.5 hours at RT, in a dark, humidified chamber. Before treatment, the FISH probes were diluted in hybridisation buffer (10 mM Tris-Cl pH 7.5, 70% formamide (47671, Sigma-Aldrich), 0.5% blocking solution (10% w/v blocking reagent (11096176001, Roche) dissolved in maleic acid buffer (100 mM maleic acid, 150 mM NaCl, pH 7.5))) and heated at 60°C for 5 minutes before use. FISH probe sequences are listed in **table 2.8**. Slides were washed for 15 minutes in hybridisation wash buffer #1 (10 mM Tris-Cl pH 7.5, 70% formamide, 0.1% BSA) and three times with hybridisation wash buffer #2 (0.1 M Tris-Cl pH 7.5, 0.15 M NaCl, 0.08% Tween-20 (P1379, Sigma-Aldrich)) for 5 minutes. To the second wash, 0.2 µg/mL DAPI was added, and the wash time increased to 10 minutes. Finally, the slides were dehydrated and dried as before and mounted with glass coverslips using Mowiol mounting medium. Samples were imaged using an Olympus FluoView

Spectral FV1200 Laser Scanning microscope using FV10-ASW software (version 4.2). Cells to be imaged and analysed were selected in an unbiased manner based on DAPI staining. Image processing and quantification are described below.

2.6.4 Chromosome-Orientation Fluorescence *In Situ* Hybridisation (CO-FISH)

Cells were synchronised as in section **2.5.7.1** with some variations. Cells were released into S phase, after double thymidine block, in the presence of 7.5 μM BrdU and 2.5 μM BrdC to label one strand of the duplex DNA. 0.4 μM APH was added to the relevant samples after 1 hour and incubated for 18 hours. Next, cells were arrested in G2 with 9 μM RO3306 for at least 5 hours. Cells were released into fresh media containing 0.1 μg/mL colcemid, 7.5 μM BrdU, and 2.5 μM BrdC for 30 minutes. Mitotic cells were collected by mitotic shake-off and metaphase spreads were generated as in **section 2.6.3**.

For CO-FISH staining, slides were rehydrated in PBS for 5 minutes at RT in Coplin jars and treated with 0.5 mg/mL RNase A for 10 minutes at 37°C in a humidified chamber. Next, slides were stained with 0.5 μg/mL Hoechst 33258 (861405, Sigma-Aldrich) in 2X saline-sodium citrate (SSC) buffer (300 mM NaCl, 30 mM sodium citrate) for 15 minutes, RT. The slides were then exposed to 312 nm UV light for $5.4x10^3$ J/m^2 (Hoefer UVC 500UV Crosslinker). The BrdU/BrdC labelled DNA strand was subsequently digested using 10 U/μL Exonuclease III (M1811, Promega) diluted in 1X Exonuclease III buffer (50 mM Tris-Cl, 5 mM $MgCl_2$, 5 mM DTT pH 8) for 30 minutes at 37°C. The slides were then washed in PBS for 5 minutes and dehydrated in a series of ethanol dilutions: 70%, 95%, and 100%, for 5 minutes each, before air drying at RT in the dark.

Slides were pre-hybridised for 30 minutes with hybridisation buffer (10 mM Tris-Cl pH 7.5, 70% formamide (47671, Sigma-Aldrich), 0.5% blocking solution (10% w/v blocking reagent (11096176001, Roche) dissolved in maleic acid buffer (100 mM maleic acid, 150 mM NaCl, pH 7.5))). Next, slides were hybridised with 500 nM CENPB-A488 (F3004, PNABio), diluted in hybridisation buffer, for 1.5 hours at RT, in a dark, humidified chamber. The slides were rinsed briefly in hybridisation wash buffer #1 (10 mM Tris-Cl pH 7.5, 70% formamide, 0.1%

BSA) before incubating with 500 nM CENPB-RC-Cy3 (F3009, PNABio) for a further 1.5 hours. Probe sequences are listed in **table 2.8** and both FISH probes were heated at 60°C for 5 minutes before use. The slides were washed in hybridisation wash buffer #1 for 15 minutes and thrice with hybridisation wash buffer #2 (0.1 M Tris-Cl pH 7.5, 0.15 M NaCl, 0.08% Tween-20 (P1379, Sigma-Aldrich)) for 5 minutes. To the second wash, 1 µg/mL DAPI was added. Finally, the slides were dehydrated and dried as before and mounted with glass coverslips using ProLong Gold antifade reagent with DAPI (P36935, Invitrogen).

Samples were imaged using an Olympus FluoView Spectral FV1000 laser scanning microscope with Becker and Hickel FLIM system using FV10-ASW software (version 4.2). Metaphase spreads to be imaged and analysed were selected in an unbiased manner based on DAPI staining.

2.6.5 Chromosome 17 FISH staining

Cells were enriched in mitosis through the addition of 0.1 µg/mL colcemid for 3-5 hours (see **section 2.5.7.2**). Mitotic cells were collected through mitotic shake-off and metaphase spreads were prepared as above (**section 2.6.3**).

For FISH staining against Chromosome 17, metaphase spreads were rehydrated in PBS for 5 minutes before dehydrating again in increasing ethanol concentrations (70%, 95%, 100%) for 5 minutes each. Once air-dry, Iso(17q) FISH probe (D-5048-100-OG, Metasystems) was applied to the spreads and topped with a glass slide. The slide was then denatured at 75°C for 3 minutes and incubated in a humidified dark box at 37°C overnight. Samples were washed in preheated 0.4X SSC pH 7 (60 mM NaCl, 6 mM sodium citrate) at 72°C for 3 minutes before washing in 2X SSC (300 mM NaCl, 30 mM sodium citrate) with 0.05% v/v Tween-20 pH 7 at RT for 1 minute. The slides were rinsed with dH2O, incubated with 0.2 µg/mL DAPI for 10 minutes, washed three more times in dH2O, and dehydrated in sequential ethanol concentrations as before. Slides were left to air dry for at least 30 minutes before mounting with Mowiol mounting medium.

Samples were imaged using Olympus FluoView FV1200 using FV10-ASW software (version 4.2). Frequency of aberrations on labelled Chromosome 17 were scored as a percentage of total chromosomes/spread.

2.6.6 Live Cell Imaging

Live cell imaging experiments were conducted by Isabel Wassing (Wassing et al., 2021). U2OS cell lines expressing GFP-Lamin B1 and mCherry-H2B were synchronised as in **section 2.5.7.1** except 9 μM RO3306 was added to the cells for 12 hours. Cells were released from RO3306 arrest and immediately imaged using a Zeiss 880 inverted confocal microscope with Zen Black software (version 14.0.22.201). Images were captured every 5 minutes for at least 6 hours. Cells that failed to display nuclear envelope breakdown within 4 hours of mitotic release were excluded from analysis. Mitotic duration was measured using ImageJ.

2.7 Molecular biology techniques

2.7.1 Western blotting (WB)

After the required treatments, cells were harvested by trypsinisation and washed with PBS. Cell pellet weight was measured and pellets resuspended in NETN150 buffer (50 mM Tris-HCl pH 8, 150 mM NaCl, 2 mM EDTA pH 8, 0.5% v/v NP-40 (492018, Millipore), 2.5 mM $MgCl_2$, 1X Protease Inhibitor Cocktail (P2714, Sigma-Aldrich), 10 mM benzamidine hydrochloride hydrate (B6506, Sigma-Aldrich), 20 mM NaF, 1 mM Na_3VO_4 (S6508, Sigma-Aldrich), 20 mM sodium β-glycerophosphate) plus 125 U/mL benzonase (71206-25KUN, Millipore) so that 50 μL lysis buffer was added per 10 mg cells.

The pellets were digested on ice for at least 30 minutes before centrifugation at 16100 x g for at least 15 minutes at 4°C and the supernatant collected as whole cell extract (WCE). Protein concentration was measured using a Bradford assay (#5000006, Bio-Rad), according to manufacturer's instructions. WCEs were diluted to 1 mg/mL and 1X NuPAGE LDS sample buffer (NP0007, Invitrogen) with 200 mM DTT (D0632, Sigma-Aldrich) was

added. Samples were denatured at 85°C for 3 minutes, briefly centrifuged, and ~15 µg protein was loaded on a NuPAGE 4-12% Bis-Tris protein gel (NP0322BOX, Fisher Scientific) with 2.5 µL protein ladder (S6-0024, Geneflow). The SDS-PAGE was run at 150 V for 1-1.5 hours in 1X MOPS running buffer (50 mM MOPS (RDD003, Sigma-Aldrich), 50 mM Tris, 3.5 mM SDS, 1 mM EDTA).

Proteins were then transferred onto a 0.45 µm nitrocellulose membrane using wet transfer as per the manufacturer's instructions. Transfer was performed at 100 V for 1 hour in 1X transfer buffer (100 mM Tris, 767 mM glycine, 10% v/v methanol). Successful protein transfer was confirmed using Ponceau (0.1% w/v Ponceau S in 5% acetic acid) before blocking with 5% w/v skimmed milk in PBST (PBS+0.05% v/v Tween-20) for at least 30 minutes. Membranes were incubated with primary antibodies (**table 2.6**) in blocking buffer at 4°C overnight. The next day, the membranes were washed three times for 5 minutes in PBST and subsequently incubated with secondary antibodies (**table 2.7**) at RT for at least 1 hour. The membranes were washed again as before and incubated with 1:1 ECL Western Blotting detection solution (RPN2106, Amersham) for 30 seconds and developed using chemiluminescence film (28906837, Cytiva) in a Xograph developer as necessary.

2.7.2 Immunoprecipitation (IP)

IgG (02-6502, Invitrogen) or BRCA2 antibodies (OP95, Calbiochem) were conjugated to Affi-Prep Protein A agarose beads (1560006, Bio-Rad) using the following protocol. The beads were washed twice with PBS before incubating with the relevant antibody (2 µL antibody per 5 µL beads) on a rotor wheel at RT for 3 hours. Antibody-crosslinked beads were pelleted (800 x g, 4 minutes) and washed twice in coupling buffer (27 mM sodium tetraborate (221732, Sigma-Aldrich), 73 mM boric acid (B7660, Sigma-Aldrich)), once in DIM-PIM buffer (56 mM dimethyl pimelimidate dihydrochloride (D8388, Sigma-Aldrich), 0.1 M sodium tetraborate), and then incubated in DIM-PIM buffer overnight, 4°C. Beads were subsequently washed thrice in coupling buffer and once in 1 M Tris pH 9. Further 1 M Tris pH 9 was added for 10 minutes, RT. Finally, the beads were washed thrice in storage buffer

(6.5 mM sodium tetraborate, 93.5 mM boric acid) and kept at 4°C until required. Before incubation with protein lysate, antibody-crosslinked beads were prewashed three times with wash buffer (50 mM Tris-HCl pH 8, 150 mM NaCl, 2 mM EDTA, 5 mM $MgCl_2$).

For IP, cells were trypsinised, washed with PBS, and lysed in NETN150 buffer (50 mM Tris-HCl pH 8, 150 mM NaCl, 2 mM EDTA pH 8, 0.5% v/v NP-40 (492018, Millipore), 2.5 mM $MgCl_2$, 1X Protease Inhibitor Cocktail (P2714, Sigma-Aldrich), 10 mM benzamidine hydrochloride hydrate (B6506, Sigma-Aldrich), 20 mM NaF, 1 mM Na_3VO_4 (S6508, Sigma-Aldrich), 20 mM sodium β-glycerophosphate (35675, Calbiochem)) with 125 U/mL benzonase (71206-25KUN, Millipore) on ice for 1 hour. Lysed cells were centrifuged (16100 x g, 20 minutes, 4°C) and supernatant collected as whole cell extract (WCE). Protein concentration was determined using a Bradford Protein assay (#5000006Bio-Rad) according to manufacturer's instructions. After protein input sample was taken (~10 µL) and stored at -20°C, WCEs were diluted to 1 mg/mL and incubated with 10 µL antibody-crosslinked beads on a rotor wheel, overnight, 4C.

Protein-bound beads were pelleted and washed 4 times with wash buffer. Beads and input samples were resuspended in 1X NuPAGE LDS sample buffer (NP0007, Invitrogen) with 200 mM DTT (D0632, Sigma-Aldrich). Input samples were denatured at 85°C for 5 minutes and the beads for 10 minutes before western blotting as described previously (**section 2.8**).

2.7.3 Pulsed-Field Gel Electrophoresis (PFGE)

Mitotic cells were collected by mitotic shake-off after the relevant drug treatments and time periods. Cells were washed with PBS and counted and $2.5x10^5$ cells were collected per agarose DNA plug. DNA plugs were made according to manufacturer's instructions (1703591, Bio-Rad). In short, 2% CleanCut agarose (1703594, Bio-Rad) was melted and equilibrated to 50°C. Cell pellets were then resuspended in 0.63 mL Cell Suspension Buffer per mL of agarose plug and equilibrated to 50°C for ~20 minutes. 0.37 mL of 2% CleanCut agarose per mL of agarose plug was then mixed thoroughly but gently into the cell suspension and 100 µL cell mixture added to each plug mould. Plugs were allowed to

solidify on ice for ~15 minutes. Next, DNA plugs were digested with 1 mg/mL proteinase K in proteinase K reaction buffer (100 mM EDTA pH 8, 1% N-Lauroyl Sarcosine, 0.2% Na-Deoxycholate) overnight at 50°C. Finally, DNA plugs were then washed four times for 1 hour in 1X Wash buffer (20 mM Tris pH 8, 50 mM EDTA) with 1 mM PMSF (11359061001, Roche) added to the third wash to inactivate residual proteinase K. The plugs were stored at 4°C for up to 3 months.

A 0.9% agarose gel was made from Pulsed Field Certified agarose (1620137, Bio-Rad) in 0.5X TBE buffer. The agarose was allowed to set at RT for ~2 hours before being transferred to 4°C overnight. Once set, the plugs were cut in half and loaded into the gel, avoiding air bubbles. The gel was then sealed using 2% CleanCut agarose. 1/5th DNA Lambda ladder plug was used as a DNA size control (1703635, Bio-Rad). The gel and 0.5X TBE running buffer were equilibrated to 14°C before completing electrophoresis using the CHEF Mapper XA system (Bio-Rad) for 15 hours to separate 1-100 kb size DNA bands according to the following settings: two state, 120° included angle (2x60°), 200V (6V/cm), an initial switch time of 0.05 seconds to a final switch time of 10 seconds, and a linear ramping factor. Afterwards, the gel was washed with dH_2O for 10 minutes at RT and stained with 3 µg/mL Ethidium Bromide in 0.5X TBE for 30 minutes. The gel was subsequently washed twice with dH_2O for 30 minutes and DNA bands visualised using a UV transilluminator (UVP). Band intensity was measured in ImageJ and normalised to untreated controls.

2.7.4 Flow cytometry

Cells were harvested by trypsinisation, washed with PBS, and counted. Equal cell numbers were collected (0.5-1x10^6 cells) and fixed in 70% ethanol, overnight, 4°C, on a rotor wheel. All subsequent steps were performed on ice and centrifugation steps performed at 1000 x g for 5 minutes at 4°C. Fixed cells were permeabilised in PBS-TriBSA (0.1% v/v Triton X-100, 1% w/v BSA, PBS) for 15 minutes and washed twice in PBST-BSA (0.1% v/v Tween-20, 1% w/v BSA, PBS). For EdU labelling to mark cell proliferation, the Click-IT reaction was conducted as in **section 2.6.2**. Next, samples were washed twice with PBST-BSA and

incubated with primary and secondary antibodies (**tables 2.6 and 2.7**), both diluted in PBST-BSA, for 1 hour and 30 minutes, respectively. Finally, cells were counter-stained with DAPI staining solution (0.1% BSA, 0.1 mg/mL RNase A, 1 µg/mL DAPI, PBS) for at least 30 minutes before analysing.

Cell cycle distribution of $1x10^4$ cells was analysed using the CytoFLEX LX (Beckman Coulter) equipped with the CytExpert program (version 2.3.0.84). Obtained data was analysed using FlowJo analysis software (version 10.7.2). Cell debris was excluded through FSC vs SSC gating and single cells identified through FSC-H vs FSC-W gating. Percentage cells in G1, S, and G2/M were obtained through gating distinct cell populations.

2.7.5 WST-1 cell proliferation assay

To validate the HCT116 OsTIR1 mAID cell lines, 3000 cells were seeded per well in a 96-well plate in technical triplicate. 24 hours post seeding, 500 µM Indole-3-acetic acid (IAA) (I5148, Sigma-Aldrich) was added to the relevant wells and incubated for 2 hours to promote protein depletion. The relevant drugs were prepared by serial dilution and added to the required wells along with additional IAA to maintain a final concentration of 500 µM. After 5 days, cells were incubated with complete media containing 10% WST-1 reagent (5015944001, Roche) for 1 hour at 37°C. Plate absorbance was measured at 450 nm and 650 nm and cell survival was calculated as 450 nm readings subtracted from the 650 nm background readings and presented as a percentage of the negative control.

2.7.6 Clonogenic cell survival assay

To assess the long-term impact of IAA on HCT116 OsTIR1 mAID cells, 600 cells were seeded per well into a 6-well plate. Cells were seeded in conditioned media (70% fresh complete media, 30% used media), in triplicate. 24 hours post seeding, 500 µM IAA was added to the relevant wells and incubated for 10 days until colony formation. Fresh drug added after 5 days. To visualise colonies, media was removed from the wells and cells washed with PBS. Cells were stained and fixed using Crystal Violet staining solution (0.005% w/v Crystal Violet, 25% v/v methanol, water) for 30 minutes in the dark before

washing thoroughly in distilled water. Samples were left to air dry and imaged using a Nikon D3200 camera.

Colonies were counted automatically using ImageJ. Colonies were defined through thresholding of 8-bit images and the 'Analyze Particles' function quantified the number of colonies displaying 0.01-1.00 circularity. Percentage survival was calculated relative to the untreated control.

2.8 Data analysis

2.8.1 Statistics

Statistical analysis was performed using Graphpad Prism 8 and 9. The means of three independent experiments were compared using the specified statistical test in the figure legends. P-values were depicted as follows; $p<0.05$ = *, $p<0.01$ = **, $p<0.001$ = ***, $p<0.0001$ = ****.

2.8.2 IF quantification in Chapter 3 using FindFoci in ImageJ

Quantification of foci in mitotic cells to investigate mitotic DNA synthesis was conducted using ImageJ and the GDSC FindFoci GUI plugin (Herbert et al., 2014). Firstly, .oib images were processed into individual .tif images for each channel and subsequently processed as required e.g. "subtract background" and "despeckle" functionalities to reduce noise or uneven background signal. The DAPI channel was used to create a mask and define regions of interest (ROI). Next, the FindFoci GUI was used to define the optimal parameters for foci detection for each channel from representative images before the FindFoci Batch function was used to apply these parameters and analysis to all images for each channel. The identified foci were projected onto the DAPI-defined ROIs and foci were counted within each nucleus using "Assign foci to objects" within the FindFoci plugin.

Colocalisation was measured using the GDSC Colocalisation plugin from ImageJ. Foci identified through the previous steps for the relevant channels were used to create a mask and "Particle Overlap" was used to detect the degree of overlap i.e. colocalisation where '1'

indicates 100% colocalisation. Automated quantification scripts are provided in **Appendix 1**.

2.8.3 Exo-FISH and IF quantification in Chapter's 4 and 5

Firstly, cells were defined as regions of interest (ROI) according to DAPI staining. For foci counting, foci were automatically selected using an arbitrarily chosen threshold (usually ~500 arbitrary units) and counted per ROI.

For quantification of Exo-FISH foci signal intensity, cenFISH and telFISH foci were automatically detected using an arbitrarily chosen threshold, as before, and a 10x10-12x12 pixel box was generated around each focus (~2x2/2.5x2.5 μm box where approximately 1 pixel equals 0.207 μm, images taken at 100X magnification), within which the pixel intensity was measured and saved. The median signal of all foci across the given cell (i.e. ROI) was calculated to generate a "median focus" per cell. The median value of the box perimeter readings was then used to estimate the background signal, and this was subtracted from the median focus. Representative median foci were plotted using seaborn (v.0.12.1) (Waskom, 2021). For plotting in Graphpad Prism, the median fluorescence signal within the background-subtracted median focus was calculated to represent both focus intensity and size.

For IF analysis, a similar approach was applied. CENP-B foci were automatically selected using an arbitrarily chosen threshold and used to define the 10x10-12x12 pixel box. The background-subtracted signal intensity of CENP-B as well as the secondary signal e.g. CENP-A, was then calculated within the CENP-B-defined box. Signal intensity was normalised to control samples. Automated quantification scripts are provided in the **Appendices 2 and 3**.

Chapter 3 - Investigating RAD51 function in mitotic DNA synthesis

3.1 Introduction

RAD51 is recruited to mitotic chromatin in a PLK1-dependent manner (**section 1.6.3.2**). In this chapter, I aimed to explore the role of RAD51 in mitosis. To this end, I synchronised U2OS cells to observe RAD51's impact on MiDAS (**section 1.5.3.1**) and subsequent mitotic progression and stability. These findings are now included as part of a publication describing RAD51's role in protecting mitotic chromatin (Wassing et al., 2021).

3.2 Results

3.2.1 RAD51 is required for MiDAS

Given that RAD51 is recruited to mitotic chromatin, I sought to investigate the potential role of RAD51 in MiDAS. Firstly, U2OS cells were synchronised at the G1/S phase boundary using a double thymidine block (dT-B/R) and then released into S phase (**figure 3.1A**). After 1 hour, low dose aphidicolin (APH) was added to the cells to induce replication stress for 23 hours. APH inhibits B-family DNA polymerases α, δ, and ε, blocking their DNA binding and synthesis activity (Dhillon et al., 2003; Krokan et al., 1981). Next, RO3306, a CDK1 inhibitor, was added to the cells to arrest the cells at the G2/M phase boundary. Cells were subsequently released into mitosis (m-R) in the presence of the thymidine analogue, EdU, to mark sites of DNA synthesis in early mitosis. Cells were also treated with RAD51 inhibitor, B02. B02 inhibits *de novo* RAD51 DNA binding without disrupting RAD51 filaments already present on the chromatin (Huang & Mazin, 2014; Wassing et al., 2021). Use of B02 ensures that RAD51 loaded on DNA in the previous S phase is not impacted, as it could be with siRNA use, and that any phenotypes are specific to its role in mitosis. After 30 minutes, cells were collected by mitotic shake-off (m-SO), immunofluorescence performed, and EdU foci counted as a read-out of MiDAS events. This synchronisation protocol has previously been demonstrated to enrich for mitotic cells and induce MiDAS (Wassing et al., 2021).

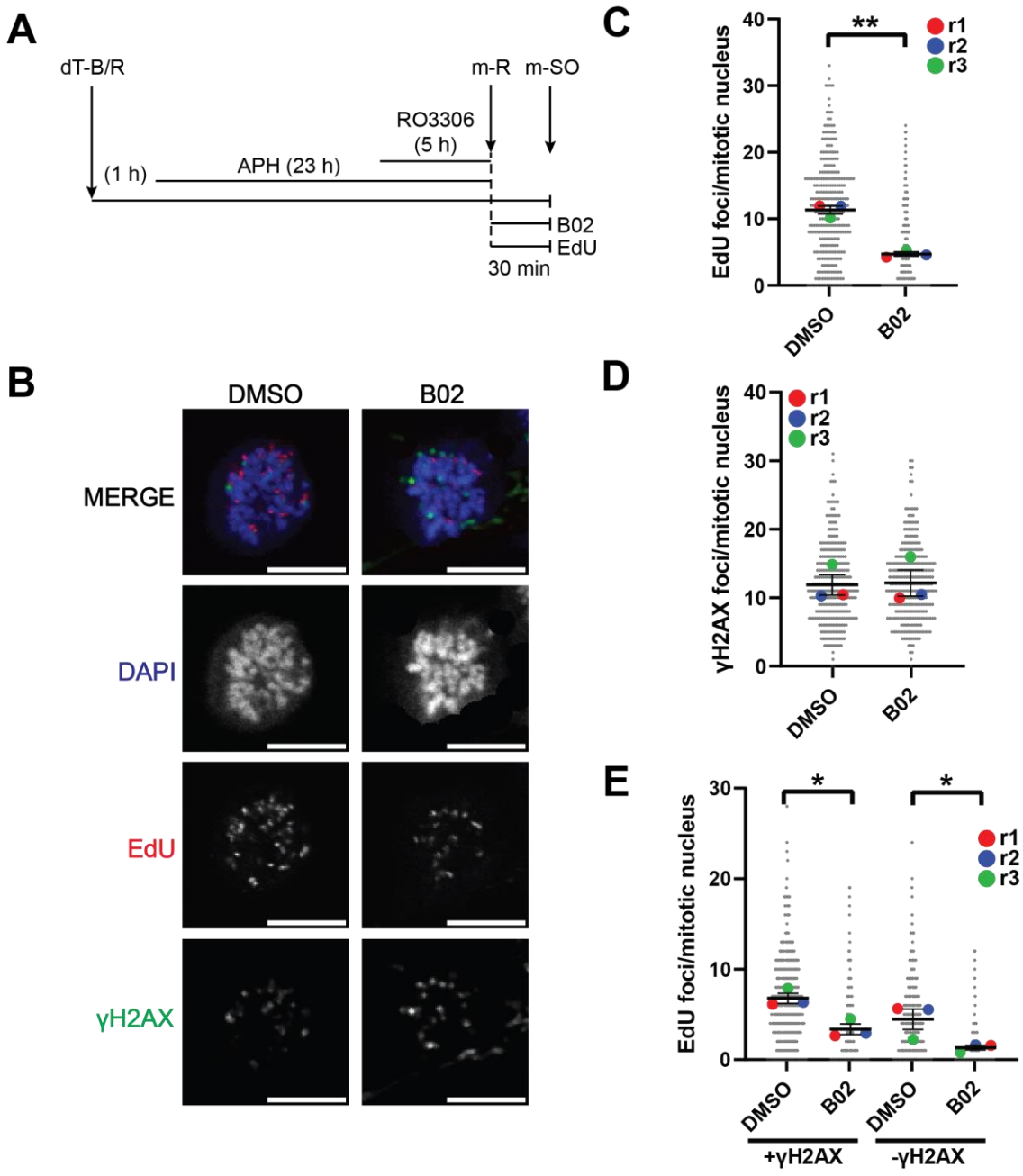


Figure 3.1 Assessing the impact of RAD51 inhibition on MiDAS
A Schematic showing U2OS cell synchronisation protocol to study mitotic DNA synthesis. **B** Representative images of mitotic U2OS cells after synchronisation. Scale bar is equal to 10μm. **C** Graph displaying number of EdU foci per mitotic nucleus. Unpaired t-test. **D** Graph showing number of γH2AX foci per mitotic nucleus. Unpaired t-test. **E** Graph showing number of EdU foci that colocalise with (+γH2AX) or without (-γH2AX) foci. Unpaired one-way ANOVA with Sidak's multiple comparisons test. All error bars represent S.E.M. Mean of each repeat displayed as larger, coloured data points. n=3. At least 100 cells analysed per repeat. dT-B/R = double thymidine block/release. m-R = mitotic release. m-SO = mitotic shake off.

RAD51 inhibition resulted in a significant decrease in the number of EdU foci suggesting that RAD51 may be important for facilitating MiDAS in U2OS cells (**figures 3.1B and C**).

ɣH2AX foci form at sites of DNA damage and replication stress (Gagou et al., 2010). Interestingly, there was no concurrent change in ɣH2AX foci formation (**figure 3.1D**). Furthermore, I next quantified EdU foci that colocalise with ɣH2AX or not (**figure 3.1E**). B02 resulted in a significant decrease in EdU signal overlapping with and without ɣH2AX. This indicates that RAD51 inhibition causes a global reduction in MiDAS events in U2OS cells at broken and unbroken replication forks. Overall, these data indicate that *de novo* RAD51 recruitment may be required to facilitate MiDAS in U2OS cells and that not all MiDAS events may occur at ɣH2AX-positive loci, as previously described (Minocherhomji et al., 2015).

3.2.2 Utilising RAD51 separation-of-function mutants to identify its mitotic function

Next, I wanted to understand more about how RAD51 was contributing to MiDAS. RAD51 is a multi-functional protein that possesses strand exchange and ssDNA binding activity. By exploiting several RAD51 mutants (**figure 3.2A**), it is possible to distinguish between RAD51's known functions and their importance in MiDAS. The RAD51 K133R mutant can bind ATP but has impaired ATP hydrolysis activity. Therefore, it retains high-affinity ssDNA binding and strand exchange activity but has defective filament disassembly so that repair intermediates cannot be fully resolved (Schlacher et al., 2012; Stark et al., 2002). Fanconi Anaemia-associated RAD51 T131P has DNA-independent ATPase activity resulting in marked destabilisation of the RAD51 filament, impairing ssDNA binding and protection. Despite this, heterozygous RAD51 T131P mutant cells remain HR proficient when endogenous RAD51 WT is also expressed (Wang et al., 2015; Zadorozhny et al., 2017). Both mutants are described as dominant negative against endogenous RAD51 WT activity.

Isabel Wassing utilised U2OS Flp-In T-REx cells to generate doxycycline (DOX)-inducible cell lines expressing FLAG-tagged RAD51 WT, K133R, or T131P mutants. I synchronised the cell lines as in **figure 3.2B**, and the expression of the RAD51 separation-of-function mutants was validated by western blot (**figure 3.2C**). Endogenous WT RAD51 remains expressed in these cells and represents the lower band present in all samples. Exogenous

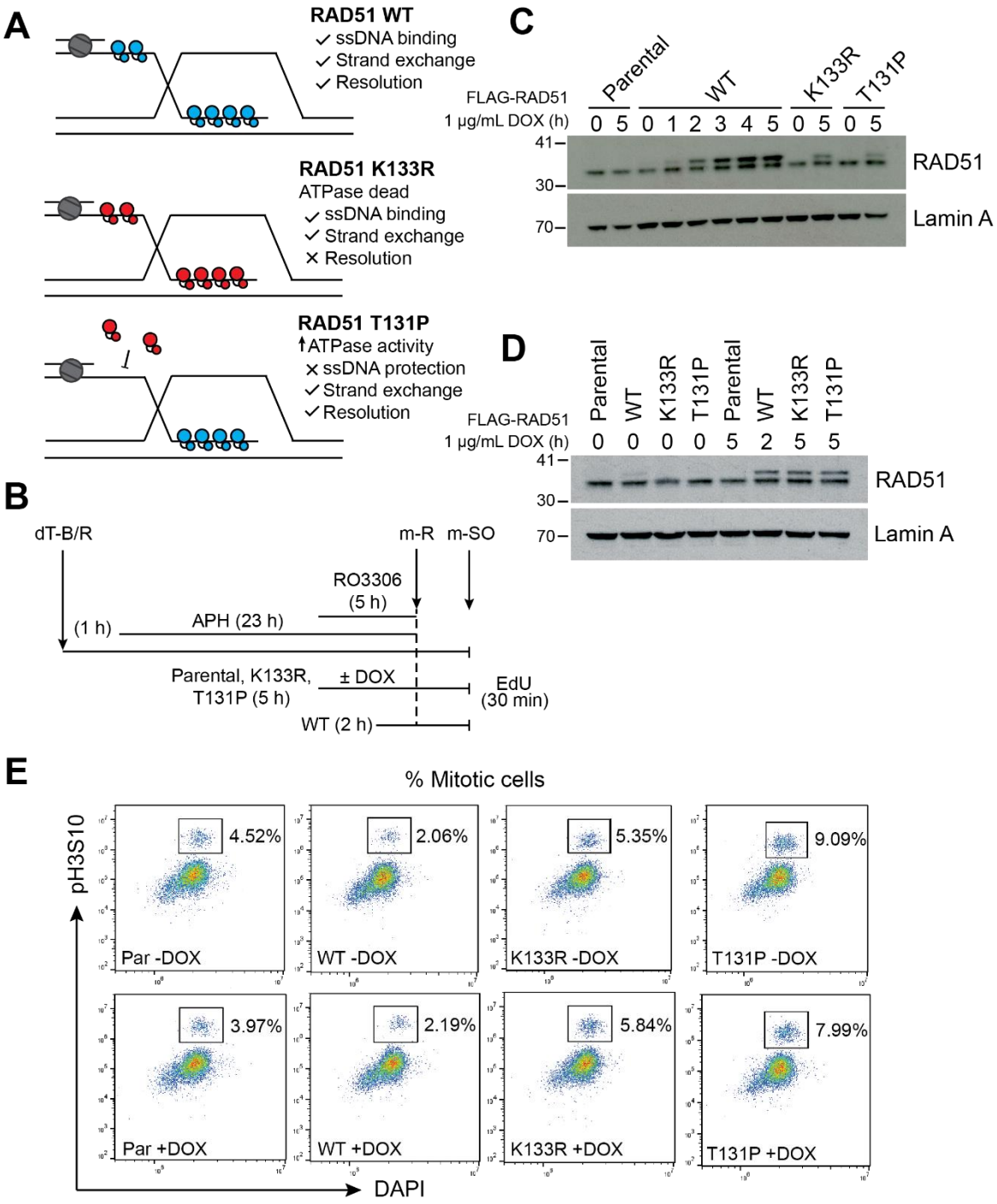


Figure 3.2 Validation of U2OS Flp-In T-REx RAD51 separation-of-function cell lines
A Schematic showing properties of different RAD51 separation-of-function mutants (red) in ssDNA binding and DSB repair. In this context, cells retain endogenous WT RAD51 (blue) expression. **B** Schematic of synchronisation of U2OS RAD51 separation-of-function mutants to assess their role in MiDAS. Lamin A was used as a loading control. **C** Western blot showing time course induction of FLAG-tagged RAD51 separation-of-function mutants in mitosis with 1 µg/mL DOX. **D** Western blot showing induction of expression of FLAG-tagged RAD51 separation-of-function mutants in mitosis after 2 or 5 hours of 1 µg/mL DOX treatment. Lamin A was used as a loading control. **E** Cell cycle analysis of U2OS RAD51 separation-of-function mutants with or without 1 µg/mL DOX treatment. Mitotic cells were gated based on DAPI and pH3S10 staining.

RAD51 WT expresses at a higher level than the RAD51 K133R and T131P mutants, as seen in (Wang et al., 2015). Due to this, DOX was added to the cell lines at different time points to ensure similar levels of exogenous RAD51 expression to aid comparability between the cell lines (**figure 3.2C**). Exogenous RAD51 WT displayed good expression after only 2 hours DOX treatment, whereas RAD51 K133R and T131P showed a similar level of expression after 5 hours DOX treatment (**figure 3.2D**).

Furthermore, to verify that exogenous expression of the RAD51 separation-of-function mutants did not significantly impact their ability to be synchronised, I conducted flow cytometry looking at histone H3 serine 10 phosphorylation (pH3S10), a marker for mitotic cells, and DAPI staining. **Figure 3.2E** shows that DOX addition does not greatly impact the enrichment of mitotic cells after synchronisation. RAD51 K133R and T131P cells did display a slightly higher level of mitotic cells overall, although this was not influenced by the addition of DOX.

3.2.3 RAD51 promotes non-DDR associated MiDAS

I next used these RAD51 separation-of-function cell lines to identify the role of RAD51 in MiDAS. The cells were synchronised as before (**figure 3.2B**), and the number of EdU and γH2AX foci quantified. Expression of the different RAD51 mutants showed no significant differences in EdU or γH2AX levels (**figure 3.3A, B, and C**). However, when measuring the levels of γH2AX-positive or -negative EdU foci, I observed an insignificant but modest increase ($p=0.0825$) in MiDAS events that do not colocalise with γH2AX in the RAD51 K133R mutants (**figure 3.3D**). This could indicate that ssDNA binding over DNA repair activity is most important to facilitate MiDAS and that RAD51 chromatin binding protects against mitotic DNA damage and γH2AX signalling to promote non-DDR associated MiDAS.

On the other hand, surprisingly RAD51 T131P expression also contributes to a small insignificant increase in γH2AX-negative EdU foci ($p=0.0714$) (**figure 3.3D**). Heterozygous RAD51 T131P cells have impaired ssDNA protection activity but remain HR proficient (**figure 3.2A**) (Wang et al., 2015). This could indicate that in the absence of functional

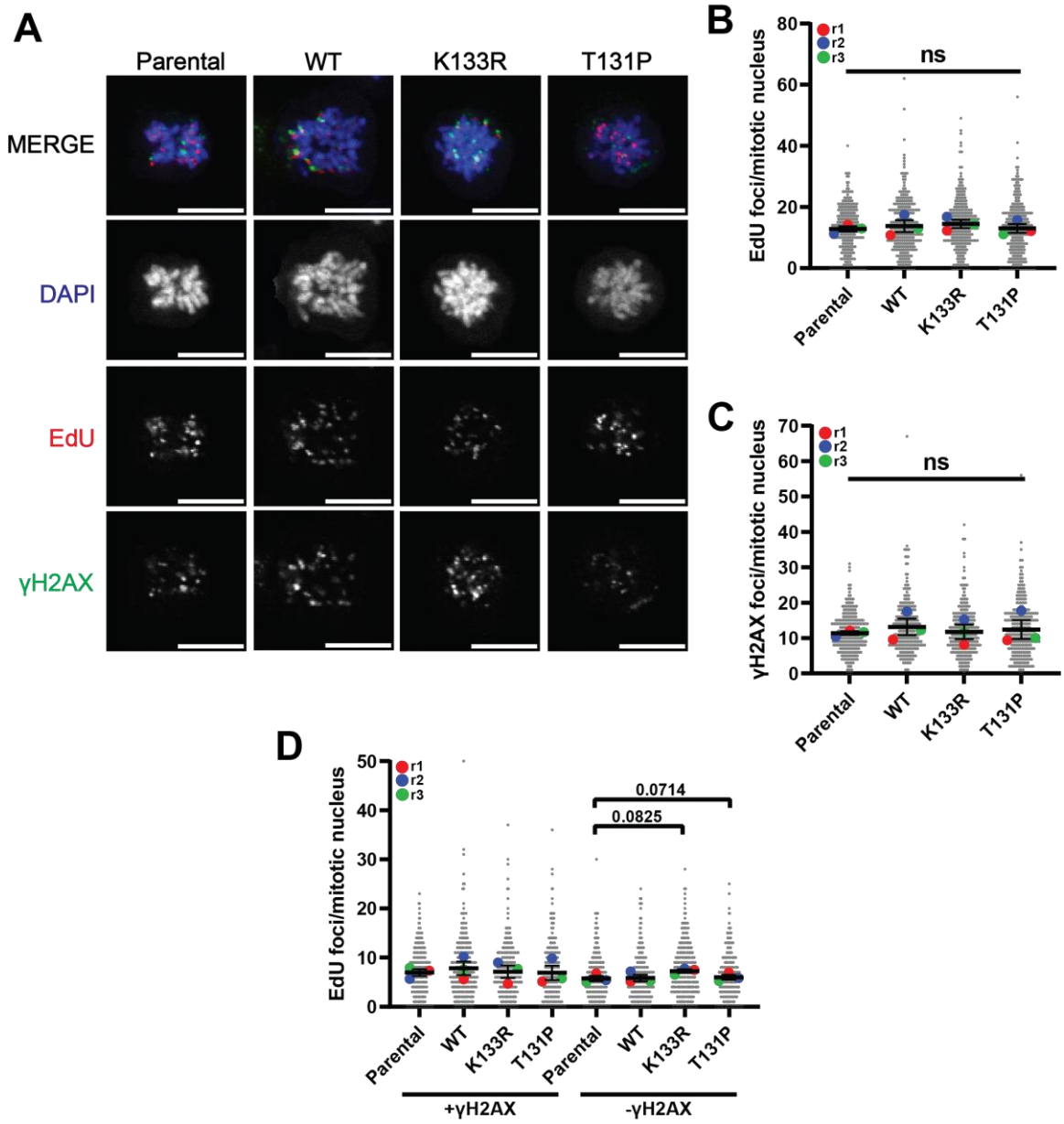


Figure 3.3 Assessing RAD51 separation-of-function mutant impact on MiDAS
A Representative images of cell lines after synchronisation. Scale bar equals 10μm. **B** Quantification of the number of EdU foci per mitotic nucleus. **C** Graph showing number of γH2AX foci per mitotic nucleus. **D** Graph showing quantification of EdU foci colocalising with (+γH2AX) or without (-γH2AX) γH2AX. All error bars represent S.E.M. At least 100 cells analysed per repeat. n=3. Mean of each repeat displayed as larger, coloured data point. Paired one-way ANOVA, uncorrected Fisher's LSD.

RAD51, there are multiple mechanisms that protect under-replicated DNA and promote MiDAS.

Overall, utilising RAD51 separation-of-function mutants enabled me to gain insight into the specific role of RAD51 in MiDAS. We have found evidence suggesting that RAD51 is most

important at γH2AX-negative sites for non-DDR associated MiDAS. This likely requires RAD51's ssDNA binding activity, although this requires further investigation.

3.2.4 RAD51 depletion in early mitosis leads to increased mitotic DNA damage

Previously, MiDAS has been linked to DDR-associated loci where MUS81 and other nucleases cleave the stalled fork to create a one-ended DSB to facilitate RAD52-dependent BIR (**figure 1.3**) (**section 1.5.3.1**) (Bhowmick et al., 2016; Calzetta et al., 2020; Minocherhomji et al., 2015).

This is converse to the suggestion that RAD51 appears to be most important for non-DDR associated MiDAS (**section 3.2.3**). Previously, RAD52 inhibition using AICAR in U2OS cells was shown to modestly reduce mitotic EdU foci formation suggesting that RAD51 may play a greater contribution to MiDAS than RAD52 (Wassing et al., 2021).

I next wanted to explore more closely the impact of RAD51 and RAD52 on mitotic DNA breaks and MiDAS. I utilised pulsed-field gel electrophoresis (PFGE) to separate intact and broken DNA fragments ranging from 1 to 100 kb. U2OS cells were synchronised as in **figure 3.4A** and released into mitosis in the presence of B02, high dose APH (APH-M), or AICAR. High doses of APH induce fork stalling, fork collapse, and complete inhibition of MiDAS (Minocherhomji et al., 2015).

The PFGE shown in **Figure 3.4B** demonstrates that B02 treatment leads to a 2.8X increase in broken DNA compared to the DMSO control. This suggests that failure of RAD51 to protect mitotic ssDNA leads to an accumulation of DNA breaks. More modest changes in broken DNA were observed after APH-M and AICAR treatment, at a 1.2X and 1.7X increase, respectively, further indicating that MiDAS inhibition leads to increased nucleolytic processing of stalled replication forks in mitosis.

Overall, B02 treatment leads to a significant increase in mitotic DNA damage suggesting that inhibition of RAD51-dependent non-DDR-associated MiDAS leads to increased

nucleolytic cleavage of stalled replication forks in mitosis, potentially requiring BIR-associated MiDAS or other RAD51-independent mechanisms for repair.

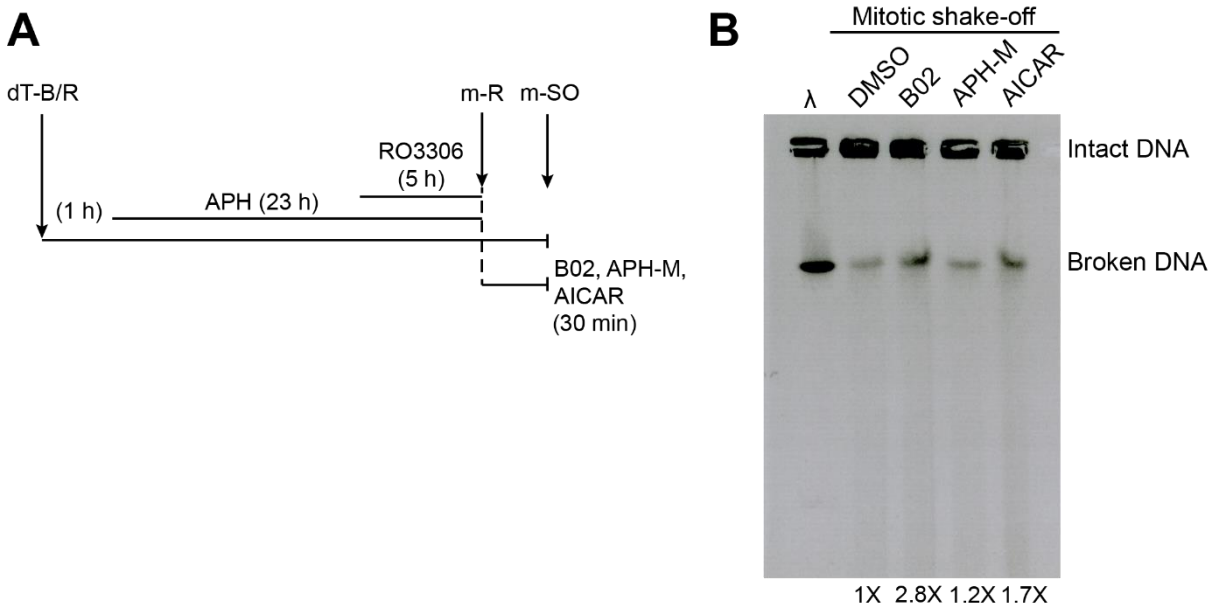


Figure 3.4 RAD51 depletion in early mitosis leads to increased mitotic DNA damage
A Schematic of U2OS cell synchronisation and drug treatments before PFGE. **B** PFGE where DNA fragments 1-100 kb were separated from the bulk DNA population. λ refers to lambda DNA ladder used as a DNA fragment size control. Band intensity was quantified and normalised to DMSO vehicle control. This normalisation is displayed at the bottom.

3.2.5 Inhibiting RAD51's role in MiDAS promotes mitotic defects

Isabel Wassing conducted experiments to investigate the consequences of RAD51 and MiDAS inhibition during early mitosis on downstream chromosome segregation. Failure to resolve under-replicated DNA is strongly associated with mitotic defects such as chromosome missegregation and breakage. SAC maintenance is vital for cell survival after extensive replication stress to allow the cell to resolve aberrant DNA entanglements before anaphase onset (**section 1.7.2**).

To examine this, we employed live cell microscopy. U2OS cells expressing GFP-tagged Lamin B1 and mCherry-tagged Histone H2B were used to assess chromatin dynamics between nuclear envelope breakdown (NEBD) and anaphase onset (AO) (**figures 3.5A and D**). U2OS cells were synchronised (**figures 3.5A and B**) and treated with different

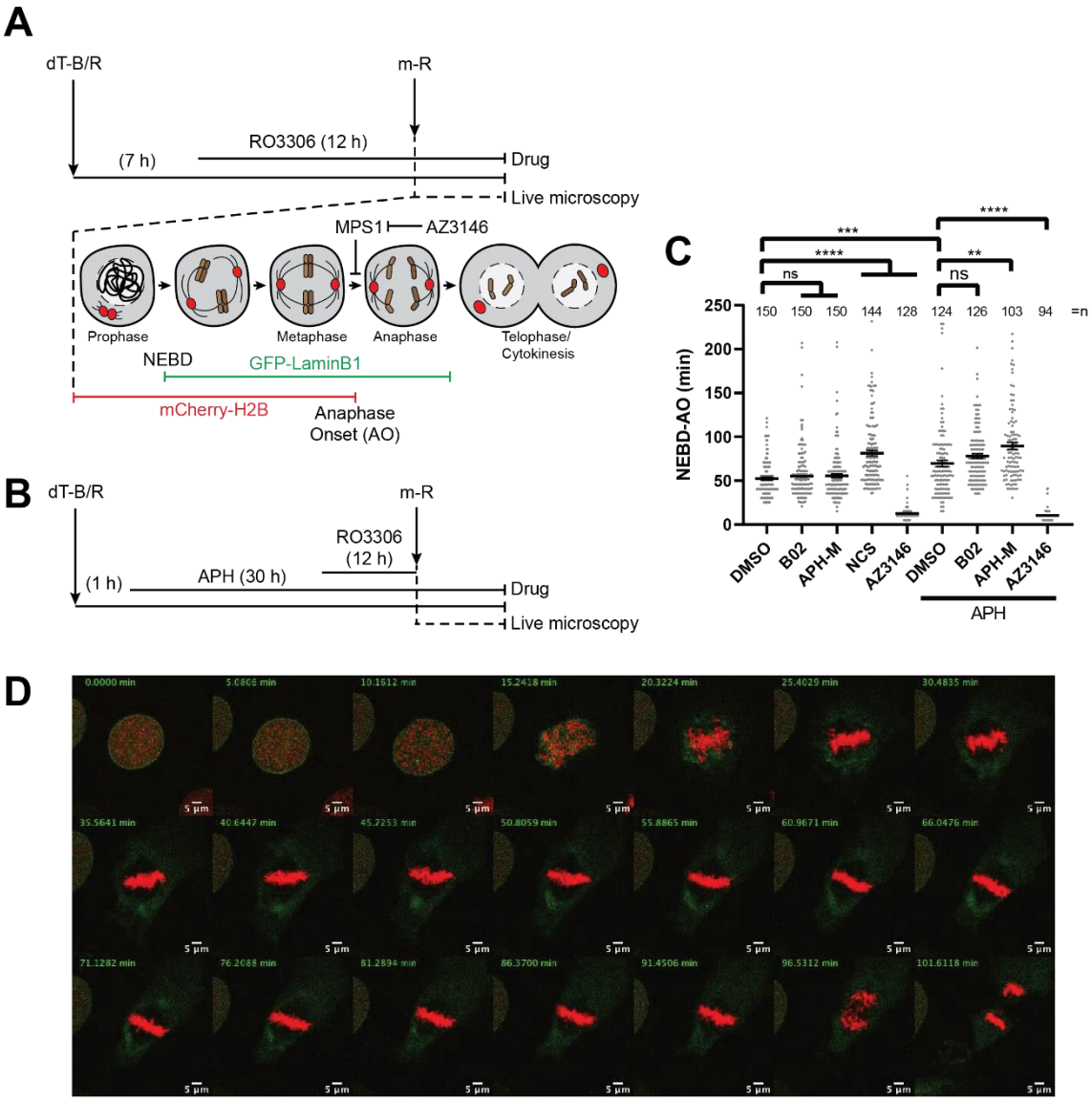


Figure 3.5 Inhibiting RAD51's role in MiDAS promotes delayed anaphase onset
A Schematic of U2OS cell synchronisation and expression profile of mCherry-Histone H2B and GFP-Lamin B1 across mitosis. **B** Schematic of U2OS cell synchronisation when combined with low dose (0.4 μM) APH. **C** Quantification of time between NEBD to AO in minutes. Combination of three independent repeats. Total cells analysed (=n) for each sample is displayed above the data points. Brown-Forsythe and Welch (unpaired) ANOVA with Dunnett's T3 multiple comparisons test. **D** Representative images of cell progression from NEBD to AO. Images taken every 5 minutes. Scale bar is equal to 5 μm. These experiments were conducted by Isabel Wassing (Wassing et al., 2021).

agents impacting MiDAS to observe their effect on mitotic timings. As expected, MPS1 inhibitor, AZ3146, drastically shortened the NEBD-AO timing as there was no SAC activation to delay chromosome segregation (**figure 3.5C**). In the absence of replication stress (**figures 3.5A and C**), B02 and APH-M show little impact on NEBD-AO timing compared to the DMSO control. However, neocarzinostatin (NCS), a radio-mimetic drug

that induces extensive DNA breaks (Kuo et al., 1984), produced a significant delay in AO (**figure 3.5C**).

Addition of mild replication stress in the preceding S phase (**figure 3.5B**) produced an overall increase in NEBD-AO time across all conditions, excluding AZ3146 (**figure 3.5C**). While B02 treatment had no significant impact, APH-M treatment delayed AO suggesting that under-replicated and/or broken mitotic DNA may activate the SAC until it is processed. NCS and AZ3146 treatment produced significantly increased levels of mitotic aberrations including lagging chromosomes and micronuclei (**figure 3.6A**), agreeing with previous findings that prevalent DNA breaks can promote inaccurate microtubule-kinetochore attachments (Calzetta et al., 2020). Addition of replication stress, as in **figure 3.5B**, also leads to a significant increase in aberrant mitotic features (**figure 3.6A**). This indicates that under-replicated DNA arising from MiDAS inhibition leads to chromosome segregation defects.

Extensive mitotic defects and DNA damage can result in mitotic cell death. NCS treatment did not significantly increase mitotic cell death (**figure 3.6B**). Alternatively APH-M treatment after replication stress significantly increased mitotic cell death (**figure 3.6B**), indicating that under-replicated DNA and DNA lesions are toxic.

Overall, we have demonstrated that the SAC delays AO to resolve under-replicated DNA through MiDAS. When MiDAS is impaired, either through addition of B02 or APH-M, there is a significant increase in aberrant mitotic phenotypes and cell death. This highlights the connection between the SAC and MiDAS in maintaining genome stability and survival.

3.2.6 RAD51 inhibition in mitosis impacts centromere integrity

Evidence indicates that the SAC is activated by DNA damage at centromeres but not chromosome arms (Mikhailov et al., 2002). Centromeres experience replication stress (**section 1.7.4.2**) but have not previously been associated with MiDAS. In fact, Wassing et

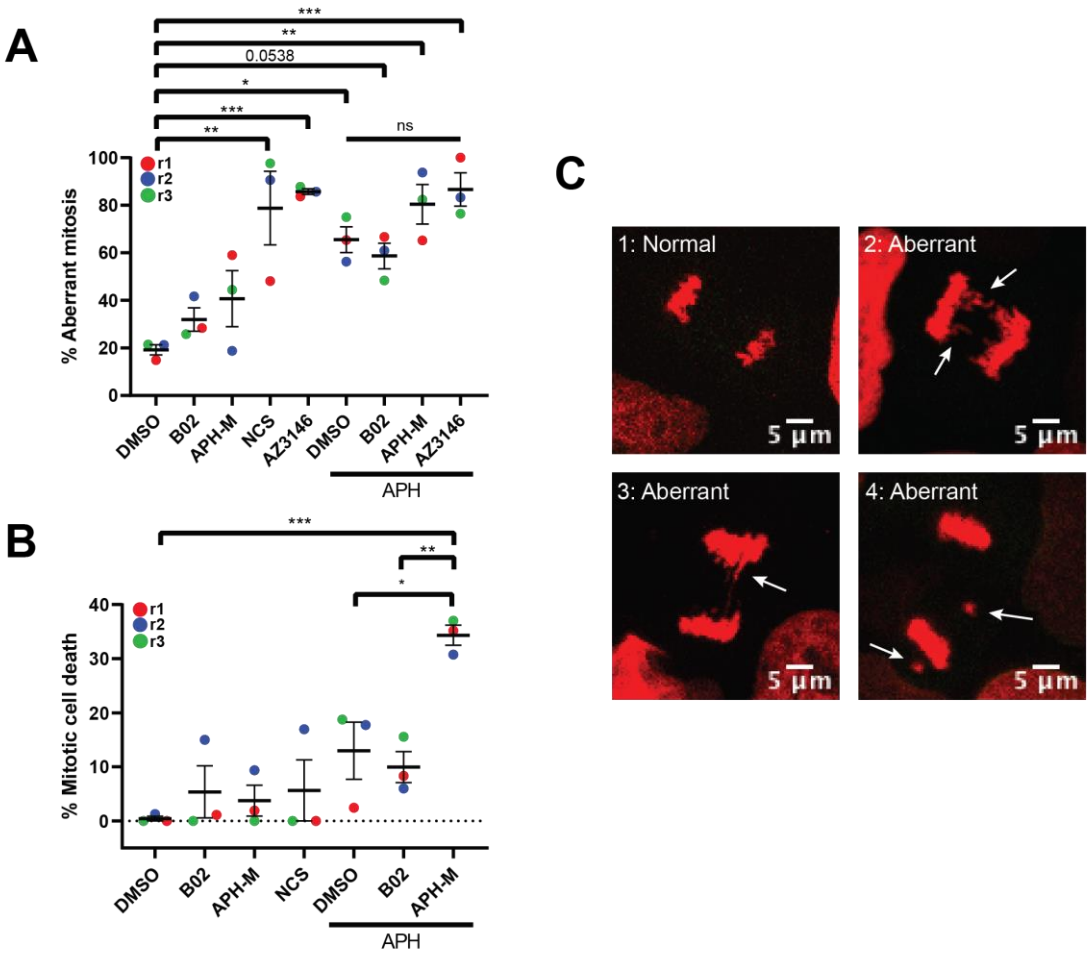


Figure 3.6 Assessing the consequences of MiDAS inhibition on mitotic aberrations
A Graph showing average percentage of cells displaying mitotic aberrations. **B** Graph showing average percentage of cells that undergo mitotic cell death. **C** Representative images of normal (1) and aberrant (2-4) mitoses. Arrows point to lagging chromosomes (2 and 3) and micronuclei (4). Scale bar represents 5 µm. Unpaired one-way ANOVA with Tukey's mulitple comparisons test. Scale bars represent S.E.M. These experiments were conducted by Isabel Wassing (Wassing et al., 2021).

al., were unable to observe significant colocalisation of EdU foci and centromeres in mitosis (Wassing et al., 2021). RAD51 has a well-characterised role in HR (**section 1.4.2**). While a majority of HR events are resolved through non-crossover mechanisms, some resolution events can produce crossovers (**section 1.7.4.2.3**). We wanted to investigate how RAD51 inhibition in early mitosis and non-DDR associated MiDAS may influence centromere repair and recombination.

Chromosome-orientated fluorescence *in situ* hybridisation (CO-FISH) (**figure 3.7A**) is a method to differentially label centromeres of sister chromatid pairs

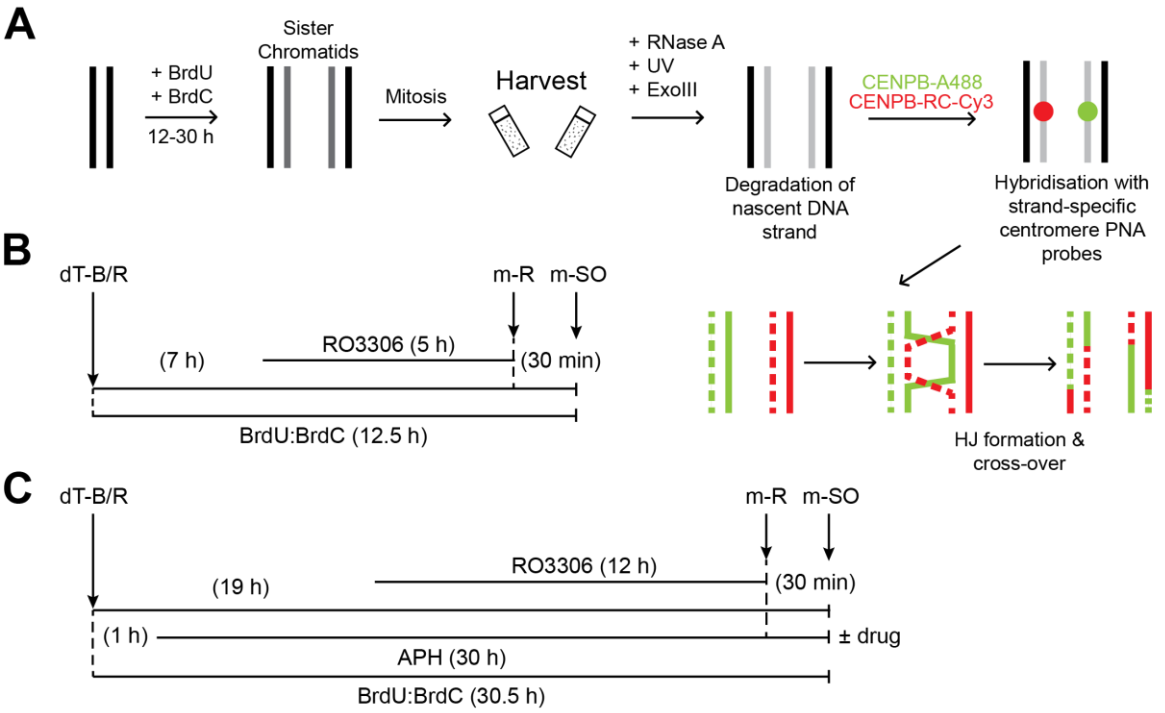


Figure 3.7 CO-FISH to detect centromeric SCEs
A Schematic of CO-FISH protocol and generation of cross-over recombination products. **B** Schematic of U2OS cell synchronisation and BrdU:BrdC treatment protocol for CO-FISH. **C** Schematic of U2OS cell synchronisation and BrdU:BrdC treatment protocol for CO-FISH combined with low dose replication stress (APH). These experiments were conducted by Isabel Wassing (Wassing et al., 2021).

(Giunta & Funabiki, 2017). In short, synchronised cells are incubated with nucleoside analogues, BrdU and BrdC, for one replicative cycle to label one strand of the DNA helix. Mitotic cells are then collected and metaphase spreads produced. The nascent BrdU:BrdC-labelled DNA strand is then degraded and the chromatin labelled with FISH probes specific for the centromeric CENP-B box. The pattern of centromeric FISH probe labelling can then be visualised by microscopy as an indication of sister chromatid exchange (cen-SCE) events (**figure 3.8C**). Centromeres have previously been shown to display high levels of cen-SCEs upon replication stress and various cancerous backgrounds (**section 1.7.4.2.3**) (Giunta et al., 2021; Giunta & Funabiki, 2017).

Isabel Wassing synchronised U2OS cells with or without APH to induce MiDAS for CO-FISH analysis (**figures 3.7B and C**). Low dose APH treatment increased the percentage of metaphase spreads displaying increased aberrant centromere FISH signal. This was further

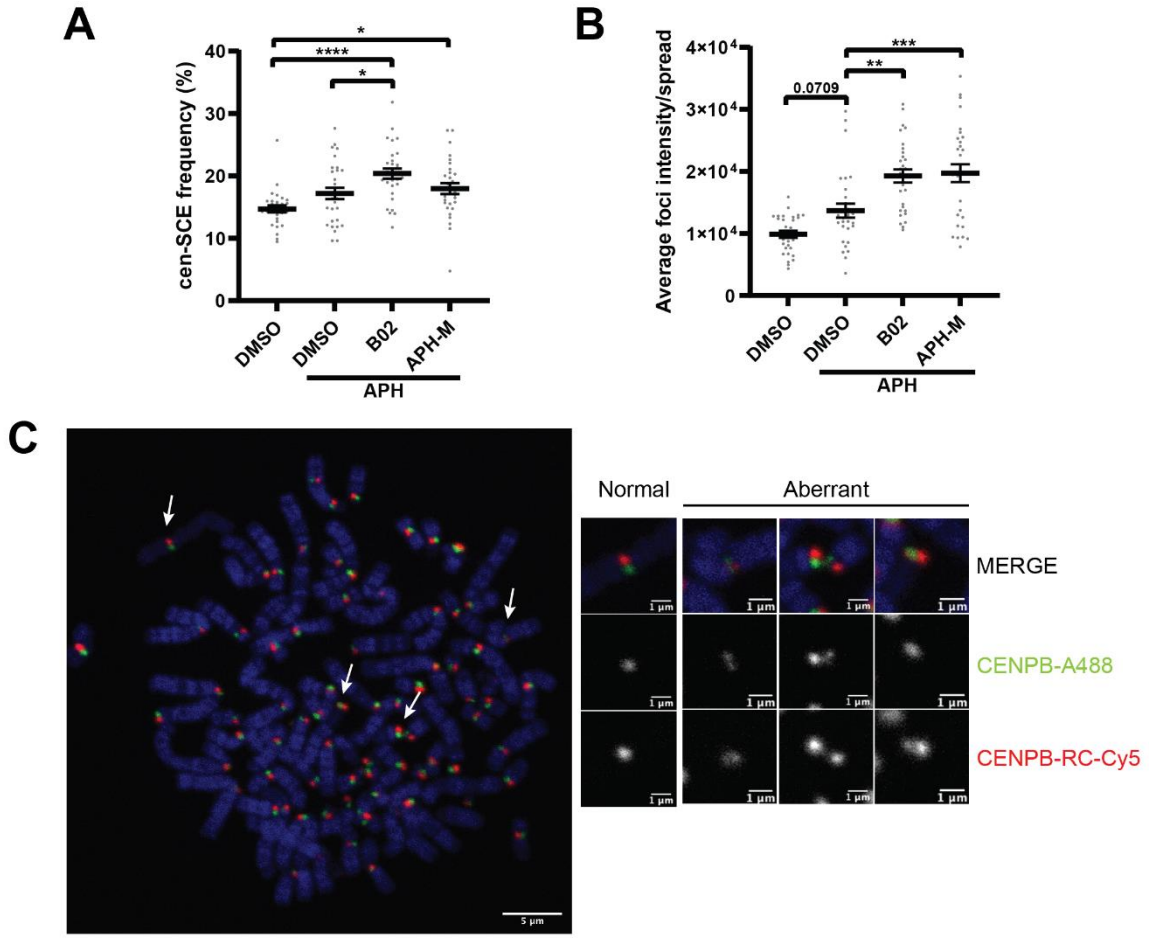


Figure 3.8 Analysing cen-SCE occurrence upon MiDAS inhibition
A Graph showing percentage of metaphase spreads displaying aberrant centromere FISH signals (cen-SCEs). **B** Graph showing average foci intensity of CENPB-RC-Cy5 probe per metaphase spread. **C** Representative image showing CO-FISH staining on metaphase spread. Scale bar equals 5µm. Arrows point to normal and aberrant centromere staining, enlarged on the right of the panel. Scale bar represents 1 µm. Data obtained from 3 independent repeats. n=30 (10 metaphase spreads per repeat). Error bars represent S.E.M. Unpaired one-way ANOVA with Tukey's multiple comparisons. These experiments were conducted by Isabel Wassing (Wassing et al., 2021).

enhanced upon mitotic RAD51 inhibition (**figures 3.8A and C**). However, APH-M treatment, and therefore MiDAS inhibition, did not rescue divergent CO-FISH signals suggesting that the increased cen-SCEs and/or other structural aberrations upon APH treatment do not necessarily result from MiDAS events.

HR can produce non-crossover events which are not detectable by CO-FISH. Therefore, Isabel Wassing also quantified the average FISH foci intensity per spread (**figure 3.8B**). B02 and APH-M treatment significantly increased foci intensity compared to the DMSO

control. This suggests that centromeric ssDNA is enriched upon MiDAS inhibition; whether this is a consequence of DNA under-replication or sample preparation is still unclear.

Overall, these results suggest that mild replication stress and MiDAS inhibition contribute to centromere fragility and ssDNA accumulation.

3.3 Discussion

3.3.1 A role for RAD51 in MiDAS

In this chapter, I identified a role for *de novo* RAD51 recruitment in facilitating MiDAS (**figure 3.1**). Utilising the RAD51 inhibitor, B02, mitotic U2OS cells displayed a reduction in EdU incorporation indicating impaired MiDAS in these cells (**figure 3.1C**). RAD51 ssDNA binding and replication fork protection activity seems to be most important to conduct these MiDAS events although some strand exchange and recombination activity may still be required in some contexts (**figures 3.2 and 3.3**). RAD51's MiDAS activity likely occurs largely independently of ɣH2AX induction and the DDR (**figures 3.1 and 3.3**). Therefore, this RAD51-mediated MiDAS pathway appears to be distinct from the previously described RAD52-dependent MiDAS mechanism (Bhowmick et al., 2016; Minocherhomji et al., 2015).

A role for RAD51 in MiDAS disagrees with the previous publication describing RAD51 and BRCA2 as dispensable (Bhowmick et al., 2016). This difference may stem from the use of siRNA in these studies which we observed to cause substantial cell cycle delay under mild replication stress (Wassing et al., 2021). Since this work was conducted, further evidence describing a role for RAD51 in MiDAS at the fragile X locus has emerged (Garribba et al., 2020). Interestingly, under these conditions, RAD51 was concluded to promote a unique sub-pathway of BIR that requires SLX1/SLX4, RAD51, and POLD3 but was independent of MUS81-EME1. These findings could indicate that MiDAS is a highly variable process with several different compensatory protein pathways at different gene loci. RAD52-mediated MiDAS is strongly associated with CFSs (Bhowmick et al., 2016), RAD51-mediated BIR-like MiDAS is associated with fragile X loci, and the RAD51-mediated MiDAS described

above could be considered a broader pathway required for both γH2AX-positive and -negative events (**figure 3.1E**) (Wassing et al., 2021).

RAD51 is classically associated with its S/G2 phase role in DSB repair and replication stress response where it is recruited to the chromatin in a BRCA2-dependent pathway (Davies & Pellegrini, 2007; Esashi et al., 2007). As described previously (**section 1.6.3.2**), RAD51 can also be recruited by a PLK1-dependent pathway which is active in the later stages of the cell cycle (Yata et al., 2012, 2014). Given this novel role for RAD51 in early mitosis (**figure 3.1**) and evidence that a majority of the DDR is downregulated in mitosis, this raises the question as to how RAD51 is recruited to MiDAS loci. Wassing et al., utilised RAD51 S14 mutants to demonstrate that RAD51 recruitment to under-replicated DNA in mitosis is PLK1-dependent (Wassing et al., 2021). Furthermore, TOPBP1, which plays a role in PLK1-dependent RAD51 recruitment (Moudry et al., 2016), has also been shown to facilitate MiDAS (Minocherhomji et al., 2015; Pedersen et al., 2015).

3.3.2 DDR vs non-DDR associated MiDAS

Next, I explored the role of RAD51 in MiDAS in more depth. Exploiting RAD51 separation-of-function mutants (**figure 3.2**), I found that expression of the RAD51 K133R mutant led to an insignificant increase in EdU foci that do not colocalise with γH2AX (**figure 3.3D**). The lack of γH2AX signalling correlates with MiDAS events at loci that are undamaged or have escaped from the DDR i.e. non-DDR associated MiDAS. As RAD51 K133R retains ssDNA binding activity but no HR-mediated repair activity, this suggests that RAD51 promotes non-DDR associated MiDAS through its ssDNA protection activity.

Surprisingly, RAD51 T131P mutant expression also produces a small insignificant increase in EdU foci without γH2AX (**figure 3.3D**). RAD51 T131P forms unstable nucleoprotein filaments and is therefore considered to have lost its ssDNA protection activity (Wang et al., 2015; Zadorozhny et al., 2017). However, its HR and strand exchange activity is preserved when WT RAD51 expression is retained in the cell (Wang et al., 2015), as is the case in these experiments. This contradicts the RAD51 K133R mutant results, therefore it is

currently unclear exactly which function(s) of RAD51 are required for MiDAS. In the future, homozygous RAD51 T131P cells i.e. depletion of endogenous WT RAD51 protein, and loss of both ssDNA binding and strand exchange activity, would provide a more distinct understanding of the role of RAD51 in MiDAS.

Bright RAD51 foci indicative of HR-mediated DSB repair were not visible in early mitosis (Wassing et al., 2021). RAD51-mediated replication fork protection is not associated with foci formation (Petermann et al., 2010). Therefore, although RAD51's strand exchange activity may contribute to MiDAS to some extent, its ssDNA binding and protection activity is likely most important for resolving under-replicated mitotic DNA.

RAD51-II3A is another described separation-of-function variant containing three amino acid substitutions (R130A, R303A, and K313A) within its second low-affinity DNA-binding domain. Mutations at these sites inhibit RAD51's ability to facilitate the DNA homology search and strand exchange but ssDNA binding activity is retained (Mason et al., 2019). Addition of this mutant to this study would further increase our confidence that RAD51's ssDNA binding activity is required to facilitate non-DDR-associated MiDAS.

To look more directly at mitotic DNA damage upon RAD51 and RAD52 inhibition, I conducted PFGE (**figure 3.4**). Analysis of global DNA breaks after addition of mild replication stress showed that RAD51 inhibition leads to a 2.8X increase in mitotic DNA damage. In the absence of RAD51-mediated stalled fork protection, branched DNA structures can be subject to cleavage by nucleases, generating DNA breaks which can be detected by PFGE. Preliminary investigations show that increased mitotic DNA damage after RAD51 inhibition is not dependent on MRE11 (Isabel Wassing, unpublished). This indicates that RAD51's role in mitosis is distinct from its role in S/G2 phase where it protects nascent DNA from MRE11-mediated nucleolytic degradation (Hashimoto et al., 2010; Schlacher et al., 2011, 2012).

The observed increase in broken DNA by PFGE differs from **figure 3.3D** where no increase in ɣH2AX signalling was observed upon RAD51 inhibition in mitosis. This supports a role for RAD51 in facilitating mitotic DNA repair downstream of DSB generation. Alternatively, this may reflect the delayed kinetics of ɣH2AX signal induction versus physical DNA breaks. After ionising radiation (IR), physical DNA breaks can be immediately detected by PFGE whereas ɣH2AX signal was not maximal until 15-30 minutes post IR (Kinner et al., 2008). Therefore, the short time frame of these experiments (**figures 3.1A and 3.4A**), when MiDAS is most active, may limit the number of ɣH2AX foci that can be observed.

RAD52 inhibition and APH-M treatment resulted in a more modest induction of mitotic DNA breaks despite both reducing or completely abrogating MiDAS events and increasing ɣH2AX signalling (Wassing et al., 2021). Under these conditions, it is plausible that some DSBs at sites of under-replicated DNA may already be commencing strand exchange and BIR, producing DNA repair/replication intermediates such as D-loops. Branched DNA structures can become trapped in the gel matrix, reducing their mobility and detection by PFGE (Barnard et al., 2013; Mateos, 1996), thus explaining this result. Furthermore, it should not be discounted that RAD51 appears to promote MiDAS at broken and unbroken forks (**figure 3.1E**). Upon AICAR treatment, RAD51 remains functional and may facilitate protection of unbroken stalled forks and MiDAS intermediates, or else repair at under-replicated loci, perhaps also explaining the relatively low levels of DNA breaks by PFGE. Therefore overall, further work is needed to establish the exact mechanism by which RAD51 promotes MiDAS and protects under-replicated DNA.

An inability to resolve under-replicated DNA through MiDAS can lead to a persistence of these lesions through mitosis and into the following cell cycle which can be detected as 53BP1 nuclear bodies (Bhowmick et al., 2016; Lukas et al., 2011; Minocherhomji et al., 2015; Naim et al., 2013; Pedersen et al., 2015). 53BP1 nuclear bodies mark under-replicated DNA regions to protect them from error-prone repair pathways or excessive resection until the following S phase, where they can be repaired through HR-mediated

mechanisms. Although I did not explore this, the same may be true for RAD51 and MiDAS inhibition in early mitosis.

Overall, this work supports a role for RAD51 in non-DDR-associated MiDAS through its ssDNA binding activity. Previous reports of MiDAS have been described as a conservative process involving RAD52-mediated BIR after MUS81-dependent DSB formation and γH2AX signalling (Bhowmick et al., 2016; Lai et al., 2017; Minocherhomji et al., 2015). Recently, MiDAS events in U2OS cells have also been identified as predominantly semi-conservative (Chappidi et al., 2020), correlating with HR-mediated replication fork restart (Miyabe et al., 2015). This suggests that RAD51 and RAD52 may have distinct roles in MiDAS (**figure 3.9**). It could be proposed that RAD51 is protecting stalled or reversed replication forks at late replicating regions. These replication intermediates fail to activate the replication checkpoint and are transferred into mitosis. While some of these structures may be cleaved by MUS81 to facilitate RAD52-dependent BIR, *de novo* RAD51 recruitment may also protect some of these replication intermediates, possibly retaining the DNA replication machinery, to promote completion of replication through a non-DDR associated, as yet unknown, mechanism. This mechanism has not been explored here but several RAD51-mediated, HR-dependent and -independent mechanisms for protecting and restarting stalled forks have been described previously (Wassing & Esashi, 2021). While RAD51 has been associated with BIR, RAD51-dependent, DDR-associated MiDAS may not be favoured in mitosis due to the potential formation of aberrant chromosome fusions (Giunta et al., 2010).

3.3.3 MiDAS at centromeres and centromere fragility

Incomplete replication and the resulting mitotic defects were explored in **figures 3.5 and 3.6**. Using live cell microscopy, we demonstrated that inhibition of RAD51-mediated MiDAS leads to an insignificant delay in AO (**figure 3.5C**) indicating that persistent under-replicated DNA in mitosis prevents timely SAC satisfaction. In turn, this prolonged mitosis correlates with increased mitotic defects including lagging chromosomes, micronuclei, and mitotic cell

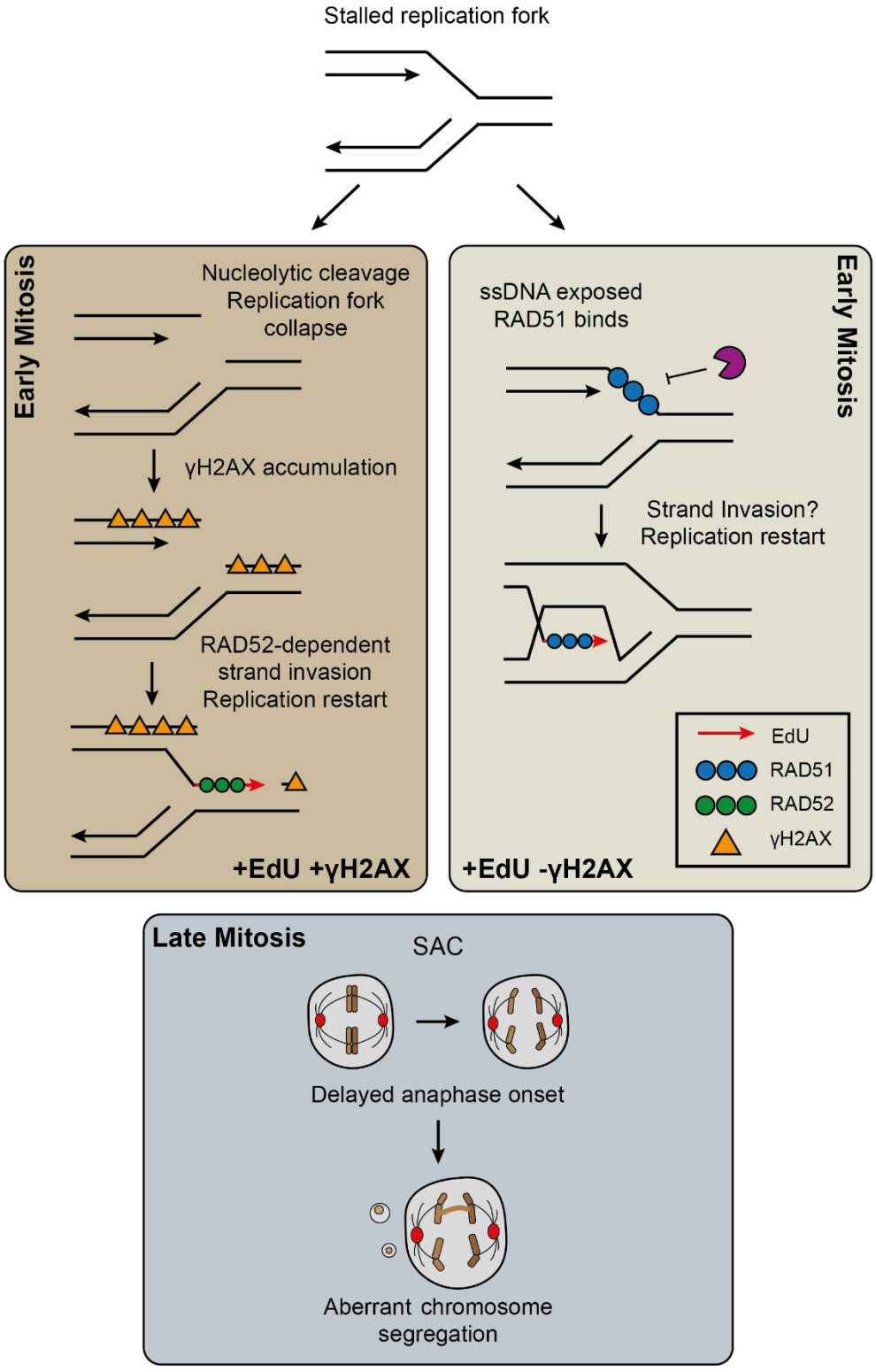


Figure 3.9 Model for RAD51-mediated MiDAS
Stalled replication forks in S phase are maintained into early mitosis where they are processed using two different pathways. The stalled fork can undergo nucleolytic cleavage, γH2AX signalling, and RAD52-dependent replication fork restart using BIR, producing EdU foci that colocalise with γ H2AX. Alternatively, ssDNA at stalled forks can be protected by RAD51 which then promotes fork restart through an unknown mechanism e.g. strand invasion or through retention of replication machinery. This is γH2AX-independent. MiDAS in early mitosis leads to delayed anaphase onset through SAC activation. Failure to complete MiDAS and premature SAC satisfaction leads to mitotic aberrations and chromosome missegregation.

death (**figure 3.6**). Under-replicated DNA has previously been associated with chromosome segregation defects and mitotic DNA damage (Calzetta et al., 2020), thereby providing further evidence that RAD51 is important for resolving under-replicated DNA in mitosis.

Replication stress and under-replicated DNA have previously associated with FANCD2-positive ultrafine anaphase bridges (FS-UFBs). FS-UFBs are thought to originate from CFSs and require structure-specific nucleases, MUS81 and GEN1, for their resolution (Chan et al., 2009). In fact, inhibition of RAD52-mediated MiDAS increases the prevalence of these FS-UFBs (Bhowmick et al., 2016; Minocherhomji et al., 2015). RAD51 has been associated with an alternative subset of UFBs termed HR-UFBs which are understood to arise from unresolved recombination intermediates or upregulated HR (Chan et al., 2018; Chan & West, 2018). In the future, it would be intriguing to investigate the connection between RAD51's mitotic role and UFB generation and whether FS-UFBs can be associated with chromatin loci other than CFSs.

There are several potential explanations for why AO is delayed upon RAD51 inhibition (**figure 3.5C**). Firstly, increased DNA damage could activate the DNA damage checkpoint to halt mitotic progression. Additionally, the SAC has previously been demonstrated to detect DNA damage at the centromere but not chromosome arms (Mikhailov et al., 2002). To further distinguish this mechanism and understand the source of delayed mitotic progression, Cas9-mediated DNA cleavage against specific centromere and chromosome regions, or other global DNA damaging agents such as TOP2 inhibitor etoposide, can be utilised alongside ATM/ATR inhibitors to assess activation of the DNA damage checkpoint, such as phosphorylation of known downstream effectors or SAC components, as has been shown previously in yeast (Kim & Burke, 2008). Furthermore, assessment of SAC protein localisation and phosphorylation at broken kinetochores in mitotic cells using IF could give additional indication of SAC activation upon DNA damage.

Nevertheless, from this we hypothesised that centromeric DNA may be enriched for damage resulting from RAD51-mediated MiDAS inhibition. Using CO-FISH to differentially

label each centromere of the sister chromatids, we examined aberrant centromere signals. **Figure 3.8A** suggests that RAD51 inhibition contributes to an accumulation of aberrant recombination events after mild replicative stress. A primary interpretation of this is that failure of RAD51 to protect under-replicated DNA and subsequent induction of DSBs may promote recombinogenic repair through a cross-over-mediated mechanism.

Cross-over recombination at the centromere is understood to drive evolution and amplification. Centromeres are considered highly recombinogenic regions of the genome (Jaco et al., 2008), nevertheless, cross-over recombination is normally suppressed at centromeres to preserve repeat integrity (Giunta & Funabiki, 2017). Given that cen-SCEs are typically suppressed in somatic cells (**section 1.7.4.2.3**), it is surprising that RAD51 (and HR) inhibition increased their prevalence .

POLQ, also known as Polθ, is largely known for its role in error-prone alt-EJ (**section 1.4.3**). POLQ has recently been linked to mutagenic SCE generation in mitosis after perturbed replication in HR-deficient cells (Heijink et al., 2021). These HR-independent SCEs were enriched in difficult-to-replicate loci including CFSs and centromeres, but not telomeres. Thus, it could be hypothesised that increased aberrant CO-FISH signals after mild replication stress in RAD51 inhibited cells may originate from ssDNA gap processing and recombination by POLQ. It would be interesting to further explore the components of MiDAS-dependent SCEs using drug inhibitors or siRNAs to understand how mitotic under-replication promotes cross-over recombination events.

Alternatively, APH-M treatment in mitosis did not significantly increase aberrant centromeric signal after replication stress compared to the DMSO treated control (**figure 3.8A**). Under this condition, MiDAS is completely abrogated and DSBs are generated. RAD51 (and RAD52) remain functional suggesting that they promote DSB repair in a non-crossover dependent manner, either through HJ dissolution or another repair pathway, which is not detectable through CO-FISH.

Additionally, we showed that both B02 and APH-M treatment led to a significant increase in centromere FISH probe signal intensity after mild replication stress (**figure 3.8B**). In CO-FISH, the centromeric FISH probes bind ssDNA and therefore this intensity measurement correlates with the prevalence of exposed ssDNA on the metaphase chromosomes. These gaps may arise due to loss of RAD51-mediated ssDNA protection, increased aberrant processing of under-replicated DNA, or as a consequence of sample generation and treatment during the CO-FISH protocol. ssDNA gaps or breaks are generally referred to as "fragility" thereby indicating that RAD51 and MiDAS function protect against centromere fragility by minimising aberrant DNA processing.

PLK1-dependent phosphorylation is required for *de novo* RAD51 recruitment to mitotic chromatin (**section 1.6.3.2**) (Wassing et al., 2021). PLK1 activity is enriched at centromeres in mitosis (Kim, 2022) providing further support for a role of RAD51 at under-replicated centromeres. However, despite this cumulative evidence, it is important to note that mitotic EdU incorporation has not been significantly observed at centromeres (Minocherhomji et al., 2015; Wassing et al., 2021). The proposed reason for this is due to the cohesin-mediated compact nature of centromeres in mitosis which may limit EdU incorporation and tract length in these regions (Wassing et al., 2021). Other sequencing-based methods have since been optimised to detect MiDAS events across the genome (Macheret et al., 2020; Macheret & Halazonetis, 2019). When combined with the recently completed full human reference genome derived from the CHM13-hTERT cell line (Nurk et al., 2022), which contains the previously excluded repetitive DNA regions including centromeres, a clearer picture of MiDAS events across all difficult-to-replicate loci will be possible to ascertain.

Overall, in this chapter, I demonstrate evidence for a role for *de novo* RAD51 recruitment in mitosis to protect under-replicated DNA and promote non-DDR-associated MiDAS. This appears to be distinct from RAD52-mediated, BIR-dependent MiDAS which requires replication fork cleavage by mitotic nucleases such as MUS81. These RAD51-dependent

MiDAS events are important for promoting timely mitotic progression and minimising mitotic chromosome segregation defects in anaphase.

Chapter 4 – Investigating the role of homologous recombination in centromere stability in RPE1 cells

4.1 Introduction

Centromeres are defined epigenetically through the presence of histone H3 variant, CENP-A. CENP-A deposition is regulated by several factors including the MIS18 complex, HJURP, and transcription (**sections 1.7.3**). Furthermore, centromeres are considered fragile regions of the genome. They are subject to numerous lesions throughout the cell cycle and studies are now beginning to explore how this damage is repaired (**section 1.7.4**).

In the previous chapter, I described evidence suggesting a role for RAD51 in protecting centromeres in mitosis in cells exposed to mild replication stress using CO-FISH (Wassing et al., 2021). Subsequently, RAD51 was identified to repair TOP2B-induced centromeric DNA breaks in quiescent non-cancerous RPE1 cells (Saayman et al., 2023). TOP2 enzymes induce DSBs to relieve torsional stress and promote efficient chromosome segregation by resolving catenated sister chromatids. Replication and transcription involve unwinding of duplex DNA which generates positively supercoiled DNA in front of the fork, and negatively supercoiled DNA behind the fork. TOP1 and TOP2 can resolve this stress to promote fork progression (Nitiss, 2009).

In this chapter, I aimed to explore the role of core canonical HR regulators: BRCA2, PALB2, and RAD51 (**section 1.4.2**), at the centromere in RPE1 cells. I investigated their importance on CENP-A levels and centromere identity, and centromere stability using Exo-FISH, a microscopy-based method utilising FISH probes to detect DNA breaks at repetitive regions (Saayman et al., 2023).

4.2 Results

4.2.1 Depleting the canonical HR factors in RPE1 cells

To investigate the role of HR factors: BRCA2, PALB2, and RAD51, in centromere identity and stability, I first depleted the proteins from RPE1 cells using siRNA. RPE1 cells were targeted with siRNA against CENP-A, BRCA2, PALB2, and RAD51 for 72 hours, by which time significant loss of protein levels could be observed by western blot, compared to the non-targeting Mission Negative (MisNeg) control (**figure 4.1A-D**).

These proteins have various cellular functions across the cell cycle and siRNA can produce indirect secondary effects which may impact interpretation of any results. Therefore, I next verified the impact of siRNA depletion for 96 hours on cell cycle progression by flow cytometry. **Figure 4.1E** shows cell cycle distribution after asynchronous cells were treated with EdU for 30 minutes to label replicating, S phase cells, and visualised using the EdU Click-IT reaction and DAPI staining. The percentage of cells in G1, S, and G2/M phase are displayed in **figure 4.1F**. siCENP-A treatment leads to a significant decrease in the S phase population and a subsequent increase in the G1 phase population. Conversely, BRCA2 and PALB2 depletion reduced the percentage of cells in G1 and markedly enriched S and G2/M phase populations. RAD51 depletion led to a significant enrichment of G2/M phase cells at 34.4% compared to 7.19% in the control sample. This agrees with previous findings that RAD51 loss impacts cell cycle progression, especially mitotic entry (Sonoda et al., 1998).

Overall, for the purpose of this study, HR factors can be depleted from RPE1 cells and so can be used to study the role of these proteins at centromeres. Nevertheless, the impact of HR factor depletion on cell cycle distribution should be taken into consideration when interpreting any results.

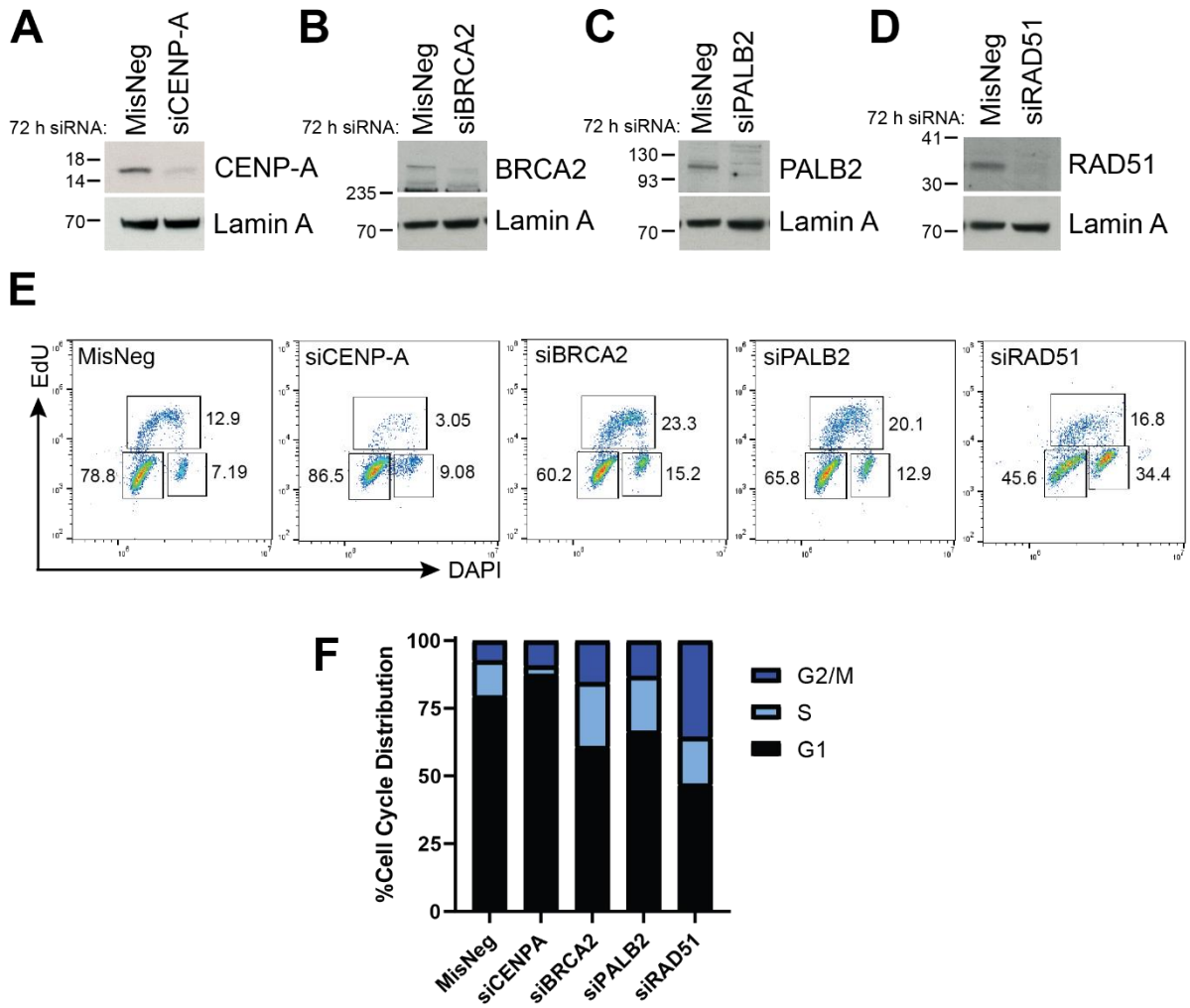


Figure 4.1 Depletion of HR factors using siRNA in RPE1 cells
A-D Depletion of CENP-A (A), BRCA2 (B), PALB2 (C), and RAD51 (D) in RPE1 cells using siRNA for 72 h. MisNeg was used as a negative control. Lamin A was used as a loading control. **E** Flow cytometry of RPE1 cells after 96 h siRNA depletion and EdU and DAPI staining. Cells in G1, S, and G2/M phase are gated and percentage of cells in each gate displayed. **F** Graph displaying quantification of percentage of cells in each cell cycle stage after siRNA depletion, as shown in E.

4.2.2 RAD51 and BRCA2, but not PALB2, impact centromere identity

Several DDR-associated factors have been linked to centromere identity across several different organisms (Mitra et al., 2014; Racca et al., 2021; Saayman et al., 2023; Yilmaz et al., 2021). Most recently, RAD51 was shown to be required to maintain CENP-A levels at the human centromere in quiescent RPE1 cells (Saayman et al., 2023). I aimed to expand on this study and investigate the impact of BRCA2 and PALB2 depletion on CENP-A levels and centromere identity.

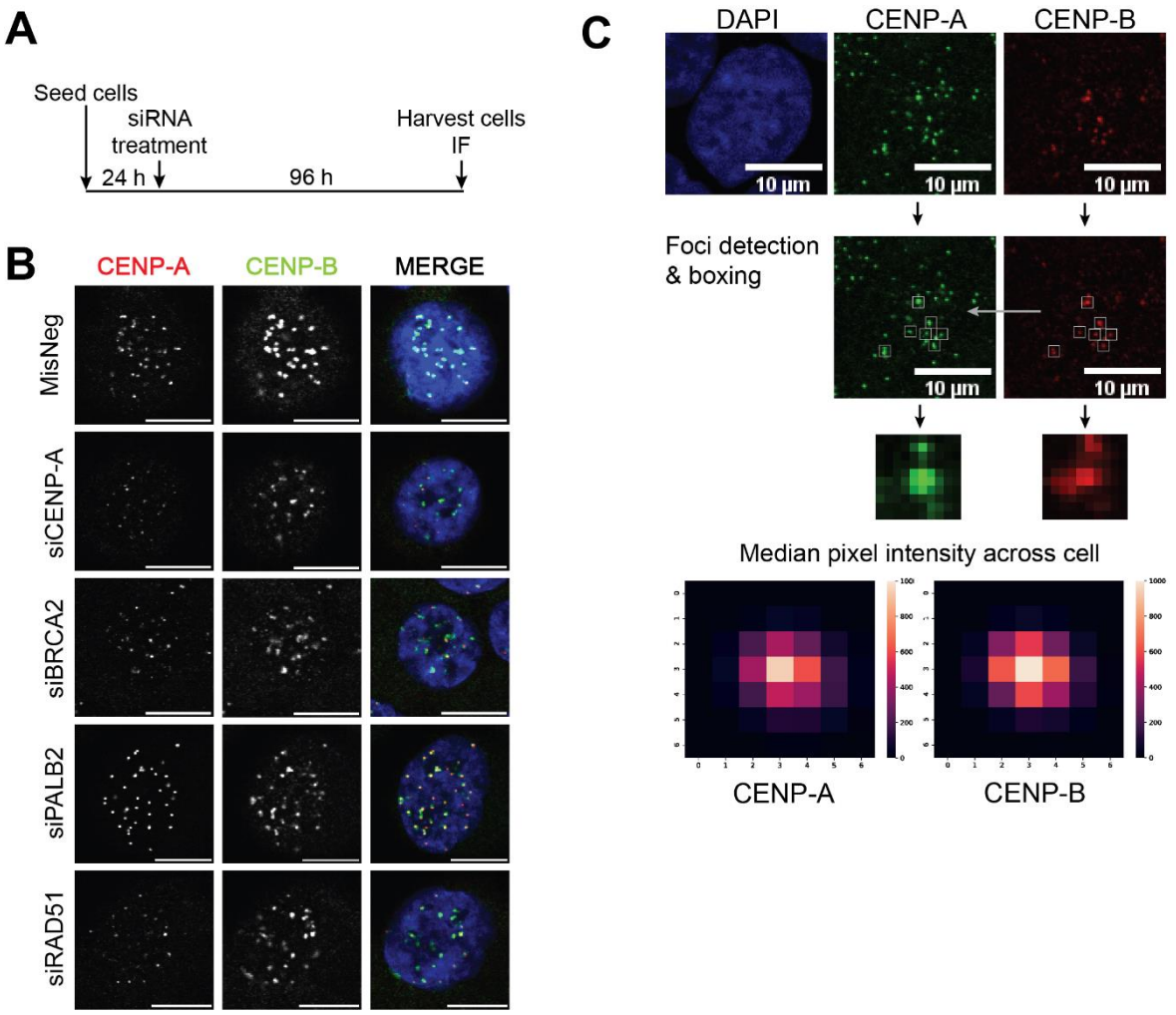


Figure 4.2 Measuring CENP-A levels at CENP-B-defined centromeres using IF
A Schematic of treatment protocol. **B** Representative images after 96 h siRNA treatment in asynchronous RPE1 cells. Scale bar equals 10 µm. **C** Schematic of analysis pipeline for CENP-A and CENP-B foci intensity quantification. Scale bar equals 10 µm.

To this end, I conducted IF against CENP-A and CENP-B on asynchronous RPE1 cells after 96 hour siRNA treatment (**figures 4.2A and B**). CENP-B was used to define the centromere as a sequence-specific member of the CCAN. To analyse CENP-A levels at CENP-B-defined centromeres, CENP-A and CENP-B foci were detected in each DAPI-defined nucleus using ImageJ analysis software. Using the defined CENP-B locus, a 10x10 or 12x12 pixel box (~2x2/2.5x2.5 µm box where 1 pixel equals approximately 0.2 µm, images taken at 100X magnification) was drawn around the foci and transposed onto the CENP-A image. The CENP-B and CENP-A foci intensity within this box was then measured

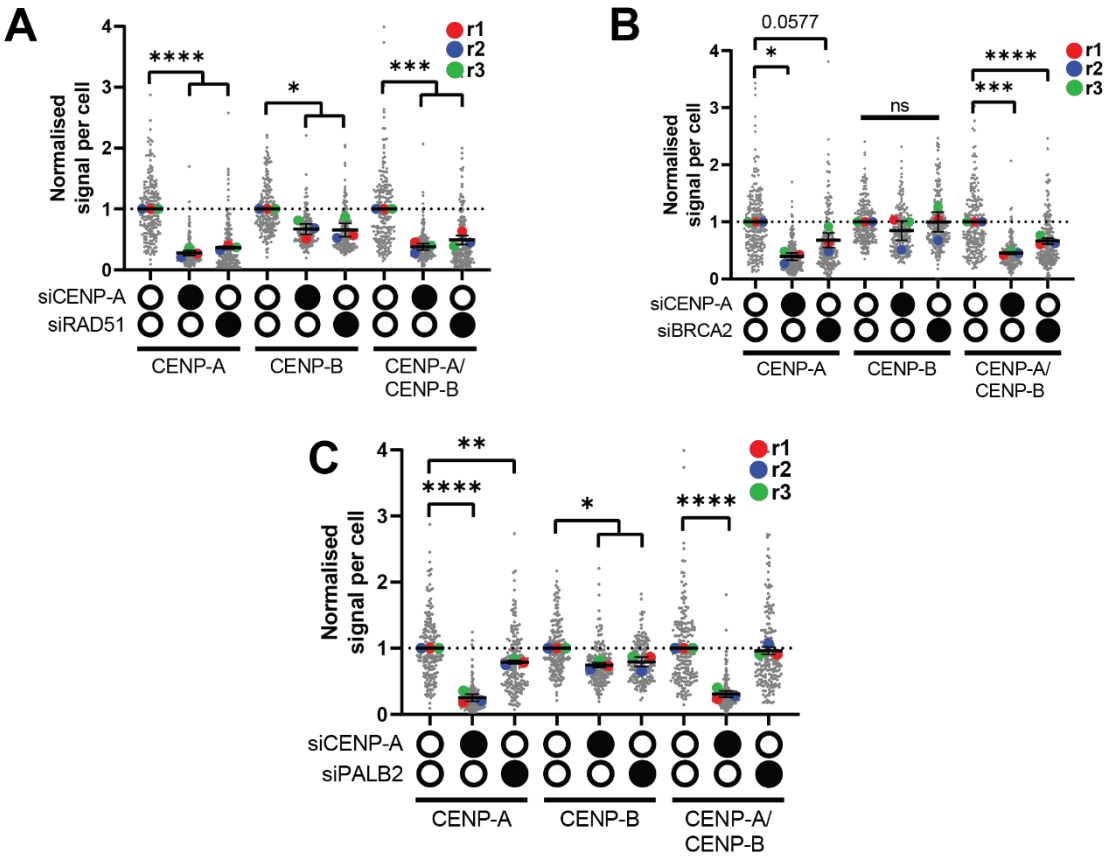


Figure 4.3 HR factor depletion impacts centromere identity
A-C Quantification of CENP-A foci signal, CENP-B foci signal, and normalised CENP-A/CENP-B signal for CENP-A, RAD51 (A), BRCA2 (B), and PALB2 (C) depleted RPE1 cells. For each measurement, signal was normalised to the MisNeg control. n=3. At least 100 cells analysed per condition, per repeat. Large coloured dots represent the mean of each repeat. Error bars represent S.E.M. Unpaired one-way ANOVA with Dunnett's multiple comparisons test. Filled circles represent treated sample.

and the median foci intensity across the nucleus was calculated using Python and plotted using a heatmap with or without background signal subtraction (**figure 4.2C, section 2.8.3**). The median pixel intensity was plotted and compared across different conditions.

As expected, CENP-A and CENP-B largely colocalised within the nucleus (**figure 4.2B**). CENP-A depletion was included as a positive control, producing a significant decrease in CENP-A signal per cell but largely unaffecting CENP-B signal (**figure 4.3A-C**). In agreement with previous publications, RAD51 depletion also resulted in a significant reduction in CENP-A signal intensity, both alone and when normalised to CENP-B levels (**figure 4.3A**) (Saayman et al., 2023).

Interestingly, upon BRCA2 depletion, there was a mild decrease in CENP-A levels compared to MisNeg treated controls (**figure 4.3B**). This significance was increased when the CENP-A signal was normalised to CENP-B. Surprisingly, while PALB2 depletion led to a very modest but significant decrease in CENP-A levels, this difference was lost when normalised to CENP-B signal (**figure 4.3C**). This indicates that while RAD51 and BRCA2 appear to impact centromere identity in asynchronous RPE1 cells, PALB2 is distinct from this function and does not significantly influence CENP-A levels at the CENP-B-defined centromere.

4.2.3 Impact of BRCA2 on centromere identity in non-cycling cells

CENP-A levels fluctuate throughout the cell cycle. CENP-A nucleosomes are diluted between replicated daughter DNA strands in S phase (Zasadzińska et al., 2018) and new CENP-A is not loaded at the centromere until the following G1 phase (**section 1.7.3**) (Jansen et al., 2007). Therefore, I next wanted to explore the impact of the cell cycle on centromere identity after BRCA2 and RAD51 depletion in RPE1 cells.

To address this, I induced a state of quiescence (G_0) in RPE1 cells using serum-starvation. Quiescence is a state of reversible growth arrest where cells cease to divide but is distinct from senescence and terminal differentiation as cells maintain the capacity to restart cell division once serum-starvation is removed. Serum contains a combination of growth factors that promote cellular proliferation; removal of these factors results in growth factor deprivation and induces quiescence via inhibition of growth factor signalling pathways (Marescal & Cheeseman, 2020). In short, cells were incubated with cell culture medium supplemented with 0.1% FBS for 24 hours to induce a quiescence-like state before siRNA transfection, the cells were then replenished with fresh serum-starved media every 24 hours (**figure 4.4A**). CENP-A, BRCA2, RAD51, and PALB2 can all be substantially depleted from serum-starved RPE1

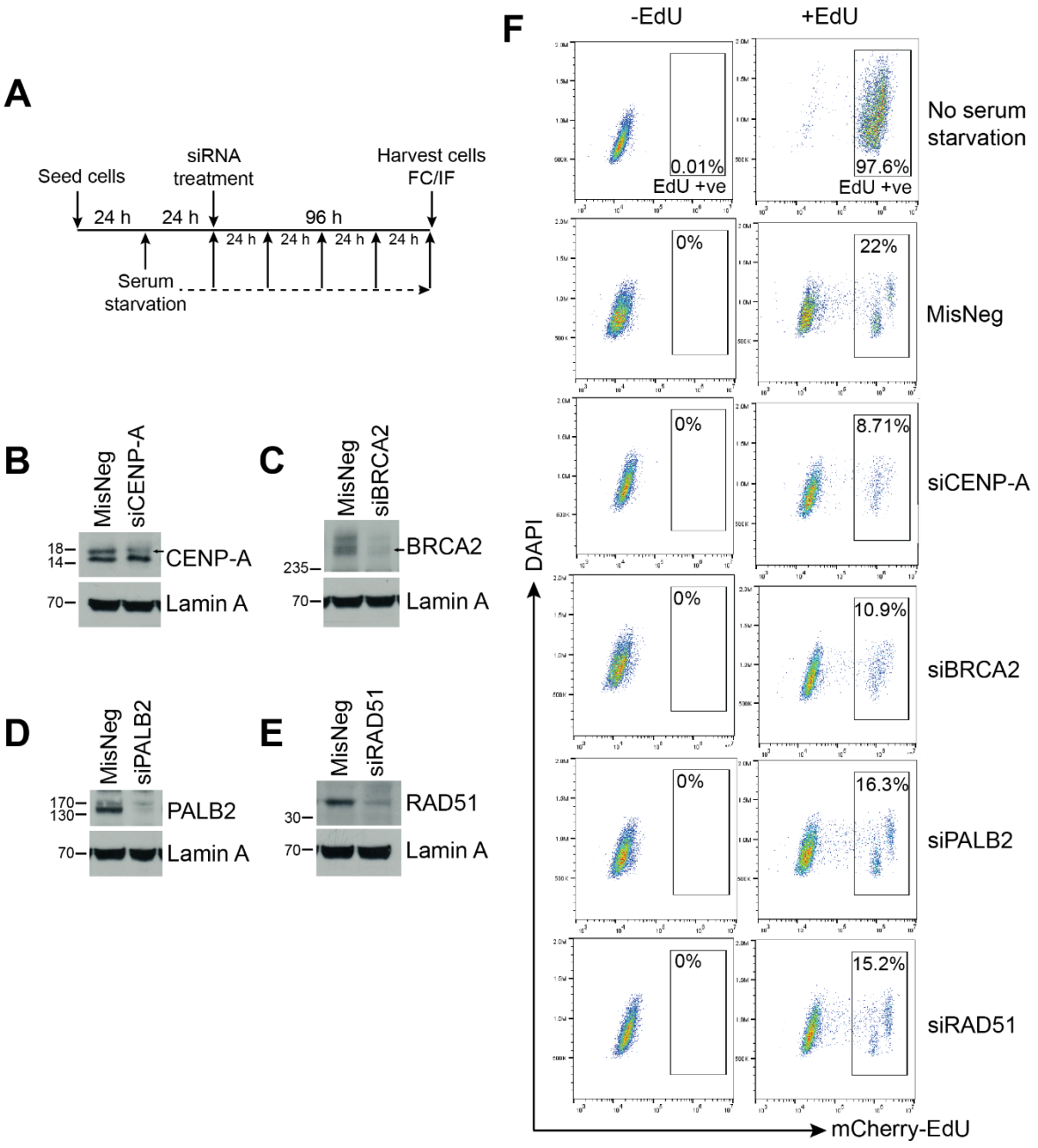


Figure 4.4 Inducing quiescence in HR-depleted RPE1 cells
A Schematic of protocol to induce quiescence and siRNA depletion in RPE1 cells using serum-starved culture media. Serum-starved media was replaced every 24 h. Cells were harvested for flow cytometry (FC) or IF after 96 h. **B-E** Western blots showing siRNA depletion of CENP-A (B), BRCA2 (C), PALB2 (D), and RAD51 (E) compared to siRNA control (MisNeg) after 96 h in serum-starved RPE1 cells. Lamin A was used as a loading control. **F** Flow cytometry profiles showing percentage of cells displaying EdU incorporation after 96 h siRNA depletion and quiescence, compared to normal cycling cells (no serum starvation).

cells (**figure 4.4B-E**) and show marked reduction in EdU incorporation compared to untreated, cycling controls by flow cytometry (**figure 4.4F**).

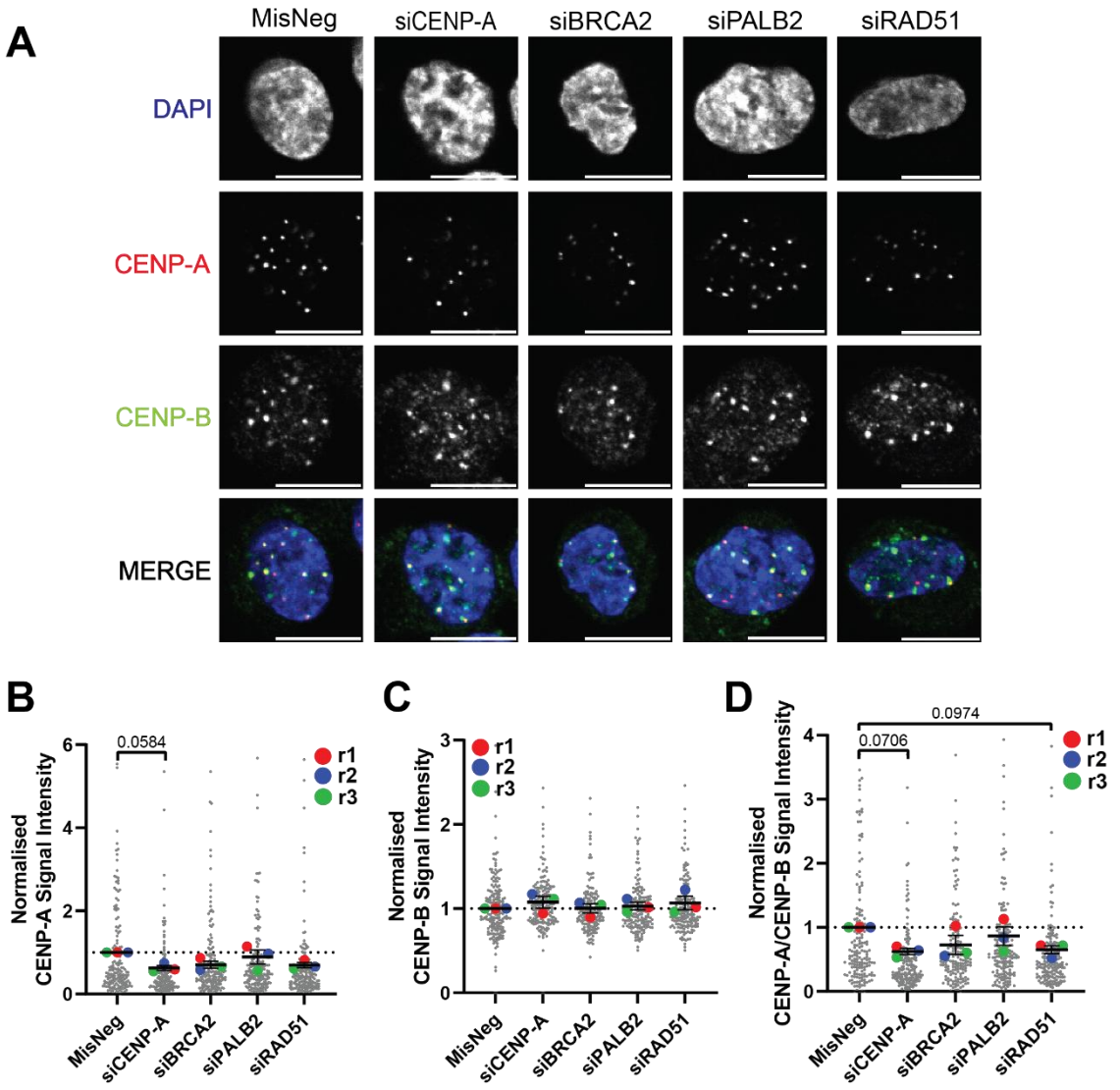


Figure 4.5 The impact of HR factors on centromere identity in quiescence RPE1 cells
A Representative images of IF staining for CENP-A and CENP-B in serum-starved RPE1 cells after 96 h siRNA depletion. Scale bar equals 10 μm. **B** Graph showing CENP-A signal intensity in serum-starved RPE1 cells after 96 h siRNA treatment. Samples normalised to MisNeg control. **C** Graph showing CENP-B signal intensity in serum-starved RPE1 cells after 96 h siRNA treatment. Samples normalised to MisNeg control. **D** Graph showing normalised CENP-A/CENP-B signal intensity in serum-starved RPE1 cells after 96 h siRNA treatment. Samples also normalised to MisNeg control. Large coloured data points represent average of each repeat. n=3. At least 100 cells analysed per repeat. Error bars represent S.E.M. Unpaired one-way ANOVA with Dunnett's multiple comparison's test.

Using these quiescent cells, I next assessed the impact of HR factor depletion on CENP-A levels as before in **section 4.2.2**. Quantification of CENP-A and CENP-B signal intensity in serum-starved RPE1 cells (**figure 4.5A**) showed no significant differences in CENP-A or CENP-B signal intensity across all samples (**figure 4.5B and C**). However, only RAD51

depletion produced a consistent but insignificant decrease in signal intensity when the CENP-A signal was normalised to CENP-B (**figure 4.5D**). This might suggest that BRCA2 and RAD51 influence CENP-A levels through different mechanisms and the impact of BRCA2 depletion on CENP-A levels is dependent on the cell cycle.

4.2.4 BRCA2 impacts centromeric ssDNA gaps but not DNA breaks

Centromeres have been described as highly recombinogenic regions of the genome (Giunta & Funabiki, 2017; Jaco et al., 2008) (**section 1.7.4.2.3**) suggesting that they are subject to frequent DNA breaks that may require the HR machinery for repair. In fact, RAD51 has now been associated with limiting spontaneous DNA breaks at the centromere in quiescent RPE1 cells (Saayman et al., 2023).

Since BRCA2, PALB2, and RAD51 form a tight complex in HR-mediated DNA break repair, I next wanted to explore their potential role in maintaining centromere stability and integrity in RPE1 cells. To do this, I employed Exo-FISH, a technique first described and utilised in (Saayman et al., 2023). Exo-FISH is a microscopy-based technique that can be used to detect SSBs, including DNA nicks and gaps, and DSBs generated *in vivo* on a single-cell level (**figure 4.6A**). Firstly, asynchronous interphase cells are collected, fixed, and dropped onto glass slides. The cells then undergo a series of pre-treatment steps including RNase A treatment to remove RNA molecules including RNA-DNA hybrids, before the SSBs and DSBs are digested using Exonuclease III (ExoIII) to generate regions of ssDNA. ExoIII is a DNA specific exonuclease that catalyses nucleotide removal in a 3’ to 5’ direction from DNA nicks or blunt-ended and 5’ overhang DSBs. Exposed ssDNA can subsequently be detected using fluorescently labelled complementary FISH probes. Therefore, any increase in centromeric DNA breaks will allow increased ExoIII digestion, exposing more ssDNA, and generating higher FISH signal intensities. In these experiments, I used FISH probes complementary to the 17 bp CENP-B box present throughout the centromeric α-satellite repeats to label the centromeres (cenFISH) and probes complementary to telomeric repeats to label telomeres (telFISH). Exo-FISH images were analysed using a similar

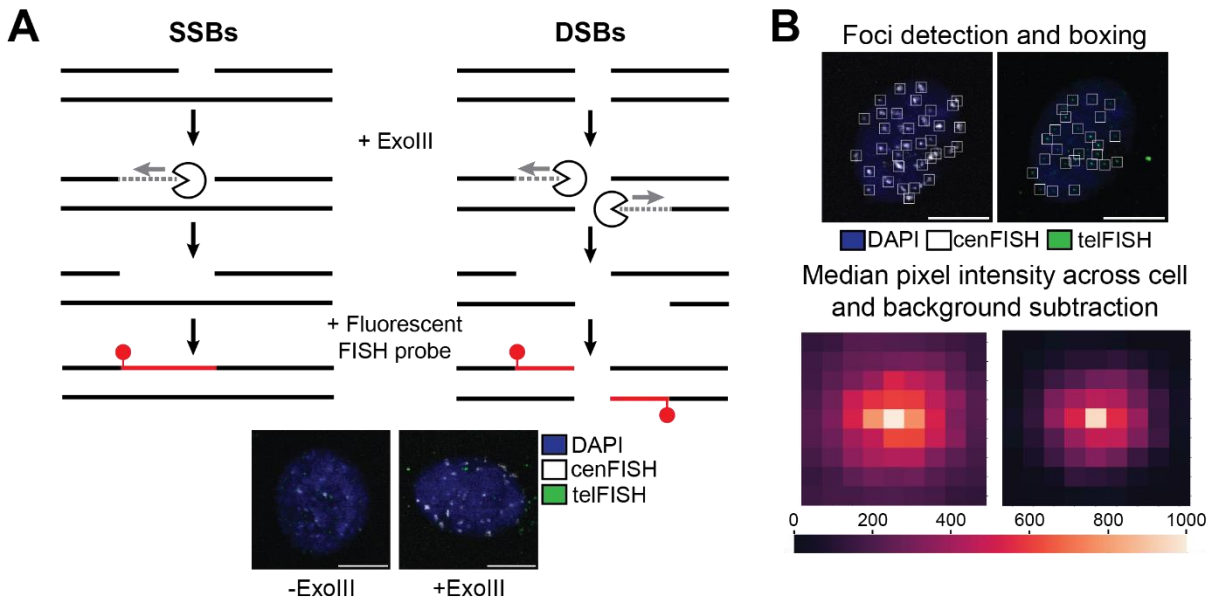


Figure 4.6 Exo-FISH to measure centromere stability
A Schematic of Exo-FISH protocol. SSBs and DSBs generated *in vivo* are digested by Exonuclease III (ExoIII) *in vitro* exposing ssDNA which can be detected using centromere (cenFISH) or telomeric (telFISH) specific FISH probes by microscopy. Scale bar equals 10 μm. **B** Work flow of Exo-FISH analysis. Scale bar equals 10 μm.

methodology to CENP-A level analysis described in **section 4.2.2** (**figure 4.6B**) except cenFISH and telFISH foci were defined and measured separately.

To assess the role of BRCA2, PALB2, and RAD51 in centromere stability, I treated asynchronous RPE1 cells with siRNA, as before, and processed the samples for Exo-FISH (**figure 4.7A**). Overall, ExoIII treatment produced an increase in cenFISH signal intensity (**figure 4.7B**). Interestingly, telFISH signal intensity was significantly lower than cenFISH signal and was generally less responsive to ExoIII or siRNA treatment (**figure 4.7C-F**). **Figures 4.7C-F** show that ExoIII treatment on MisNeg control samples leads to an increase in cenFISH signal, likely representing digestion of spontaneous DNA breaks that arise at the centromere across the cell cycle (Saayman et al., 2023). Surprisingly, BRCA2 depletion produces a significant increase in cenFISH signal, irrespective of ExoIII treatment (**figure 4.7C**). This could indicate increased exposure of ssDNA under these conditions, but that this is not necessarily dependent on DNA break induction as there is no additional increase

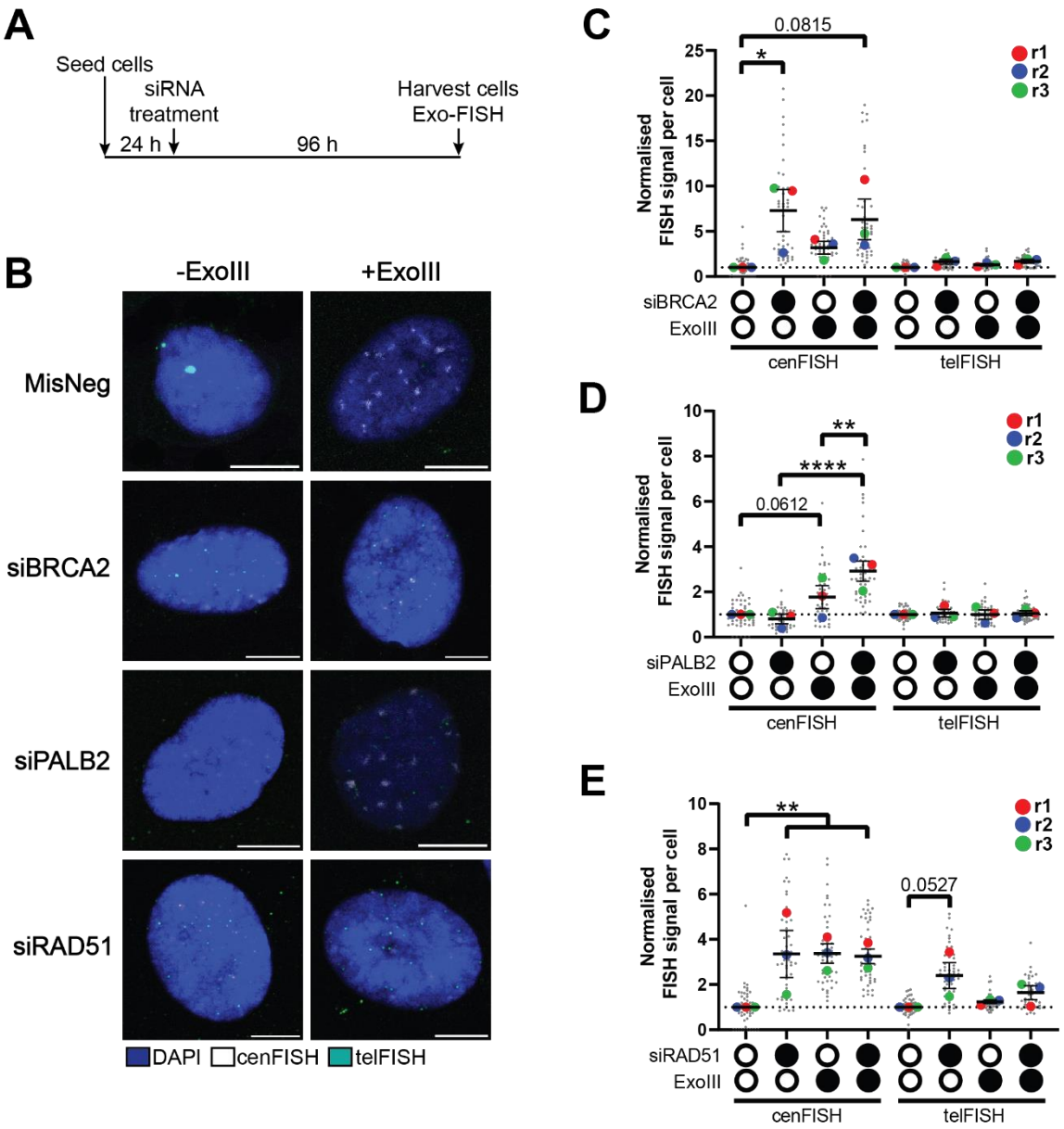


Figure 4.7 The impact of HR factors on centromere stability using Exo-FISH
A Schematic of siRNA treatment protocol for Exo-FISH. **B** Representative images of Exo-FISH after 96 h siRNA treatment. Scale bar equals 10 μm. **C-E** Graphs showing impact of HR factor depletion (BRCA2 (C), PALB2 (D), and RAD51 (E)) on Exo-FISH signal. Samples were normalised to MisNeg cenFISH or telFISH signal without ExoIII treatment. Large coloured datapoints represent average of each independent repeat. n=3. At least 15 cells analysed per condition, per repeat. Error bars represent S.E.M. Unpaired one-way ANOVA with uncorrected Fisher's LSD.

after ExoIII digestion. Conversely, PALB2 depletion produced no significant difference in cenFISH signal in the absence of ExoIII treatment (**figure 4.7D**). However, upon ExoIII treatment PALB2 depletion resulted in a significant increase in cenFISH signal compared to MisNeg, suggesting that PALB2 is important for minimising or repairing DNA breaks at

centromeres. Finally, similar to BRCA2 depleted samples, although to a lesser extent, RAD51 depletion increased cenFISH signal in the absence of ExoIII treatment suggesting that these samples also have increased ssDNA exposure (**figure 4.7E**). Furthermore, ExoIII treatment did not cause an additional increase in cenFISH signal. Intriguingly, telFISH signal was more sensitive to siRAD51 treatment, creating larger fluctuations compared to BRCA2 and PALB2 depleted samples. This suggests that RAD51 impacts both centromeres and telomere stability in asynchronous RPE1 cells.

Overall, these findings indicate that in asynchronous RPE1 cells, BRCA2 depletion increases the level of exposed ssDNA at centromeres, but not necessarily DNA breaks. PALB2 depletion leads to a significant increase in centromeric DNA breaks, and RAD51 impacts both centromere and telomere stability.

The centromeric chromatin contains large proteinaceous complexes i.e. CENP-A and the CCAN (**section 1.7.1**), and complex secondary DNA structures including DNA hairpin loops maintained by condensin molecules (Aze et al., 2016) (**section 1.7.4.2**). Furthermore, various DNA repair intermediates, breaks, or ssDNA stretches may be protected by DNA binding proteins such as RPA or RAD51. Collectively, this complex chromatin environment may conceal DNA substrates from ExoIII digestion, limiting the sensitivity of cenFISH signal generation. To explore this idea, I modified the Exo-FISH protocol to include a pepsin pre-treatment step (**figure 4.8A**). Pepsin is a protease that removes chromatin-bound proteins and so I propose that inclusion of this step may expose additional regions of ssDNA or DNA breaks susceptible to ExoIII-mediated digestion and FISH probe binding.

Hence, asynchronous RPE1 cells were treated as in **figure 4.7A** and processed for Exo-FISH staining, this time including a pepsin pre-treatment step. Pepsin treatment itself increased the FISH signal intensity although telFISH signal remained overall less responsive to ExoIII and siRNA treatment (**figure 4.8B**). Inclusion of the pepsin pre-treatment step in BRCA2 depleted cells still generates significantly increased cenFISH signal in the absence of ExoIII treatment, compared to the MisNeg control, again indicating

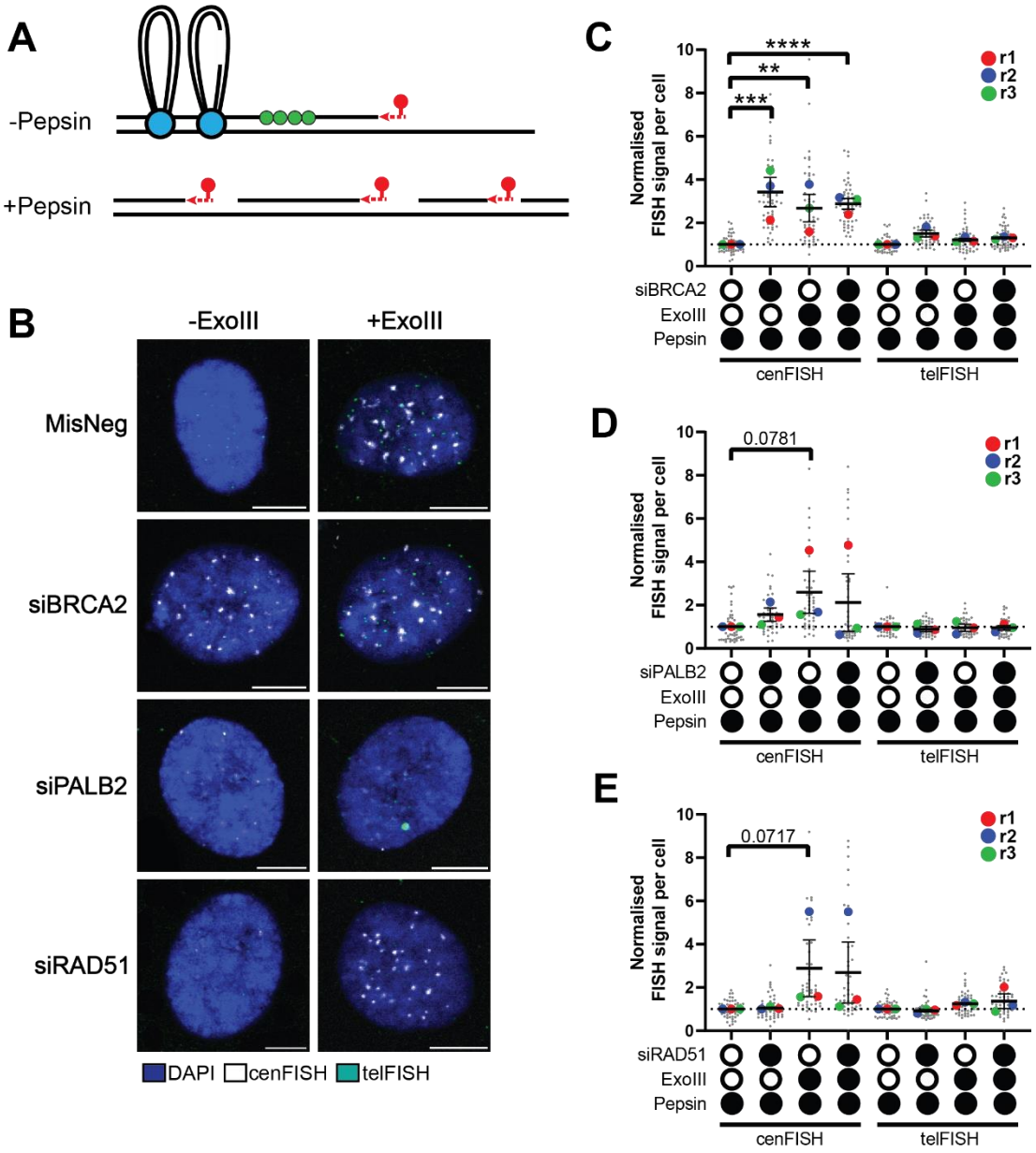


Figure 4.8 Impact of HR factors on centromere stability by Exo-FISH after pepsin pretreatment
A Model for the proposed impact of pepsin pre-treatment on Exo-FISH signal. Red arrowed probes reflect sites exposed for ExoIII digestion and FISH probe binding. **B** Representative images of asynchronous interphase RPE1 cells after Exo-FISH staining including pepsin pre-treatment. Scale bar equals 10 µm. **C-E** Graphs showing cenFISH and telFISH signal after 96 h siRNA depletion (BRCA2 (C), PALB2 (D), and RAD51 (E)) and pepsin treatment. Large coloured data points represent the average of each independent repeat. n=3. At least 15 cells imaged per condition, per repeat. Signal was normalised to MisNeg -ExoIII control of cenFISH and telFISH, respectively. Unpaired one-way ANOVA with uncorrected Fisher's LSD.

that ssDNA is enriched at the centromere under these conditions (**figure 4.8C**). While ExoIII digestion significantly increased cenFISH signal in MisNeg treated samples, there was no significant difference upon BRCA2 depletion and no further increase compared to the ExoIII

untreated sample. Neither PALB2 nor RAD51 depletion significantly increased cenFISH signal compared to MisNeg controls in the ExoIII untreated sample suggesting that these proteins do not influence the exposure of ssDNA on centromeric chromatin (**figure 4.8D and E**). With ExoIII treatment, while cenFISH signal increased, this was not significantly different from MisNeg treated samples in either PALB2 or RAD51 depleted conditions.

Combined, these results suggest that BRCA2 is important in regulating the levels of ssDNA at centromeres in asynchronous RPE1 cells but does not appear to influence the level of centromeric DNA breaks. PALB2 may have some impact on centromeric DNA breaks and stability although this is highly variable. And finally, RAD51 also likely maintains centromere and telomere stability but does not appear to influence centromeric ssDNA exposure in cycling RPE1 cells.

4.2.5 BRCA2-dependent centromeric ssDNA exposure is cell cycle-dependent

ssDNA can originate from several sources including replication, transcription/replication stress, for example torsional stress resulting from dsDNA unwinding, and DNA repair intermediates. Centromeres have previously been characterised as difficult-to-replicate regions and are susceptible to replication stress (**section 1.7.4.2**) (Aze et al., 2016; Black & Giunta, 2018; Giunta et al., 2021). I demonstrated in **section 4.2.4** that BRCA2 depletion results in an accumulation of endogenous centromeric ssDNA, as detected by Exo-FISH. I next aimed to further explore the source of this ssDNA by utilising serum-starvation in RPE1 cells to determine whether this signal was cell cycle-dependent. Serum-starvation and siRNA-mediated protein depletion was employed as described previously (**figure 4.4A**) and Exo-FISH signal assessed with or without pepsin pre-treatment (**figure 4.9**).

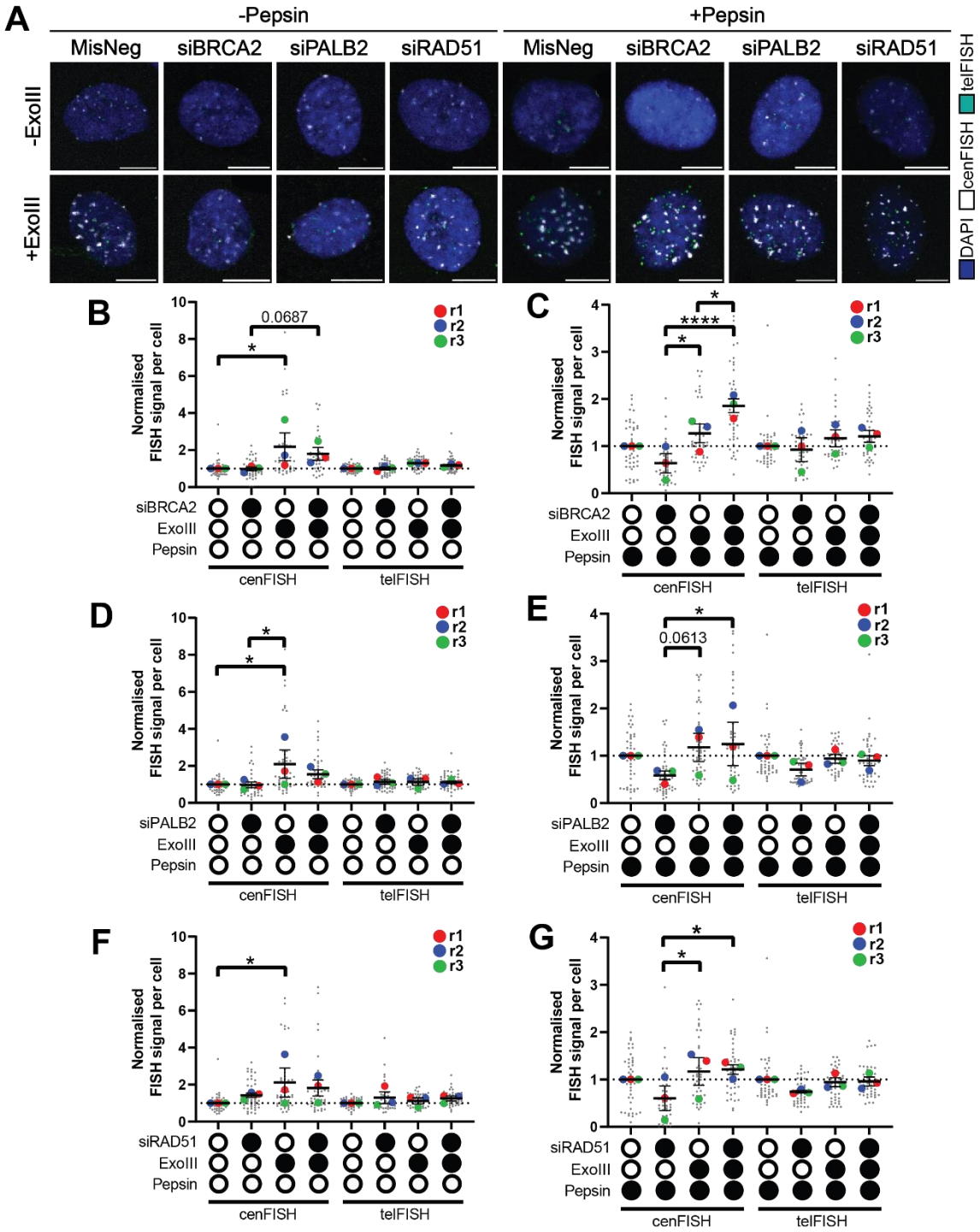


Figure 4.9 Impact of HR factors on centromere stability using Exo-FISH in quiescent RPE1 cells
A Representative images of Exo-FISH in serum-starved RPE1 cells after 96 h siRNA depletion. Scale bar represents 10 µm. **B,D,F** Exo-FISH, without pepsin pre-treatment, after 96 h siRNA depletion (BRCA2 (B), PALB2 (D), RAD51 (F)) in serum-starved RPE1 cells. **C,E,G** Exo-FISH, including pepsin pre-treatment, after 96 h siRNA depletion (BRCA2 (C), PALB2 (E), RAD51 (G)) in serum-starved RPE1 cells. Error bars represent S.E.M. Signal normalised to MisNeg -ExoIII cenFISH or telFISH signal. Large coloured datapoints represent average of each independent repeat. At least 15 cells analysed per condition, per repeat. Unpaired one-way ANOVA with uncorrected Fisher's LSD.

cenFISH and telFISH signal generation was not affected by serum-starvation (**figure 4.9A**). Upon serum-starvation, in the absence or presence of pepsin pre-treatment, the increased cenFISH signal without ExoIII treatment was abrogated in BRCA2 depleted cells (**figure 4.9B and C**). This indicates that the increased centromeric ssDNA that accumulated in BRCA2 deficient cells was cell cycle-dependent. Interestingly, with pepsin pre-treatment, BRCA2 depletion now leads to an increased cenFISH signal compared to MisNeg controls after ExoIII treatment (**figure 4.9C**) suggesting that BRCA2 plays a role in repairing DNA lesions in non-cycling, quiescent RPE1 cells. Exo-FISH results after PALB2 and RAD51 depletion in serum-starved RPE1 cells reflect what was observed previously (**section 4.2.4**) (**figures 4.9D,E,F,G**). PALB2 and RAD51 depletion did not significantly alter cenFISH signal after ExoIII treatment compared to the MisNeg control, with or without pepsin pre-treatment. It is also important to note that decreased cenFISH signal was observed in pepsin treated, ExoIII untreated, quiescent cells when all three HR factors were depleted (**figure 4.9C,E,G**).

In conclusion, these experiments suggest that BRCA2 may function to limit ssDNA accumulation or dsDNA unwinding at centromeres and that this ssDNA generation is dependent on the cell cycle. This subsequently revealed a potential role for BRCA2 in repairing or mitigating centromere DNA breaks in quiescent cells. RAD51 likely functions to maintain both centromere and telomere stability in asynchronous but not quiescent RPE1 cells. PALB2 does not consistently impact centromere stability, either through ssDNA accumulation or DNA break induction, in asynchronous and serum-starved RPE1 cells. Ultimately suggesting that the canonical HR pathway may not be vital for maintaining centromere stability.

4.3 Discussion

4.3.1 Understanding the role of HR factors in centromere identity

In this chapter, I demonstrated the effect of BRCA2, PALB2, and RAD51 factor depletion on CENP-A levels and centromere identity. RAD51 was shown to lead to a decrease in

CENP-A levels in asynchronous and serum-starved RPE1 cells (**figures 4.3A and 4.5D**). BRCA2 was also observed to reduce CENP-A levels at CENP-B-defined centromeres when depleted from asynchronous cells (**figure 4.3B**), however this phenotype was lost upon serum-starvation (**figure 4.5D**). Intriguingly, PALB2 depletion did not significantly impact centromere identity under any of the conditions analysed (**figures 4.3C and 4.5D**). This implies that canonical HR does not play a role in maintaining CENP-A levels and that BRCA2 and RAD51 play a distinct role from PALB2 in this context at centromeres.

The finding that RAD51 depletion correlates with a reduction in CENP-A levels at CENP-B-defined centromeres in asynchronous and quiescent cells agrees with previous publications (Saayman et al., 2023). RAD51 depletion using siRNA delays the cell cycle through activation of G2 arrest (**figure 4.1F**) (Sonoda et al., 1998). While Saayman et al., also used siRNA to deplete RAD51 from RPE1 cells it is unlikely that this centromere phenotype is an artefact of RNA interference as small molecular inhibitor of RAD51, B02, also recapitulates the reduced CENP-A levels (Xanita Saayman, unpublished). Furthermore, RAD51 depletion also reduces CENP-A levels at centromeres in serum-starved, non-cycling RPE1 cells (**figure 4.5D**), implying that this is not a cell cycle artefact.

Similarly, BRCA2 depletion reduced CENP-A levels at centromeres in asynchronous but not serum-starved cells (**figure 4.3B and 4.5D**). This suggests that BRCA2's role across the cell cycle is important for maintaining centromere identity. Chromatin-bound CENP-A levels fluctuate throughout the cell cycle. During S phase and DNA replication, HJURP associates with the MCM2/7 helicase complex to bind CENP-A-containing nucleosomes and promote their retention and incorporation into the replicated daughter strands, thus diluting CENP-A across the chromatin (Zasadzińska et al., 2018). This is distinct from canonical nucleosomes which are disassembled ahead of the advancing replication fork. Empty DNA patches are filled with histone H3.3-containing nucleosomes as place holders until they can be replaced with nascent CENP-A molecules in the following G1 phase (Dunleavy et al., 2011; Jansen et al., 2007). New CENP-A-containing nucleosomes are

deposited onto chromatin by the MIS18 complex and HJURP (**section 1.7.3**) (Barnhart et al., 2011; Fujita et al., 2007; Hayashi et al., 2004; Moree et al., 2011; Wang et al., 2014). Given this information, siRNA-mediated BRCA2 depletion leads to a small enrichment of S phase cells (**figure 4.1F**) which could partially explain the impact on CENP-A levels. However, this is unlikely as PALB2 depletion produced a similar effect on cell cycle distribution but does not significantly impact centromere identity (**figure 4.3C**), ultimately indicating that BRCA2 activity is specifically influencing CENP-A levels through an unknown mechanism.

PALB2 depletion did not significantly impact CENP-A levels in either asynchronous or serum-starved RPE1 cells (**figure 4.3C and 4.5D**). This could imply that BRCA2 and RAD51 have a role in protecting centromere identity which is separate and distinct from their role in canonical HR repair with PALB2. Therefore, the question remains as to what function BRCA2 and RAD51 may be serving to regulate centromeric CENP-A levels. In quiescent RPE1 cells, it was identified that RAD51 promotes *de novo* CENP-A deposition and repair at sites of TOP2B-induced DNA breaks (Saayman et al., 2023). The exact purpose of CENP-A turnover in quiescent-like cells is still unknown although it is thought to be required to facilitate future chromosome segregation and maintain the proliferative potential (Swartz et al., 2019). The redundancy of PALB2 and BRCA2 in this context suggests that other, currently unknown factors are required for RAD51 recruitment and function in quiescent cells.

It remains possible that RAD51 differentially regulates CENP-A levels in asynchronous cells, dependent or independent of BRCA2 activity. Unpublished work from my lab demonstrates that RAD51 depletion reduces *de novo* CENP-A deposition at centromeres in HeLa cells (Xanita Saayman, unpublished). It is currently unknown whether BRCA2 is impacting nascent CENP-A loading or maintenance within the centromeric chromatin across the cell cycle. Several cellular systems have been generated to investigate this including exogenously overexpressed SNAP-CENP-A (Jansen et al., 2007) and

endogenously tagged Halo-CENP-A (Swartz et al., 2019). Both systems involve the modification of CENP-A with a tag which can be covalently and irreversibly inactivated or labelled. Utilising various pulse-chase and quench-chase-pulse experiments, CENP-A turnover or loading at centromeres can be visualised by microscopy. Experiments such as these would ultimately increase our confidence that BRCA2 is directly regulating *de novo* CENP-A deposition in G1 or maintenance during S phase, rather than producing artefacts of cell cycle differences and S phase dilution.

Overall, I have provided evidence suggesting a role for BRCA2 and RAD51 in influencing CENP-A levels at CENP-B-defined centromeres, which is likely separate from their canonical role in HR with PALB2. However further work needs to be conducted to establish the exact mechanism of this relationship.

4.3.2 Understanding the role HR factors in centromere stability

The canonical HR factors are most strongly associated with DNA break repair and replication fork stability by limiting extended ssDNA gap formation (**sections 1.4.2 and 1.5**). Centromeres have been shown to be highly recombinogenic regions of the genome (Giunta & Funabiki, 2017; Jaco et al., 2008) and RAD51 has previously been demonstrated to repair centromere DNA breaks in quiescent RPE1 cells (Saayman et al., 2023). Hence, I next wanted to expand these findings and explore the role of BRCA2, PALB2, and RAD51 in centromere stability.

I utilised Exo-FISH, a microscopy-based technique to visualise DNA breaks generated *in vivo* at centromeres, at a single cell level (Saayman et al., 2023). Addition of ExoIII to asynchronous RPE1 cells treated with MisNeg control siRNA revealed the presence of spontaneous DNA centromere breaks (**figures 4.7C-F and 4.8C-E)**, as shown previously in (Saayman et al., 2023). This is not inherently surprising as it is understood that human cells undergo approximately 70,000 lesions per day (Lindahl & Barnes, 2000) and Exo-FISH can theoretically detect endogenous DNA nicks including Okazaki fragments. Centromeres themselves are subject to topoisomerase activity including TOP1 in S phase (Aze et al.,

2016) and TOP2A and TOP2B in S phase and mitosis, to resolve torsional stress and DNA catenanes (Pommier et al., 2022), and quiescent cells to promote CENP-A loading (Saayman et al., 2023).

Interestingly, telFISH signal using telomere-specific probes was not significantly influenced by ExoIII treatment across almost all conditions (**figures 4.7C-D and 4.8C-E**). This is likely due to the presence of T-loops which may not be susceptible to ExoIII-mediated digestion. Due to this, future experiments could be improved through inclusion of FISH probes specific to chromatin environments that are more similar to the core functional centromere such as pericentromere-associated satellite repeats: human satellites 2 and 3. This would allow more direct comparisons and increase the confidence that any proteins-of-interest function at centromeres specifically.

Depletion of the canonical HR factors in asynchronous RPE1 cells showed varying phenotypes. BRCA2 depletion showed increased cenFISH signal, even in the absence of ExoIII treatment (**figure 4.7C**). Given the absence of DNA digestion under this condition, this implies an endogenous accumulation of ssDNA that can bind cenFISH probes. This result was further confirmed when I modified the Exo-FISH protocol to include a pepsin pre-treatment step (**figures 4.8A and C**), removing chromatin-bound proteins to theoretically further expose centromeric ssDNA and DNA breaks. ssDNA can arise from replication- and transcription-associated torsional stress, PRIMPOL-mediated repriming, displaced ssDNA from R-loops, or DNA resection and DNA repair intermediates. Centromeres are transcriptionally active regions of the genome where R-loops can accumulate and cause TRCs (Giunta et al., 2021) (**section 1.7.4.2.2**). BRCA2 protects against R-loop formation and aids in their resolution (**section 1.6.2.3.4**). Exo-FISH includes an RNase A treatment step which removes RNA:DNA hybrids. Therefore, exposed ssDNA resulting from R-loop accumulation could be detected by Exo-FISH and would not be responsive to ExoIII treatment due to the absence of a physical DNA break (**figures 4.7C and 4.8C**).

Reconstitution of human centromere replication using BACs in *Xenopus laevis* egg extract showed that the highly repetitive human α-satellite DNA sequences display extensive TOP1-dependent DNA loops, DNA supercoiling, and enrichment of DDR factors suggesting ssDNA and replication stress is common in these regions (Aze et al., 2016) (**section 1.7.4.2**). Therefore, BRCA2 may function to suppress torsional stress at centromeres along with topoisomerases. Furthermore, BRCA2 protects against extensive MRE11-mediated digestion of nascent DNA after replication stress (Schlacher et al., 2011), signifying another potential source of centromeric ssDNA under these conditions. BRCA2 also restrains fork progression after replication stress by suppressing PRIMPOL-mediated repriming and ssDNA gap formation (Kang et al., 2021) (**sections 1.5.1 and 1.6.2.3.3**).

Another theory is that DNA resection early in the DNA repair pathway could also represent the ssDNA signal in BRCA2 deficient RPE1 cells. An inability to complete HR at DNA breaks results in persistent 3' ssDNA overhangs which could be targeted for more extensive resection to facilitate repair through other, more error-prone pathways, such as alt-EJ and SSA, which have been associated with repetitive DNA regions (Ceccaldi et al., 2015; Sfeir & Symington, 2015; Truong et al., 2013). Collectively, this suggests that there is increased requirement for BRCA2 and its role in restricting exposed ssDNA, through managing R-loop accumulation, replication stress, or indirectly limiting DNA break resection, at centromeres in asynchronous RPE1 cells.

Upon ExoIII treatment with BRCA2 depletion, there is no additional increase in cenFISH signal, regardless of pepsin pre-treatment (**figures 4.7C and 4.8C**). This was surprising as it implies that facilitating DNA digestion of spontaneous DNA breaks/gaps, as in MisNeg samples, does not produce amplified cenFISH signal on top of the ssDNA signal. As discussed previously, this could signify that the cenFISH signal originates from dsDNA unwinding and ssDNA bubbles from R-loop formation, which is independent of DNA break induction. On the other hand, this could also reflect a key limitation of the Exo-FISH assay (**figure 4.10**). It is plausible that on centromeric chromatin there is accumulation of DSBs

and SSBs. ssDNA gaps can be easily detected through cenFISH probe binding, even in the absence of ExoIII-mediated digestion. Upon addition of ExoIII, DSBs, SSBs, and ssDNA gaps are all susceptible to nucleolytic degradation in a 3' to 5' direction. ExoIII digests approximately 500 nucleotides per minute *in vitro*, although this depends on temperature, salt concentration, and the DNA:enzyme molar ratio (Guo & Wu, 1982). Under these experimental conditions, extensive loss of genetic material after ExoIII digestion could limit cenFISH probe binding and signal amplification compared to ExoIII untreated conditions. Understanding these kinetics in more detail will enable us to further optimise the Exo-FISH protocol in the future.

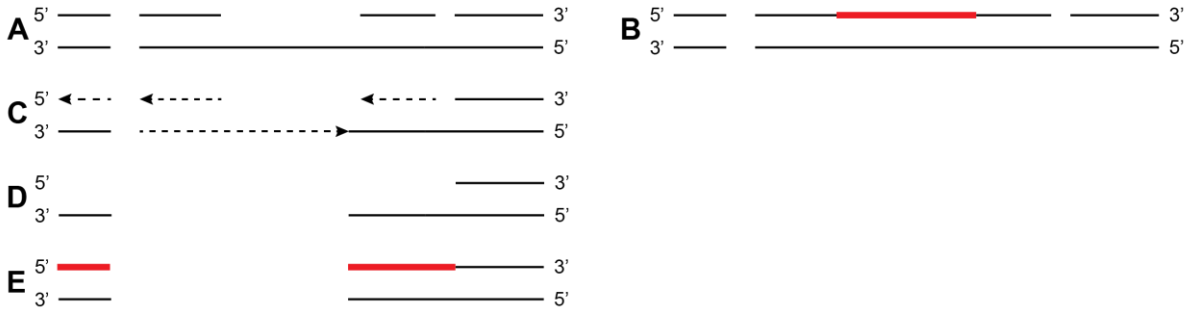


Figure 4.10 ExoIII digestion may lead to loss of genetic material
A Potential DNA template containing DSB, ssDNA, and SSB. **B** In the absence of ExoIII treatment, ssDNA regions can be detected by cenFISH probe binding (red line) but DSBs and SSBs are undetectable. **C** Addition of ExoIII digests DNA in a 3'-5' direction. **D** Extensive and unrestricted digestion by ExoIII results in loss of genetic material. **E** Loss of DNA sequences limits cenFISH probe binding, limiting signal amplification from A.

PALB2 depletion in asynchronous RPE1 cells resulted in increased cenFISH signal upon ExoIII treatment (**figure 4.7D**) suggesting an increased prevalence of DNA breaks under these conditions. However, this effect was lost with pepsin pre-treatment (**figure 4.8D**). It is possible that ExoIII treatment combined with pepsin pre-treatment obscures the increase in cenFISH signal, as discussed in **figure 4.10**, thus it is currently not possible to confirm the importance of PALB2 in maintaining centromere stability using Exo-FISH alone. Curiously, neither BRCA2 nor RAD51 depletion correlates with increased cenFISH signal upon ExoIII treatment in asynchronous RPE1 cells, so this could indicate a novel, HR-independent role for PALB2 in maintaining centromere stability but this needs to be explored further.

RAD51 depletion produced a similar effect on cenFISH signal as BRCA2 depletion (**figure 4.7E**), where increased cenFISH signal was observed even without ExoIII treatment. Intriguingly, siRAD51 treatment significantly impacted telFISH signal which was unique compared to siBRCA2 and siPALB2 treated samples. RAD51 has been linked to mitigating telomere replicative stress by promoting telomere maintenance, ssDNA fill-in synthesis, and replication restart through interaction with the CST complex (Chastain et al., 2016), as well as implicated in alternative lengthening of telomeres (ALT) (Cho et al., 2014), hence this could explain the apparent sensitivity of telomeres to RAD51 depletion. On the other hand, pepsin pre-treatment in RAD51 depleted cells did not significantly impact centromere stability (**figure 4.8E**), which could also potentially be explained by ExoIII over-digestion (**figure 4.10**).

To reveal more information about the source of centromeric ssDNA, I utilised the Exo-FISH assay in serum-starved, quiescent RPE1 cells (**figure 4.9**). BRCA2 depletion no longer caused increased cenFISH signal in the absence of ExoIII treatment in non-cycling cells (**figure 4.9B and C**) suggesting that this ssDNA accumulation is cell cycle-dependent. Centromere transcription in maintained in quiescent cells (Swartz et al., 2019) and can generate R-loops (Cristini et al., 2019). R-loops can be resolved through BRCA2 independent mechanisms, potentially explaining this loss of ssDNA signal (Hegazy et al., 2020). This is supported by the observation that BRCA2 expression is downregulated in response to serum deprivation (Rajan et al., 1996). Hence, the exposed ssDNA in asynchronous RPE1 cells may arise from replication-associated processes such as dsDNA unwinding upon torsional stress or PRIMPOL-mediated repriming, for example. Interestingly, when pepsin pre-treatment was included, BRCA2 depletion led to an increase in cenFISH signal after ExoIII treatment compared to MisNeg controls (**figure 4.9C**). This result suggests that pepsin pre-treatment and removal of chromatin-bound proteins exposes centromeric DNA breaks (**figure 4.8A**), perhaps through relaxation of chromatin compaction or removal of covalently-bound topoisomerase cleavage complexes, so that

breaks are susceptible to ExoIII digestion, ultimately indicating that BRCA2 is required to repair centromeric DNA breaks. It is currently unclear whether this finding is also present in asynchronous RPE1 cells as the ssDNA-related cenFISH signal may have been obscuring the phenotype.

Similar to **figures 4.7D and 4.8D**, PALB2 depletion also causes variable cenFISH signals upon serum-starvation. With or without pepsin pre-treatment, PALB2 depletion with ExoIII treatment did not significantly change cenFISH signal (**figure 4.9D and E**). Additionally, RAD51 depletion had no significant impact on cenFISH signal, regardless of pepsin pre-treatment (**figure 4.9F and G**). Of note, telFISH signal is more variable in serum-starved RPE1 cells (**figure 4.9**), possibly reflecting changes in chromatin compaction, which is important to consider when interpreting results.

Previous studies found that RAD51 depletion increased cenFISH signal and *de novo* centromeric DNA lesions in quiescent RPE1 cells (Saayman et al., 2023). This contrast in our observations could originate from the different concentrations of ExoIII we utilised. Saayman et al., used 4X the concentration of ExoIII that I used during these experiments. I found that pepsin pre-treatment sensitised cells to ExoIII treatment and reduced cenFISH signal, suggesting over-digestion may be occurring under those conditions (**figure 4.10**). Therefore, I employed a lower concentration of ExoIII in my experiments to minimise this impact. Unfortunately, as a result, it could be feasible that not all DNA substrates are digested under my experimental conditions, obscuring any differences that may occur. Interestingly, Saayman et al., found that cenFISH signal and centromere damage levels fluctuated over time in quiescent cells: first decreasing from 0 to 3 days serum-starvation before increasing again up to day 7 (Saayman et al., 2023). This demonstrates that centromere DNA breaks are initially proliferation dependent, before being induced *de novo* during quiescence. Investigating the requirement of BRCA2 and PALB2 in preventing centromeric DNA breaks across different time points in quiescent cells would be valuable to study in the future. In fact, the different cenFISH signals after BRCA2 depletion in

asynchronous and serum-starved cells could indicate dual functions: BRCA2 minimises ssDNA accumulation after transcription/replication stress in proliferating cells (**figures 4.7C and 4.8C**) and also protects against *de novo* DNA lesions in quiescent cells (**figure 4.9C**).

The question remains as to how BRCA2 depletion stimulates ssDNA accumulation, but not PALB2 and RAD51 depletion. BRCA2 has been strongly linked to restricting R-loop formation and promoting their resolution (**section 1.6.2.3.4**). RAD51 has been proposed to both promote R-loop formation and removal (Nascakova et al., 2021; Tan-Wong & Proudfoot, 2013). This balance may explain the accumulation of ssDNA upon RAD51 depletion, regardless of ExoIII treatment (**figure 4.7E**), but to a lesser extent than BRCA2 depletion (**figure 4.7A**). ssDNA after RAD51 depletion is lost after pepsin pre-treatment, although the exact reason for this is currently unclear (**figures 4.8E and 4.10**). Another possibility is that BRCA2 functions separately from PALB2 and RAD51 to suppress torsional stress by supporting topoisomerase activity during DNA replication/transcription, although the mechanism for this is currently unknown. Finally, given their collective role in facilitating HR-mediated repair, ssDNA resulting from extensive DNA resection at DNA repair intermediates might be expected to affect all conditions equally. Furthermore, as RAD51 has been linked to the replication stress response to limit ssDNA accumulation, like BRCA2 (Schlacher et al., 2011, 2012), it remains surprising to observe different phenotypes with the Exo-FISH assay. One possible explanation could relate to replication fork remodelling and reversal. At reversed forks, BRCA2 is proposed to promote RAD51 loading and filament formation at exposed DNA ends to protect against nucleolytic degradation (Schlacher et al., 2011). In the absence of BRCA2 and RAD51 loading, MRE11-mediated digestion can occur generating extensive ssDNA gaps. RAD51 can promote replication fork remodelling (Zellweger et al., 2015). Consequently, in the absence of RAD51, fewer reversed fork structures may be present, reducing MRE11-mediated degradation and ssDNA accumulation. Instead, stalled forks would likely remain protected by RPA binding or

otherwise unsusceptible to ExoIII-mediated digestion. In the future, it would be interesting to explore the impact of MRE11 inhibition on cenFISH signal after BRCA2 depletion.

Loss of ExoIII-independent cenFISH signal in quiescent cells further implies the importance of cell cycle progression in centromeric ssDNA. This reduced cenFISH signal is therefore likely DNA break-independent and could signify reduced replication-dependent dsDNA unwinding and ssDNA exposure. Alternatively, the involvement of DNA resection and cell cycle regulated repair pathways should not be excluded. NHEJ is the predominant repair pathway utilised in quiescent cells (Dutta et al., 2017) and includes minimal DNA end processing and so would not be detectable without ExoIII treatment. Furthermore, alt-EJ/SSA and the associated DNA resection occurs at low levels in G_0 cells (Truong et al., 2013). Overall, further work is still needed to understand the source of ssDNA at centromeres and how HR factors, primarily BRCA2, influence this.

There are several additional experiments that would support and improve the validity of the findings discussed above. PFGE combined with southern blotting to visualise DNA breaks *in vitro* using centromere-specific DNA probes will enable the direct assessment of DNA breaks, distinguishing them from SSBs including DNA nicks and gaps. To investigate the source of centromeric ssDNA, centromeric R-loops upon BRCA2 depletion could be detected using DNA-RNA immunoprecipitation (DRIP), and replication fork processivity and degradation could be assessed using DNA fiber assays combined with FISH probes against α-satellite DNA sequences (Gamba et al., 2022; Giunta et al., 2021). Inhibition of topoisomerases or depletion of PRIMPOL using RNA interference followed by Exo-FISH or non-denaturing BrdU assays may reveal more information on the source of ssDNA. ssDNA resulting from DNA resection and repair intermediates could again be identified using non-denaturing BrdU assays. Altogether, a novel and exciting mechanism for HR factors in maintaining centromere DNA stability and integrity could be obtained in the future.

4.3.3 A requirement for DNA breaks in CENP-A deposition at centromeres?

An increasing number of publications are linking centromere breaks to CENP-A occupancy at centromeres (Giunta et al., 2021; Saayman et al., 2023; Yilmaz et al., 2021).

Firstly, resected DNA was observed to promote CENP-A incorporation and HR-mediated repair in G1 cells (Yilmaz et al., 2021) (**section 1.7.4.1**). Alternatively, Giunta et al., demonstrated a role for CENP-A in minimising centromeric replication stress and aneuploidy (Giunta et al., 2021) (**section 1.7.4.2.2**). Finally, Saayman et al., proposed that DNA lesions induced by TOP2B at the centromere in quiescent cells are targets for RAD51-mediated recombination, in turn promoting CENP-A recruitment and occupancy (Saayman et al., 2023) (**section 1.7.4.4**). Previous unpublished work from my lab showed that RAD51 depletion in HeLa cells reduces deposition of *de novo* CENP-A at CENP-B-defined centromeres using the SNAP-tag system (Jansen et al., 2007) (Xanita Saayman, unpublished). This suggests that RAD51 is required to promote CENP-A deposition and not retention of existing CENP-A already present in the chromatin, although this needs to be confirmed in RPE1 cells.

Given this information and that RAD51 and BRCA2 depletion both impact CENP-A levels in asynchronous RPE1 cells (**figure 4.3A and B**), it is tempting to speculate that this could be a consequence of defective centromeric DNA repair. In fact, CENP-A was observed to be recruited to I-SceI endonuclease- and laser-induced DSBs throughout interphase and although this was found to correlate with NHEJ activity (Helfricht et al., 2013; Zeitlin et al., 2009), CENP-A and other centromeric proteins recruited after DNA damage were also observed to colocalise with RAD51 (Zeitlin et al., 2009). Furthermore, other HR factors have been linked to CENP-A deposition in several organisms (Mitra et al., 2014; Racca et al., 2021).

Additionally, CENP-A chaperone, HJURP, was first described for its role in HR-mediated repair and its interaction with MSH5 and NBS1, where *in vitro* assays found it able to directly bind HJs and rDNA arrays (Kato et al., 2007). HJs arise at sites of strand invasion and D-

loop formation in HR, further suggesting that BRCA2-RAD51 activity could promote HJURP and CENP-A recruitment at centromeric DNA breaks, under certain conditions. Regardless, PALB2 and RAD51 depletion did not show consistent impacts on centromere stability by Exo-FISH under the conditions I employed (**figures 4.7, 4.8, 4.9**) and PALB2 did not affect CENP-A levels at centromeres. Therefore, this possible connection between canonical HR factors and CENP-A occupancy still needs further exploration and validation using robust and reliable techniques, as discussed previously.

Chapter 5 – Exploring the impact of BRCA2 and PALB2 on chromosome stability in HCT116 cells

5.1 Introduction

5.1.1 Gross chromosomal rearrangements (GCRs) drive tumourigenesis

Gross chromosomal rearrangements (GCRs) such as translocations, inversions, and deletions are hallmarks of tumourigenesis (Tiwari et al., 2018). These structural rearrangements can impact gene copy number, altering gene expression and cell behaviour towards a cancerous phenotype (Dahiya et al., 2022).

Heterozygous germline mutations in BRCA2 and PALB2 can predispose patients to breast, ovarian, and pancreatic cancers, among others, due to loss of their tumour suppressor activity (Roy et al., 2012; Wu et al., 2020). Furthermore, biallelic mutations in both proteins have been associated with cancer predisposition syndrome, Fanconi Anaemia (FA-D1 and FA-N) (Howlett et al., 2002; Xia et al., 2007). Accurate DNA repair via HR is important for limiting tumourigenesis and GCRs commonly arise from inaccurate DNA repair including NHEJ of non-neighbouring sequences, or mutagenic recombination between non-allelic chromosomes or heterologous sequences through SSA or alt-EJ.

5.1.2 Centromere research in RPE1 and HCT116 cells

Our understanding of centromere biology and stability has increased substantially over the last decade, however there is much we still do not understand. It is well established that phenotypes can vary across different cell lines due to variable gene expression, for example. Combining my findings described in **chapter 4** and recent publications (Saayman et al., 2023), the involvement of HR factors at centromeres in RPE1 cells is becoming clearer. However, whether these findings are reproducible and consistent in other cell types is yet to be determined.

RPE1 cells are human retinal pigment epithelial cells, immortalised using human telomerase reverse transcriptase (hTERT). They are non-cancerous, karyotypically stable, and near-diploid. Microscopy-based analysis, using IF and Exo-FISH, has revealed a role for RAD51 and BRCA2 in maintaining centromere identity and stability in these cells (**sections 4.3.1 and 4.3.2**) (Saayman et al., 2023). On the other hand, the human colorectal carcinoma cell line, HCT116, displays microsatellite instability due to loss of the mismatch repair (MMR) protein, MLH1. MMR functions in post-replicative DNA repair and promotes HR by rejecting homeologous recombination by aborting the formation of recombination intermediates, or else accommodating homeologous recombination by repairing nucleotide mismatches during RAD51-dependent strand invasion and branch migration (Spies & Fishel, 2015) (**section 1.5.4**). Despite this, MMR-deficient HCT116 cells are p53-positive and considered near-diploid, although they contain several described chromosomal rearrangements (Knutsen et al., 2010). So far, DNA break analysis using publicly available datasets has revealed an enrichment of DNA breaks at HCT116 centromeres (Saayman et al., 2023). However, no further microscopy-based analysis has been conducted. Past studies have indicated a role for MMR factors at centromeres (Aze et al., 2016), therefore HCT116 cells could be a valuable model system to understand the function of MMR in regulating centromere stability, perhaps in relation to HR.

In this chapter, I aimed to employ an auxin-inducible degron (AID) system to rapidly and specifically deplete BRCA2 and PALB2 from HCT116 cells. Utilising this, I investigated the long-term consequences of BRCA2 and PALB2 depletion on chromosomal aberrations and explored the role of HR at HCT116 centromeres, similar to **chapter 4**.

5.2 Results

5.2.1 Generation and validation of an auxin-inducible degron (AID)-tagged BRCA2/PALB2 system in HCT116 cells

Previously in **chapter 4**, I utilised siRNA to study the role of HR factors: BRCA2, PALB2, and RAD51, at centromeres in RPE1 cells. siRNA can produce indirect secondary effects,

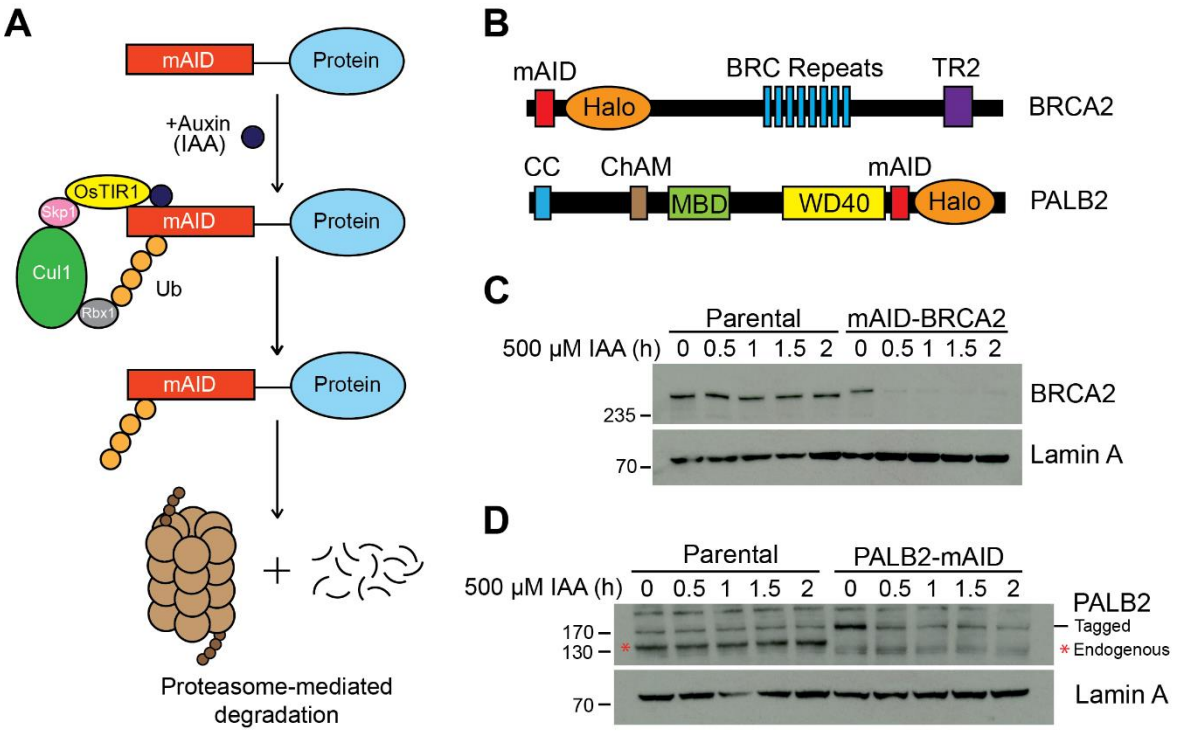


Figure 5.1 Generation and validation of auxin inducible degron (AID)-tagged BRCA2/PALB2 system in HCT116 cells
A Schematic of auxin inducible degron (AID) system to degrade proteins of interest. **B** Schematic of BRCA2 and PALB2 mAID-Halo tagging. mAID = mini Auxin-inducible degron. CC = Coiled-coil. ChAM = Chromatin-association motif. MBD = MRG15-binding domain. **C** Western blot showing degradation of BRCA2 within 30 minutes 500 μm IAA treatment. Lamin A used as a loading control. **D** Western blot showing degradation of PALB2 within 30 minutes 500 μm IAA treatment. Red asterisk refers to endogenous PALB2 protein. Lamin A used as a loading control.

incomplete and variable degradation, and cannot be used to study dynamic protein functions across the cell cycle. Therefore, I next aimed to explore the role of BRCA2 and PALB2 in chromosome and centromere stability using the auxin-inducible degron (AID) system (Natsume et al., 2016) (**figure 5.1A**). The AID system involves tagging the protein-of-interest with the Arabidopsis IAA17-derived, mini-AID tag (mAID) in cells expressing the F-box protein, Oryza sativa TIR1 (OsTIR1). OsTIR1 forms part of the SCF E3 ubiquitin ligase complex with endogenous SKP1, CUL1, and F-box. Upon addition of auxin (indole-3-acetic acid, IAA), SCF rapidly ubiquitinates the mAID-tagged protein-of-interest for proteasomal degradation.

We utilised CRISPR/Cas9 technology to generate clonal Halo- and mAID-tagged BRCA2 and PALB2 HCT116 cell lines (Christine Ralf, Fumiko Esashi, Lucia Rampazzo) (**figure**

5.1B) where Halo is a fusion tag useful for protein visualisation. I also attempted to generate degron-tagged RAD51 cell lines but was unable to obtain any successful clones (data not shown). Both cell lines are henceforth referred to as HCT116 mAID-BRCA2 and HCT116 PALB2-mAID. In these cells, as seen by western blot, addition of Halo and mAID tags produces a size shift of approximately 40 kDa and BRCA2 and PALB2 can be rapidly degraded within 30 minutes of 500 μM IAA treatment (**figures 5.1C and D**).

Successful protein tagging was further validated by PCR (**figure 5.2A**). Accurate, homozygous mAID-BRCA2 tagging was confirmed by Lucia Rampazzo (data not shown). Three primer pairs were used to validate PALB2 tagging (primer sets 1 and 2) and template plasmid integration (primer set 3). The band present in both HCT116 OsTIR1 parental and PALB2-mAID cells using primer set 3 represents non-specific banding and the plasmid template is not believed to have been incorporated. HCT116 PALB2-mAID showed a clear band at the expected size after amplification with primer set 2, which was not present in HCT116 OsTIR1 parental cells, indicating incorporation of the mAID-Halo tag. Interestingly, HCT116 PALB2-mAID cells also generated a DNA band correlating with endogenous PALB2 after amplification with primer set 1. Sequencing of this DNA band revealed the presence of an 11 amino acid deletion within the C-terminus of PALB2 (**figure 5.2B**). Given that complete PALB2 loss is visible after IAA treatment (**figure 5.1D**), I reasoned that this mutant, untagged allele of PALB2, is unstable and non-functional. This was further supported with a BRCA2 pulldown where 2 hours IAA treatment in HCT116 PALB2-mAID cells completely abrogated its interaction with BRCA2 (**figure 5.2C**).

In summary, these results demonstrate that BRCA2 and PALB2 can be rapidly degraded using the AID system in HCT116 cells. While gene editing by CRISPR/Cas9 was not completely effective (HCT116 PALB2-mAID, **figures 5.2A-B**), IAA treatment completely removed the HR-dependent interaction between BRCA2 and PALB2 (**figure 5.2C**), indicating that these cell lines can be useful tools to investigate the function of these proteins.

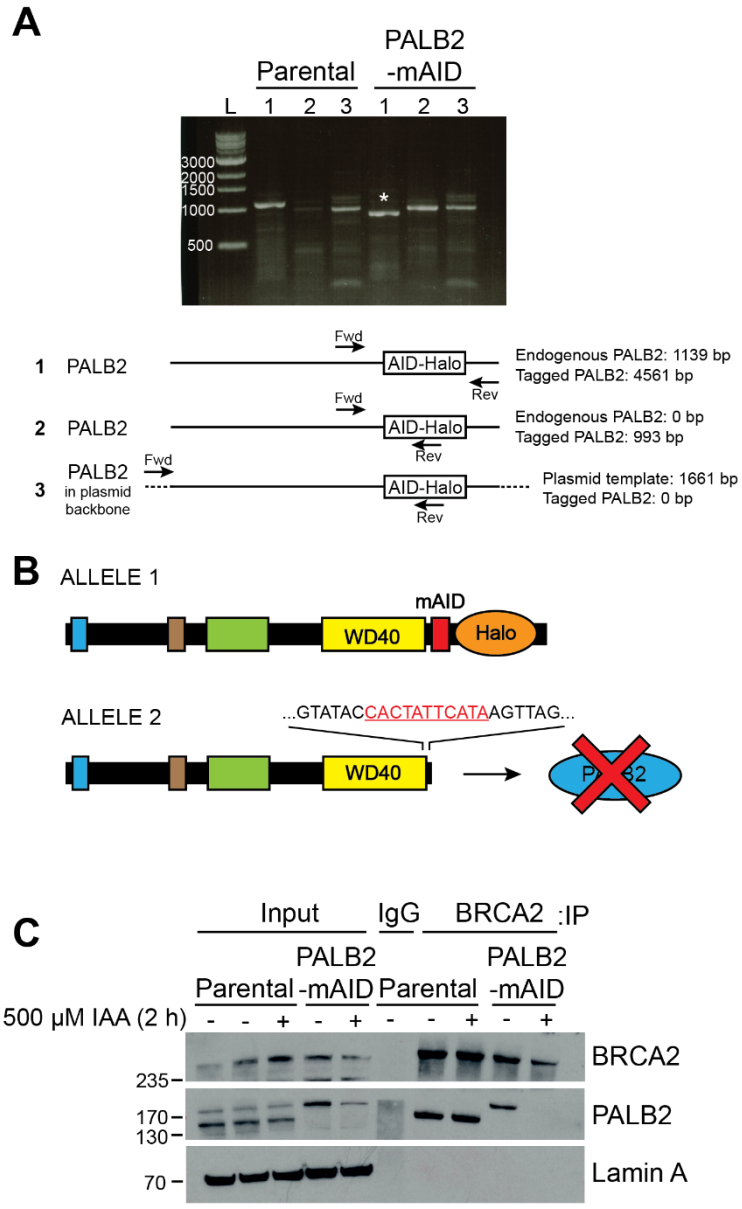


Figure 5.2 Impact of PALB2 and BRCA2 depletion in HCT116 cells
A Agarose gel image of PCR validating C-terminal tagging of PALB2 with mAID and Halo. Three set of primer pairs were used, the expected size of each amplified DNA fragments are displayed. Asterisk marks band sent for sequencing. **B** Schematic of two alleles of PALB2 gene and the deleted region indicated in red. **C** Immunoprecipitation showing loss of PALB2-BRCA2 interaction upon 2 h 500 µm IAA treatment. Lamin A used as a loading control for the inputs.

5.2.2 Short-term BRCA2/PALB2 depletion impacts cellular functions

BRCA2 and PALB2 are important for cellular survival in response to genome stability, where loss of these proteins results in defects in the DDR and ultimately cell death (Jurkovicova et al., 2022). Therefore, I wanted to further validate these HCT116 mAID cell lines by

exploring the short-term consequences of BRCA2 and PALB2 depletion after exogenous DNA damage.

Mitomycin C (MMC) is an inter-strand crosslinking agent that impedes replication and transcription machinery and requires HR for repair (Deans & West, 2011) (**section 1.6.2.3.2**). Olaparib is a PARP1 inhibitor that traps PARP1 on DNA, increasing replication fork progression and replication stress. This can contribute to ssDNA accumulation, replication fork collapse, and one-ended DSBs that require HR-mediated repair (Hopkins et al., 2019; Maya-Mendoza et al., 2018). Using these agents, I assessed cell survival after PALB2 and BRCA2 depletion via WST-1 cell proliferation assays (**figure 5.3A**) (Jacob Wall conducted HCT116 mAID-BRCA2 WST-1 experiments). Protein depletion in HCT116 mAID-BRCA2 and PALB2-mAID cell lines produced a significant decrease in cell survival after MMC and Olaparib treatment while HCT116 OsTIR1 parental cells remained largely unaffected by IAA treatment (**figures 5.3B-E**). This indicates that rapid depletion of BRCA2 and PALB2 in HCT116 mAID cell lines produces the expected HR repair defect, correlating with decreased cell survival.

Additionally, I utilised immunofluorescence (IF) to observe DDR signalling and HR-mediated repair more directly (**figure 5.4**). Jacob Wall conducted IF experiments in HCT116 mAID-BRCA2 cells. H2AX is phosphorylated at S139 at sites of DNA damage to generate ɣH2AX. This DDR signalling marker stimulates DNA repair factor recruitment including the HR repair machinery. In this context, PALB2 acts to recruit BRCA2 to DNA lesions where it subsequently facilitates RAD51 loading onto 3’ ssDNA overhangs to form nucleoprotein filaments that promote strand invasion and DNA repair (Esashi et al., 2007; Zhang et al., 2009a). After MMC treatment in HCT116 OsTIR1 parental cells, ɣH2AX and RAD51 foci were induced, regardless of IAA treatment (**figures 5.5A and D**), demonstrating intact DDR and HR pathways. In HCT116 mAID-BRCA2 and PALB2-mAID cells, MMC treatment also produces ɣH2AX and RAD51 foci. As expected, upon IAA-induced BRCA2/PALB2

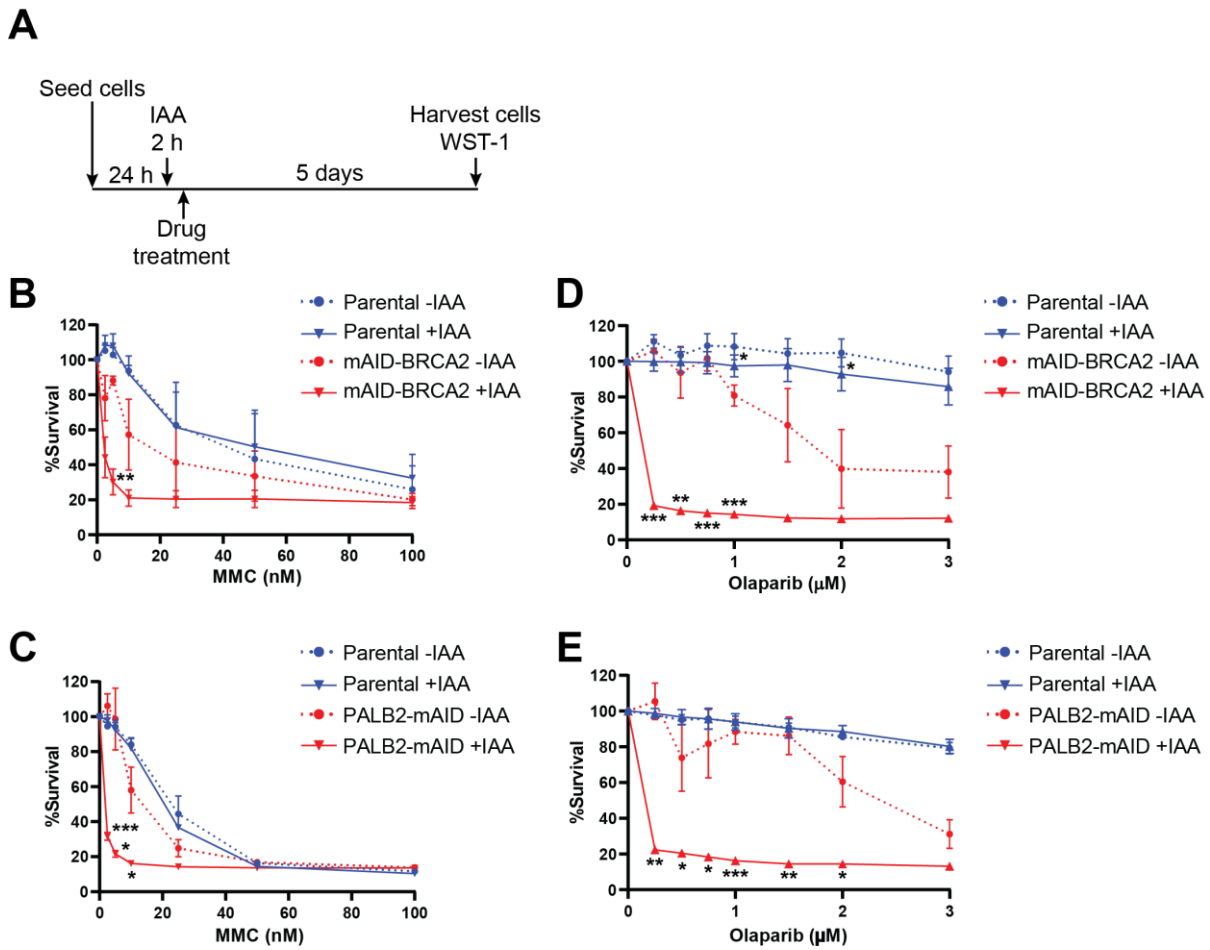


Figure 5.3 BRCA2 and PALB2 depletion sensitises HCT116 cells to DNA damaging agents
A Schematic of WST-1 protocol. **B** Graph showing percentage cell survival after MMC and 500 μM IAA treatment in HCT116 OsTIR1 parental and mAID-BRCA2 cell lines. **C** Graph showing percentage cell survival after MMC and 500 μM IAA treatment in HCT116 OsTIR1 parental and PALBB2-mAID cell lines. **D** Graph showing percentage cell survival after Olaparib and 500 μM IAA treatment in HCT116 OsTIR1 parental and mAID-BRCA2 cell lines. **D** Graph showing percentage cell survival after Olaparib and 500 μM IAA treatment in HCT116 OsTIR1 parental and PALB2-mAID cell lines. Points represent average of three independent experiments. Error bars represent S.E.M. Two-tailed T-test comparing -IAA vs +IAA for each cell line. **B** and **C** conducted by Jacob Wall.

depletion, there is no longer a significant increase in RAD51 foci formation while γH2AX induction is unaffected (**figures 5.5B, C, E, and F**), indicating a failure to facilitate HR-mediated repair under these conditions while early DDR signalling remains functional. The same trends can be observed upon olaparib treatment (**figures 5.5G-L**).

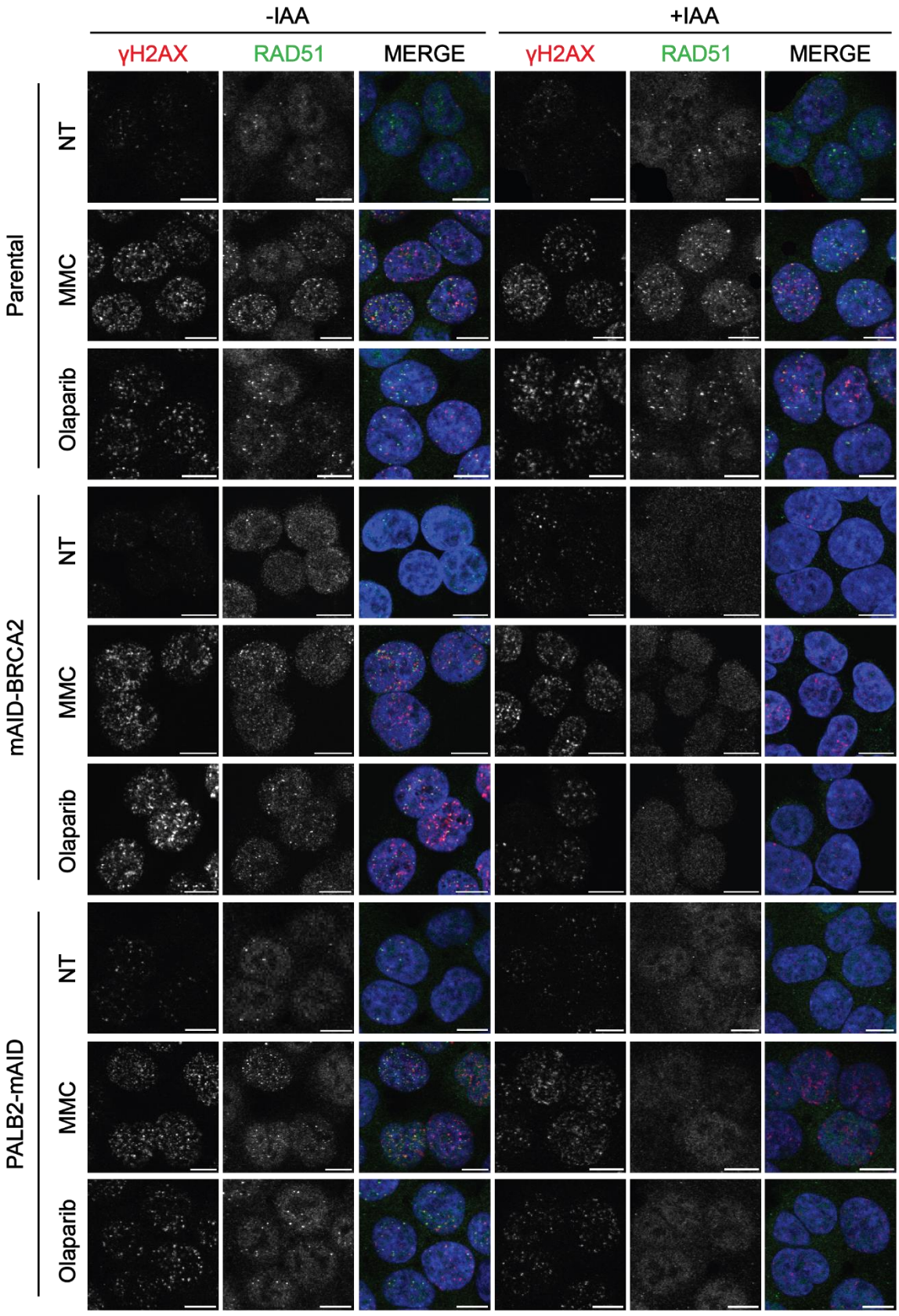


Figure 5.4 Representative images RAD51 and γH2AX signalling after BRCA2 and PALB2 depletion in HCT116 cells.
Images to complement analysis shown in figure 5.5. Scale bar equals 10 μm. mAID-BRCA2 images obtained by Jacob Wall.

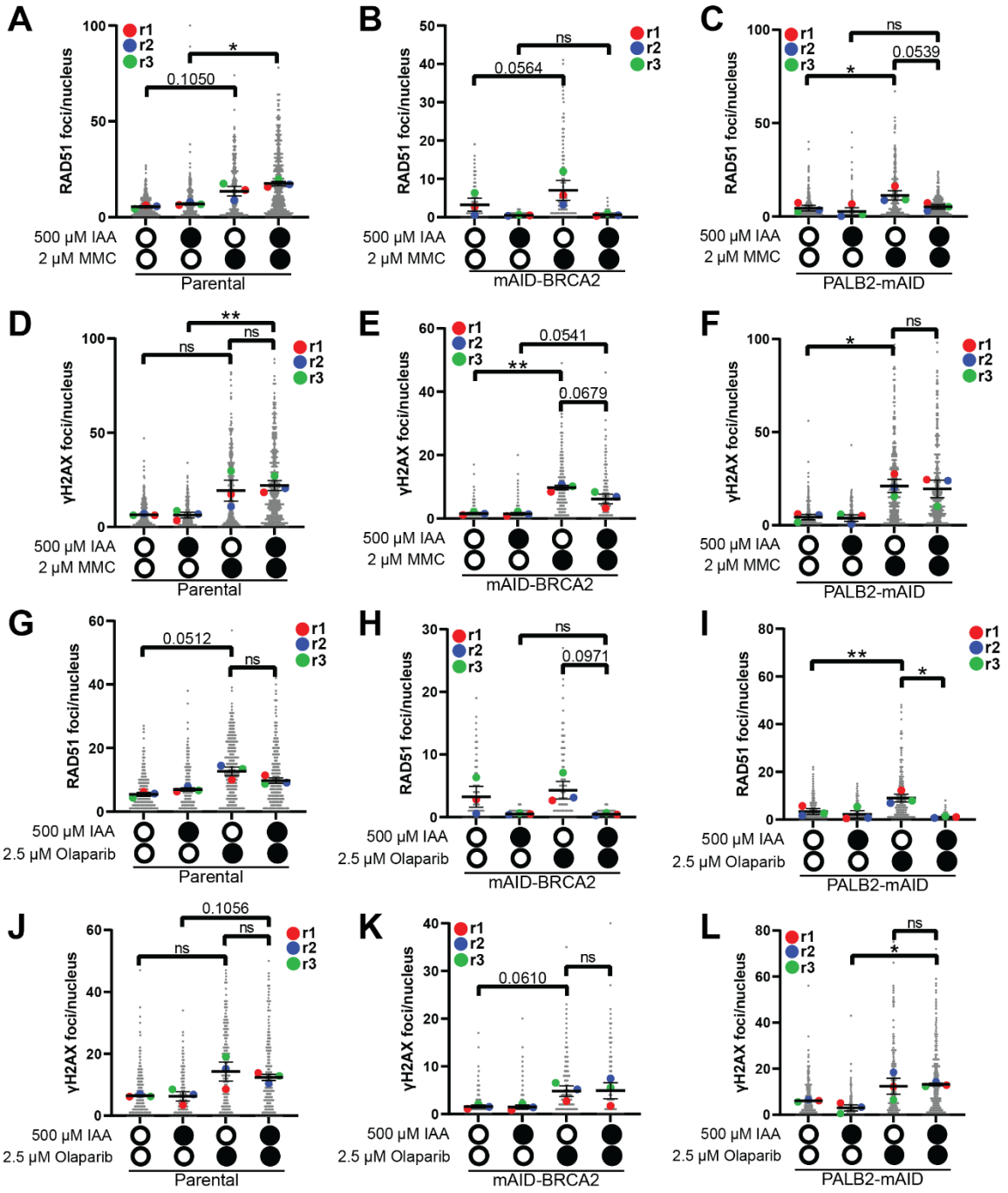


Figure 5.5 Short-term BRCA2 and PALB2 depletion in HCT116 cells produces a HR repair defect
A-C Quantification of RAD51 foci count per nucleus after MMC treatment in HCT116 OsTIR1 parental (A), mAID-BRCA2 (B), and PALB2-mAID cells (C). **D-F** Quantification of γH2AX foci count per nucleus after MMC treatment in HCT116 OsTIR1 parental (D), mAID-BRCA2 (E), and PALB2-mAID cells (F). **G-I** Quantification of RAD51 foci count per nucleus after olaparib treatment in HCT116 OsTIR1 parental (G), mAID-BRCA2 (H), and PALB2-mAID cells (I). **J-L** Quantification of γH2AX foci count per nucleus after olaparib treatment in HCT116 OsTIR1 parental (J), mAID-BRCA2 (K), and PALB2-mAID cells (L). Cells were incubated with or without 500 μM IAA for 2 h before treatment with 2 μM MMC or 2.5 μM olaparib. At least 100 cells were quantified per condition, per repeat. n=3. Large coloured foci represent the average of each repeat. Error bars represent S.E.M. Paired t-test. Data in graphs **B, E, H, K** from HCT116 mAID-BRCA2 cells obtained by Jacob Wall.

Overall, these findings establish that the generated HCT116 mAID-BRCA2 and PALB2-mAID cell lines are valuable tools to investigate the function of BRCA2 and PALB2 in mitigating chromosome and centromere instability.

5.2.3 Long-term BRCA2/PALB2 depletion reveals distinct chromosome phenotypes

Using this degron system, I next aimed to further understand the role of BRCA2 and PALB2 in HCT116 cell stability after endogenous DNA damage. I conducted a clonogenic survival assay where HCT116 mAID-BRCA2 and PALB2-mAID cells were treated with 500 μM IAA for 10 days (**figure 5.6A**). Both cell lines revealed an approximately 75% drop in cell survival compared to untreated samples (**figures 5.6C and D**) indicating BRCA2's and PALB2's importance in normal cell survival after endogenous genotoxic stressors. HCT116 OsTIR1 parental cells showed only a modest drop in cell survival after IAA treatment (**figure 5.6B**). BRCA2 and PALB2 depletion was confirmed by western blot and a slight increase in p21 and p53 signalling was visible under these conditions (**figure 5.6E**).

Intriguingly, these results suggest that a proportion of cells can survive in the absence of PALB2 and BRCA2, despite their importance in cell survival. I subsequently hypothesised that this surviving population of cells may have accumulated chromosomal aberrations that facilitate their continued survival. BRCA2 and PALB2 germline mutations, and subsequent loss-of-function, are associated with several cancers including breast and ovarian cancers, and medulloblastomas (Waszak et al., 2018). Isochromosome 17q (Iso(17q)) formation is specifically associated with a subset of medulloblastoma patients displaying BRCA2 and PALB2 mutations. Chromosome 17 (Chr17) contains the TP53 gene within its p-arm (**figure 5.7A**) and structural aberrations of Chr17 have been additionally linked to colorectal cancers and gastroesophageal adenocarcinomas (Birkness et al., 2018; Sawai et al., 1997).

I aimed to examine the impact of BRCA2 and PALB2 depletion on the occurrence of various Chr17 aberrations to give insight into how cells may adapt and promote cell survival despite defects in DDR signalling and chromosomal instability (**figure 5.6**). The AID system is

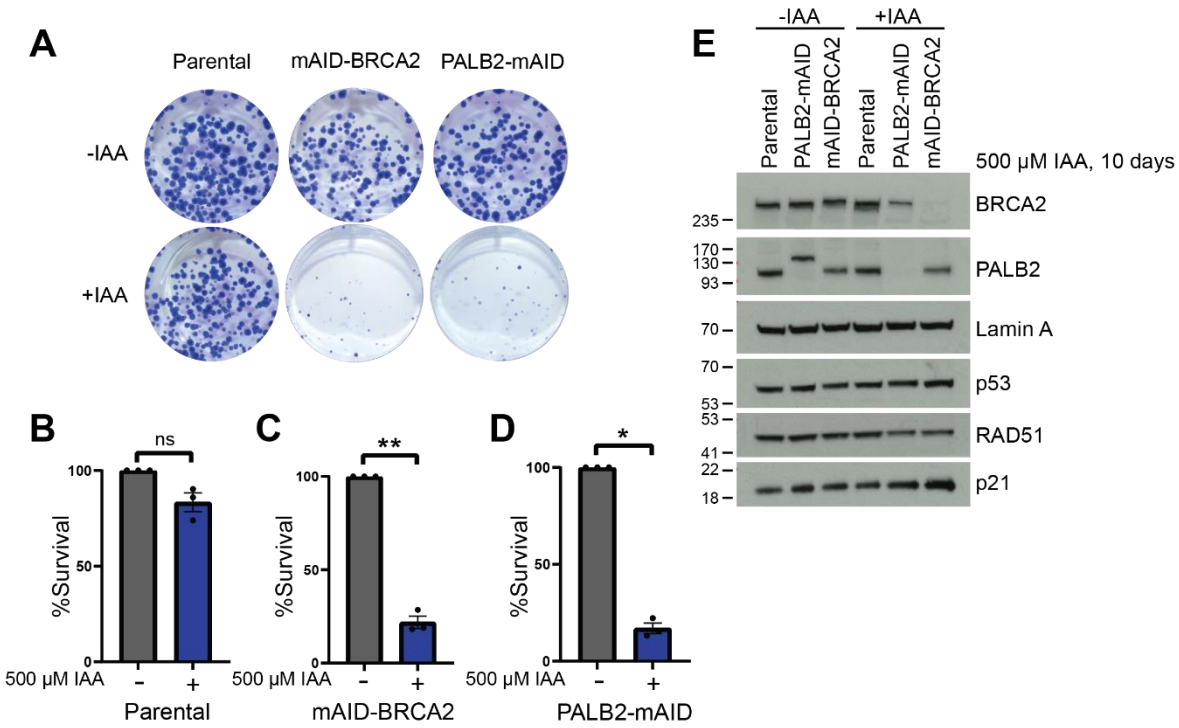


Figure 5.6 Long-term BRCA2 and PALB2 depletion decreases cell survival without exogenous DNA damage
A Representative images of colony growth in HCT116 OsTIR1 parental or mAID-degron cell lines with or without 500 μM IAA treatment for 10 days. **B** Clonogenic cell survival of HCT116 OsTIR1 parental cells upon treatment with 500 μM IAA. Error bars represent S.E.M. from three techninical repeats. n=3. Unpaired t-test. **C** Clonogenic cell survival of HCT116 mAID-BRCA2 cells upon treatment with 500 μM IAA. Error bars represent S.E.M. from three techninical repeats. n=3. Unpaired t-test. **D** Clonogenic cell survival of HCT116 PALB2-mAID cells upon treatment with 500 μM IAA. Error bars represent S.E.M. from three techninical repeats. n=3. Unpaired t-test. **E** Western blot showing BRCA2 and PALB2 depletion after 10 days, 500 μM IAA treatment. Lamin A used as a loading control.

beneficial for this as it allows the precise control of BRCA2/PALB2 depletion to track chromosomal aberrations over time. The three HCT116 cell lines were cultured in the presence or absence of 500 μM IAA for 24 hours or 1 month before FISH analysis of Chr17 on metaphase spreads. Chr17 p- and q-arms were differentially labelled and any aberrations scored. A normal HCT116 metaphase spread and Chr17 staining is displayed in **figure 5.7A** where the two copies, with red and green staining, are visible. HCT116 cells also contain a Chr17 translocation (t(4;17)) (Knutsen et al., 2010) resulting in an additional chromosome displaying red q-arm signal only. Various aberrations were visible on Chr17 including chromosome breaks, duplications, chromosome arm loss, inversions, and isochromosomes (**figure 5.7B**).

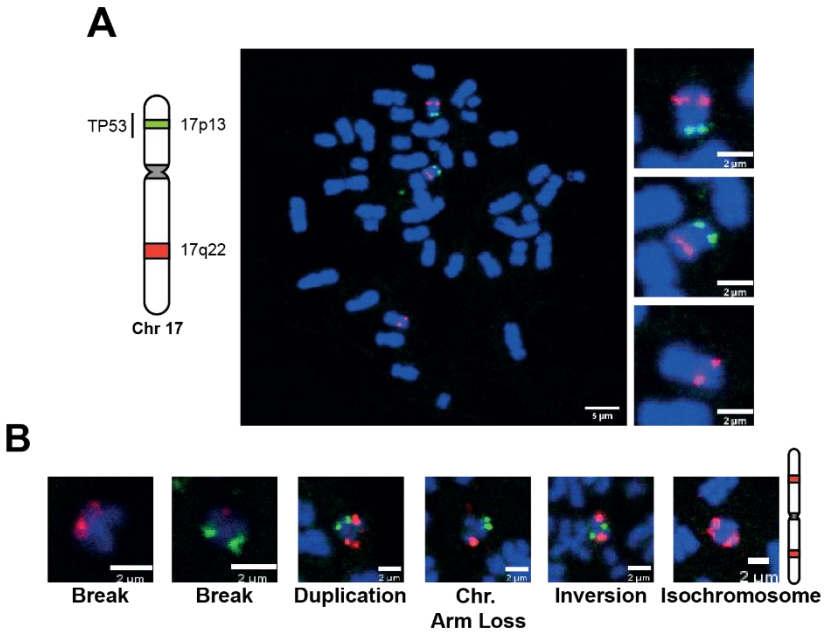


Figure 5.7 Long-term depletion of BRCA2 and PALB2 reveals distinct Chr17 aberrations
A Representative image of HCT116 cell metaphase spread with chromosome 17 p- and q- arms labelled green and red, respectively. Scale bar equals 5 µm and 2 µm. **B** Representative images of different observed Chr17 aberrations. Scale bar equals 2 µm.

I first evaluated Chr17 aberrations that arise after 24 hours IAA treatment to identify the baseline level of aberrations that occur after short-term BRCA2 and PALB2 depletion. Cell cycle analysis by flow cytometry revealed minimal impact of IAA treatment in the HCT116 cell lines (**figure 5.8A**). In fact, the percentage of cells in each cell cycle phase was comparable across all three cell lines (**figure 5.8B**). HCT116 OsTIR1 parental cells showed low levels of metaphase spreads containing Chr17 aberrations and this decreased by 9% upon IAA addition (**figure 5.8C**). Interestingly, BRCA2 depletion did not substantially impact the level of Chr17 aberrations after 24 hours IAA treatment (**figure 5.8D**), while PALB2 depletion resulted in an 8% increase in metaphase spreads displaying aberrant Chr17 FISH probe staining patterns (**figure 5.8E**). Despite these relatively small changes, the specific types of Chr17 aberrations arising were variable across the cell lines. The predominant Chr17 aberrations occurring in HCT116 OsTIR1 parental and PALB2-mAID cell lines were inversions, chromosome arm loss, missegregation, and duplications (**figure 5.8F and H**): metaphase spreads displaying duplications and arm loss were most prevalent in OsTIR1

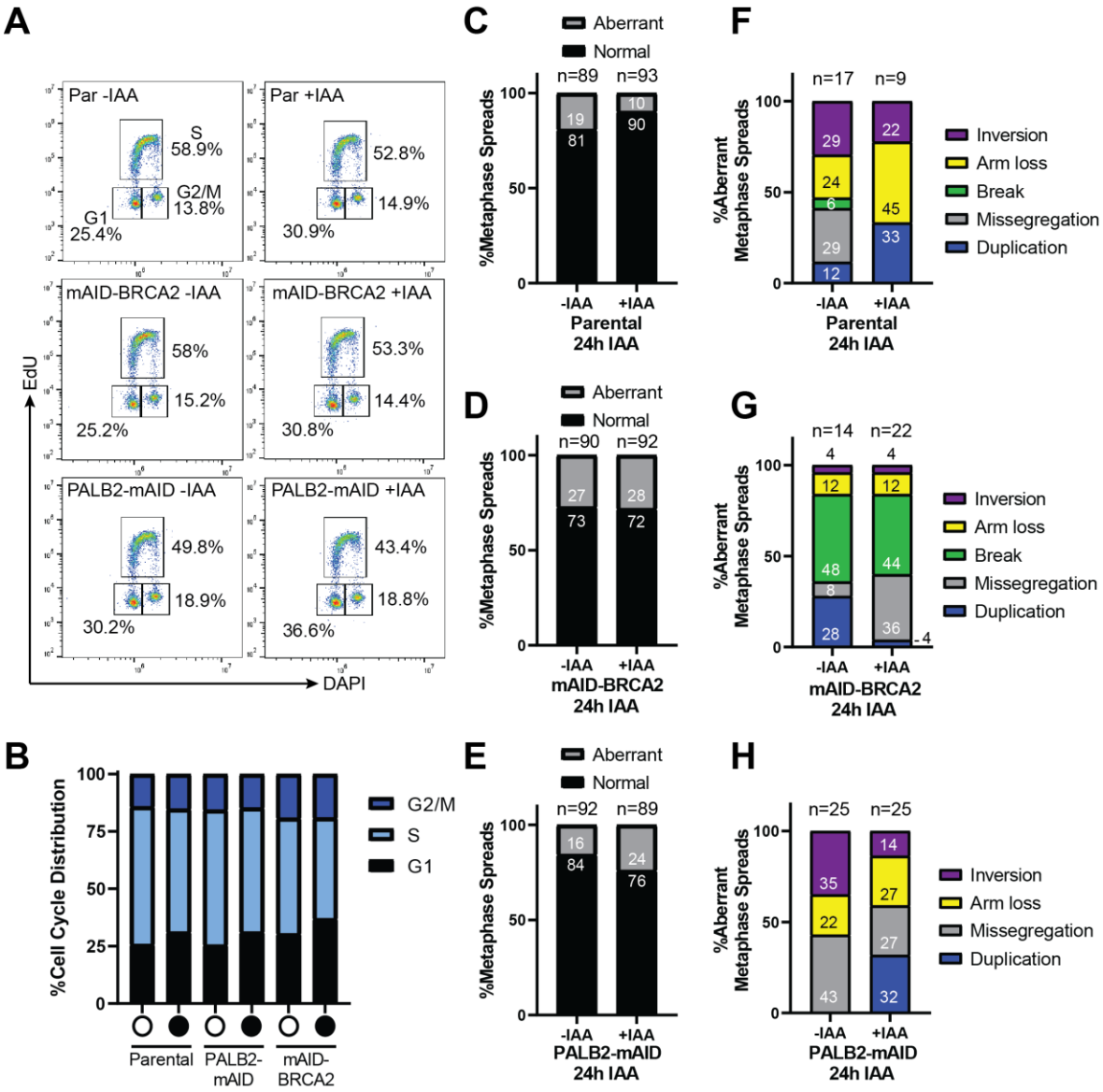


Figure 5.8 The effect of BRCA2 and PALB2 depletion for 24 h on Chr17 stability
A Cell cycle profile of HCT116 mAID-degron cells stained with EdU and DAPI. Gates show percentage of cells in G1, S, and G2/M phase after 24 h 500 μM IAA. **B** Graph showing quantification of percentage of HCT116 mAID-degron cells in the different cell cycle stages, as determined by A. **C-E** Quantification of metaphase spreads showing normal vs aberrant Chr17 FISH probe signal after 24 h 500 μM IAA treatment in HCT116 OsTIR1 parental (C), mAID-BRCA2 (D), and PALB2-mAID (E) cells. Numbers represent the percentage of metaphase spreads, rounded to the nearest whole number. At least 90 metaphase spreads analysed per condition from 3 independent repeats. **F-H** Graphs showing quantification of types of Chr17 aberrations appearing after 24 h 500 μM IAA treatment in HCT116 OsTIR1 parental (F), mAID-BRCA2 (E), and PALB2-mAID (H) cells. Numbers represent the percentage occurance out of aberrant metaphase spreads shown in C-E, rounded to the nearest whole number. Precise n displayed above each sample.

parental cells after IAA treatment while duplications were highest in PALB2-mAID cells. However, HCT116 mAID-BRCA2 cells displayed relatively high levels of Chr17 breaks resulting in p- and q-arm separation, and missegregation (**figures 5.8G and 5.7B**). Furthermore, despite no significant changes in metaphase spreads displaying aberrant FISH signals (**figure 5.8D**), there was increased missegregation of Chr17 (**figure 5.8G**). In summary, after 24 hour IAA treatment, the level of metaphase spreads displaying aberrant Chr17 FISH staining is similar across the three cell lines analysed, however the types of Chr17 aberrations that do arise, differ, possibly reflecting the different functions of PALB2 and BRCA2.

Addition of 500 μM IAA for extended time periods further distorts cell cycle progression in HCT116 PALB2-mAID and mAID-BRCA2 cell lines. Upon 1 week IAA treatment, both PALB2 and BRCA2 depletion trigger significantly increased G1 and reduced S phase populations compared to OsTIR1 parental and untreated controls (**figures 5.9A and B**). After 1 month IAA treatment, this difference is lessened by some extent, particularly in mAID-BRCA2 cell lines, however depleted cells still display a reduced S phase population (**figures 5.9C and D**).

Next, I assessed Chr17 aberrations that occur after 1 month of 500 μM IAA treatment to understand how cells may adapt and survive in the absence of BRCA2 and PALB2. Protein depletion after 1 month was measured by WB (**figure 5.10A**). HCT116 PALB2-mAID cells maintain PALB2 degradation however mAID-BRCA2 cells restore BRCA2 expression during this time, although at slightly reduced levels compared to the untreated control. Despite this, both PALB2 and BRCA2 depletion result in elevated p53 and p21 expression indicating cell stress and instability.

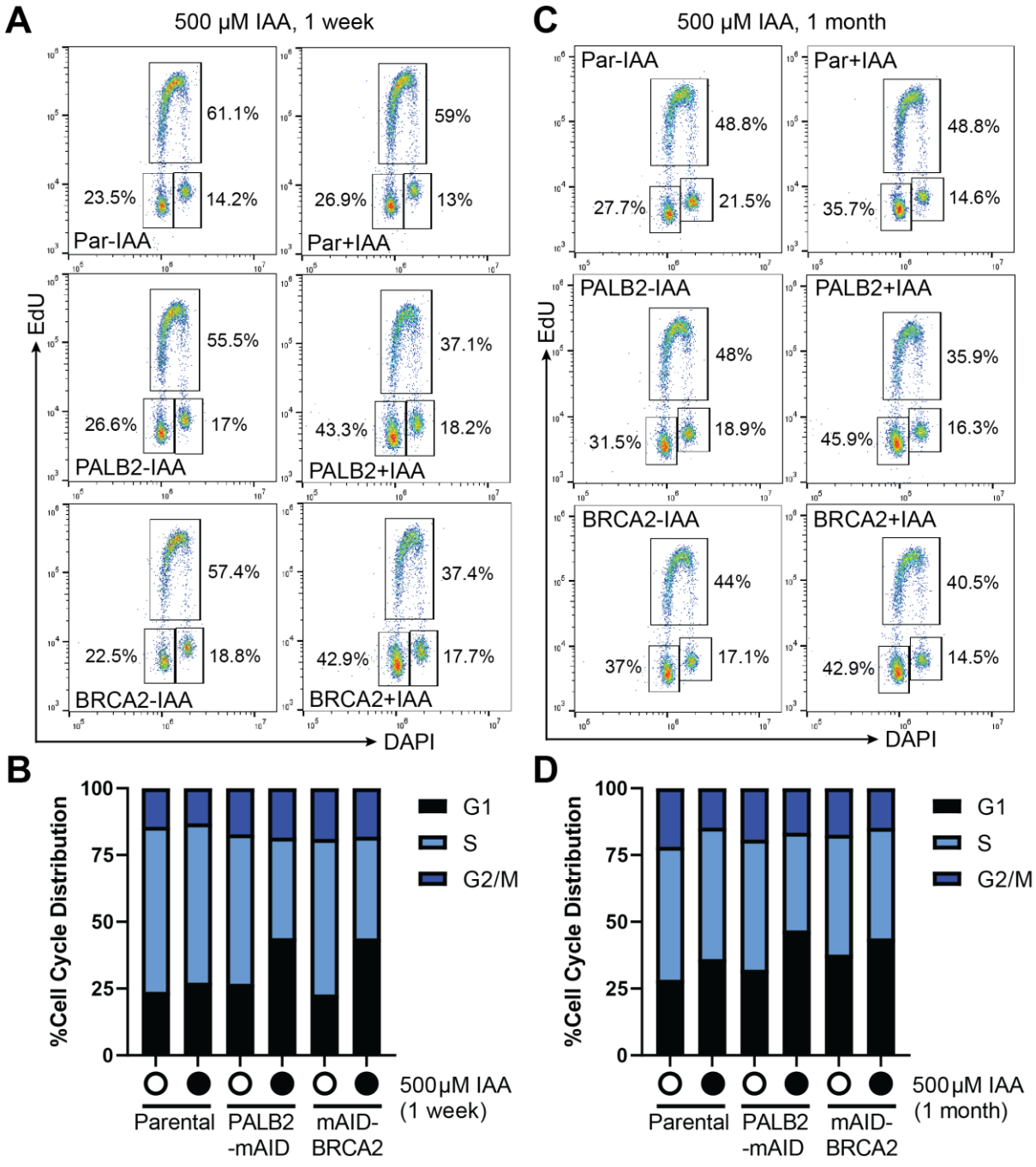


Figure 5.9 Cell cycle analysis after long-term IAA treatment
A Cell cycle profile of HCT116 mAID-degron cells stained with EdU and DAPI. Gates show percentage of cells in G1, S, and G2/M phase after 1 week 500 µM IAA. **B** Graph showing quantification of percentage of HCT116 mAID-degron cells in the different cell cycle stages, as determined by A. **C** Cell cycle profile of HCT116 mAID-degron cells stained with EdU and DAPI. Gates show percentage of cells in G1, S, and G2/M phase after 1 month 500 µM IAA. **D** Graph showing percentage of cells in each cell cycle stage, from data in C, after 1 month 500 µM IAA.

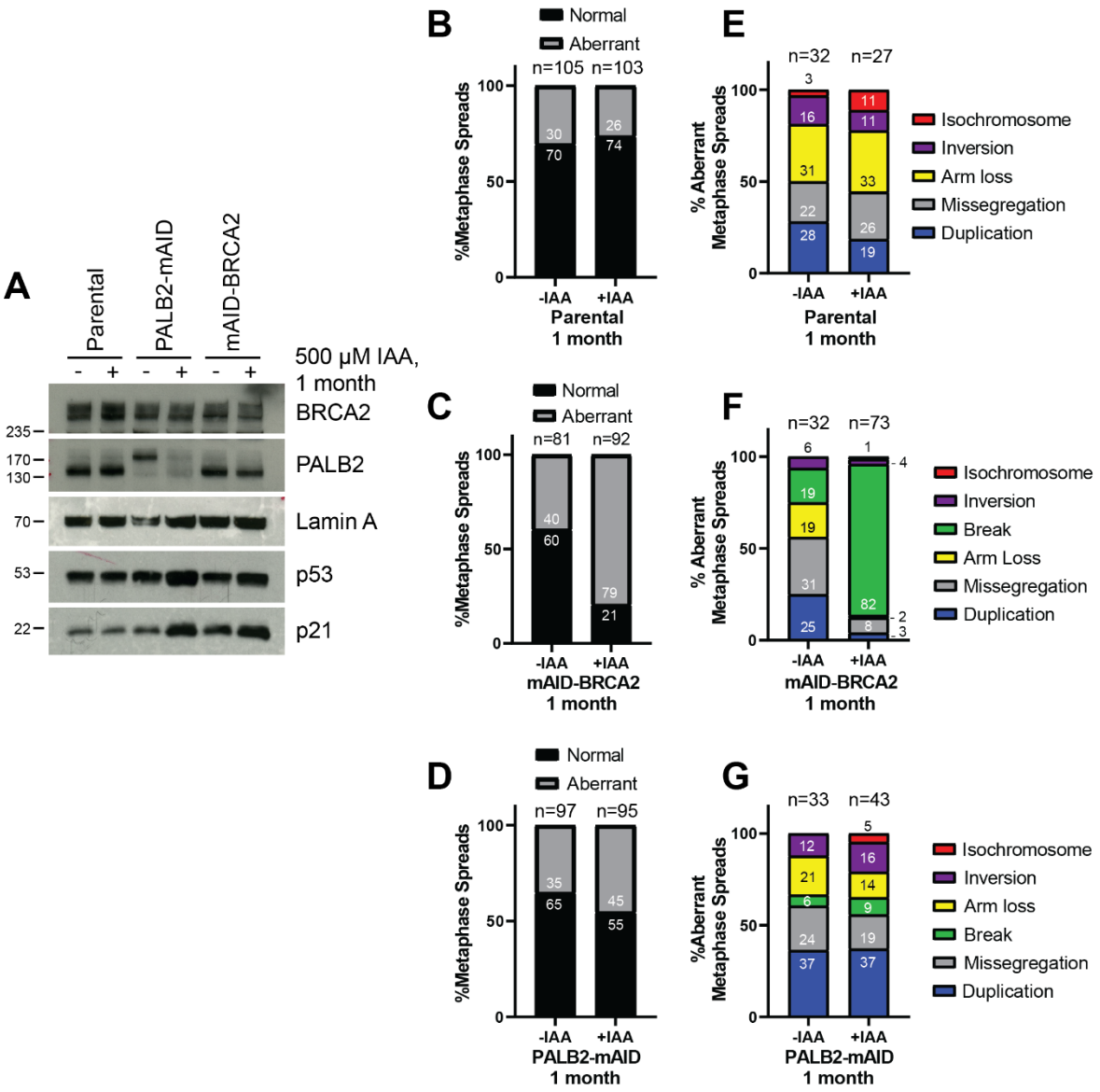


Figure 5.10 The effect of long-term (1 month) BRCA2 and PALB2 depletion on Chr17 aberrations

A Western blot showing protein levels after 1 month 500 μM IAA treatment. Lamin A was used as a loading control. **B-D** Quantification of metaphase spreads showing normal vs aberrant Chr17 FISH probe signal after 1 month 500 μM IAA treatment in HCT116 OsTIR1 parental (B), mAID-BRCA2 (C), and PALB2-mAID (D) cells. Numbers represent the percentage of metaphase spreads, rounded to the nearest whole number. At least 90 metaphase spreads analysed per condition from 3 independent repeats. **E-G** Graphs showing quantification of types of Chr17 aberrations appearing after 1 month 500 μM IAA treatment in HCT116 OsTIR1 parental (E), mAID-BRCA2 (F), and PALB2-mAID (G) cells. Numbers represent the percentage occurance out of aberrant metaphase spreads shown in B-D, rounded to the nearest whole number. Precise n displayed above each sample.

After 1 month, 500 μM IAA treatment, HCT116 OsTIR1 parental cells showed little change in the percentage of metaphase spreads with aberrant Chr17 FISH signal (**figure 5.10B**), however this was increased by ~10-20% from the 24 hour IAA condition (**figure 5.8C**).

Alternatively, PALB2 depletion for 1 month increased the percentage of aberrant metaphase spreads by 10% (**figure 5.10D**), up by 20% from 24 hour IAA treatment (**figure 5.8E**). Nevertheless, there were only slight differences in the types of Chr17 aberrations that arose after 1 month IAA treatment. HCT116 OsTIR1 parental cells showed minor increases in Chr17 missegregation, arm loss, and isochromosome formation, possibly reflecting the low level of chromosome instability that occurs throughout the cell cycle from endogenous stressors and DNA damage (**figure 5.10E**). PALB2 depletion led to small increases in chromosome breaks, inversions, and isochromosomes, indicative of its role in accurate HR-mediated DNA break repair (**figure 5.10G**).

Most intriguingly, 1 month BRCA2 depletion resulted in a 39% increase in Chr17 aberrations (**figure 5.10C**), up by approximately 50% from 24 hour IAA treated samples. 82% of these aberrations represented chromosome breaks (**figure 5.10F**). These breakage events often coincided with missegregation of the q-arm while the p-arm was retained. The substantial increase in Chr17 breaks upon long-term BRCA2 depletion correlates with its important role in maintaining genome stability.

Overall, this investigation into the long-term consequences of BRCA2 and PALB2 depletion on Chr17 stability revealed that PALB2 depletion has a more modest effect on Chr17 stability while BRCA2 depletion correlates with a large increase in Chr17 breaks and chromosome arm separation. This may provide some insight into tumourigenesis and early cancer driving events.

5.2.4 Impact of BRCA2 and PALB2 depletion on centromere identity in HCT116 cells

I demonstrated in **chapter 4** that HR factors can impact centromere identity in RPE1 cells. RAD51 was shown to be important for maintaining CENP-A levels at CENP-B-defined centromeres in asynchronous and quiescent RPE1 cells (**sections 4.2.2 and 4.2.3**) (Saayman et al., 2023) and BRCA2 depletion was shown to decrease CENP-A levels in

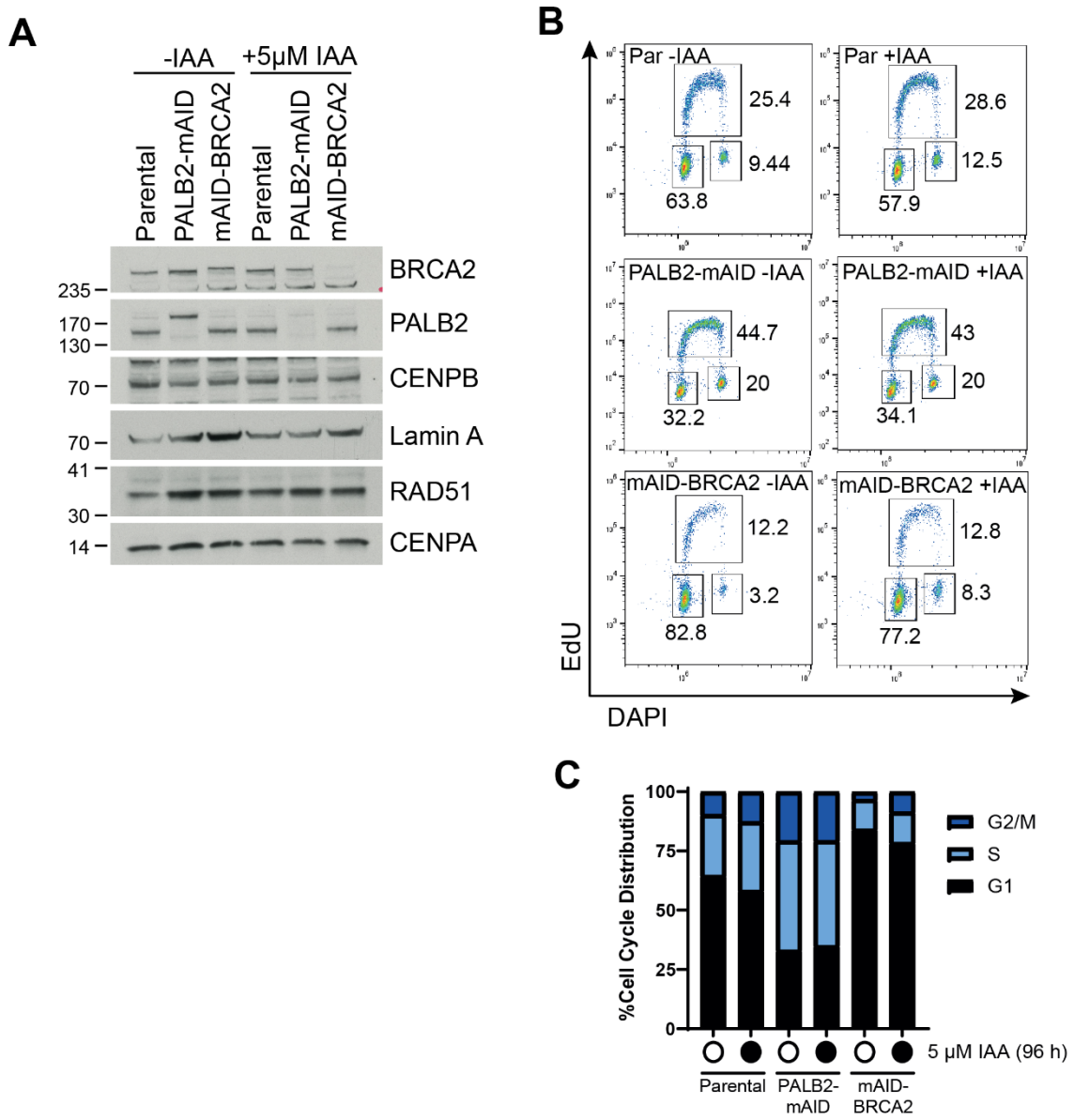


Figure 5.11 BRCA2 and PALB2 can be degraded with only 5 μM IAA
A Western blot showing PALB2 and BRCA2 degradation after 5 μM IAA treatment for 96 h. Lamin A used as a loading control. **B** Flow cytometry after 96 h 5 μM IAA treatment with EdU and DAPI staining. Percentage of cells in each gate displayed. **C** Graph showing quantification of percentage of HCT116 mAID-degron cells in the different cell cycle stages after 5 μM IAA treatment, as determined by B.

asynchronous but not quiescent cells (**sections 4.2.2 and 4.2.3**). Interestingly, PALB2 did not significantly influence CENP-A levels in RPE1 cells under any conditions (**sections 4.2.2 and 4.2.3**). Given that these studies were conducted using siRNA-mediated depletion and in non-cancerous RPE1 cells, I wanted to further explore the role of HR factors in

centromere identity using the AID system, in conjunction with siRNA, in cancerous HCT116 cells, to investigate whether these phenotypes are conserved across different cell types.

During the course of this investigation, evidence emerged that IAA can impact cellular growth and gene expression (Yesbolatova et al., 2020), hence I titrated IAA concentration to only 5 μM IAA while still maintaining rapid and complete protein depletion (**figure 5.11A**). I next assessed the consequences of PALB2 and BRCA2 depletion in HCT116 cells on cell cycle distribution. Cells were treated with 5 μM IAA for 96 hours before cell cycle analysis through EdU incorporation, to measure replicating cells, and DAPI staining (**figure 5.11B**). While OsTIR1 parental, PALB2-mAID, and mAID-BRCA2 cell lines show different cell cycle distributions, IAA treatment did not significantly alter this (**figure 5.11C**). HCT116 PALB2-mAID cells showed enrichment in S- and G2/M-phase while mAID-BRCA2 cells were enriched in G1 phase, compared to OsTIR1 parental cells. This could reflect background, leaky degradation of BRCA2 and PALB2, or else the impact of protein tagging on endogenous protein function.

To assess HR factor involvement in centromere identity, I conducted immunofluorescence experiments similar to **section 4.2.2** where HCT116 degron cells were treated with or without 5 μM IAA for 96 hours (**figure 5.10A**), consistent with siRNA depletion studies (**figures 5.13 and 5.14, section 4.2.2**). Images were collected (**figure 5.12B**) and quantified as in **figure 4.2C**. Unsurprisingly, 96 hour 5 μM IAA treatment did not significantly impact CENP-A or CENP-B levels in HCT116 OsTIR1 parental cells (**figure 5.12C**). Alternatively, BRCA2 degradation in asynchronous HCT116 mAID-BRCA2 cells produced a modest reduction in CENP-A signal, although this was variable and only notable when normalised to CENP-B signal (**figure 5.12D**). Furthermore, PALB2 depletion failed to significantly impact CENP-A levels at CENP-B-defined centromeres (**figure 5.12E**). Collectively, these data indicate that BRCA2, but not PALB2, modestly impacts centromere identity in asynchronous HCT116 cells.

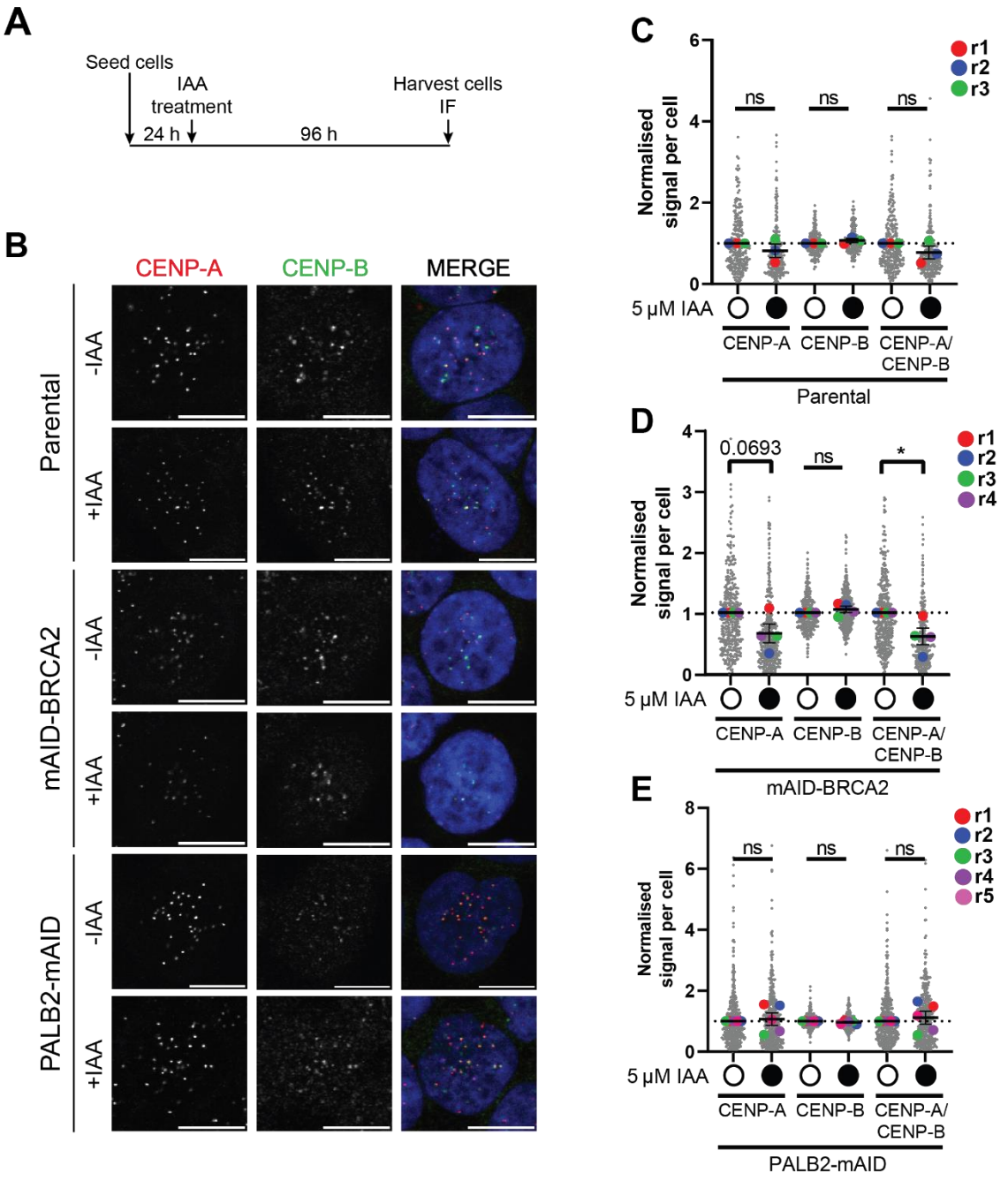


Figure 5.12 Assessing CENP-A levels in HCT116 degron cell lines
A Schematic of experimental protocol using 5 μM IAA. **B** Representative images of CENP-A and CENP-B immunofluorescence staining. Scale bar equals 10 μm. **C** CENP-A, CENP-B, or normalised CENP-A to CENP-B signal in HCT116 OsTIR1 parental cells. **D** CENP-A, CENP-B, or normalised CENP-A to CENP-B signal in HCT116 mAID-BRCA2 cells. **E** CENP-A, CENP-B, or normalised CENP-A to CENP-B signal in HCT116 PALB2-mAID cells. All samples normalised to the -IAA sample. Large coloured dots represent experiment average. At least 100 cells analysed per condition, per repeat. Unpaired t-test.

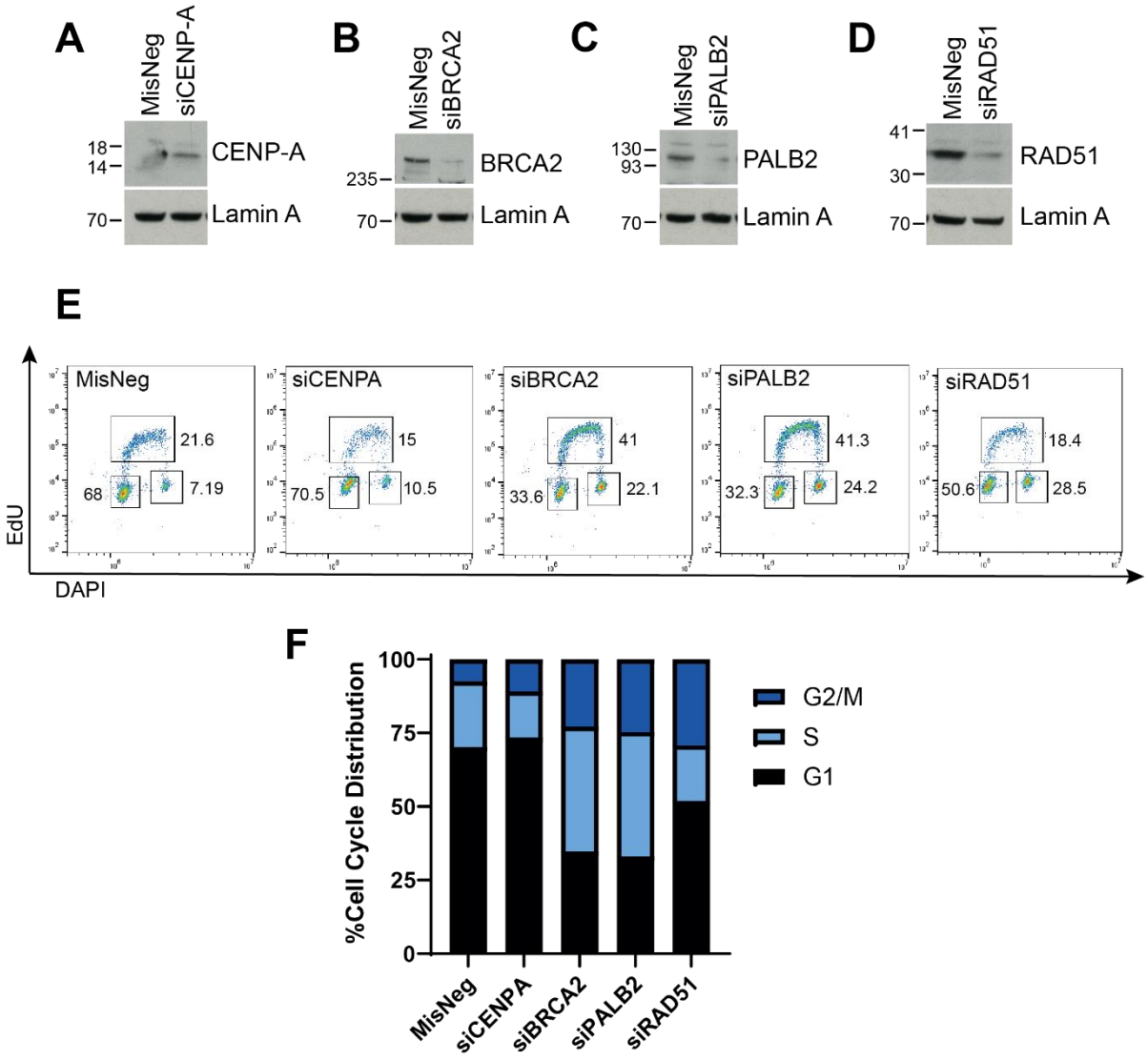


Figure 5.13 siRNA depletion of HR factors in HCT116 OsTIR1 parental cells
A-D Western blot showing siRNA mediated depletion over 72 h of CENP-A (A), BRCA2 (B), PALB2 (C), and RAD51 (D). Lamin A used as a loading control. **E** Cell cycle profile of HCT116 OsTIR1 parental cells stained with EdU and DAPI. Gates show percentage of cells in G1, S, and G2/M phase after 96 h siRNA treatment. **F** Graph showing quantification of percentage of siRNA-depleted HCT116 OsTIR1 parental cells in the different cell cycle stages, as determined by E.

I wanted to corroborate these findings using siRNA-mediated HR factor depletion, as in RPE1 cells, to compare the impact of RAD51 depletion on centromere identity in asynchronous HCT116 cells. BRCA2, PALB2, and RAD51 could all be successfully depleted from asynchronous HCT116 cells using siRNA (**figures 5.13B-D**). Complete siRNA-mediated CENP-A depletion was difficult to confirm by WB (**figure 5.13A**) but quantification by IF showed reduced levels on chromatin (**figures 5.14A-D**). Cell cycle analysis indicated some influence of siRNA depletion on cell cycle distribution (**figures**

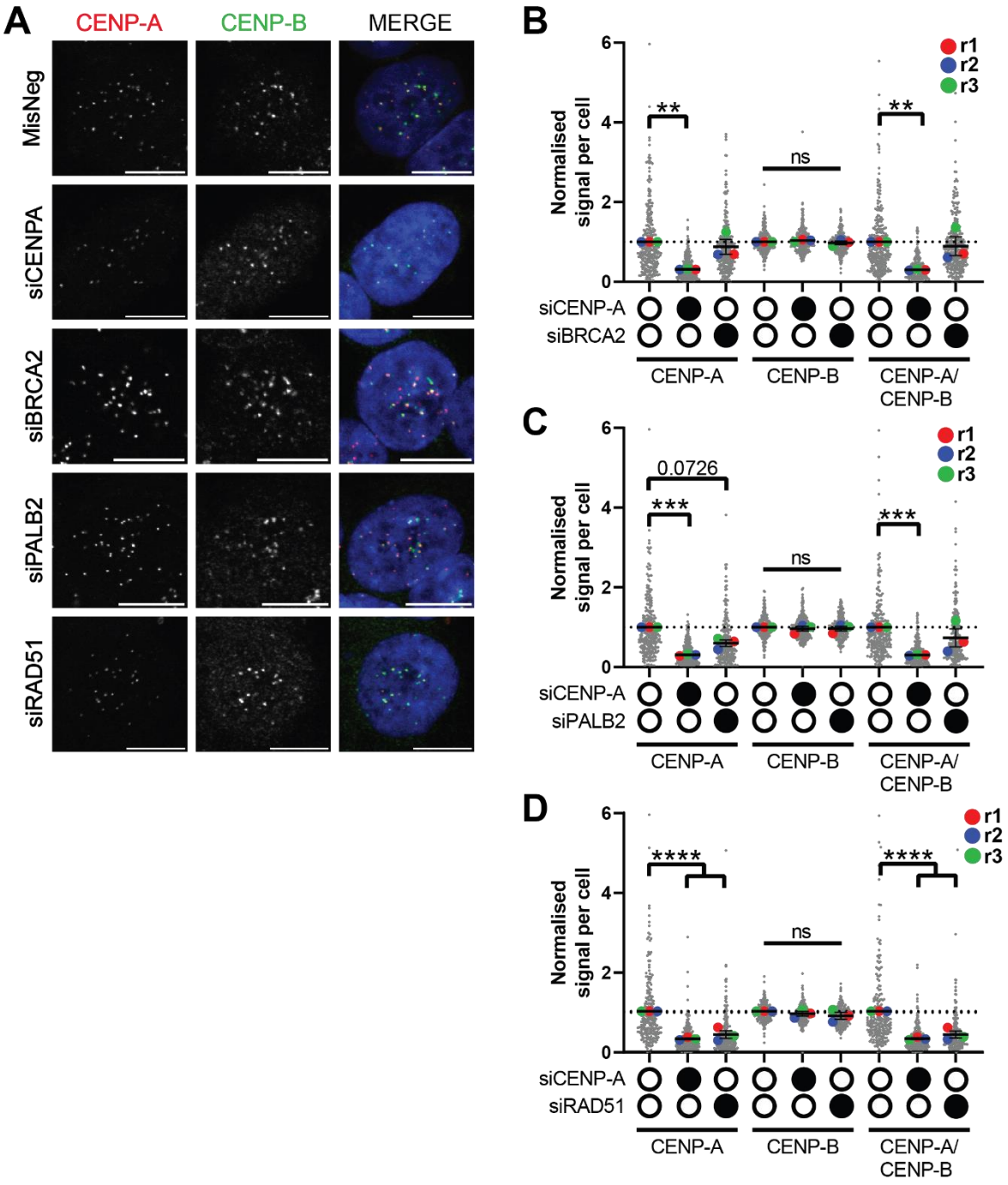


Figure 5.14 Assessing CENP-A levels after siRNA depletion in HCT116 cells
A Representative images of CENP-A and CENP-B immunofluorescence staining. Scale bar equals 10 µm. **B** CENP-A, CENP-B, or normalised CENP-A to CENP-B signal after 96 h BRCA2 depletion in HCT116 OsTIR1 parental cells. **C** CENP-A, CENP-B, or normalised CENP-A to CENP-B signal after 96 h PALB2 depletion in HCT116 OsTIR1 parental cells. **D** CENP-A, CENP-B, or normalised CENP-A to CENP-B signal after 96 h RAD51 depletion in HCT116 OsTIR1 parental cells. All samples normalised to the MisNeg sample. Large coloured dots represent experiment average. At least 100 cells analysed per condition, per repeat. Unpaired one-way ANOVA with Tukey's multiple comparisons test.

5.13E and F). Both BRCA2 and PALB2 depletion led to a substantial increase in S and G2/M phase populations while RAD51 depletion contributed to increased G2/M phase cells. Next, assessment of CENP-A and CENP-B levels after 96 hour siRNA treatment (as in **figure 4.2A**) (**figure 5.14A**) showed that BRCA2 depletion does not produce a significant decrease in CENP-A levels at CENP-B-defined centromeres in asynchronous HCT116 cells (**figure 5.14B**). Quantification of CENP-A levels revealed a modest decrease upon PALB2 depletion, however this effect was lost upon normalisation to CENP-B signal (**figure 5.14C**). On the other hand, RAD51 depletion by siRNA resulted in a significant decrease in CENP-A levels in asynchronous HCT116 cells (**figure 5.14D**).

Altogether, comparison of AID-tagged and siRNA-treated cells indicate different requirements for HR factors in HCT116 cells. siRNA-mediated RAD51 depletion suggests it is required to maintain CENP-A levels at the centromere. However, while HCT116 mAID-BRCA2 cells demonstrated a modest requirement for BRCA2 in centromere identity, BRCA2 depleted by siRNA showed no impact on CENP-A levels, most likely due to incomplete depletion. Finally, PALB2 depletion by either method demonstrated little influence on CENP-A levels and centromere identity in asynchronous HCT116 cells.

5.2.5 Impact of BRCA2/PALB2/RAD51 on centromere integrity in HCT116 cells

Expanding on this and the evidence suggesting a role for HR factors on centromere integrity in RPE1 cells (**chapter 4**) (Saayman et al., 2023), I again wanted to explore this in HCT116 cells. In quiescent RPE1 cells, RAD51 was shown to limit centromere breaks (Saayman et al., 2023), although this disagreed with my own findings, likely due to experimental differences (**sections 4.2.4, 4.2.5, 4.3.2**). Furthermore, I discussed evidence suggesting that BRCA2 may limit exposure of ssDNA at centromeres in cycling cells (**sections 4.2.4 and 4.2.5**). PALB2 depletion did not appear to significantly affect centromere integrity in RPE1 cells (**sections 4.2.4 and 4.2.5**).

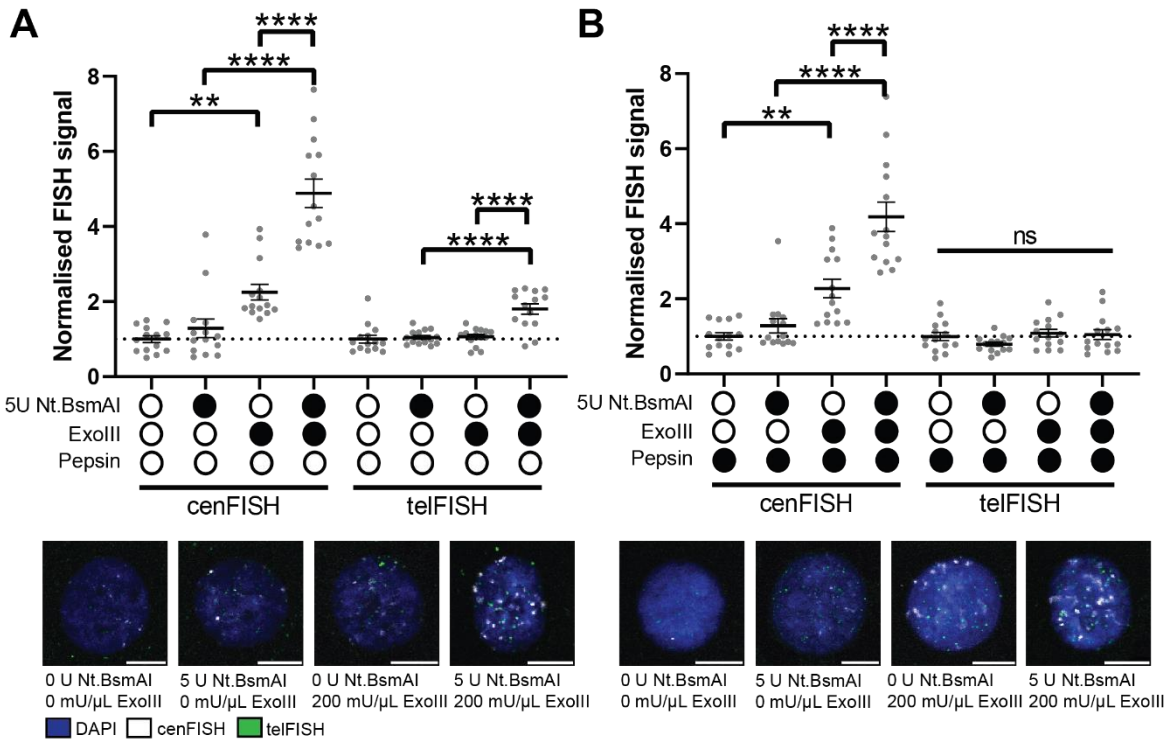


Figure 5.15 Optimisation of Exo-FISH assay in HCT116 cells
A Exo-FISH in HCT116 cells excluding pepsin pre-treatment. **B** Exo-FISH assay in HCT116 cells including a pepsin pre-treatment step. Representative images displayed underneath the graphs. Scale bar equals 10 µm. SSBs induced with 5 U Nt.BsmAI. Samples treated with 200 mU/µL ExoIII where indicated. cenFISH and telFISH signals normalised to 0 mU ExoIII condition, respectively. 14 interphase cells analysed per condition. n=1. Unpaired one-way ANOVA with Tukey's multiple comparisons test.

Like **sections 4.2.4, 4.2.5** and (Saayman et al., 2023), I employed Exo-FISH to study the role of HR factors in asynchronous HCT116 cells (**figure 4.6 and 5.12**). Exo-FISH has not previously been utilised in HCT116 cells so I first optimised the protocol for these cells. In **figure 5.15A**, asynchronous HCT116 OsTIR1 parental cells were treated without pepsin and SSBs induced using the nicking endonuclease, Nt.BsmAI. Addition of Nt.BsmAI without ExoIII treatment produced low levels of cenFISH and telFISH signal as no DNA resection occurs and limited FISH probes can bind. Upon ExoIII treatment, cenFISH signal increases as spontaneous DNA breaks are now resected to facilitate probe binding. ExoIII and Nt.BsmAI treatment further enhances cenFISH and telFISH signal due to extensive SSB induction and resection. A similar trend can also be observed with pepsin pre-treatment to remove chromatin-bound proteins (**figure 4.8A and 5.15B**).

Centromeric DNA breaks were assessed in the HCT116 mAID cell lines after 5 μM IAA treatment for 96 hours. Similar to RPE1 cells, telFISH signal was less responsive to ExoIII treatment than cenFISH signal in HCT116 cells (**figure 5.16A-F**). In HCT116 OsTIR1 parental cells, IAA treatment contributes to a small, insignificant increase in cenFISH signal, even in the absence of ExoIII. Upon ExoIII treatment, cenFISH signal further increases, especially when combined with IAA treatment, however this difference was not significant (**figure 5.16A**). HCT116 mAID-BRCA2 cells showed a similar trend however ExoIII treatment in BRCA2 depleted cells produced a notable but insignificant increase in cenFISH signal compared to IAA treated, ExoIII untreated controls (**figure 5.16B**). Interestingly however, HCT116 PALB2-mAID cells appeared largely unresponsive to ExoIII treatment and PALB2 degradation did not significantly alter cenFISH signal compared to the control (**figure 5.16C**). Collectively, this suggests that while BRCA2 could play a modest role in limiting centromere stability in asynchronous HCT116 cells, PALB2 is likely not involved in this process.

Moreover, I included a pepsin pre-treatment step within the Exo-FISH protocol to remove chromatin-bound proteins and theoretically reveal additional DNA breaks or ssDNA regions (**figure 4.8A**). Pepsin treatment produced variable results making any interpretations more difficult (**figures 5.16D, E, F**). As described above, IAA addition alone increased cenFISH signal in HCT116 OsTIR1 parental cells, and ExoIII treatment did not significantly increase cenFISH signal, regardless of IAA addition (**figure 5.16D**). Similarly, highly variable and insignificant trends were seen in both mAID-BRCA2 and PALB2-mAID cells (**figures 5.16E and F**). On the surface, these results suggest that BRCA2 and PALB2 depletion does not impact ssDNA accumulation or DNA breaks at centromeres in asynchronous HCT116 cells, however the quality of the data impedes confident conclusions.

These findings were subsequently compared to HCT116 cells treated with siRNA (**figure 5.17**). In **figure 5.17A**, siBRCA2 treatment did not contribute to a significant increase in cenFISH signal after ExoIII treatment, compared to MisNeg-treated controls. The same can

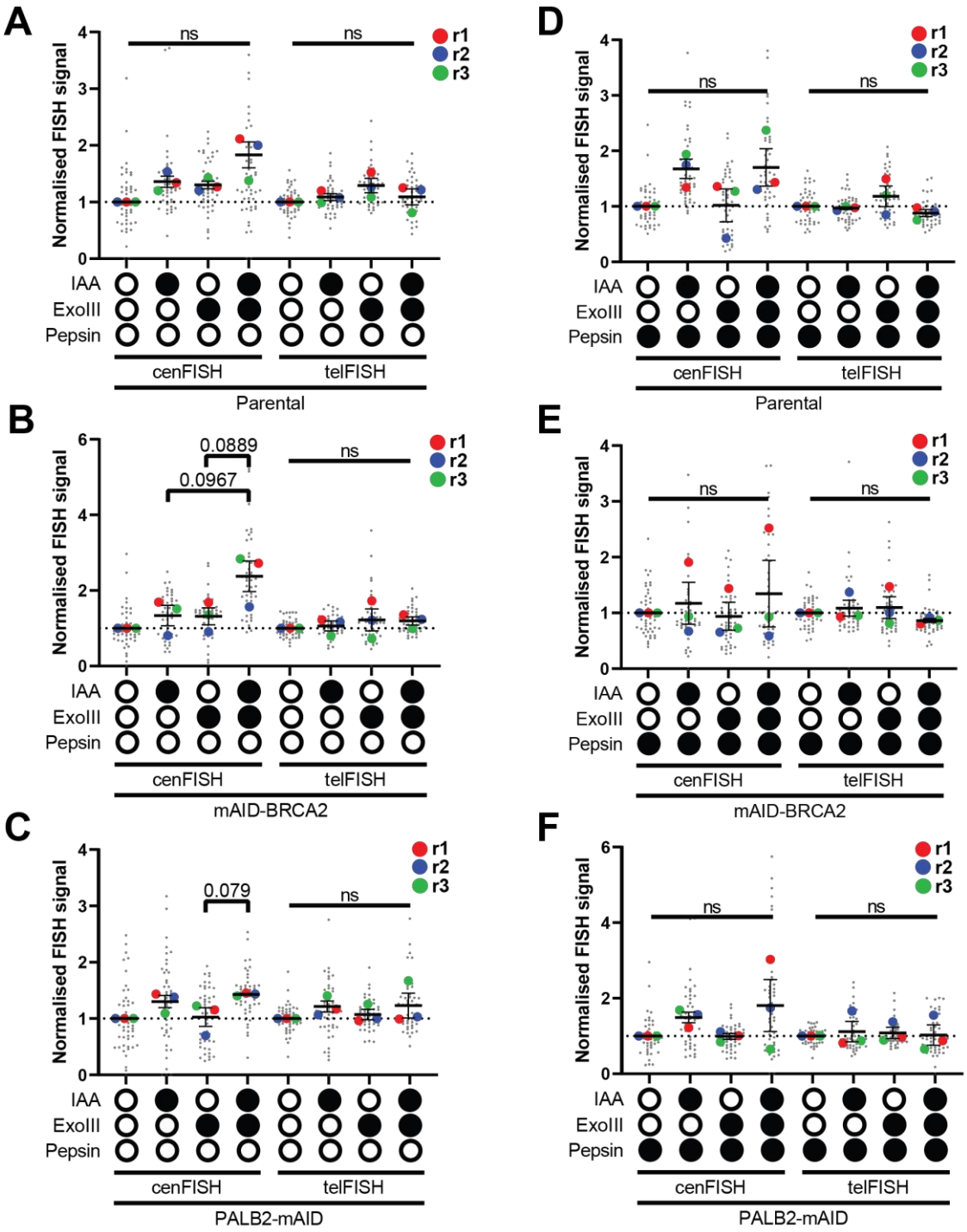


Figure 5.16 Exo-FISH assay in HCT116 degron cell lines
A Exo-FISH without pepsin pre-treatment in HCT116 OsTIR1 parental cells with or without 5 μM IAA for 96 h. **B** Exo-FISH without pepsin pre-treatment in HCT116 mAID-BRCA2 cells with or without 5 μM IAA for 96 h. **C** Exo-FISH without pepsin pre-treatment in HCT116 mAID-BRCA2 cells with or without 5 μM IAA for 96 h. **D** Exo-FISH with pepsin pre-treatment in HCT116 OsTIR1 parental cells with or without 5 μM IAA for 96 h. **E** Exo-FISH with pepsin pre-treatment in HCT116 mAID-BRCA2 cells with or without 5 μM IAA for 96 h. **F** Exo-FISH with pepsin pre-treatment in HCT116 mAID-BRCA2 cells with or without 5 μM IAA for 96 h. cenFISH and telFISH signal normalised to -IAA, -ExoIII treated samples. Large coloured dots represent average of each independent experiment. n=3. At least 15 cells analysed per condition, per repeat. Error bars represent S.E.M. Unpaired one-way ANOVA with Tukey's multiple comparisons test.

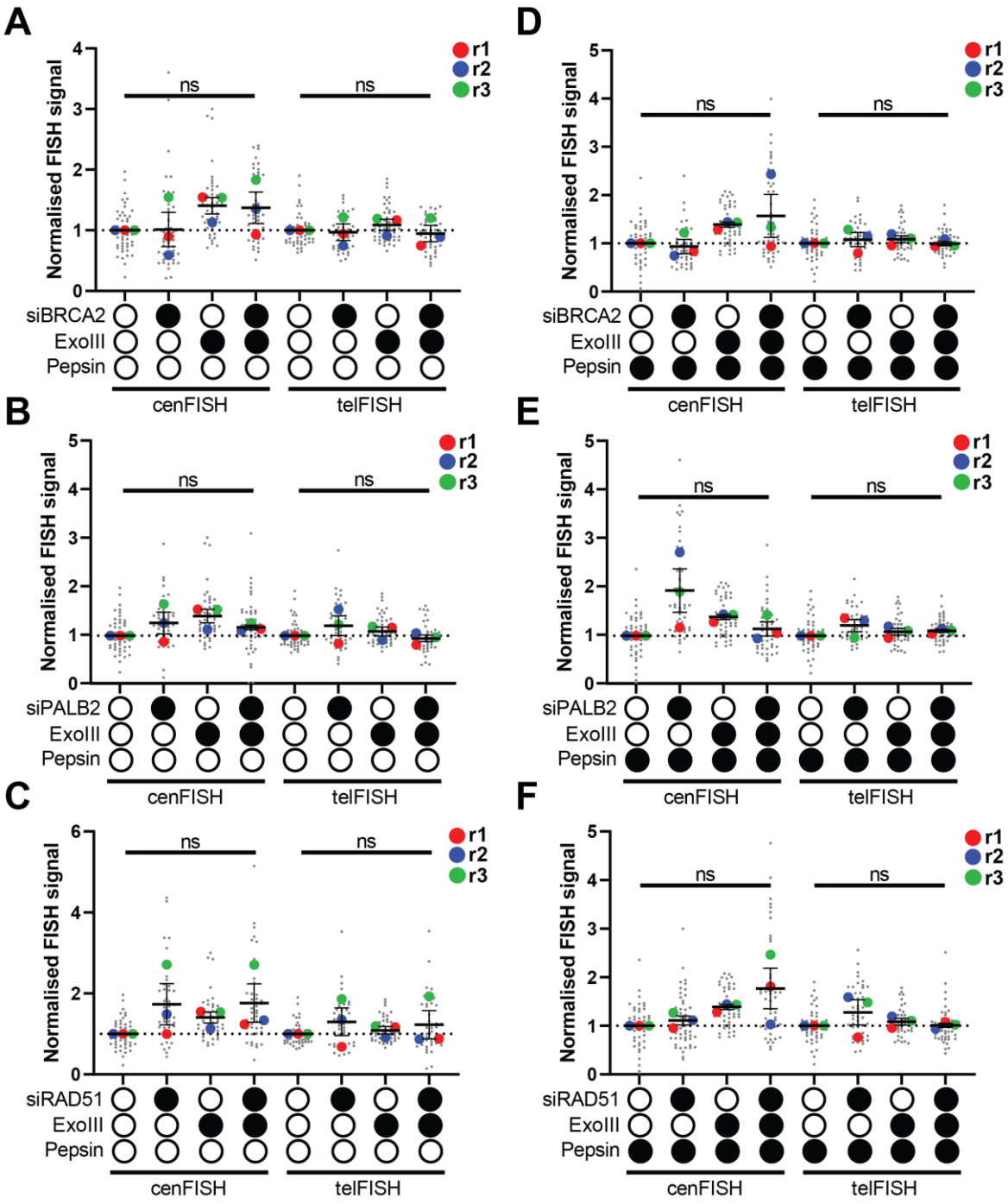


Figure 5.17 Exo-FISH assay in HCT116 cells treated with siRNA
A Exo-FISH without pepsin pre-treatment in siBRCA2 (96 h) treated HCT116 OsTIR1 parental cells. **B** Exo-FISH without pepsin pre-treatment in siPALB2 (96 h) treated HCT116 OsTIR1 parental cells. **C** Exo-FISH without pepsin pre-treatment in siRAD51 (96 h) treated HCT116 OsTIR1 Parental cells. **D** Exo-FISH with pepsin pre-treatment in siBRCA2 (96 h) treated HCT116 OsTIR1 parental cells. **E** Exo-FISH with pepsin pre-treatment in siPALB2 (96 h) treated HCT116 OsTIR1 parental cells. **F** Exo-FISH with pepsin pre-treatment in siRAD51 (96 h) treated HCT116 OsTIR1 parental cells. cenFISH and telFISH signal normalised to MisNeg, -ExoIII treated samples. Large coloured dots represent average of each independent experiment. n=4. At least 15 cells analysed per condition, per repeat. Error bars represent S.E.M. Unpaired one-way ANOVA with Tukey's multiple comparisons test.

be concluded for PALB2 (**figure 5.17B**) and RAD51 depleted cells (**figure 5.17C**). It should be noted however, that siRAD51 treatment produced particularly variable results, regardless of ExoIII treatment, resulting in slight differences compared to MisNeg treated samples. Importantly, similar to RPE1 cells (**figure 4.7E**), telFISH signal was also impacted by RAD51 depletion, again highlighting RAD51's proposed function at telomeres (**section 4.3.2**) (Chastain et al., 2016; Cho et al., 2014). Pepsin pre-treatment produced comparable results where neither BRCA2, PALB2, nor RAD51 depletion significantly altered cenFISH signal compared to the MisNeg control, irrespective of ExoIII treatment (**figures 5.17D-F**).

In conclusion, utilising AID and siRNA to investigate the role of BRCA2, PALB2, and RAD51 in centromere stability, failed to reveal evidence for these factors in regulating centromeric DNA breaks or ssDNA exposure in asynchronous HCT116 cells, although BRCA2 may have some small role.

5.3 Discussion

5.3.1 Using the AID system to study BRCA2 and PALB2 function in HCT116 cells

In this chapter, I described the successful generation and validation of HCT116 mAID-BRCA2 and PALB2-mAID cell lines (**figure 5.1**). Rapid degradation of BRCA2 and PALB2 was possible using this AID system (**figures 5.1C and D**) and produced the expected HR repair defect, as determined by WST-1 and IF experiments after MMC and olaparib treatment (**figures 5.3-5.5**).

In **figures 5.2A and B**, it became apparent that only one PALB2 allele was tagged with Halo and mAID by PCR and sequencing, due to a deletion within the C-terminal region of PALB2. PALB2 contains a seven-bladed WD40-type β-propeller within its C-terminus which forms the binding site for BRCA2 via its N-terminus (Oliver et al., 2009). Cancer-associated mutations and truncations within PALB2's C-terminal region have been shown to disrupt hydrogen bonding between amino acids, producing an incompletely folded protein that is

non-functional and likely degraded rapidly, thus not detectable by WB (Oliver et al., 2009). Therefore, I concluded that this heterozygous HCT116 PALB2-mAID clone is sufficient for the purpose of this study and any future experiments. This is supported by rapid degradation of PALB2 upon IAA treatment (**figures 5.1D and 5.11A**) and complete loss of the PALB2-BRCA2 interaction upon IAA treatment by immunoprecipitation (**figure 5.2C**). Furthermore, evidence indicates that only one functional allele of PALB2 is required to maintain adequate DDR signalling, as shown clearly in **figures 5.3C and I** where RAD51 foci are induced upon exogenous DNA damage, indicating PALB2's remaining activity is sufficient to facilitate HR-mediated repair. The HCT116 mAID-BRCA2 cell line used in this study was previously demonstrated to be homozygous (Lucia Rampazzo, data not shown).

However, it should be noted that both HCT116 mAID-BRCA2 and PALB2-mAID cell lines show reduced survival compared to HCT116 OsTIR1 parental cells, regardless of IAA treatment (**figures 5.3B-E**). During this study, it became known that the AID system can induce leaky degradation of the protein-of-interest (Yesbolatova et al., 2020). Furthermore, cells treated with 500 μM IAA can impact cell growth and gene expression (Yesbolatova et al., 2020). Therefore, it is possible that some findings in my study are impacted by leaky depletion and IAA treatment itself and so this should be considered when interpreting any results. Ultimately, it was possible to reduce the concentration of IAA by 100X and still rapidly degrade BRCA2 and PALB2 from cells (**figure 5.11A**), hence these conditions were used for the remainder of my investigation (**figures 5.12 and 5.16**). More recently, a new generation of AID system has been developed, termed AID2, which uses the osTIR1(F47G) mutant and IAA analogue 5-Ph-IAA to minimise leaky protein degradation and allow for a 670X lower ligand concentration (Yesbolatova et al., 2020), as such, it may be worth updating these HCT116 mAID cell lines for future studies.

Another potential source of variation, regardless of IAA treatment, could result from protein tagging or additional off-target mutations induced during CRISPR. CRISPR/Cas9 gene editing is a fantastic system to modify genes, however it can produce secondary mutations

due to limited specificity of the sgRNA target DNA sequence. These off-target effects are often linked to loss-of-function mutations or incorrect repair of the targeted genes (Zhu, 2022). There are now several other Cas9 variants, such as Cpf1/Cas12a, with improved accuracy which may reduce off-target impacts when directly administered to cells in complex with sgRNA (Bandyopadhyay et al., 2020; Yamagishi et al., 2019).

Surprisingly, cell cycle analysis after short-term IAA treatment showed little impact of IAA treatment on cell cycle distribution (**figures 5.11B and C, 5.8A and B**) despite BRCA2 and PALB2's role in G2/M cell cycle checkpoint activation and DNA repair in S and G2 phase (Feng & Jasin, 2017; Nikkilä et al., 2013; Patel et al., 1998). Again, this lack of response to IAA treatment could reflect leaky AID-mediated degradation of BRCA2 and PALB2 in these cell lines or the impact of secondary mutations generated during CRISPR editing (Natsume et al., 2016). Alternatively, it could be a consequence of using cancerous HCT116 cells which could more readily adapt to disturbances in the DDR due to the absence of MMR and increased homeologous recombination (Spies & Fishel, 2015). It might be interesting to further validate BRCA2's and PALB2's impact on cell cycle progression in the future by establishing the cell cycle distribution after exogenous DNA damage and stress is applied to the cells.

5.3.2 Long-term depletion of BRCA2 and PALB2 reveals distinct chromosomal aberrations

BRCA2 and PALB2 loss-of-function has been linked to tumourigenesis (Roy et al., 2012; Wu et al., 2020). Analysis of cell survival after 10 days BRCA2 or PALB2 depletion revealed a subset of cells that were able to survive in the absence of tumour suppressor activity (**figure 5.6A-D**). Germline BRCA2 and PALB2 loss has previously been associated with medulloblastoma and Iso(17q) formation (Waszak et al., 2018), hence I aimed to investigate the consequences of long-term BRCA2 and PALB2 loss on Chr17 stability (**figure 5.7**) to gain insight into how cells accumulate chromosomal aberrations and adapt to drive tumourigenesis.

I first assessed Chr17 aberrations after 24 hour 500 μM IAA treatment to establish baseline chromosomal instability (CIN) levels (**figure 5.8**). At this time point, there was little difference in the percentage of metaphase spreads containing Chr17 aberrations after IAA treatment, across the three HCT116 mAID cell lines (**figures 5.8C-E**). Short-term BRCA2/PALB2 depletion likely fails to significantly alter Chr17 aberration frequency as secondary mutations promoting cell survival after GCRs are presumably absent, thus cells displaying CIN and GCRs undergo apoptosis following p53 expression and are thereby excluded from analysis (Carlos et al., 2013; Jonkers et al., 2001). This is supported by the modest increase in p53 and p21 expression that is visible by WB after 10 days 500 μM IAA treatment (**figure 5.6E**). p53 is a tumour suppressor expressed on the p-arm of Chr17 that functions with retinoblastoma protein, Rb, and p21, to regulate several cellular processes including the cell cycle, DNA replication, DDR, chromosome segregation, and apoptosis (Engeland, 2022). The TP53 gene is mutated or deleted in approximately half of all cancers to facilitate cancer cell survival and increase proliferative potential. After 24 hour IAA treatment, most cells would be expected to contain functional p53 expression and downstream signalling pathways, limiting the accumulation of aberrant mitotic cells.

Alternatively, after 1 month of 500 μM IAA treatment, more substantial increases in p53 and p21 expression are visible by WB (**figure 5.10A**), indicative of high stress levels in these cell lines. While HCT116 OsTIR1 parental cells showed no difference, PALB2-mAID cells, and mAID-BRCA2 cells to a slightly lesser extent, displayed a large increase in p53 and p21 compared to IAA untreated controls. Unexpectedly, BRCA2 expression was restored in IAA treated mAID-BRCA2 cells. The exact explanation for this is unknown but these cells may have obtained a missense mutation within the mAID tag or OsTIR1 so that proteasomal-mediated degradation can no longer occur. Although BRCA2 depletion was not maintained for the whole experimental period, cells display stress (p53 and p21 expression) and accumulation of Chr17 aberrations (**figures 5.10C and D**), possibly

originating from previous mutational events and reflecting BRCA2's role in protecting against CIN.

PALB2 and BRCA2 depletion for 1 month produced a 10% and 40% increase in Chr17 aberrations, respectively (**figures 5.10C-D**). Meanwhile, long-term IAA treatment in HCT116 OsTIR1 parental cells produced very little change in Chr17 aberrations, decreasing by 4% (**figure 5.10B**). Nevertheless, this percentage of aberrant metaphase spreads was increased by ~10% compared to the 24 hour treated sample, although there was little change in the types of Chr17 aberrations occurring (**figures 5.10E**). This difference could reflect the consequences of long-term cell culture work and continual passaging of cells, highlighting the importance of regularly refreshing cell culture stocks to avoid spontaneous mutations and CIN from influencing experimental results.

As stated previously, 1 month of 500 μM IAA treatment in HCT116 PALB2-mAID cells produced a small increase in the percentage of metaphase spreads displaying aberrant Chr17 FISH staining (**figure 5.10D**). Despite this, similar to HCT116 OsTIR1 parental cells, there were no substantial differences in the types of Chr17 aberrations to emerge after PALB2 depletion (**figure 5.10G**) where the majority of aberrations included chromosome duplications, inversions, and missegregation. This presumably reflects aberrant DNA repair events resulting from loss of accurate HR-mediated pathways.

1 month BRCA2 depletion in HCT116 mAID-BRCA2 cells resulted in a large increase in Chr17 aberrations, specifically Chr17 breaks leading to complete separation of p- and q-arms (**figures 5.10C and F**), likely reflecting BRCA2's role in preventing DNA breaks and/or DNA repair. The overall percentage of aberrant metaphase spreads in IAA untreated cells was higher than OsTIR1 parental cells which could indicate some degree of leaky BRCA2 degradation or CRISPR off-target effects (**section 5.3.1**) (Natsume et al., 2016). As described above, Chr17 breaks after BRCA2 depletion were commonly associated with missegregation of Chr17 q-arm (red FISH probe staining). It is currently unclear whether the remaining p-arm retains TP53 functionality. It can be hypothesised that p53 activity may

be compromised due to accumulation of secondary mutations, facilitating continued cell survival. This can be confirmed through further transcriptomic- and sequencing-based methods.

Due to the complete separation of p- and q-arms of Chr17, it is tempting to speculate that these lesions may be occurring at or around the centromere. Chromosomes broken at the centromere can still be retained as an active chromosome as long as part, or a majority, of the centromere remains intact for kinetochore formation and spindle attachment (Guerrero et al., 2010). Furthermore, HCT116 cells and other colorectal cancer cell lines have been described to contain several common breakpoints within Chr17, including the centromere and pericentromere (Knutsen et al., 2010). Additionally, analysis of chromosome breakpoints in 345 cases of adenocarcinoma of the large intestine (Mitelman et al., 2008) revealed that of the 50 most common recurrent breakpoints, 50% were located within centromeric regions, the most common of which was within Chr17 (16%) (Knutsen et al., 2010). Complementary to this, analysis of publicly available GLOE-seq and END-seq datasets from HCT116 cells also uncovered an enrichment of spontaneous DNA breaks at the centromere (Canela et al., 2016; Logsdon et al., 2021; Saayman et al., 2023; Sriramachandran et al., 2020). Therefore, although it is impossible to determine the exact breakpoints frequently occurring upon BRCA2 depletion in HCT116 mAID-BRCA2 cells in this experiment, these findings could have very interesting implications for BRCA2's potential role in maintaining centromere stability (**sections 4.3.2 and 5.3.4**). Indeed, BRCA2 mutations have been associated with increased risk of colorectal cancer suggesting that BRCA2 may be particularly important in mitigating chromosome breaks that would otherwise drive tumourigenesis (Sopik et al., 2015). Furthermore, these results highlight the feasibility of MMR-deficient HCT116 cells as a model to study centromere stability (further discussed in **section 6.1.2**).

Evidence suggests that DNA breaks can drive GCRs. First described in 1942, the breakage-fusion-bridge (BFB) cycle proposes how chromosome breaks can be repaired erroneously

to produce dicentric chromosome fusions. In the following cell division, spindle pulling forces on the dicentric chromosome can trigger DNA breaks, thus repeating the cycle (McClintock, 1942). This was expanded in 2018 by Tiwari et al., who described the rupture-bridging cycle (Tiwari et al., 2018). Sister chromatid intertwinements from unresolved HR-mediated repair or replication intermediates can result in break sites close to or at centromeres in anaphase. These breaks can subsequently be erroneously repaired to drive GCRs such as whole arm deletions, translocations, duplications, and isochromosomes. This rupture-bridging cycle was found to be highest in HCT116 cells compared to other cancer cell lines and is normally suppressed by 53BP1 activity. One hypothesis could be that increased Chr17 breakage upon BRCA2 depletion may correlate with increased GCRs, through the mechanism above, across the genome with successive cell divisions. In fact, BRCA2 has previously been shown to be essential to suppress GCRs after chromosome breaks in murine cells (Yu et al., 2000). While this may be not be visible through Chr17 FISH staining alone, more in depth spectral karyotyping (SKY) could reveal further insights. However, despite germline mutations in both proteins being associated with Iso(17q) formation, I did not see significant enrichment across the cell lines (**figure 5.10E-G**). This could result from cell-type differences, or, as discussed previously, the limited experimental timeframe; therefore, increasing passage number may promote further GCR events and Iso(17q) formation.

Also, given the overlapping functions of PALB2 and BRCA2, it is intriguing that cells display distinct Chr17 aberrations upon long-term depletion. In PALB2-independent pathways, BRCA2 functions in S phase by facilitating RAD51 recruitment to stressed replication forks for phosphorylation by PLK1 and CDKs (Wassing et al., 2021; Yata et al., 2014). BRCA2 also protects stalled forks from nucleolytic processing (Schlacher et al., 2011, 2012). Therefore, a large proportion of Chr17 breaks upon BRCA2 depletion could originate from a defective replication stress response. Alternatively, Chr17 aberrations in PALB2 deficient cells are more suggestive of mutagenic recombination events e.g. SSA and alt-EJ, resulting from defective HR. Ultimately suggesting that PALB2 and BRCA2 may trigger

tumourigenesis through distinct mechanisms, and not necessarily solely HR deficiency as previously speculated.

In the absence of HR, spontaneous DNA breaks may be repaired through other erroneous pathways including NHEJ, SSA, or alt-EJ. It was therefore surprising that more translocations or inversions, common features of defective DNA repair, were not observed. The FISH probes I employed in this study only annealed to 167 kb and 343 kb DNA regions. Thus, this assay likely does not have the resolution to effectively assess a majority of GCR events upon PALB2 or BRCA2 depletion, or demonstrate how these GCRs affect gene expression to drive tumourigenesis. More extensive SKY or single-cell whole genome sequencing would ultimately be needed to investigate this in more detail, potentially revealing novel therapeutic targets.

5.3.3 A potential role for BRCA2 in centromere identity in HCT116 cells?

As part of my investigation, I was interested in assessing the role of HR factors in centromere identity. In the previous **chapter 4**, both RAD51 and BRCA2 depletion was shown to decrease CENP-A levels at CENP-B-defined centromeres in asynchronous RPE1 cells but PALB2 did not (**sections 4.2.2**). Furthermore, RAD51 was subsequently shown to be important for centromere identity in quiescent cells (**section 4.2.3**) (Saayman et al., 2023). As discussed in **section 5.1.2**, the question remained as to whether HR factors would also play an important role at centromeres in cancerous HCT116 cells due to their MMR-deficiency associated microsatellite instability.

Measuring CENP-A levels at CENP-B-defined centromeres in asynchronous HCT116 AID cell lines found that while BRCA2 degradation modestly reduced CENP-A levels (**figure 5.10D**), PALB2 depletion had no significant impact (**figure 5.10E**). IAA treatment itself in HCT116 OsTIR1 parental cells also showed little impact on CENP-A levels so this influence can be excluded from any interpretation (**figure 5.10C**). Furthermore, IAA treatment did not significantly alter cell cycle progression compared to untreated controls, as discussed in

section 5.3.1 (figures 5.11B and C), making it unlikely that this phenotype is an indirect consequence.

I next compared these results to HCT116 cells treated with siRNA to deplete BRCA2, PALB2, and RAD51 (**figure 5.14**). In these experiments, RAD51 depletion significantly reduced CENP-A levels (**figure 5.14D**), consistent with studies in asynchronous RPE1 cells (**figure 4.3A**). As discussed previously (**section 4.3.1**), this implies that RAD51 activity is central in regulating centromere identity (Saayman et al., 2023). Nevertheless, the exact function of RAD51 at centromeres remains unknown and further studies using B02-mediated RAD51 inhibition at different stages of the cell cycle and the SNAP-/Halo-tag systems (**section 4.3.1**) (Jansen et al., 2007; Swartz et al., 2019) would hopefully provide more insight into this.

PALB2 siRNA depletion showed no significant decrease in CENP-A levels when normalised to CENP-B (**figure 5.14C**), agreeing with HCT116 PALB2-mAID phenotype (**figure 5.10E**) and asynchronous RPE1 cells (**figure 4.3C**). Interestingly however, asynchronous HCT116 cells treated with siBRCA2 show no significant difference in CENP-A levels compared to the MisNeg control (**figure 5.14B**), contrasting with the modest but insignificant impact observed in HCT116 mAID-BRCA2 cells (**figure 5.12D**). siRNA depletion can produce off-target effects or inconsistent protein depletion, perhaps explaining this difference. However, these experiments are beneficial due to the inclusion of siCENP-A and siRAD51 as a positive control (**figure 5.14B-D**), which is missing from the HCT116 AID experiments (**figure 5.12**). In HCT116 cells, CENP-A depletion after siRNA treatment was difficult to assess by western blot (**figure 5.13A**), as previously described (Swartz et al., 2019). This is likely due to stable incorporation of CENP-A into chromatin and its turnover only once per cell cycle (Jansen et al., 2007). HJURP depletion has been observed to stimulate more complete loss of CENP-A from chromatin and may be useful in these studies in the future (Swartz et al., 2019). Regardless, CENP-A loss was visible by IF (**figure 5.14**) and provided

confidence that the experiments were working. Further discussion on the difference between siRNA and mAID experiments can be found in **section 5.3.5**.

In conclusion, the combination of AID and siRNA-mediated experiments in asynchronous HCT116 cells indicate a role for RAD51 in regulating CENP-A levels, while PALB2 does not appear to play a role, and the impact of BRCA2 is modest, if any. Surprisingly, this differs slightly from the observed impact in RPE1 cells (**sections 4.2.2, 4.3.1, and 6.1.2**). More detailed experiments looking at the impact of BRCA2 depletion on CENP-A loading/maintenance on centromeric chromatin using the Halo-/SNAP-tag system may provide further conclusive insight into this. Importantly, the exclusion of PALB2's influence on CENP-A implies that RAD51's function(s) at centromeres is regulated through non-canonical mechanisms. As described previously, RAD51 can be recruited to chromatin through several BRCA2-independent mechanisms across the cell cycle (Daza-Martin et al., 2019; Nakamura et al., 2019; O'Donnell et al., 2010; Park et al., 2019; Piwko et al., 2016; Saredi et al., 2016; Wassing et al., 2021; Yata et al., 2012, 2014). Therefore, knowledge of RAD51's exact function regarding CENP-A may give further indication as to how it is recruited to centromeric chromatin.

5.3.4 The role of HR factors in centromere stability in HCT116 cells

Expanding on from this, I next assessed the role of BRCA2, PALB2, and RAD51 in centromere stability in HCT116 cells using Exo-FISH. Firstly, I demonstrated that Exo-FISH can be successfully applied to asynchronous HCT116 cells as a method to measure centromeric DNA breaks (**figure 5.15**).

Exo-FISH in HCT116 mAID cell lines revealed that IAA treatment alone increases cenFISH signal (**figures 5.16A and D**). This was surprising but could reflect IAA's influence on the transcriptional landscape in human cells which may indirectly affect the centromere, altering DNA resection and FISH probe accessibility (**section 5.3.1**) (Yesbolatova et al., 2020). Pepsin pre-treatment in HCT116 OsTIR1 parental cells gave very variable results, possibly

by exposing fragile secondary DNA structures containing ssDNA, and completely obscured the impact of ExoIII-mediated digestion (**figure 5.16D**).

Asynchronous HCT116 mAID-BRCA2 cells displayed a notable but insignificant increase in cenFISH signal upon IAA and ExoIII treatment (**figure 5.16B**), indicating that the repair activity of BRCA2 may be important for mitigating centromeric DNA breaks under these conditions. Interestingly, conversely to **figures 4.7C and 4.8C** in RPE1 cells, BRCA2 depletion by IAA treatment does not influence centromeric ssDNA in HCT116 cells (**figures 5.16B and E**). While a small increase was visible, this was consistent with the impact of IAA alone (**figure 5.16A**). BRCA2's impact on centromeric DNA breaks was lost when combined with pepsin pre-treatment (**figure 5.16E**), although it is possible that the high level of variability across the three repeats conceals any subtle phenotypes, including the expected ExoIII response indicating spontaneous centromeric DNA breaks (Saayman et al., 2023). The same is also true for Exo-FISH after siRNA-mediated BRCA2 depletion (**figure 5.17A and D**); cenFISH signal does increase upon ExoIII treatment although this was insignificant and there was no observable difference between MisNeg and siBRCA2-treated asynchronous HCT116 cells. This again highlights the difference between mAID and siRNA-mediated experiments (**section 5.3.5**). Collectively, these data suggest that BRCA2 could have a small role in maintaining centromere stability, emphasising BRCA2's well-established role in HR and DNA repair.

Ribonucleotides can be erroneously incorporated into DNA by Pol α, δ, and ε during replication. These DNA mismatches are repaired through ribonucleotide excision repair (RER) involving RNase H2 or TOP1 (Kellner & Luke, 2020; Williams et al., 2016). RNase H2 incises into the nascent DNA backbone at the ribonucleotide and provides an entry point for MMR and MLH1/PMS2-mediated mismatch removal. The resulting nucleotide gap is filled by Pol δ or ε and ligated by LIG1. Alternatively, TOP1-mediated ribonucleotide excision forms an error-prone backup RER pathway where TOP1 cleaves either side of the ribonucleotide to remove it from DNA. This can produce short, 2-5 bp deletions or DSBs

which require HR for repair (**section 1.5.4**). Due to the MMR defect in HCT116 cells, RNase H2-mediated ribonucleotide processing may not be efficiently resolved by MMR, leading to increased TOP1-mediated RER. In the absence of BRCA2, TOP1-induced DSBs are left unrepaired leading to a further increase in DNA breaks. This is supported by the synthetic lethal interaction between RNase H2 and BRCA1/2 deletion in human cells (Zimmermann et al., 2018). As RAD51 depletion does not significantly increase cenFISH signal (**figures 5.17C and F**), this repair is potentially RAD51 independent. RPE1 cells are MMR proficient, potentially explaining the difference in Exo-FISH results (discussed in **section 6.1.2**). **Figure 5.10F** (**section 5.3.2**) gave some indication for long-term BRCA2 depletion increasing chromosomal DNA breaks at or around the centromere regions. While the HCT116 mAID-BRCA2 cell Exo-FISH results support this to some extent, BRCA2's role in maintaining centromere stability should be confirmed through other methods.

PALB2 depletion by IAA or siRNA did not significantly alter cenFISH signal suggesting that it does not function in maintaining centromere stability in asynchronous HCT116 cells (**figures 5.16C and F, and 5.17B and E**). In fact, upon PALB2 depletion, cells were less responsive to ExoIII treatment and inclusion of pepsin pre-treatment produced a very similar result. Intriguingly, siPALB2 treatment in asynchronous HCT116 cells produced an insignificant but consistent decrease in cenFISH signal compared to MisNeg samples after ExoIII treatment (**figure 5.17B and E**). This could correlate with the proposed role for PALB2 in facilitating transcription and ssDNA accumulation which would otherwise generate cenFISH signal (Gardini et al., 2014).

Finally, I also observed that RAD51 depletion by siRNA did not significantly impact cenFISH levels in asynchronous HCT116 cells, regardless of pepsin pre-treatment (**figure 5.17C and F**). Despite this, variation in cenFISH upon RAD51 depletion and ExoIII treatment may have disguised small differences and so confident conclusions are elusive. This result is consistent with my observations in RPE1 cells (**sections 4.2.4 and 4.3.2**). However, Saayman et al., identified RAD51's role in limiting centromere DNA breaks in quiescent

RPE1 cells (Saayman et al., 2023). Therefore, it may be interesting to expand my studies further to explore the impact of the cell cycle on centromere stability in HCT116 cells.

Spontaneous centromeric DNA breaks have previously been shown to be enriched in HCT116 cells (Canela et al., 2016; Logsdon et al., 2021; Saayman et al., 2023; Sriramachandran et al., 2020). Analysing publicly available NGS datasets, a correlation between CENP-A positioning and DNA breaks was identified at the functionally active centromere. My investigation into centromeric DNA breaks in HCT116 cells using Exo-FISH showed only modest ExoIII responsiveness indicative of spontaneous DNA breaks (**figures 5.16 and 5.17**). While validation of the Exo-FISH protocol in HCT116 cells showed a significant increase in signal upon ExoIII treatment alone (**figure 5.15**), Nt.BsmAI treatment introduces extensive SSBs compared to endogenous levels, potentially artificially amplifying the results. It is possible that extensive degradation of the DNA may be impacting break detectability (**figure 4.10**). This was evident upon Exo-FISH optimisation where increasing concentrations of the restriction endonuclease, BsmAI, decreased cenFISH signal (Xanita Saayman, unpublished). This effect is likely exacerbated and more variable in HCT116 cells, compared to RPE1 cells, due to their unstable cancerous nature (Saayman et al., 2023). Therefore, these results should be supported through additional techniques including southern blotting and sequencing-based analysis to increase the confidence in the above findings and enable adequate comparison of AID and siRNA-treated asynchronous HCT116 cells.

5.3.5 Variation between AID and siRNA studies

Throughout this chapter, several differences between HCT116 mAID cell lines and siRNA-mediated depletion studies became apparent (**figures 5.12, 5.14, 5.16, and 5.17**). Experiments assessing centromere identity and stability were often not consistent between the two systems, raising the question as to which results are most reliable and how can this be confirmed.

The most likely explanation for this difference may be due to the different extents of BRCA2 and PALB2 depletion between AID and siRNA-treated cells. The HCT116 mAID system is well-characterised to produce consistent, reliable, and rapid depletion of tagged proteins (Natsume et al., 2016) (**figures 5.1C and D, and 5.11A**), whereas siRNA-mediated depletion can be variable between experiments such that some functional protein may remain in the cell. Unfortunately, I was unable to generate HCT116 cells expressing degron-tagged RAD51 and therefore these experiments cannot be easily validated. In this context, RAD51 inhibitor, B02, may be useful. Protein depletion was not confirmed by WB for each experimental repeat and no antibodies are available to check BRCA2 and PALB2 expression by IF. Therefore, this may explain why modest phenotypes were visible in the AID cell lines but not by siRNA (**sections 5.2.4 and 5.2.5**). Experiments assessing protein function in HR, as in **figures 5.3 and 5.5**, after siRNA depletion may be a useful addition to WB validation only (**figures 5.13A-D**).

Furthermore, the different cell cycle impact of IAA and siRNA treatment can also influence results (**figures 5.11B and C, 5.13E and F**). 96 hour, 5 μM IAA treatment did not significantly alter cell cycle distribution compared to the untreated control, although there were differences between the cell lines themselves (**figure 5.11C**). Alternatively, siRNA depletion triggered a degree of cell cycle delay (**figure 5.13F**). siBRCA2 and siPALB2 treated HCT116 cells showed enrichment in S and G2/M phase whereas siRAD51 treated cells had increased G2/M and G1 phase populations. The cell cycle dependence of BRCA2 in HCT116 cell centromere identity and stability remains unclear as these experiments have only been conducted under asynchronous conditions. Further understanding of how the cell cycle influences these phenotypes may help explain the discrepancy between AID and siRNA-treated cells. Adapting my analysis to include considerations for the number of cell divisions that occur over the 96 hour analysis period may also provide a more accurate depiction of HR factor involvement. Therefore, by taking cell cycle distribution into account,

the AID and siRNA depletion experiments may become more comparable and display increased impact.

Finally, centromere-related experiments using the AID system were generally more variable than siRNA-related experiments (**figures 5.12, 5.14, 5.16, and 5.17**). This was surprising as these cell lines are clonal and should be consistent throughout the population. Therefore, this difference could reflect leaky expression of the AID system, experimental limitations, or endogenous changes in centromere stability over time, perhaps due to cell culture passaging and accumulation of spontaneous mutations (**section 5.3.2**) (Boesen et al., 1994). Inclusion of additional HCT116 mAID cell line CRISPR clones may improve confidence and repeatability, excluding the possible impact of secondary mutations. Overall, the considerations described above combined with supplementary experiments should help reconcile the differences between AID and siRNA depletion methods and improve the reliability of this work.

Chapter 6 – Discussion

6.1 Summary of thesis

Human DNA is subject to damage from many different sources. Centromeres are unique regions of the genome comprised of repetitive DNA sequences and secondary DNA structures (**sections 1.7.1 and 1.7.4**). They experience instability from various sources throughout the cell cycle including R-loops and TRCs, replication stress, and mitotic pulling forces during chromosome segregation (**section 1.7.4**). Centromeres are highly recombinogenic regions of the genome (**section 1.7.4.2.3**) and HR is an essential pathway to repair DNA breaks; regulated by key factors: BRCA2, PALB2, and RAD51 (**section 1.4.2**). In this thesis, I aimed to investigate the role of these HR modulators in maintaining centromere integrity and stability. Here, I will summarise the key findings and some remaining questions.

6.1.1 RAD51 maintains genome stability in mitosis

In **chapter 3**, I discussed my contribution towards (Wassing et al., 2021), demonstrating a novel role for *de novo* RAD51 loading in mitosis to promote MiDAS in cells exposed to mild replication stress. Use of RAD51 separation of function mutants, K133R and T131P, revealed that both ssDNA binding and strand invasion activity may be required for RAD51-dependent MiDAS, although these findings could be improved with the generation of homozygous or additional mutant (RAD51 II3A) cell lines (**section 3.3.2**). Nevertheless, consistent with the replication-associated role of RAD51 (Petermann et al., 2010), bright RAD51 foci were not visible during early mitosis (Wassing et al., 2021), suggesting that its ssDNA binding activity is primarily required to promote MiDAS. Furthermore, this function is seemingly independent of other canonical HR regulators, BRCA2 and PALB2, although I did not directly assess this, as RAD51 recruitment to mitotic chromatin is PLK1-dependent (Wassing et al., 2021; Yata et al., 2012).

I demonstrated that RAD51 promotes non-DDR-associated MiDAS, although it is also linked to DDR-associated mitosis (**figure 3.2E**). This led to the proposed model (**figure 3.9, section 3.3.2**): *de novo* RAD51 loading in early mitosis protects stalled replication forks that have escaped the replication checkpoint from nucleolytic cleavage, promoting replication completion. MiDAS in U2OS cells has been described as both conservative and semi-conservative replication events (Bhowmick et al., 2016; Chappidi et al., 2020; Minocherhomji et al., 2015) suggesting that RAD51-dependent MiDAS at unbroken, stalled forks may involve retention of the DNA replication machinery into mitosis. This is likely distinct from the RAD52-dependent MiDAS pathway that has previously been described (Bhowmick et al., 2016; Minocherhomji et al., 2015). However, as RAD51-dependent MiDAS can also colocalise with ɣH2AX, this suggests that a subset of collapsed forks may require RAD51 activity. Nuclease activity is high in mitosis (Audrey et al., 2022) therefore RAD51 may also function to protect DNA repair structures resulting from RAD52-dependent MiDAS from endonuclease activity e.g. MUS81 which can target BIR and HR intermediates, and replication forks (Duda et al., 2016; Mayle et al., 2015; Wyatt et al., 2013). The exact conditions determining RAD52 vs RAD51 mediated MiDAS is still unknown, although it is likely that the surrounding chromatin environment influences this. Indeed, RAD52-dependent MiDAS is strongly associated with CFSs (Minocherhomji et al., 2015) while RAD51-associated MiDAS is linked to the fragile X locus (Garribba et al., 2020) and potentially centromeres (**sections 3.2.6 and 3.3.3**) (Wassing et al., 2021).

Isabel Wassing expanded this, observing that mitotic RAD51 inhibition after mild replication stress results in delayed AO and mitotic defects due to increased mitotic DNA damage (**sections 3.2.5 and 3.3.3**). MiDAS is frequently observable in cancerous U2OS cells (Bhowmick et al., 2016; Minocherhomji et al., 2015), likely due to prevalent intrinsic replication stress. Therefore, this could reveal exciting new cancer therapy opportunities combining SAC and MiDAS inhibition to induce mitotic cell death. Interestingly, RAD51 inhibition after mild replication stress increased aberrant CO-FISH signals and centromere

FISH probe signal intensity (**figure 3.8, section 3.2.6**), suggesting that MiDAS is required to maintain centromere stability. This led to the hypothesis that loss of HR and RAD51-mediated fork protection, could promote POLQ-dependent alt-EJ, generating SCEs from erroneous repair of broken replication forks (**section 3.3.3**) (Heijink et al., 2021). Recombination is primarily resolved through non-crossover mechanisms in somatic cells (Scully et al., 2019). Therefore, it is possible that a large proportion of centromere breaks are not visible by CO-FISH. Since these experiments were conducted, Exo-FISH has been developed to detect DNA breaks (**figure 4.6**) (Saayman et al., 2023) and so may provide more insight into centromere fragility upon RAD51-dependent MiDAS inhibition. Measurement of centromere FISH probe signal intensity indicated an enrichment of exposed ssDNA after mild replication stress and RAD51 inhibition (**section 3.2.6**). CO-FISH involves the digestion of nascent DNA to produce ssDNA for FISH probe binding. Hence, this increased centromere signal after B02 treatment could suggest that RAD51 coats and protects centromeric DNA, blocking FISH probe binding, especially as the CO-FISH protocol does not involve protein stripping from the chromatin i.e. pepsin pre-treatment. Upon mitotic RAD51 inhibition, ssDNA is likely deprotected, leading to increased CO-FISH signal generation and centromere fragility. This proposal potentially draws interesting parallels with ssDNA accumulation upon RAD51 and BRCA2 depletion in RPE1 cells by Exo-FISH (**section 6.1.2**).

6.1.2 Distinct roles for BRCA2, PALB2, and RAD51 at centromeres

Since describing a role for RAD51 in mitosis in promoting MiDAS and maintaining centromere stability, additional work from the lab identified a role for RAD51 at TOP2B-induced centromere DNA breaks in quiescent RPE1 cells (Saayman et al., 2023). This required RAD51 strand exchange activity and is thought to promote CENP-A deposition. I aimed to expand these studies and explore the role of BRCA2 and PALB2 in centromere identity and stability in RPE1 and HCT116 cells (**chapters 4 and 5**). **Table 6.1** summarises these findings.

		Asynchronous			Quiescent		
	Depleted:	**BRCA2**	**PALB2**	**RAD51**	**BRCA2**	**PALB2**	**RAD51**
Centromere Identity	**RPE1**	↓	ns	↓	ns	ns	↓ns
	HCT116	AID: ↓ siRNA: ns	AID: ns siRNA: ns	siRNA: ↓			
Centromere Instability	**RPE1**	-pep: ↑ ssDNA +pep: ↑ ssDNA	-pep: ↑ breaks +pep: ns	-pep: ↑ telFISH and cenFISH ssDNA +pep: ns	-pep: ns +pep: ↑ breaks	-pep: ns +pep: ns	-pep: ns +pep: ns
	HCT116	AID: -pep: ↑ns breaks +pep: ns siRNA: -pep: ns +pep: ns	ns under all conditions	ns under all conditions			

Table 6.1. Summary of BRCA2, PALB2, and RAD51 depletion impact on centromere identity and stability in RPE1 and HCT116 cells. Ns = not significant. -/+pep = +/- pepsin pre-treatment. ↑ ssDNA refers to increased cenFISH signal independent of ExoIII treatment. ↑ breaks refers to increased cenFISH signal upon ExoIII treatment. Different results between AID system and siRNA depletion in HCT116 cells are indicated.

My results show that RAD51 maintains centromere identity in asynchronous RPE1 and HCT116 cells and quiescent RPE1 cells (**sections 4.2.2, 4.2.3, and 5.2.4**), agreeing with (Saayman et al., 2023). However, this maintenance of CENP-A levels and centromere identity did not correlate with increased centromere instability i.e. DNA breaks, as detected by Exo-FISH (**sections 4.2.4, 4.2.5, and 5.2.5**). This is contrary to Saayman et al., who described a role for RAD51 in limiting the level of centromeric DNA breaks in quiescent RPE1 cells (Saayman et al., 2023). This difference is believed to stem from different experimental conditions, as discussed in **section 4.3.2**, or reflect other caveats of the Exo-FISH protocol (**section 6.1.3**).

BRCA2 depletion decreased CENP-A levels in asynchronous RPE1 cells and HCT116 cells, to a lesser extent (**sections 4.2.2 and 5.2.4**). This effect was lost upon serum-starvation in RPE1 cells (**section 4.2.3**). Furthermore, in asynchronous RPE1 cells, BRCA2

depletion increased Exo-FISH centromere signal, with or without pepsin pre-treatment, indicative of exposed ssDNA (**sections 4.2.4 and 4.2.5**). This was not further increased upon ExoIII treatment, suggesting that the ssDNA signal is not associated with DNA breaks. There are several different sources of ssDNA across the cell cycle including R-loops, transcription/replication-associated torsional stress, or PRIMPOL-mediated repriming (Bainbridge et al., 2021; Kang et al., 2021; Nitiss, 2009). Loss of this ssDNA signal upon serum-starvation (**section 4.2.5**) implies that replication-associated ssDNA is the most likely source of the cenFISH signal. Centromeres are characterised as difficult-to-replicate DNA regions (Black & Giunta, 2018) and so a potential role for BRCA2 in facilitating the resolution of excessive torsional stress or restricting PRIMPOL-mediated repriming during replication is not unfounded (Kang et al., 2021). The exact source of centromeric ssDNA still needs to be explored further and co-depletion studies against topoisomerases or PRIMPOL to suppress ssDNA resolution or accumulation, could facilitate this.

Intriguingly, asynchronous HCT116 and serum-starved RPE1 cells did not show increased ExoIII-independent Exo-FISH signals upon BRCA2 depletion but did display increased ExoIII-sensitive cenFISH signal, indicative of centromeric DNA breaks (**sections 4.2.5 and 5.2.5**). This signal was potentially obscured in asynchronous RPE1 cells due to excessive ssDNA cenFISH signal. This striking difference between asynchronous HCT116 and RPE1 cells could result from their different genetic backgrounds. The RPE1 cell line is karyotypically stable and non-cancerous, whereas HCT116 cells are derived from colorectal cancer and display microsatellite instability and MMR deficiency due to a mutation within MLH1. Therefore, this striking difference between HCT116 and RPE1 cells suggests that these breaks may arise due to defective MMR. MMR can promote HR by repairing mismatches within homeologous template sequences (a more frequent mechanism in meiosis) or suppress HR by completely rejecting heteroduplex formation (the primary pathway in somatic cells) (**section 1.5.4**) (Chakraborty & Alani, 2016; Spies & Fishel, 2015). Consequently, loss of MMR could increase recombination between diverged sequences,

either through homeologous recombination or erroneous repair pathways including SSA or alt-EJ (Spies & Fishel, 2015). As MMR factors are known to associate with centromeres (Aze et al., 2016), HCT116 cells can be a useful tool to assess the importance of HR (and MMR) at centromeres.

Furthermore, MMR is also required to remove misincorporated ribonucleotides through the process of RNase H2-mediated RER (**sections 1.5.4 and 5.3.4**) (Kellner & Luke, 2020; Williams et al., 2016). I propose a model where RNase H2-mediated RER cannot adequately function in HCT116 cells, diverting repair into a TOP1-mediated pathway (**figure 6.1**). TOP1-mediated RER in the absence of MMR is error-prone, potentially producing gene conversions, crossover recombination, or DSBs which require HR for repair. In BRCA2 deficient HCT116 cells, these lesions persist and are detectable by Exo-FISH. In RPE1 cells, MMR and HR are proficient in resolving mismatches, promoting efficient centromere break repair. Therefore, increased centromere breaks upon BRCA2 depletion and RPE1 serum-starvation could possibly reflect inefficient break repair, although caveats of the Exo-FISH methodology should not be discounted (**section 6.1.3**). Nevertheless, it would be interesting to further explore this in $MLH1^{-/-}$ RPE1 cells to investigate if this relationship between MMR and HR can be recapitulated. In turn, HCT116 cells do not produce increased ExoIII-independent cenFISH signal indicative of ssDNA upon HR factor depletion. In the context of this model, this could suggest that increased TOP1 activity at centromeres in the absence of MMR may more readily relieve torsional stress, reducing ssDNA and cenFISH signals.

It is tempting to speculate that accumulated DNA breaks in BRCA2 deficient HCT116 cells may be repaired through other erroneous repair pathways which can produce crossover recombination products. Therefore, CO-FISH analysis may reveal additional insight into the repair of centromere breaks under these conditions. Curiously, preliminary investigations show few cen-SCEs by CO-FISH upon BRCA2 depletion in HCT116 cells, correlating with

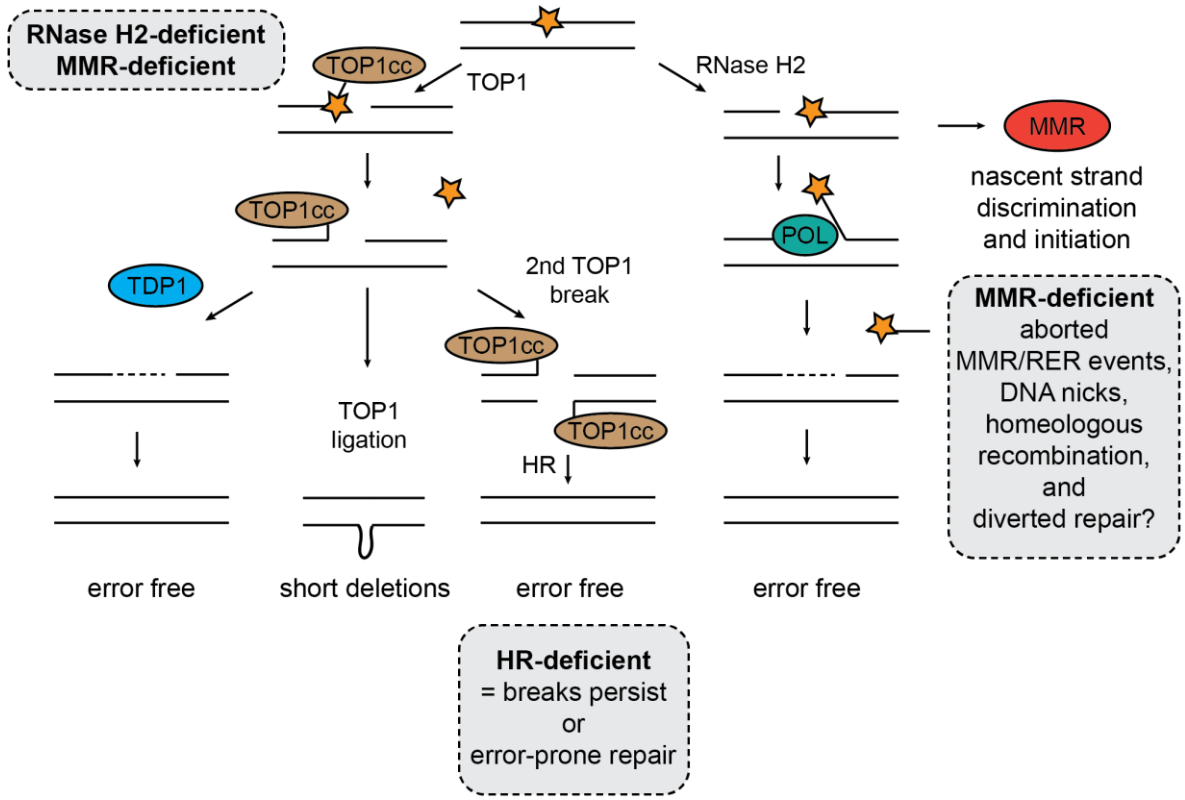


Figure 6.1. Ribonucleotide Excision Repair (RER) in MMR- and HR-deficient cells. Ribonucleotide mismatches (represented by the star) are resolved by RNase H2 and TOP1. RNase H2 induces DNA nicks at ribonucleotide mismatches. Polymerase (POL) facilitates strand displacement synthesis and FEN1/EXO1 orchestrate flap cleavage. DNA backbone is ligated. RNase H2 nicking can initiate MMR by indicating the nascent DNA strand. MMR can excise the ribonucleotide mismatch to complete RER, along with other mismatches in the vicinity. MMR deficiency may divert repair to TOP1-mediated events. TOP1 can cleave ribonucleotide mismatches, creating TOP1 cleavage complex (TOP1cc). A second TOP1 cut removes the ribonucleotide. TDP1 can remove the TOP1cc in an error free mechanism. Alternatively, religation by TOP1 can produce short deletions (2-5bp). A second TOP1-induced break produces a DSB which may require HR for repair. In HR-deficient cells, these breaks may persist or be repaired through other error-prone mechanisms.

the proposed suppression of inter-centromeric recombination (Piazza et al., 2021) (**section 1.7.4.2.3**) and non-crossover repair products produced by NHEJ, SSA, and alt-EJ.

Therefore, a potential alternative explanation could be that a portion of the DNA breaks remain unrepaired. This is supported by long-term depletion of BRCA2 in HCT116 mAID-BRCA2 cells that resulted in increased Chr17 breakages at or around the centromere region (**section 5.2.3**). Therefore, more in-depth sequencing analysis may be required to fully characterise the repair landscape at centromeres.

PALB2 consistently shows little impact on centromere identity and stability across the two cell lines (**sections 4.2.2-5 and 5.2.4-5**). This suggests that canonical HR is not predominant at centromeres. RAD51 can be recruited to chromatin via PLK1 (Yata et al., 2012, 2014), as shown for its role in MiDAS (Wassing et al., 2021). BRCA2 can further promote PLK1-dependent RAD51 phosphorylation to recruit RAD51 to DSBs in an NBS1-dependent manner to facilitate strand invasion and DNA repair (Yata et al., 2012, 2014). Collectively alleviating a need for PALB2 in promoting DNA repair in this context. Exo-FISH results in HCT116 cells suggest that BRCA2 promotes DNA integrity independently of RAD51, however it is important to consider the variable results between AID- and siRNA-mediated protein depletion, as discussed in **section 5.3.5**. Ultimately, it cannot be excluded that RAD51 plays a role in maintaining centromere integrity in asynchronous HCT116 cells and further attempts to generate RAD51 degron HCT116 cell lines would increase our understanding of this.

The connection between centromere stability and identity remains largely unknown. Centromere breaks in quiescent RPE1 cells were proposed to facilitate CENP-A loading (Saayman et al., 2023); whether this is also the case in cycling cells is yet to be determined. In **section 4.3.3**, I discussed the potential for BRCA2 and RAD51 in facilitating CENP-A deposition through repair intermediates. Alternatively, intact centromere DNA may present an essential foundation for canonical CENP-A loading in early G1, potentially also linking to the importance of RAD51-mediated MiDAS and replication completion in this process.

6.1.3 Detecting centromeric DNA breaks

In this study, I used Exo-FISH and CO-FISH as a readout of centromere instability. CO-FISH is a useful technique to differentially label the two sister chromatids and observe crossover recombination between them (cen-SCE) (**figure 3.8A**). Exo-FISH is a microscopy-based technique that can theoretically detect SSBs, including DNA nicks and gaps, and DSBs after ExoIII-mediated resection through binding of a fluorescent FISH

probe to the region of interest (**figure 4.6A**). Despite their usefulness, both techniques have caveats.

CO-FISH detects crossover recombination events which are uncommon repair events in somatic cells (Scully et al., 2019). Therefore, it is likely that a majority of DNA break and repair events remain undetected during CO-FISH analysis. On the other hand, Exo-FISH allows you to directly visualise DNA breaks, regardless of how they are repaired, and can be theoretically applied to any region of interest. Regardless, Exo-FISH has several limitations. T-loops are naturally occurring DNA "breaks" at telomeres that are protected through strand invasion into telomeric dsDNA (Ruis & Boulton, 2021), however, they are not responsive to ExoIII treatment. Therefore, Exo-FISH can presumably only detect and digest certain DNA substrates i.e. it may not detect HR repair intermediates (Saayman et al., 2023) or DNA breaks resulting from topoisomerase activity e.g. TOP1 cleavage complexes on 3' DNA ends, only digesting exposed DNA ends. Alternatively, pepsin pre-treatment may expose some additional substrates through removal of chromatin-bound proteins.

ExoIII digests DNA in a 3'-5' direction and it targets several DNA substrates including blunt-ended DSBs, 3' overhangs less than 4 bp long, and DNA nicks. Therefore, it is unclear what type of DNA lesions are enriched at centromeres. This propensity for ExoIII to cleave multiple DNA substrates could be resolved in future experiments by utilising alternative exonucleases that are specific to different DNA lesions. For example, truncated exonuclease VIII removes nucleotides from 5' end of DSBs only. Moreover, DNA breaks in close proximity to the core centromere may be digested into this region of interest upon ExoIII treatment, creating false positive signal.

I modified the Exo-FISH protocol to include a pepsin pre-treatment step to remove chromatin-bound proteins, theoretically revealing previously obscured ssDNA or breaks, to gain more insight into the function of BRCA2/PALB2/RAD51 at centromeres (**section 4.2.4**). Pepsin-mediated digestion occurs under acidified conditions which may interfere

with ExoIII functionality if not washed sufficiently. This may explain the variable Exo-FISH signal visible upon pepsin pre-treatment (**sections 4.2.5 and 5.2.5**), potentially contributing towards ExoIII under or over-digestion and loss of Exo-FISH signal (**figure 4.10**). RPE1 and HCT116 cells, asynchronous or serum-starved, with or without pepsin pre-treatment, appear to display differing responsiveness to ExoIII treatment. Asynchronous HCT116 cells and serum-starved RPE1 cells show an overall lower fold-change in cenFISH signal upon ExoIII treatment compared to asynchronous RPE1 cells. This may result from several sources including reduced replicative DNA damage in quiescent RPE1 cells or an altered heterochromatic status. For example, colorectal cancer cell lines, including HCT116 cells, commonly display increased HP1ɣ expression, associated with heterochromatin formation (Liu et al., 2015). Reduced HP1α, but not HP1β and HP1ɣ in serum-starved human primary fibroblast cell lines and quiescent MCF7 breast carcinoma cell lines also suggest changes in heterochromatin organisation under these conditions (De Koning et al., 2009). Therefore, increased heterochromatin formation could potentially restrict ExoIII-mediated digestion and FISH signal amplification. Ultimately, Exo-FISH may have different applications and usability across different cell lines (Saayman et al., 2023)

6.1.4 Chromosome instability after BRCA2 and PALB2 depletion

Finally, I also utilised HCT116 mAID-BRCA2 and PALB2-mAID cell lines to investigate their impact on chromosome stability after long-term depletion (**sections 5.2.3 and 5.3.2**). These studies revealed a surprising distinction between BRCA2 and PALB2 depletion on Chr17 stability. While BRCA2 depletion led to a significant increase in Chr17 breaks, potentially localised around the centromere and agreeing with the Exo-FISH findings**,** PALB2 depletion resulted in Chr17 duplications, inversions, and missegregation, indicative of aberrant recombination events. Although loss of both proteins has been associated with cancer (Fradet-Turcotte et al., 2016; Wu et al., 2020), this investigation provided surprising insight into potential mechanisms driving early tumourigenesis in these cells.

6.2 Concluding remarks

Canonical HR modulators BRCA2, PALB2, and RAD51 are essential to maintain genome stability through DNA repair and resolution of replication stress, among other processes. Centromeres are unique regions of the genome that display instability from a range of sources. This thesis first reveals a role for *de novo* RAD51 recruitment in mitosis to promote MiDAS after replication stress to prevent DNA under-replication. Particularly important at centromeres, further investigation of these HR factors at this region in two different cell lines implied distinct functions for these proteins in maintaining centromere integrity. Moreover, I discuss a potential exciting relationship between MMR and HR at centromeres which should be explored further. Finally, generation and validation of a rapid degron system in HCT116 cells emphasised the importance of BRCA2 and PALB2 in early tumourigenesis for maintaining chromosome stability. As such, this work provides intriguing insight into the requirement of BRCA2, PALB2, and RAD51 at centromeres and forms an exciting stepping-stone to expand our understanding of centromere stability in unperturbed cells.

Bibliography

Addis Jones, O., Tiwari, A., Olukoga, T., Herbert, A., & Chan, K.-L. (2019). PLK1 facilitates chromosome biorientation by suppressing centromere disintegration driven by BLM-mediated unwinding and spindle pulling. *Nature Communications*, *10*(1), 2861. https://doi.org/10.1038/s41467-019-10938-y

Albers, E., Sbroggiò, M., Pladevall-Morera, D., Bizard, A. H., Avram, A., Gonzalez, P., Martin-Gonzalez, J., Hickson, I. D., & Lopez-Contreras, A. J. (2018). Loss of PICH Results in Chromosomal Instability, p53 Activation, and Embryonic Lethality. *Cell Reports*, *24*(12), 3274–3284. https://doi.org/10.1016/j.celrep.2018.08.071

Altemose, N., Logsdon, G. A., Bzikadze, A. V, Sidhwani, P., Langley, S. A., Caldas, G. V, Hoyt, S. J., Uralsky, L., Ryabov, F. D., Shew, C. J., Sauria, M. E. G., Borchers, M., Gershman, A., Mikheenko, A., Shepelev, V. A., Dvorkina, T., Kunyavskaya, O., Vollger, M. R., Rhie, A., … Miga, K. H. (2023). Complete genomic and epigenetic maps of human centromeres. *Science*, *376*(6588), eabl4178. https://doi.org/10.1126/science.abl4178

Ameziane, N., May, P., Haitjema, A., van de Vrugt, H. J., van Rossum-Fikkert, S. E., Ristic, D., Williams, G. J., Balk, J., Rockx, D., Li, H., Rooimans, M. A., Oostra, A. B., Velleuer, E., Dietrich, R., Bleijerveld, O. B., Maarten Altelaar, A. F., Meijers-Heijboer, H., Joenje, H., Glusman, G., … Dorsman, J. C. (2015). A novel Fanconi anaemia subtype associated with a dominant-negative mutation in RAD51. *Nature Communications*, *6*(1), 8829. https://doi.org/10.1038/ncomms9829

Amir-Aslani, A., Mauffret, O., Bittoun, P., Sourgen, F., Monnot, M., Lescot, E., & Fermandjian, S. (1995). Hairpins in a DNA site for topoisomerase II studied by 1 H-and 31 P-NMR. *Nucleic Acids Research*, *23*(19), 3850–3857. https://doi.org/10.1093/nar/23.19.3850

Amir-Aslani, A., Mauffret, O., Sourgen, F., Neplaz, S., Maroun, R. G., Lescot, E., Tevanian, G., & Fermandjian, S. (1996). The Hairpin Structure of a Topoisomerase II Site DNA Strand Analyzed by Combined NMR and Energy Minimization Methods. *Journal of Molecular Biology*, *263*(5), 776–788. https://doi.org/https://doi.org/10.1006/jmbi.1996.0615

Anand, R. P., Lovett, S. T., & Haber, J. E. (2013). Break-Induced DNA Replication. *Cold Spring Harbor Perspectives in Biology*, *5*(12). https://doi.org/10.1101/cshperspect.a010397

Andersen, C. L., Wandall, A., Kjeldsen, E., Mielke, C., & Koch, J. (2002). Active, but not inactive, human centromeres display topoisomerase II activity in vivo. *Chromosome Research*, *10*(4), 305–312. https://doi.org/10.1023/A:1016571825025

Audrey, A., de Haan, L., van Vugt, M. A. T. M., & de Boer, H. R. (2022). Processing DNA lesions during mitosis to prevent genomic instability. *Biochemical Society Transactions*, *50*(4), 1105–1118. https://doi.org/10.1042/BST20220049

Ayoub, N., Rajendra, E., Su, X., Jeyasekharan, A. D., Mahen, R., & Venkitaraman, A. R. (2009). The carboxyl terminus of Brca2 links the disassembly of Rad51

complexes to mitotic entry. *Current Biology : CB*, *19*(13), 1075–1085. https://doi.org/10.1016/j.cub.2009.05.057

Aze, A., Sannino, V., Soffientini, P., Bachi, A., & Costanzo, V. (2016). Centromeric DNA replication reconstitution reveals DNA loops and ATR checkpoint suppression. *Nature Cell Biology*, *18*(6), 684–691. https://doi.org/10.1038/ncb3344

Bainbridge, L. J., Teague, R., & Doherty, A. J. (2021). Repriming DNA synthesis: an intrinsic restart pathway that maintains efficient genome replication. *Nucleic Acids Research*, *49*(9), 4831–4847. https://doi.org/10.1093/nar/gkab176

Bandyopadhyay, A., Kancharla, N., Javalkote, V. S., Dasgupta, S., & Brutnell, T. P. (2020). CRISPR-Cas12a (Cpf1): A Versatile Tool in the Plant Genome Editing Tool Box for Agricultural Advancement. *Frontiers in Plant Science*, *11*. https://www.frontiersin.org/articles/10.3389/fpls.2020.584151

Barnard, S., Bouffler, S., & Rothkamm, K. (2013). The shape of the radiation dose response for DNA double-strand break induction and repair. *Genome Integrity*, *4*(1), 1. https://doi.org/10.1186/2041-9414-4-1

Barnhart, M. C., Kuich, P. H. J. L., Stellfox, M. E., Ward, J. A., Bassett, E. A., Black, B. E., & Foltz, D. R. (2011). HJURP is a CENP-A chromatin assembly factor sufficient to form a functional de novo kinetochore. *Journal of Cell Biology*, *194*(2), 229–243. https://doi.org/10.1083/jcb.201012017

Barra, V., & Fachinetti, D. (2018). The dark side of centromeres: types, causes and consequences of structural abnormalities implicating centromeric DNA. *Nature Communications*, *9*(1), 4340. https://doi.org/10.1038/s41467-018-06545-y

Bassett, E. A., DeNizio, J., Barnhart-Dailey, M. C., Panchenko, T., Sekulic, N., Rogers, D. J., Foltz, D. R., & Black, B. E. (2012). HJURP Uses Distinct CENP-A Surfaces to Recognize and to Stabilize CENP-A/Histone H4 for Centromere Assembly. *Developmental Cell*, *22*(4), 749–762. https://doi.org/10.1016/j.devcel.2012.02.001

Baumann, Benson, F. E., & West, S. C. (1996). Human Rad51 Protein Promotes ATP-Dependent Homologous Pairing and Strand Transfer Reactions In Vitro. *Cell*, *87*(4), 757–766. https://doi.org/10.1016/S0092-8674(00)81394-X

Baumann, C., Körner, R., Hofmann, K., & Nigg, E. A. (2007). PICH, a Centromere-Associated SNF2 Family ATPase, Is Regulated by Plk1 and Required for the Spindle Checkpoint. *Cell*, *128*(1), 101–114. https://doi.org/https://doi.org/10.1016/j.cell.2006.11.041

Baxter, J. (2015). 'Breaking up is hard to do': the formation and resolution of sister chromatid intertwines. *Journal of Molecular Biology*, *427*(3), 590–607. https://doi.org/10.1016/j.jmb.2014.08.022

Belan, O., Sebald, M., Adamowicz, M., Anand, R., Vancevska, A., Neves, J., Grinkevich, V., Hewitt, G., Segura-Bayona, S., Bellelli, R., Robinson, H. M. R., Higgins, G. S., Smith, G. C. M., West, S. C., Rueda, D. S., & Boulton, S. J. (2022). POLQ seals post-replicative ssDNA gaps to maintain genome stability in BRCA-deficient cancer cells. *Molecular Cell*, *82*(24), 4664-4680.e9. https://doi.org/10.1016/j.molcel.2022.11.008

Bellacosa, A., Godwin, A. K., Peri, S., Devarajan, K., Caretti, E., Vanderveer, L., Bove, B., Slater, C., Zhou, Y., Daly, M., Howard, S., Campbell, K. S., Nicolas, E., Yeung, A. T., Clapper, M. L., Crowell, J. A., Lynch, H. T., Ross, E., Kopelovich, L., & Knudson, A. G. (2010). Altered Gene Expression in Morphologically Normal Epithelial Cells from Heterozygous Carriers of BRCA1 or BRCA2 Mutations. *Cancer Prevention Research*, *3*(1), 48–61. https://doi.org/10.1158/1940-6207.CAPR-09-0078

Bennardo, N., Cheng, A., Huang, N., & Stark, J. M. (2008). Alternative-NHEJ Is a Mechanistically Distinct Pathway of Mammalian Chromosome Break Repair. *PLOS Genetics*, *4*(6), e1000110-. https://doi.org/10.1371/journal.pgen.1000110

Bensasson, D. (2011). Evidence for a high mutation rate at rapidly evolving yeast centromeres. *BMC Evolutionary Biology*, *11*(1), 211. https://doi.org/10.1186/1471-2148-11-211

Benson, F. E., Stasiak, A., & West, S. C. (1994). Purification and characterization of the human Rad51 protein, an analogue of E. coli RecA. *The EMBO Journal*, *13*(23), 5764–5771. https://doi.org/https://doi.org/10.1002/j.1460-2075.1994.tb06914.x

Bergmann, J. H., Rodríguez, M. G., Martins, N. M. C., Kimura, H., Kelly, D. A., Masumoto, H., Larionov, V., Jansen, L. E. T., & Earnshaw, W. C. (2011). Epigenetic engineering shows H3K4me2 is required for HJURP targeting and CENP-A assembly on a synthetic human kinetochore. *The EMBO Journal*, *30*(2), 328–340. https://doi.org/https://doi.org/10.1038/emboj.2010.329

Bernad, R., Sánchez, P., Rivera, T., Rodríguez-Corsino, M., Boyarchuk, E., Vassias, I., Ray-Gallet, D., Arnaoutov, A., Dasso, M., Almouzni, G., & Losada, A. (2011). Xenopus HJURP and condensin II are required for CENP-A assembly. *Journal of Cell Biology*, *192*(4), 569–582. https://doi.org/10.1083/jcb.201005136

Berti, M., Ray Chaudhuri, A., Thangavel, S., Gomathinayagam, S., Kenig, S., Vujanovic, M., Odreman, F., Glatter, T., Graziano, S., Mendoza-Maldonado, R., Marino, F., Lucic, B., Biasin, V., Gstaiger, M., Aebersold, R., Sidorova, J. M., Monnat, R. J., Lopes, M., & Vindigni, A. (2013). Human RECQ1 promotes restart of replication forks reversed by DNA topoisomerase I inhibition. *Nature Structural & Molecular Biology*, *20*(3), 347–354. https://doi.org/10.1038/nsmb.2501

Berti, M., & Vindigni, A. (2016). Replication stress: getting back on track. *Nature Structural & Molecular Biology*, *23*(2), 103–109. https://doi.org/10.1038/nsmb.3163

Bhatia, V., Barroso, S. I., García-Rubio, M. L., Tumini, E., Herrera-Moyano, E., & Aguilera, A. (2014). BRCA2 prevents R-loop accumulation and associates with TREX-2 mRNA export factor PCID2. *Nature*, *511*(7509), 362–365. https://doi.org/10.1038/nature13374

Bhowmick, R., Minocherhomji, S., & Hickson, I. D. (2016). RAD52 Facilitates Mitotic DNA Synthesis Following Replication Stress. *Molecular Cell*, *64*(6), 1117–1126. https://doi.org/10.1016/j.molcel.2016.10.037

Bianchi, J., Rudd, S. G., Jozwiakowski, S. K., Bailey, L. J., Soura, V., Taylor, E., Stevanovic, I., Green, A. J., Stracker, T. H., Lindsay, H. D., & Doherty, A. J.

(2013). PrimPol Bypasses UV Photoproducts during Eukaryotic Chromosomal DNA Replication. *Molecular Cell*, *52*(4), 566–573. https://doi.org/https://doi.org/10.1016/j.molcel.2013.10.035

Biebricher, A., Hirano, S., Enzlin, J. H., Wiechens, N., Streicher, W. W., Huttner, D., Wang, L. H.-C., Nigg, E. A., Owen-Hughes, T., Liu, Y., Peterman, E., Wuite, G. J. L., & Hickson, I. D. (2013). PICH: A DNA Translocase Specially Adapted for Processing Anaphase Bridge DNA. *Molecular Cell*, *51*(5), 691–701. https://doi.org/https://doi.org/10.1016/j.molcel.2013.07.016

Bignell, G., Micklem, G., Stratton, M. R., Ashworth, A., & Wooster, R. (1997). The BRC Repeats are Conserved in Mammalian BRCA2 Proteins. *Human Molecular Genetics*, *6*(1), 53–58. https://doi.org/10.1093/hmg/6.1.53

Birkness, J. E., Spada, N. G., Miller, C., Luketich, J. D., Nason, K. S., Sun, W., & Davison, J. M. (2018). Extreme chromosome 17 copy number instability is a prognostic factor in patients with gastroesophageal adenocarcinoma: A retrospective cohort study. *Genes, Chromosomes and Cancer*, *57*(1), 28–34. https://doi.org/https://doi.org/10.1002/gcc.22504

Bizard, A. H., & Hickson, I. D. (2018). Anaphase: a fortune-teller of genomic instability. *Current Opinion in Cell Biology*, *52*, 112–119. https://doi.org/https://doi.org/10.1016/j.ceb.2018.02.012

Black, & Giunta, S. (2018). Repetitive Fragile Sites: Centromere Satellite DNA as a Source of Genome Instability in Human Diseases. In *Genes* (Vol. 9, Issue 12). https://doi.org/10.3390/genes9120615

Black, Jansen, L. E. T., Maddox, P. S., Foltz, D. R., Desai, A. B., Shah, J. V, & Cleveland, D. W. (2007). Centromere Identity Maintained by Nucleosomes Assembled with Histone H3 Containing the CENP-A Targeting Domain. *Molecular Cell*, *25*(2), 309–322. https://doi.org/10.1016/j.molcel.2006.12.018

Bleuyard, J.-Y., Buisson, R., Masson, J.-Y., & Esashi, F. (2012). ChAM, a novel motif that mediates PALB2 intrinsic chromatin binding and facilitates DNA repair. *EMBO Reports*, *13*(2), 135–141. https://doi.org/https://doi.org/10.1038/embor.2011.243

Bleuyard, J.-Y., Fournier, M., Nakato, R., Couturier, A. M., Katou, Y., Ralf, C., Hester, S. S., Dominguez, D., Rhodes, D., Humphrey, T. C., Shirahige, K., & Esashi, F. (2017). MRG15-mediated tethering of PALB2 to unperturbed chromatin protects active genes from genotoxic stress. *Proceedings of the National Academy of Sciences*, *114*(29), 7671–7676. https://doi.org/10.1073/pnas.1620208114

Blower, M. D. (2016). Centromeric Transcription Regulates Aurora-B Localization and Activation. *Cell Reports*, *15*(8), 1624–1633. https://doi.org/10.1016/j.celrep.2016.04.054

Bobkov, G. O. M., Gilbert, N., & Heun, P. (2018). Centromere transcription allows CENP-A to transit from chromatin association to stable incorporation. *Journal of Cell Biology*, *217*(6), 1957–1972. https://doi.org/10.1083/jcb.201611087

Bodor, D. L., Valente, L. P., Mata, J. F., Black, B. E., & Jansen, L. E. T. (2013). Assembly in G1 phase and long-term stability are unique intrinsic features of

CENP-A nucleosomes. *Molecular Biology of the Cell*, *24*(7), 923–932. https://doi.org/10.1091/mbc.e13-01-0034

Boesen, J. J. B., Niericker, M. J., Dieteren, N., & Simons, J. W. I. M. (1994). How variable is an spontaneous mutation rate in cultured mammalian cells? *Mutation Research/Fundamental and Molecular Mechanisms of Mutagenesis*, *307*(1), 121–129. https://doi.org/https://doi.org/10.1016/0027-5107(94)90284-4

Bonilla, B., Hengel, S. R., Grundy, M. K., & Bernstein, K. A. (2020). RAD51 Gene Family Structure and Function. *Annual Review of Genetics*, *54*(1), 25–46. https://doi.org/10.1146/annurev-genet-021920-092410

Bork, P., Blomberg, N., & Nilges, M. (1996). Internal repeats in the BRCA2 protein sequence. *Nature Genetics*, *13*(1), 22–23. https://doi.org/10.1038/ng0596-22

Broderick, R., & Niedzwiedz, W. (2015). Sister chromatid decatenation: bridging the gaps in our knowledge. *Cell Cycle (Georgetown, Tex.)*, *14*(19), 3040–3044. https://doi.org/10.1080/15384101.2015.1078039

Broderick, R., Nieminuszczy, J., Blackford, A. N., Winczura, A., & Niedzwiedz, W. (2015). TOPBP1 recruits TOP2A to ultra-fine anaphase bridges to aid in their resolution. *Nature Communications*, *6*, 6572. https://doi.org/10.1038/ncomms7572

Brough, R., Bajrami, I., Vatcheva, R., Natrajan, R., Reis-Filho, J. S., Lord, C. J., & Ashworth, A. (2012). APRIN is a cell cycle specific BRCA2-interacting protein required for genome integrity and a predictor of outcome after chemotherapy in breast cancer. *The EMBO Journal*, *31*(5), 1160–1176. https://doi.org/https://doi.org/10.1038/emboj.2011.490

Buisson, R., Dion-Côté, A.-M., Coulombe, Y., Launay, H., Cai, H., Stasiak, A. Z., Stasiak, A., Xia, B., & Masson, J.-Y. (2010). Cooperation of breast cancer proteins PALB2 and piccolo BRCA2 in stimulating homologous recombination. *Nature Structural & Molecular Biology*, *17*(10), 1247–1254. https://doi.org/10.1038/nsmb.1915

Buisson, R., Niraj, J., Pauty, J., Maity, R., Zhao, W., Coulombe, Y., Sung, P., & Masson, J.-Y. (2014). Breast Cancer Proteins PALB2 and BRCA2 Stimulate Polymerase η in Recombination-Associated DNA Synthesis at Blocked Replication Forks. *Cell Reports*, *6*(3), 553–564. https://doi.org/https://doi.org/10.1016/j.celrep.2014.01.009

Burma, S., Chen, B. P., Murphy, M., Kurimasa, A., & Chen, D. J. (2001). ATM Phosphorylates Histone H2AX in Response to DNA Double-strand Breaks. *Journal of Biological Chemistry*, *276*(45), 42462–42467. https://doi.org/10.1074/jbc.C100466200

Bury, L., Moodie, B., Ly, J., McKay, L. S., Miga, K. H. H., & Cheeseman, I. M. (2020). Alpha-satellite RNA transcripts are repressed by centromere–nucleolus associations. *ELife*, *9*, e59770. https://doi.org/10.7554/eLife.59770

Caldecott, K. W. (2008). Single-strand break repair and genetic disease. *Nature Reviews Genetics*, *9*(8), 619–631. https://doi.org/10.1038/nrg2380

Callegari, A. J., Clark, E., Pneuman, A., & Kelly, T. J. (2010). Postreplication gaps at UV lesions are signals for checkpoint activation. *Proceedings of the National*

Academy of Sciences, *107*(18), 8219–8224. https://doi.org/10.1073/pnas.1003449107

Calzetta, N. L., González Besteiro, M. A., & Gottifredi, V. (2020). Mus81-Eme1–dependent aberrant processing of DNA replication intermediates in mitosis impairs genome integrity. *Science Advances*, *6*(50), eabc8257. https://doi.org/10.1126/sciadv.abc8257

Canela, A., Sridharan, S., Sciascia, N., Tubbs, A., Meltzer, P., Sleckman, B. P., & Nussenzweig, A. (2016). DNA Breaks and End Resection Measured Genome-wide by End Sequencing. *Molecular Cell*, *63*(5), 898–911. https://doi.org/10.1016/j.molcel.2016.06.034

Carlos, A. R., Escandell, J. M., Kotsantis, P., Suwaki, N., Bouwman, P., Badie, S., Folio, C., Benitez, J., Gomez-Lopez, G., Pisano, D. G., Jonkers, J., & Tarsounas, M. (2013). ARF triggers senescence in Brca2-deficient cells by altering the spectrum of p53 transcriptional targets. *Nature Communications*, *4*(1), 2697. https://doi.org/10.1038/ncomms3697

Carnie, C. J., Armstrong, L., Sebesta, M., Ariza, A., Wang, X., Graham, E., Zhu, K., & Ahel, D. (2023). ERCC6L2 mitigates replication stress and promotes centromere stability. *Cell Reports*, *42*(4). https://doi.org/10.1016/j.celrep.2023.112329

Carreira, A., Hilario, J., Amitani, I., Baskin, R. J., Shivji, M. K. K., Venkitaraman, A. R., & Kowalczykowski, S. C. (2009). The BRC repeats of BRCA2 modulate the DNA-binding selectivity of RAD51. *Cell*, *136*(6), 1032–1043. https://doi.org/10.1016/j.cell.2009.02.019

Carreira, A., & Kowalczykowski, S. C. (2011). Two classes of BRC repeats in BRCA2 promote RAD51 nucleoprotein filament function by distinct mechanisms. *Proceedings of the National Academy of Sciences*, *108*(26), 10448–10453. https://doi.org/10.1073/pnas.1106971108

Carroll, C. W., Milks, K. J., & Straight, A. F. (2010). Dual recognition of CENP-A nucleosomes is required for centromere assembly. *Journal of Cell Biology*, *189*(7), 1143–1155. https://doi.org/10.1083/jcb.201001013

Carroll, C. W., Silva, M. C. C., Godek, K. M., Jansen, L. E. T., & Straight, A. F. (2009). Centromere assembly requires the direct recognition of CENP-A nucleosomes by CENP-N. *Nature Cell Biology*, *11*(7), 896–902. https://doi.org/10.1038/ncb1899

Castellano-Pozo, M., Santos-Pereira, J. M., Rondón, A. G., Barroso, S., Andújar, E., Pérez-Alegre, M., García-Muse, T., & Aguilera, A. (2013). R Loops Are Linked to Histone H3 S10 Phosphorylation and Chromatin Condensation. *Molecular Cell*, *52*(4), 583–590. https://doi.org/10.1016/j.molcel.2013.10.006

Ceccaldi, R., Liu, J. C., Amunugama, R., Hajdu, I., Primack, B., Petalcorin, M. I. R., O'Connor, K. W., Konstantinopoulos, P. A., Elledge, S. J., Boulton, S. J., Yusufzai, T., & D'Andrea, A. D. (2015). Homologous-recombination-deficient tumours are dependent on Polθ-mediated repair. *Nature*, *518*(7538), 258–262. https://doi.org/10.1038/nature14184

Ceccaldi, R., Rondinelli, B., & D'Andrea, A. D. (2016). Repair Pathway Choices and Consequences at the Double-Strand Break. *Trends in Cell Biology*, *26*(1), 52–64. https://doi.org/https://doi.org/10.1016/j.tcb.2015.07.009

Chakraborty, U., & Alani, E. (2016). Understanding how mismatch repair proteins participate in the repair/anti-recombination decision. *FEMS Yeast Research*, *16*(6), fow071. https://doi.org/10.1093/femsyr/fow071

Chan, Fugger, K., & West, S. C. (2018). Unresolved recombination intermediates lead to ultra-fine anaphase bridges, chromosome breaks and aberrations. *Nature Cell Biology*, *20*(1), 92–103. https://doi.org/10.1038/s41556-017-0011-1

Chan, Marshall, O. J., Saffery, R., Won Kim, B., Earle, E., Choo, K. H. A., & Wong, L. H. (2012). Active transcription and essential role of RNA polymerase II at the centromere during mitosis. *Proceedings of the National Academy of Sciences*, *109*(6), 1979–1984. https://doi.org/10.1073/pnas.1108705109

Chan, North, P. S., & Hickson, I. D. (2007). BLM is required for faithful chromosome segregation and its localization defines a class of ultrafine anaphase bridges. *The EMBO Journal*, *26*(14), 3397 LP – 3409. https://doi.org/10.1038/sj.emboj.7601777

Chan, Palmai-Pallag, T., Ying, S., & Hickson, I. D. (2009). Replication stress induces sister-chromatid bridging at fragile site loci in mitosis. *Nature Cell Biology*, *11*(6), 753–760. https://doi.org/10.1038/ncb1882

Chan, & West, S. C. (2018). A new class of ultrafine anaphase bridges generated by homologous recombination. *Cell Cycle (Georgetown, Tex.)*, *17*(17), 2101–2109. https://doi.org/10.1080/15384101.2018.1515555

Chappidi, N., Nascakova, Z., Boleslavska, B., Zellweger, R., Isik, E., Andrs, M., Menon, S., Dobrovolna, J., Balbo Pogliano, C., Matos, J., Porro, A., Lopes, M., & Janscak, P. (2020). Fork Cleavage-Religation Cycle and Active Transcription Mediate Replication Restart after Fork Stalling at Co-transcriptional R-Loops. *Molecular Cell*, *77*(3), 528-541.e8. https://doi.org/10.1016/j.molcel.2019.10.026

Chardon, F., Japaridze, A., Witt, H., Velikovsky, L., Chakraborty, C., Wilhelm, T., Dumont, M., Yang, W., Kikuti, C., Gangnard, S., Mace, A.-S., Wuite, G., Dekker, C., & Fachinetti, D. (2022). CENP-B-mediated DNA loops regulate activity and stability of human centromeres. *Molecular Cell*, *82*(9), 1751-1767.e8. https://doi.org/10.1016/j.molcel.2022.02.032

Chastain, M., Zhou, Q., Shiva, O., Fadri-Moskwik, M., Whitmore, L., Jia, P., Dai, X., Huang, C., Ye, P., & Chai, W. (2016). Human CST Facilitates Genome-wide RAD51 Recruitment to GC-Rich Repetitive Sequences in Response to Replication Stress. *Cell Reports*, *16*(5), 1300–1314. https://doi.org/https://doi.org/10.1016/j.celrep.2016.06.077

Chatterjee, G., Jimenez-Sainz, J., Presti, T., Nguyen, T., & Jensen, R. B. (2016). Distinct binding of BRCA2 BRC repeats to RAD51 generates differential DNA damage sensitivity. *Nucleic Acids Research*, *44*(11), 5256–5270. https://doi.org/10.1093/nar/gkw242

Cheeseman, I. M., & Desai, A. (2008). Molecular architecture of the kinetochore–microtubule interface. *Nature Reviews Molecular Cell Biology*, *9*(1), 33–46. https://doi.org/10.1038/nrm2310

Chen, Bowers, S., Lipinszki, Z., Palladino, J., Trusiak, S., Bettini, E., Rosin, L., Przewloka, M. R., Glover, D. M., O'Neill, R. J., & Mellone, B. G. (2015). Establishment of Centromeric Chromatin by the CENP-A Assembly Factor CAL1 Requires FACT-Mediated Transcription. *Developmental Cell*, *34*(1), 73–84. https://doi.org/10.1016/j.devcel.2015.05.012

Chen, C.-F., Chen, P.-L., Zhong, Q., Sharp, Z. D., & Lee, W.-H. (1999). Expression of BRC Repeats in Breast Cancer Cells Disrupts the BRCA2-Rad51 Complex and Leads to Radiation Hypersensitivity and Loss of G2/M Checkpoint Control. *Journal of Biological Chemistry* , *274*(46), 32931–32935. https://doi.org/10.1074/jbc.274.46.32931

Chen, P.-L., Chen, C.-F., Chen, Y., Xiao, J., Sharp, Z. D., & Lee, W.-H. (1998a). The BRC repeats in BRCA2 are critical for RAD51 binding and resistance to methyl methanesulfonate treatment. *Proceedings of the National Academy of Sciences*, *95*(9), 5287–5292. https://doi.org/10.1073/pnas.95.9.5287

Chen, J., Silver, D. P., Walpita, D., Cantor, S. B., Gazdar, A. F., Tomlinson, G., Couch, F. J., Weber, B. L., Ashley, T., Livingston, D. M., & Scully, R. (1998b). Stable Interaction between the Products of the BRCA1 and BRCA2 Tumor Suppressor Genes in Mitotic and Meiotic Cells. *Molecular Cell*, *2*(3), 317–328. https://doi.org/10.1016/S1097-2765(00)80276-2

Chen, Zhang, Q., Teng, Z., & Liu, H. (2021). Centromeric transcription maintains centromeric cohesion in human cells. *Journal of Cell Biology*, *220*(7), e202008146. https://doi.org/10.1083/jcb.202008146

Cho, N. W., Dilley, R. L., Lampson, M. A., & Greenberg, R. A. (2014). Interchromosomal Homology Searches Drive Directional ALT Telomere Movement and Synapsis. *Cell*, *159*(1), 108–121. https://doi.org/https://doi.org/10.1016/j.cell.2014.08.030

Choi, Park, P.-G., Lee, H., Lee, Y.-K., Kang, G. H., Lee, J. W., Han, W., Lee, H. C., Noh, D.-Y., Lekomtsev, S., & Lee, H. (2012). BRCA2 Fine-Tunes the Spindle Assembly Checkpoint through Reinforcement of BubR1 Acetylation. *Developmental Cell*, *22*(2), 295–308. https://doi.org/10.1016/j.devcel.2012.01.009

Choi, Strålfors, A., Castillo, A. G., Durand-Dubief, M., Ekwall, K., & Allshire, R. C. (2011). Identification of Noncoding Transcripts from within CENP-A Chromatin at Fission Yeast Centromeres. *Journal of Biological Chemistry*, *286*(26), 23600–23607. https://doi.org/10.1074/jbc.M111.228510

Ciccia, A., & Elledge, S. J. (2010). The DNA Damage Response: Making It Safe to Play with Knives. *Molecular Cell*, *40*(2), 179–204. https://doi.org/10.1016/j.molcel.2010.09.019

Cimprich, K. A., & Cortez, D. (2008). ATR: an essential regulator of genome integrity. *Nature Reviews Molecular Cell Biology*, *9*(8), 616–627. https://doi.org/10.1038/nrm2450

Cong, K., Peng, M., Kousholt, A. N., Lee, W. T. C., Lee, S., Nayak, S., Krais, J., VanderVere-Carozza, P. S., Pawelczak, K. S., Calvo, J., Panzarino, N. J., Turchi, J. J., Johnson, N., Jonkers, J., Rothenberg, E., & Cantor, S. B. (2021). Replication gaps are a key determinant of PARP inhibitor synthetic lethality with BRCA deficiency. *Molecular Cell*, *81*(15), 3128-3144.e7. https://doi.org/10.1016/j.molcel.2021.06.011

Conway, A. B., Lynch, T. W., Zhang, Y., Fortin, G. S., Fung, C. W., Symington, L. S., & Rice, P. A. (2004). Crystal structure of a Rad51 filament. *Nature Structural & Molecular Biology*, *11*(8), 791–796. https://doi.org/10.1038/nsmb795

Costantino, L., Sotiriou, S. K., Rantala, J. K., Magin, S., Mladenov, E., Helleday, T., Haber, J. E., Iliakis, G., Kallioniemi, O. P., & Halazonetis, T. D. (2014). Break-Induced Replication Repair of Damaged Forks Induces Genomic Duplications in Human Cells. *Science*, *343*(6166), 88–91. https://doi.org/10.1126/science.1243211

Cristini, A., Ricci, G., Britton, S., Salimbeni, S., Huang, S. N., Marinello, J., Calsou, P., Pommier, Y., Favre, G., Capranico, G., Gromak, N., & Sordet, O. (2019). Dual Processing of R-Loops and Topoisomerase I Induces Transcription-Dependent DNA Double-Strand Breaks. *Cell Reports*, *28*(12), 3167-3181.e6. https://doi.org/https://doi.org/10.1016/j.celrep.2019.08.041

Crosetto, N., Mitra, A., Silva, M. J., Bienko, M., Dojer, N., Wang, Q., Karaca, E., Chiarle, R., Skrzypczak, M., Ginalski, K., Pasero, P., Rowicka, M., & Dikic, I. (2013). Nucleotide-resolution DNA double-strand break mapping by next-generation sequencing. *Nature Methods*, *10*(4), 361–365. https://doi.org/10.1038/nmeth.2408

Dahiya, R., Hu, Q., & Ly, P. (2022). Mechanistic origins of diverse genome rearrangements in cancer. *Seminars in Cell & Developmental Biology*, *123*, 100–109. https://doi.org/https://doi.org/10.1016/j.semcdb.2021.03.003

D'Alessandro, G., Whelan, D. R., Howard, S. M., Vitelli, V., Renaudin, X., Adamowicz, M., Iannelli, F., Jones-Weinert, C. W., Lee, M., Matti, V., Lee, W. T. C., Morten, M. J., Venkitaraman, A. R., Cejka, P., Rothenberg, E., & d'Adda di Fagagna, F. (2018). BRCA2 controls DNA:RNA hybrid level at DSBs by mediating RNase H2 recruitment. *Nature Communications*, *9*(1), 5376. https://doi.org/10.1038/s41467-018-07799-2

Dambacher, S., Deng, W., Hahn, M., Sadic, D., Fröhlich, J., Nuber, A., Hoischen, C., Diekmann, S., Leonhardt, H., & Schotta, G. (2012). CENP-C facilitates the recruitment of M18BP1 to centromeric chromatin. *Nucleus*, *3*(1), 101–110. https://doi.org/10.4161/nucl.18955

Daniels, M. J., Wang, Y., Lee, M., & Venkitaraman, A. R. (2004). Abnormal Cytokinesis in Cells Deficient in the Breast Cancer Susceptibility Protein BRCA2. *Science*, *306*(5697), 876 LP – 879. https://doi.org/10.1126/science.1102574

Davies, Masson, J.-Y., McIlwraith, M. J., Stasiak, A. Z., Stasiak, A., Venkitaraman, A. R., & West, S. C. (2001). Role of BRCA2 in Control of the RAD51 Recombination and DNA Repair Protein. *Molecular Cell*, *7*(2), 273–282. https://doi.org/https://doi.org/10.1016/S1097-2765(01)00175-7

Davies, & Pellegrini, L. (2007). Interaction with the BRCA2 C terminus protects RAD51-DNA filaments from disassembly by BRC repeats. *Nature Structural & Molecular Biology*, *14*(6), 475–483. https://doi.org/10.1038/nsmb1251

Davis, L., & Maizels, N. (2014). Homology-directed repair of DNA nicks via pathways distinct from canonical double-strand break repair. *Proceedings of the National Academy of Sciences*, *111*(10), E924–E932. https://doi.org/10.1073/pnas.1400236111

Daza-Martin, M., Starowicz, K., Jamshad, M., Tye, S., Ronson, G. E., MacKay, H. L., Chauhan, A. S., Walker, A. K., Stone, H. R., Beesley, J. F. J., Coles, J. L., Garvin, A. J., Stewart, G. S., McCorvie, T. J., Zhang, X., Densham, R. M., & Morris, J. R. (2019). Isomerization of BRCA1–BARD1 promotes replication fork protection. *Nature*, *571*(7766), 521–527. https://doi.org/10.1038/s41586-019-1363-4

De Koning, L., Savignoni, A., Boumendil, C., Rehman, H., Asselain, B., Sastre-Garau, X., & Almouzni, G. (2009). Heterochromatin protein 1α: a hallmark of cell proliferation relevant to clinical oncology. *EMBO Molecular Medicine*, *1*(3), 178–191. https://doi.org/https://doi.org/10.1002/emmm.200900022

Deans, A. J., & West, S. C. (2011). DNA interstrand crosslink repair and cancer. *Nature Reviews Cancer*, *11*(7), 467–480. https://doi.org/10.1038/nrc3088

Deem, A., Keszthelyi, A., Blackgrove, T., Vayl, A., Coffey, B., Mathur, R., Chabes, A., & Malkova, A. (2011). Break-Induced Replication Is Highly Inaccurate. *PLOS Biology*, *9*(2), e1000594-. https://doi.org/10.1371/journal.pbio.1000594

Depinet, T. W., Zackowski, J. L., Earnshaw, W. C., Kaffe, S., Sekhon, G. S., Stallard, R., Sullivan, B. A., Vance, G. H., Van Dyke, D. L., Willard, H. F., Zinn, A. B., & Schwartz, S. (1997). Characterization of Neo-Centromeres in Marker Chromosomes Lacking Detectable Alpha-satellite DNA. *Human Molecular Genetics*, *6*(8), 1195–1204. https://doi.org/10.1093/hmg/6.8.1195

Deveryshetty, J., Peterlini, T., Ryzhikov, M., Brahiti, N., Dellaire, G., Masson, J.-Y., & Korolev, S. (2019). Novel RNA and DNA strand exchange activity of the PALB2 DNA binding domain and its critical role for DNA repair in cells. *ELife*, *8*, e44063. https://doi.org/10.7554/eLife.44063

Dhillon, V. S., Husain, S. A., & Ray, G. N. (2003). Expression of aphidicolin-induced fragile sites and their relationship between genetic susceptibility in breast cancer, ovarian cancer, and non-small-cell lung cancer patients. *Teratogenesis, Carcinogenesis, and Mutagenesis*, *23*(S1), 35–45. https://doi.org/https://doi.org/10.1002/tcm.10068

Dilley, R. L., Verma, P., Cho, N. W., Winters, H. D., Wondisford, A. R., & Greenberg, R. A. (2016). Break-induced telomere synthesis underlies alternative telomere maintenance. *Nature*, *539*(7627), 54–58. https://doi.org/10.1038/nature20099

Donoho, G., Brenneman, M. A., Cui, T. X., Donoviel, D., Vogel, H., Goodwin, E. H., Chen, D. J., & Hasty, P. (2003). Deletion of Brca2 exon 27 causes hypersensitivity to DNA crosslinks, chromosomal instability, and reduced life span in mice. *Genes, Chromosomes and Cancer*, *36*(4), 317–331. https://doi.org/https://doi.org/10.1002/gcc.10148

Duda, H., Arter, M., Gloggnitzer, J., Teloni, F., Wild, P., Blanco, M. G., Altmeyer, M., & Matos, J. (2016). A Mechanism for Controlled Breakage of Under-replicated Chromosomes during Mitosis. *Developmental Cell*, *39*(6), 740–755. https://doi.org/10.1016/j.devcel.2016.11.017

Dunleavy, E. M., Almouzni, G., & Karpen, G. H. (2011). H3.3 is deposited at centromeres in S phase as a placeholder for newly assembled CENP-A in G1 phase. *Nucleus*, *2*(2), 146–157. https://doi.org/10.4161/nucl.2.2.15211

Dunleavy, E. M., Roche, D., Tagami, H., Lacoste, N., Ray-Gallet, D., Nakamura, Y., Daigo, Y., Nakatani, Y., & Almouzni-Pettinotti, G. (2009). HJURP Is a Cell-Cycle-Dependent Maintenance and Deposition Factor of CENP-A at Centromeres. *Cell*, *137*(3), 485–497. https://doi.org/10.1016/j.cell.2009.02.040

Dutta, A., Eckelmann, B., Adhikari, S., Ahmed, K. M., Sengupta, S., Pandey, A., Hegde, P. M., Tsai, M.-S., Tainer, J. A., Weinfeld, M., Hegde, M. L., & Mitra, S. (2017). Microhomology-mediated end joining is activated in irradiated human cells due to phosphorylation-dependent formation of the XRCC1 repair complex. *Nucleic Acids Research*, *45*(5), 2585–2599. https://doi.org/10.1093/nar/gkw1262

Earnshaw, W. C., & Rothfield, N. (1985). Identification of a family of human centromere proteins using autoimmune sera from patients with scleroderma. *Chromosoma*, *91*(3), 313–321. https://doi.org/10.1007/BF00328227

Ehlén, Å., Martin, C., Miron, S., Julien, M., Theillet, F.-X., Ropars, V., Sessa, G., Beaurepere, R., Boucherit, V., Duchambon, P., El Marjou, A., Zinn-Justin, S., & Carreira, A. (2020). Proper chromosome alignment depends on BRCA2 phosphorylation by PLK1. *Nature Communications*, *11*(1), 1819. https://doi.org/10.1038/s41467-020-15689-9

El Amri, C., Mauffret, O., Monnot, M., Tevanian, G., Lescot, E., Porumb, H., & Fermandjian, S. (1999). A DNA hairpin with a single residue loop closed by a strongly distorted watson-crick G x C base-pair. *Journal of Molecular Biology*, *294*(2), 427–442. https://doi.org/https://doi.org/10.1006/jmbi.1999.3270

Elvers, I., Johansson, F., Groth, P., Erixon, K., & Helleday, T. (2011). UV stalled replication forks restart by re-priming in human fibroblasts. *Nucleic Acids Research*, *39*(16), 7049–7057. https://doi.org/10.1093/nar/gkr420

Engeland, K. (2022). Cell cycle regulation: p53-p21-RB signaling. *Cell Death & Differentiation*, *29*(5), 946–960. https://doi.org/10.1038/s41418-022-00988-z

Esashi, F., Christ, N., Gannon, J., Liu, Y., Hunt, T., Jasin, M., & West, S. C. (2005). CDK-dependent phosphorylation of BRCA2 as a regulatory mechanism for recombinational repair. *Nature*, *434*(7033), 598–604. https://doi.org/10.1038/nature03404

Esashi, F., Galkin, V. E., Yu, X., Egelman, E. H., & West, S. C. (2007). Stabilization of RAD51 nucleoprotein filaments by the C-terminal region of BRCA2. *Nature Structural & Molecular Biology*, *14*(6), 468–474. https://doi.org/10.1038/nsmb1245

Fachinetti, D., Diego Folco, H., Nechemia-Arbely, Y., Valente, L. P., Nguyen, K., Wong, A. J., Zhu, Q., Holland, A. J., Desai, A., Jansen, L. E. T., & Cleveland, D. W. (2013). A two-step mechanism for epigenetic specification of centromere

identity and function. *Nature Cell Biology*, *15*(9), 1056–1066. https://doi.org/10.1038/ncb2805

Fachinetti, D., Han, J. S., McMahon, M. A., Ly, P., Abdullah, A., Wong, A. J., & Cleveland, D. W. (2015). DNA Sequence-Specific Binding of CENP-B Enhances the Fidelity of Human Centromere Function. *Developmental Cell*, *33*(3), 314–327. https://doi.org/10.1016/j.devcel.2015.03.020

Falk, S. J., Guo, L. Y., Sekulic, N., Smoak, E. M., Mani, T., Logsdon, G. A., Gupta, K., Jansen, L. E. T., Van Duyne, G. D., Vinogradov, S. A., Lampson, M. A., & Black, B. E. (2015). CENP-C reshapes and stabilizes CENP-A nucleosomes at the centromere. *Science*, *348*(6235), 699–703. https://doi.org/10.1126/science.1259308

Feng, W., & Jasin, M. (2017). BRCA2 suppresses replication stress-induced mitotic and G1 abnormalities through homologous recombination. *Nature Communications*, *8*(1), 525. https://doi.org/10.1038/s41467-017-00634-0

Floridia, G., Zatterale, A., Zuffardi, O., & Tyler-Smith, C. (2000). Mapping of a human centromere onto the DNA by topoisomerase II cleavage. *EMBO Reports*, *1*(6), 489–493. https://doi.org/https://doi.org/10.1093/embo-reports/kvd110

Foltz, D. R., Jansen, L. E. T., Bailey, A. O., Yates III, J. R., Bassett, E. A., Wood, S., Black, B. E., & Cleveland, D. W. (2009). Centromere-Specific Assembly of CENP-A Nucleosomes Is Mediated by HJURP. *Cell*, *137*(3), 472–484. https://doi.org/10.1016/j.cell.2009.02.039

Foltz, D. R., Jansen, L. E. T., Black, B. E., Bailey, A. O., Yates, J. R., & Cleveland, D. W. (2006). The human CENP-A centromeric nucleosome-associated complex. *Nature Cell Biology*, *8*(5), 458–469. https://doi.org/10.1038/ncb1397

Fournier, M., Orpinell, M., Grauffel, C., Scheer, E., Garnier, J.-M., Ye, T., Chavant, V., Joint, M., Esashi, F., Dejaegere, A., Gönczy, P., & Tora, L. (2016). KAT2A/KAT2B-targeted acetylome reveals a role for PLK4 acetylation in preventing centrosome amplification. *Nature Communications*, *7*(1), 13227. https://doi.org/10.1038/ncomms13227

Fournier, M., Rodrigue, A., Milano, L., Bleuyard, J.-Y., Couturier, A. M., Wall, J., Ellins, J., Hester, S., Smerdon, S. J., Tora, L., Masson, J.-Y., & Esashi, F. (2022). KAT2-mediated acetylation switches the mode of PALB2 chromatin association to safeguard genome integrity. *ELife*, *11*, e57736. https://doi.org/10.7554/eLife.57736

Fradet-Turcotte, A., Sitz, J., Grapton, D., & Orthwein, A. (2016). BRCA2 functions: from DNA repair to replication fork stabilization. *Endocrine-Related Cancer*, *23*(10), T1–T17. https://doi.org/10.1530/ERC-16-0297

Froelich-Ammon, S. J., Gale, K. C., & Osheroff, N. (1994). Site-specific cleavage of a DNA hairpin by topoisomerase II. DNA secondary structure as a determinant of enzyme recognition/cleavage. *Journal of Biological Chemistry*, *269*(10), 7719–7725. https://doi.org/https://doi.org/10.1016/S0021-9258(17)37346-5

Fujita, Y., Hayashi, T., Kiyomitsu, T., Toyoda, Y., Kokubu, A., Obuse, C., & Yanagida, M. (2007). Priming of Centromere for CENP-A Recruitment by

Human hMis18alpha, hMis18beta, and M18BP1. *Developmental Cell*, *12*(1), 17–30. https://doi.org/10.1016/j.devcel.2006.11.002

Futamura, M., Arakawa, H., Matsuda, K., Katagiri, T., Saji, S., Miki, Y., & Nakamura, Y. (2000). Potential Role of BRCA2 in a Mitotic Checkpoint after Phosphorylation by hBUBR1. *Cancer Research*, *60*(6), 1531 LP – 1535.

Gagou, M. E., Zuazua-Villar, P., & Meuth, M. (2010). Enhanced H2AX Phosphorylation, DNA Replication Fork Arrest, and Cell Death in the Absence of Chk1. *Molecular Biology of the Cell*, *21*(5), 739–752. https://doi.org/10.1091/mbc.e09-07-0618

Gamba, R., Mazzucco, G., Wilhelm, T., Velikovsky, L., Salinas-Luypaert, C., Chardon, F., Picotto, J., Bohec, M., Baulande, S., Doksani, Y., & Fachinetti, D. (2022). Enrichment of centromeric DNA from human cells. *PLOS Genetics*, *18*(7), e1010306-. https://doi.org/10.1371/journal.pgen.1010306

Gan, W., Guan, Z., Liu, J., Gui, T., Shen, K., Manley, J. L., & Li, X. (2011). R-loop-mediated genomic instability is caused by impairment of replication fork progression. *Genes & Development*, *25*(19), 2041–2056. https://doi.org/10.1101/gad.17010011

Gao, X. D., Tu, L.-C., Mir, A., Rodriguez, T., Ding, Y., Leszyk, J., Dekker, J., Shaffer, S. A., Zhu, L. J., Wolfe, S. A., & Sontheimer, E. J. (2018). C-BERST: defining subnuclear proteomic landscapes at genomic elements with dCas9–APEX2. *Nature Methods*, *15*(6), 433–436. https://doi.org/10.1038/s41592-018-0006-2

Garavís, M., Escaja, N., Gabelica, V., Villasante, A., & González, C. (2015). Centromeric Alpha-Satellite DNA Adopts Dimeric i-Motif Structures Capped by AT Hoogsteen Base Pairs. *Chemistry – A European Journal*, *21*(27), 9816–9824. https://doi.org/10.1002/chem.201500448

Garavís, M., Méndez-Lago, M., Gabelica, V., Whitehead, S. L., González, C., & Villasante, A. (2015). The structure of an endogenous Drosophila centromere reveals the prevalence of tandemly repeated sequences able to form i-motifs. *Scientific Reports*, *5*(1), 13307. https://doi.org/10.1038/srep13307

Garcia, V., Phelps, S. E. L., Gray, S., & Neale, M. J. (2011). Bidirectional resection of DNA double-strand breaks by Mre11 and Exo1. *Nature*, *479*(7372), 241–244. https://doi.org/10.1038/nature10515

García-Gómez, S., Reyes, A., Martínez-Jiménez, M. I., Chocrón, E. S., Mourón, S., Terrados, G., Powell, C., Salido, E., Méndez, J., Holt, I. J., & Blanco, L. (2013). PrimPol, an Archaic Primase/Polymerase Operating in Human Cells. *Molecular Cell*, *52*(4), 541–553. https://doi.org/10.1016/j.molcel.2013.09.025

García-Rubio, M. L., Pérez-Calero, C., Barroso, S. I., Tumini, E., Herrera-Moyano, E., Rosado, I. V, & Aguilera, A. (2015). The Fanconi Anemia Pathway Protects Genome Integrity from R-loops. *PLoS Genetics*, *11*(11), e1005674–e1005674. https://doi.org/10.1371/journal.pgen.1005674

Gardini, A., Baillat, D., Cesaroni, M., & Shiekhattar, R. (2014). Genome-wide analysis reveals a role for BRCA1 and PALB2 in transcriptional co-activation. *The EMBO Journal*, *33*(8), 890–905. https://doi.org/https://doi.org/10.1002/embj.201385567

Garribba, L., Bjerregaard, V. A., Gonçalves Dinis, M. M., Özer, Ö., Wu, W., Sakellariou, D., Pena-Diaz, J., Hickson, I. D., & Liu, Y. (2020). Folate stress induces SLX1- and RAD51-dependent mitotic DNA synthesis at the fragile X locus in human cells. *Proceedings of the National Academy of Sciences*, *117*(28), 16527–16536. https://doi.org/10.1073/pnas.1921219117

Gascoigne, K. E., & Cheeseman, I. M. (2013). CDK-dependent phosphorylation and nuclear exclusion coordinately control kinetochore assembly state. *Journal of Cell Biology*, *201*(1), 23–32. https://doi.org/10.1083/jcb.201301006

Ge, X. Q., Jackson, D. A., & Blow, J. J. (2007). Dormant origins licensed by excess Mcm2–7 are required for human cells to survive replicative stress. *Genes & Development*, *21*(24), 3331–3341. https://doi.org/10.1101/gad.457807

Ghodgaonkar, M. M., Lazzaro, F., Olivera-Pimentel, M., Artola-Borán, M., Cejka, P., Reijns, M. A., Jackson, A. P., Plevani, P., Muzi-Falconi, M., & Jiricny, J. (2013). Ribonucleotides Misincorporated into DNA Act as Strand-Discrimination Signals in Eukaryotic Mismatch Repair. *Molecular Cell*, *50*(3), 323–332. https://doi.org/10.1016/j.molcel.2013.03.019

Giunta, S., Belotserkovskaya, R., & Jackson, S. P. (2010). DNA damage signaling in response to double-strand breaks during mitosis. *The Journal of Cell Biology*, *190*(2), 197–207. https://doi.org/10.1083/jcb.200911156

Giunta, S., & Funabiki, H. (2017). Integrity of the human centromere DNA repeats is protected by CENP-A, CENP-C, and CENP-T. *Proceedings of the National Academy of Sciences*, *114*(8), 1928–1933. https://doi.org/10.1073/pnas.1615133114

Giunta, S., Hervé, S., White, R. R., Wilhelm, T., Dumont, M., Scelfo, A., Gamba, R., Wong, C. K., Rancati, G., Smogorzewska, A., Funabiki, H., & Fachinetti, D. (2021). CENP-A chromatin prevents replication stress at centromeres to avoid structural aneuploidy. *Proceedings of the National Academy of Sciences*, *118*(10), e2015634118. https://doi.org/10.1073/pnas.2015634118

Gravel, S., Chapman, J. R., Magill, C., & Jackson, S. P. (2008). DNA helicases Sgs1 and BLM promote DNA double-strand break resection. *Genes & Development*, *22*(20), 2767–2772. https://doi.org/10.1101/gad.503108

Greenfeder, S. A., & Newlon, C. S. (1992). Replication Forks Pause at Yeast Centromeres. *Molecular and Cellular Biology*, *12*(9), 4056–4066. https://doi.org/10.1128/mcb.12.9.4056-4066.1992

Groth, P., Orta, M. L., Elvers, I., Majumder, M. M., Lagerqvist, A., & Helleday, T. (2012). Homologous recombination repairs secondary replication induced DNA double-strand breaks after ionizing radiation. *Nucleic Acids Research*, *40*(14), 6585–6594. https://doi.org/10.1093/nar/gks315

Gu, W., Zhang, F., & Lupski, J. R. (2008). Mechanisms for human genomic rearrangements. *PathoGenetics*, *1*(1), 4. https://doi.org/10.1186/1755-8417-1-4

Guerrero, A. A., Gamero, M. C., Trachana, V., Fütterer, A., Pacios-Bras, C., Díaz-Concha, N. P., Cigudosa, J. C., Martínez-A., C., & van Wely, K. H. M. (2010). Centromere-localized breaks indicate the generation of DNA damage by the

mitotic spindle. *Proceedings of the National Academy of Sciences*, *107*(9), 4159 LP – 4164. https://doi.org/10.1073/pnas.0912143106

Guo, L.-H., & Wu, R. (1982). New rapid methods for DNA sequencing based on exonuclease III digestion followed by repair synthesis. *Nucleic Acids Research*, *10*(6), 2065–2084. https://doi.org/10.1093/nar/10.6.2065

Haas, K. T., Lee, M., Esposito, A., & Venkitaraman, A. R. (2018). Single-molecule localization microscopy reveals molecular transactions during RAD51 filament assembly at cellular DNA damage sites. *Nucleic Acids Research*, *46*(5), 2398–2416. https://doi.org/10.1093/nar/gkx1303

Hagen, K. G. Ten, Gilbert, D. M., Willard, H. F., & Cohen, S. N. (1990). Replication Timing of DNA Sequences Associated with Human Centromeres and Telomeres. *Molecular and Cellular Biology*, *10*(12), 6348–6355. https://doi.org/10.1128/mcb.10.12.6348-6355.1990

Håkansson, S., Johannsson, O., Johansson, U., Sellberg, G., Loman, N., Gerdes, A. M., Holmberg, E., Dahl, N., Pandis, N., Kristoffersson, U., Olsson, H., & Borg, A. (1997). Moderate frequency of BRCA1 and BRCA2 germ-line mutations in Scandinavian familial breast cancer. *American Journal of Human Genetics*, *60*(5), 1068–1078.

Hamperl, S., Bocek, M. J., Saldivar, J. C., Swigut, T., & Cimprich, K. A. (2017). Transcription-Replication Conflict Orientation Modulates R-Loop Levels and Activates Distinct DNA Damage Responses. *Cell*, *170*(4), 774-786.e19. https://doi.org/10.1016/j.cell.2017.07.043

Hashimoto, Y., Puddu, F., & Costanzo, V. (2011). RAD51- and MRE11-dependent reassembly of uncoupled CMG helicase complex at collapsed replication forks. *Nature Structural & Molecular Biology*, *19*(1), 17–24. https://doi.org/10.1038/nsmb.2177

Hashimoto, Y., Ray Chaudhuri, A., Lopes, M., & Costanzo, V. (2010). Rad51 protects nascent DNA from Mre11-dependent degradation and promotes continuous DNA synthesis. *Nature Structural & Molecular Biology*, *17*(11), 1305–1311. https://doi.org/10.1038/nsmb.1927

Hayakawa, T., Zhang, F., Hayakawa, N., Ohtani, Y., Shinmyozu, K., Nakayama, J., & Andreassen, P. R. (2010). MRG15 binds directly to PALB2 and stimulates homology-directed repair of chromosomal breaks. *Journal of Cell Science*, *123*(7), 1124 LP – 1130. https://doi.org/10.1242/jcs.060178

Hayashi, T., Fujita, Y., Iwasaki, O., Adachi, Y., Takahashi, K., & Yanagida, M. (2004). Mis16 and Mis18 Are Required for CENP-A Loading and Histone Deacetylation at Centromeres. *Cell*, *118*(6), 715–729. https://doi.org/10.1016/j.cell.2004.09.002

Hegazy, Y. A., Fernando, C. M., & Tran, E. J. (2020). The balancing act of R-loop biology: The good, the bad, and the ugly. *Journal of Biological Chemistry*, *295*(4), 905–913. https://doi.org/https://doi.org/10.1016/S0021-9258(17)49903-0

Heijink, A. M., Stok, C., Porubsky, D., Manolika, E. M., Kok, Y. P., Everts, M., de Boer, H. R., Audrey, A., Wierenga, E., Guryev, V., Spierings, D. C. J., Knipscheer, P., Chaudhuri, A. R., Lansdorp, P. M., & van Vugt, M. A. T. M.

(2021). Sister chromatid exchanges induced by perturbed replication are formed independently of homologous recombination factors. *BioRxiv*, 2021.09.17.460736. https://doi.org/10.1101/2021.09.17.460736

Helfricht, A., Wiegant, W., Thijssen, P., Vertegaal, A., Luijsterburg, M., & van Attikum, H. (2013). Remodeling and spacing factor 1 (RSF1) deposits centromere proteins at DNA double-strand breaks to promote non-homologous end-joining. *Cell Cycle*, *12*(18), 3070–3082. https://doi.org/10.4161/cc.26033

Heller, R. C., & Marians, K. J. (2006). Replication fork reactivation downstream of a blocked nascent leading strand. *Nature*, *439*(7076), 557–562. https://doi.org/10.1038/nature04329

Herbert, A. D., Carr, A. M., & Hoffmann, E. (2014). FindFoci: A Focus Detection Algorithm with Automated Parameter Training That Closely Matches Human Assignments, Reduces Human Inconsistencies and Increases Speed of Analysis. *PLOS ONE*, *9*(12), e114749-. https://doi.org/10.1371/journal.pone.0114749

Heun, P., Erhardt, S., Blower, M. D., Weiss, S., Skora, A. D., & Karpen, G. H. (2006). Mislocalization of the Drosophila Centromere-Specific Histone CID Promotes Formation of Functional Ectopic Kinetochores. *Developmental Cell*, *10*(3), 303–315. https://doi.org/10.1016/j.devcel.2006.01.014

Hoffmann, S., Dumont, M., Barra, V., Ly, P., Nechemia-Arbely, Y., McMahon, M. A., Hervé, S., Cleveland, D. W., & Fachinetti, D. (2016). CENP-A Is Dispensable for Mitotic Centromere Function after Initial Centromere/Kinetochore Assembly. *Cell Reports*, *17*(9), 2394–2404. https://doi.org/10.1016/j.celrep.2016.10.084

Hoffmann, S., Izquierdo, H. M., Gamba, R., Chardon, F., Dumont, M., Keizer, V., Hervé, S., McNulty, S. M., Sullivan, B. A., Manel, N., & Fachinetti, D. (2020). A genetic memory initiates the epigenetic loop necessary to preserve centromere position. *The EMBO Journal*, *39*(20), e105505. https://doi.org/https://doi.org/10.15252/embj.2020105505

Hopkins, T. A., Ainsworth, W. B., Ellis, P. A., Donawho, C. K., DiGiammarino, E. L., Panchal, S. C., Abraham, V. C., Algire, M. A., Shi, Y., Olson, A. M., Johnson, E. F., Wilsbacher, J. L., & Maag, D. (2019). PARP1 Trapping by PARP Inhibitors Drives Cytotoxicity in Both Cancer Cells and Healthy Bone Marrow. *Molecular Cancer Research : MCR*, *17*(2), 409–419. https://doi.org/10.1158/1541-7786.MCR-18-0138

Howlett, N. G., Taniguchi, T., Olson, S., Cox, B., Waisfisz, Q., de Die-Smulders, C., Persky, N., Grompe, M., Joenje, H., Pals, G., Ikeda, H., Fox, E. A., & D'Andrea, A. D. (2002). Biallelic Inactivation of BRCA2 in Fanconi Anemia. *Science*, *297*(5581), 606–609. https://doi.org/10.1126/science.1073834

Howman, E. V, Fowler, K. J., Newson, A. J., Redward, S., MacDonald, A. C., Kalitsis, P., & Choo, K. H. A. (2000). Early disruption of centromeric chromatin organization in centromere protein A (Cenpa) null mice. *Proceedings of the National Academy of Sciences*, *97*(3), 1148–1153. https://doi.org/10.1073/pnas.97.3.1148

Hu, L., Zhao, C., Liu, M., Liu, S., Ye, J., Wang, K., Shi, J., Tian, W., & He, X. (2023). CENP-I directly targets centromeric DNA to support CENP-A deposition and

centromere maintenance. *Proceedings of the National Academy of Sciences*, *120*(11), e2219170120. https://doi.org/10.1073/pnas.2219170120

Huang, F., & Mazin, A. v. (2014). A Small Molecule Inhibitor of Human RAD51 Potentiates Breast Cancer Cell Killing by Therapeutic Agents in Mouse Xenografts. *PLOS ONE*, *9*(6), e100993-. https://doi.org/10.1371/journal.pone.0100993

Hudson, D. F., Fowler, K. J., Earle, E., Saffery, R., Kalitsis, P., Trowell, H., Hill, J., Wreford, N. G., de Kretser, D. M., Cancilla, M. R., Howman, E., Hii, L., Cutts, S. M., Irvine, D. V, & Choo, K. H. A. (1998). Centromere Protein B Null Mice are Mitotically and Meiotically Normal but Have Lower Body and Testis Weights. *Journal of Cell Biology*, *141*(2), 309–319. https://doi.org/10.1083/jcb.141.2.309

Ikeno, M., Masumoto, H., & Okazaki, T. (1994). Distribution of CENP-B boxes reflected in CREST centromere antigenic sites on long-range α-satellite DNA arrays of human chromosome 21. *Human Molecular Genetics*, *3*(8), 1245–1257. https://doi.org/10.1093/hmg/3.8.1245

Iliakis, G., Wang, Y., Guan, J., & Wang, H. (2003). DNA damage checkpoint control in cells exposed to ionizing radiation. *Oncogene*, *22*(37), 5834–5847. https://doi.org/10.1038/sj.onc.1206682

Ishikura, S., Nakabayashi, K., Nagai, M., Tsunoda, T., & Shirasawa, S. (2020). ZFAT binds to centromeres to control noncoding RNA transcription through the KAT2B–H4K8ac–BRD4 axis. *Nucleic Acids Research*, *48*(19), 10848–10866. https://doi.org/10.1093/nar/gkaa815

Ishikura, S., Yoshida, K., Hashimoto, S., Nakabayashi, K., Tsunoda, T., & Shirasawa, S. (2021). CENP-B promotes the centromeric localization of ZFAT to control transcription of noncoding RNA. *Journal of Biological Chemistry*, *297*(4). https://doi.org/10.1016/j.jbc.2021.101213

Jackson, & Bartek, J. (2009). The DNA-damage response in human biology and disease. *Nature*, *461*(7267), 1071–1078. https://doi.org/10.1038/nature08467

Jackson, M. S., See, C. G., Mulligan, L. M., & Lauffart, B. F. (1996). A 9.75-Mb Map across the Centromere of Human Chromosome 10. *Genomics*, *33*(2), 258–270. https://doi.org/https://doi.org/10.1006/geno.1996.0190

Jaco, I., Canela, A., Vera, E., & Blasco, M. A. (2008). Centromere mitotic recombination in mammalian cells . *Journal of Cell Biology*, *181*(6), 885–892. https://doi.org/10.1083/jcb.200803042

Jansen, L. E. T., Black, B. E., Foltz, D. R., & Cleveland, D. W. (2007). Propagation of centromeric chromatin requires exit from mitosis. *Journal of Cell Biology*, *176*(6), 795–805. https://doi.org/10.1083/jcb.200701066

Jensen, R. B., Carreira, A., & Kowalczykowski, S. C. (2010). Purified human BRCA2 stimulates RAD51-mediated recombination. *Nature*, *467*(7316), 678–683. https://doi.org/10.1038/nature09399

Jonkers, J., Meuwissen, R., van der Gulden, H., Peterse, H., van der Valk, M., & Berns, A. (2001). Synergistic tumor suppressor activity of BRCA2 and p53 in a conditional mouse model for breast cancer. *Nature Genetics*, *29*(4), 418–425. https://doi.org/10.1038/ng747

Jonstrup, A. T., Thomsen, T., Wang, Y., Knudsen, B. R., Koch, J., & Andersen, A. H. (2008). Hairpin structures formed by alpha satellite DNA of human centromeres are cleaved by human topoisomerase IIalpha. *Nucleic Acids Research*, *36*(19), 6165–6174. https://doi.org/10.1093/nar/gkn640

Jurga, M., Abugable, A. A., Goldman, A. S. H., & El-Khamisy, S. F. (2021). USP11 controls R-loops by regulating senataxin proteostasis. *Nature Communications*, *12*(1), 5156. https://doi.org/10.1038/s41467-021-25459-w

Jurkovicova, D., Neophytou, C. M., Gašparović, A. Č., & Gonçalves, A. C. (2022). DNA Damage Response in Cancer Therapy and Resistance: Challenges and Opportunities. *International Journal of Molecular Sciences*, *23*(23). https://doi.org/10.3390/ijms232314672

Kabeche, L., Nguyen, H. D., Buisson, R., & Zou, L. (2018). A mitosis-specific and R loop-driven ATR pathway promotes faithful chromosome segregation. *Science (New York, N.Y.)*, *359*(6371), 108–114. https://doi.org/10.1126/science.aan6490

Kang, Z., Fu, P., Alcivar, A. L., Fu, H., Redon, C., Foo, T. K., Zuo, Y., Ye, C., Baxley, R., Madireddy, A., Buisson, R., Bielinsky, A.-K., Zou, L., Shen, Z., Aladjem, M. I., & Xia, B. (2021). BRCA2 associates with MCM10 to suppress PRIMPOL-mediated repriming and single-stranded gap formation after DNA damage. *Nature Communications*, *12*(1), 5966. https://doi.org/10.1038/s41467-021-26227-6

Kapoor, M., Montes de Oca Luna, R., Liu, G., Lozano, G., Cummings, C., Mancini, M., Ouspenski, I., Brinkley, B. R., & May, G. S. (1998). The cenpB gene is not essential in mice. *Chromosoma*, *107*(8), 570–576. https://doi.org/10.1007/s004120050343

Kasinathan, S., & Henikoff, S. (2018). Non-B-Form DNA Is Enriched at Centromeres. *Molecular Biology and Evolution*, *35*(4), 949–962. https://doi.org/10.1093/molbev/msy010

Kato, Jiang, J., Zhou, B.-R., Rozendaal, M., Feng, H., Ghirlando, R., Xiao, T. S., Straight, A. F., & Bai, Y. (2013). A Conserved Mechanism for Centromeric Nucleosome Recognition by Centromere Protein CENP-C. *Science*, *340*(6136), 1110–1113. https://doi.org/10.1126/science.1235532

Kato, Sato, N., Hayama, S., Yamabuki, T., Ito, T., Miyamoto, M., Kondo, S., Nakamura, Y., & Daigo, Y. (2007). Activation of Holliday Junction–Recognizing Protein Involved in the Chromosomal Stability and Immortality of Cancer Cells. *Cancer Research*, *67*(18), 8544–8553. https://doi.org/10.1158/0008-5472.CAN-07-1307

Keen, B. A., Jozwiakowski, S. K., Bailey, L. J., Bianchi, J., & Doherty, A. J. (2014). Molecular dissection of the domain architecture and catalytic activities of human PrimPol. *Nucleic Acids Research*, *42*(9), 5830–5845. https://doi.org/10.1093/nar/gku214

Kellner, V., & Luke, B. (2020). Molecular and physiological consequences of faulty eukaryotic ribonucleotide excision repair. *The EMBO Journal*, *39*(3). https://doi.org/10.15252/embj.2019102309

Kile, A. C., Chavez, D. A., Bacal, J., Eldirany, S., Korzhnev, D. M., Bezsonova, I., Eichman, B. F., & Cimprich, K. A. (2015). HLTF's Ancient HIRAN Domain Binds 3′ DNA Ends to Drive Replication Fork Reversal. *Molecular Cell*, *58*(6), 1090–1100. https://doi.org/https://doi.org/10.1016/j.molcel.2015.05.013

Kim. (2022). Recent Progress on the Localization of PLK1 to the Kinetochore and Its Role in Mitosis. *Int. J. Mol. Sci.*, *23*(9), 5252.

Kim, & Burke, D. J. (2008). DNA damage activates the SAC in an ATM/ATR-dependent manner, independently of the kinetochore. *PLoS Genetics*, *4*(2), e1000015–e1000015. https://doi.org/10.1371/journal.pgen.1000015

King, G. A., Peterman, E. J. G., & Wuite, G. J. L. (2016). Unravelling the structural plasticity of stretched DNA under torsional constraint. *Nature Communications*, *7*(1), 11810. https://doi.org/10.1038/ncomms11810

Kinner, A., Wu, W., Staudt, C., & Iliakis, G. (2008). γ-H2AX in recognition and signaling of DNA double-strand breaks in the context of chromatin. *Nucleic Acids Research*, *36*(17), 5678–5694. https://doi.org/10.1093/nar/gkn550

Knutsen, T., Padilla-Nash, H. M., Wangsa, D., Barenboim-Stapleton, L., Camps, J., McNeil, N., Difilippantonio, M. J., & Ried, T. (2010). Definitive molecular cytogenetic characterization of 15 colorectal cancer cell lines. *Genes, Chromosomes and Cancer*, *49*(3), 204–223. https://doi.org/https://doi.org/10.1002/gcc.20730

Kolinjivadi, A. M., Sannino, V., de Antoni, A., Técher, H., Baldi, G., & Costanzo, V. (2017a). Moonlighting at replication forks – a new life for homologous recombination proteins BRCA1, BRCA2 and RAD51. *FEBS Letters*, *591*(8), 1083–1100. https://doi.org/https://doi.org/10.1002/1873-3468.12556

Kolinjivadi, A. M., Sannino, V., De Antoni, A., Zadorozhny, K., Kilkenny, M., Técher, H., Baldi, G., Shen, R., Ciccia, A., Pellegrini, L., Krejci, L., & Costanzo, V. (2017b). Smarcal1-Mediated Fork Reversal Triggers Mre11-Dependent Degradation of Nascent DNA in the Absence of Brca2 and Stable Rad51 Nucleofilaments. *Molecular Cell*, *67*(5), 867-881.e7. https://doi.org/10.1016/j.molcel.2017.07.001

Krokan, H., Wist, E., & Krokan, R. H. (1981). Aphidicolin inhibits DNA synthesis by DNA polymerase alpha and isolated nuclei by a similar mechanism. *Nucleic Acids Research*, *9*(18), 4709–4719. https://doi.org/10.1093/nar/9.18.4709

Kuo, W. L., Meyn, R. E., & Haidle, C. W. (1984). Neocarzinostatin-mediated DNA damage and repair in wild-type and repair-deficient Chinese hamster ovary cells. *Cancer Research*, *44*(5), 1748–1751.

Lai, X., Broderick, R., Bergoglio, V., Zimmer, J., Badie, S., Niedzwiedz, W., Hoffmann, J.-S., & Tarsounas, M. (2017). MUS81 nuclease activity is essential for replication stress tolerance and chromosome segregation in BRCA2-deficient cells. *Nature Communications*, *8*(1), 15983. https://doi.org/10.1038/ncomms15983

Lara-Gonzalez, P., Pines, J., & Desai, A. (2021). Spindle assembly checkpoint activation and silencing at kinetochores. *Seminars in Cell & Developmental*

Biology, *117*, 86–98. https://doi.org/https://doi.org/10.1016/j.semcdb.2021.06.009

Lawrimore, J., & Bloom, K. (2019). The regulation of chromosome segregation via centromere loops. *Critical Reviews in Biochemistry and Molecular Biology*, *54*(4), 352–370. https://doi.org/10.1080/10409238.2019.1670130

Le, H. P., Ma, X., Vaquero, J., Brinkmeyer, M., Guo, F., Heyer, W.-D., & Liu, J. (2020). DSS1 and ssDNA regulate oligomerization of BRCA2. *Nucleic Acids Research*. https://doi.org/10.1093/nar/gkaa555

Lee, M., Daniels, M. J., & Venkitaraman, A. R. (2004). Phosphorylation of BRCA2 by the Polo-like kinase Plk1 is regulated by DNA damage and mitotic progression. *Oncogene*, *23*(4), 865–872. https://doi.org/10.1038/sj.onc.1207223

Lekomtsev, S., Guizetti, J., Pozniakovsky, A., Gerlich, D. W., & Petronczki, M. (2010). Evidence that the tumor-suppressor protein BRCA2 does not regulate cytokinesis in human cells. *Journal of Cell Science*, *123*(9), 1395 LP – 1400. https://doi.org/10.1242/jcs.068015

Lemaçon, D., Jackson, J., Quinet, A., Brickner, J. R., Li, S., Yazinski, S., You, Z., Ira, G., Zou, L., Mosammaparast, N., & Vindigni, A. (2017). MRE11 and EXO1 nucleases degrade reversed forks and elicit MUS81-dependent fork rescue in BRCA2-deficient cells. *Nature Communications*, *8*(1), 860. https://doi.org/10.1038/s41467-017-01180-5

Li, Z., Liu, B., Jin, W., Wu, X., Zhou, M., Liu, V. Z., Goel, A., Shen, Z., Zheng, L., & Shen, B. (2018). hDNA2 nuclease/helicase promotes centromeric DNA replication and genome stability. *The EMBO Journal*, *37*(14), e96729. https://doi.org/https://doi.org/10.15252/embj.201796729

Liebman, S. W., Symington, L. S., & Petes, T. D. (1988). Mitotic recombination within the centromere of a yeast chromosome. *Science*, *241*(4869), 1074–1077. https://doi.org/10.1126/science.3137657

Lin, H.-R., Ting, N. S. Y., Qin, J., & Lee, W.-H. (2003). M Phase-specific Phosphorylation of BRCA2 by Polo-like Kinase 1 Correlates with the Dissociation of the BRCA2-P/CAF Complex. *Journal of Biological Chemistry* , *278*(38), 35979–35987. https://doi.org/10.1074/jbc.M210659200

Lindahl, T., & Barnes, D. E. (2000). Repair of Endogenous DNA Damage. *Cold Spring Harbor Symposia on Quantitative Biology*, *65*, 127–134. https://doi.org/10.1101/sqb.2000.65.127

Liu, Carvalho, C. M. B., Hastings, P. J., & Lupski, J. R. (2012). Mechanisms for recurrent and complex human genomic rearrangements. *Current Opinion in Genetics & Development*, *22*(3), 211–220. https://doi.org/https://doi.org/10.1016/j.gde.2012.02.012

Liu, Huang, F., Zhang, D., Ju, J., Wu, X.-B., Wang, Y., Wang, Y., Wu, Y., Nie, M., Li, Z., Ma, C., Chen, X., Zhou, J.-Y., Tan, R., Yang, B.-L., Zen, K., Zhang, C.-Y., Chen, Y.-G., & Zhao, Q. (2015). Heterochromatin Protein HP1γ Promotes Colorectal Cancer Progression and Is Regulated by miR-30a. *Cancer Research*, *75*(21), 4593–4604. https://doi.org/10.1158/0008-5472.CAN-14-3735

Liu, Y., Liu, Q., Su, H., Liu, K., Xiao, X., Li, W., Sun, Q., Birchler, J. A., & Han, F. (2021). Genome-wide mapping reveals R-loops associated with centromeric repeats in maize. *Genome Research*, *31*(8), 1409–1418. https://doi.org/10.1101/gr.275270.121

Liu, Yi, C., Zhang, Z., Su, H., Liu, C., Huang, Y., Li, W., Hu, X., Liu, C., Birchler, J. A., Liu, Y., & Han, F. (2023). Non–B-form DNA tends to form in centromeric regions and has undergone changes in polyploid oat subgenomes. *Proceedings of the National Academy of Sciences*, *120*(1), e2211683120. https://doi.org/10.1073/pnas.2211683120

Logsdon, G. A., Barrey, E. J., Bassett, E. A., DeNizio, J. E., Guo, L. Y., Panchenko, T., Dawicki-McKenna, J. M., Heun, P., & Black, B. E. (2015). Both tails and the centromere targeting domain of CENP-A are required for centromere establishment. *Journal of Cell Biology*, *208*(5), 521–531. https://doi.org/10.1083/jcb.201412011

Logsdon, G. A., Vollger, M. R., Hsieh, P., Mao, Y., Liskovykh, M. A., Koren, S., Nurk, S., Mercuri, L., Dishuck, P. C., Rhie, A., de Lima, L. G., Dvorkina, T., Porubsky, D., Harvey, W. T., Mikheenko, A., Bzikadze, A. V, Kremitzki, M., Graves-Lindsay, T. A., Jain, C., … Eichler, E. E. (2021). The structure, function and evolution of a complete human chromosome 8. *Nature*, *593*(7857), 101–107. https://doi.org/10.1038/s41586-021-03420-7

Lomonosov, M., Anand, S., Sangrithi, M., Davies, R., & Venkitaraman, A. R. (2003). Stabilization of stalled DNA replication forks by the BRCA2 breast cancer susceptibility protein. *Genes & Development*, *17*(24), 3017–3022. https://doi.org/10.1101/gad.279003

Lopes, M., Foiani, M., & Sogo, J. M. (2006). Multiple Mechanisms Control Chromosome Integrity after Replication Fork Uncoupling and Restart at Irreparable UV Lesions. *Molecular Cell*, *21*(1), 15–27. https://doi.org/10.1016/j.molcel.2005.11.015

Lujan, S. A., Williams, J. S., Clausen, A. R., Clark, A. B., & Kunkel, T. A. (2013). Ribonucleotides Are Signals for Mismatch Repair of Leading-Strand Replication Errors. *Molecular Cell*, *50*(3), 437–443. https://doi.org/10.1016/j.molcel.2013.03.017

Lukas, C., Savic, V., Bekker-Jensen, S., Doil, C., Neumann, B., Sølvhøj Pedersen, R., Grøfte, M., Chan, K. L., Hickson, I. D., Bartek, J., & Lukas, J. (2011). 53BP1 nuclear bodies form around DNA lesions generated by mitotic transmission of chromosomes under replication stress. *Nature Cell Biology*, *13*(3), 243–253. https://doi.org/10.1038/ncb2201

Macheret, M., Bhowmick, R., Sobkowiak, K., Padayachy, L., Mailler, J., Hickson, I. D., & Halazonetis, T. D. (2020). High-resolution mapping of mitotic DNA synthesis regions and common fragile sites in the human genome through direct sequencing. *Cell Research*, *30*(11), 997–1008. https://doi.org/10.1038/s41422-020-0358-x

Macheret, M., & Halazonetis, T. D. (2019). Monitoring early S-phase origin firing and replication fork movement by sequencing nascent DNA from synchronized cells. *Nature Protocols*, *14*(1), 51–67. https://doi.org/10.1038/s41596-018-0081-y

Macůrek, L., Lindqvist, A., Lim, D., Lampson, M. A., Klompmaker, R., Freire, R., Clouin, C., Taylor, S. S., Yaffe, M. B., & Medema, R. H. (2008). Polo-like kinase-1 is activated by aurora A to promote checkpoint recovery. *Nature*, *455*(7209), 119–123. https://doi.org/10.1038/nature07185

Maddox, P. S., Hyndman, F., Monen, J., Oegema, K., & Desai, A. (2007). Functional genomics identifies a Myb domain–containing protein family required for assembly of CENP-A chromatin. *Journal of Cell Biology*, *176*(6), 757–763. https://doi.org/10.1083/jcb.200701065

Magdalou, I., Lopez, B. S., Pasero, P., & Lambert, S. A. E. (2014). The causes of replication stress and their consequences on genome stability and cell fate. *Seminars in Cell & Developmental Biology*, *30*, 154–164. https://doi.org/https://doi.org/10.1016/j.semcdb.2014.04.035

Mah, L.-J., El-Osta, A., & Karagiannis, T. C. (2010). γH2AX: a sensitive molecular marker of DNA damage and repair. *Leukemia*, *24*(4), 679–686. https://doi.org/10.1038/leu.2010.6

Mahtani, M. M., & Willard, H. F. (1998). Physical and Genetic Mapping of the Human X Chromosome Centromere: Repression of Recombination. *Genome Research*, *8*(2), 100–110. https://doi.org/10.1101/gr.8.2.100

Mao, Z., Bozzella, M., Seluanov, A., & Gorbunova, V. (2008). DNA repair by nonhomologous end joining and homologous recombination during cell cycle in human cells. *Cell Cycle*, *7*(18), 2902–2906. https://doi.org/10.4161/cc.7.18.6679

Marescal, O., & Cheeseman, I. M. (2020). Cellular Mechanisms and Regulation of Quiescence. *Developmental Cell*, *55*(3), 259–271. https://doi.org/10.1016/j.devcel.2020.09.029

Marnef, A., & Legube, G. (2021). R-loops as Janus-faced modulators of DNA repair. *Nature Cell Biology*, *23*(4), 305–313. https://doi.org/10.1038/s41556-021-00663-4

Marshall, O. J., Chueh, A. C., Wong, L. H., & Choo, K. H. A. (2008). Neocentromeres: New Insights into Centromere Structure, Disease Development, and Karyotype Evolution. *The American Journal of Human Genetics*, *82*(2), 261–282. https://doi.org/10.1016/j.ajhg.2007.11.009

Marston, N. J., Richards, W. J., Hughes, D., Bertwistle, D., Marshall, C. J., & Ashworth, A. (1999). Interaction between the Product of the Breast Cancer Susceptibility Gene BRCA2 and DSS1, a Protein Functionally Conserved from Yeast to Mammals. *Molecular and Cellular Biology*, *19*(7), 4633–4642. https://doi.org/10.1128/MCB.19.7.4633

Martinez, J. S., Baldeyron, C., & Carreira, A. (2015). Molding BRCA2 function through its interacting partners. *Cell Cycle*, *14*(21), 3389–3395. https://doi.org/10.1080/15384101.2015.1093702

Martrat, G., Maxwell, C. A., Tominaga, E., Porta-de-la-Riva, M., Bonifaci, N., Gómez-Baldó, L., Bogliolo, M., Lázaro, C., Blanco, I., Brunet, J., Aguilar, H., Fernández-Rodríguez, J., Seal, S., Renwick, A., Rahman, N., Kühl, J., Neveling, K., Schindler, D., Ramírez, M. J., … Collaborators, G. S. (2011). Exploring the link

between MORF4L1 and risk of breast cancer. *Breast Cancer Research*, *13*(2), R40. https://doi.org/10.1186/bcr2862

Mason, J. M., Chan, Y.-L., Weichselbaum, R. W., & Bishop, D. K. (2019). Non-enzymatic roles of human RAD51 at stalled replication forks. *Nature Communications*, *10*(1), 4410. https://doi.org/10.1038/s41467-019-12297-0

Masumoto, H., Masukata, H., Muro, Y., Nozaki, N., & Okazaki, T. (1989). A human centromere antigen (CENP-B) interacts with a short specific sequence in alphoid DNA, a human centromeric satellite. *Journal of Cell Biology*, *109*(5), 1963–1973. https://doi.org/10.1083/jcb.109.5.1963

Mateos, S. (1996). Cell-cycle variation in DNA migration in pulsed-field gel electrophoresis. *International Journal of Radiation Biology*, *69*(6), 687–693. https://doi.org/10.1080/095530096145427

Mauffret, O., Amir-Aslani, A., Maroun, R. G., Monnot, M., Lescot, E., & Fermandjian, S. (1998). Comparative structural analysis by [1H, 31P]-NMR and restrained molecular dynamics of two DNA hairpins from a strong DNA topoisomerase II cleavage site. *Journal of Molecular Biology*, *283*(3), 643–655. https://doi.org/https://doi.org/10.1006/jmbi.1998.2095

Maya-Mendoza, A., Moudry, P., Merchut-Maya, J. M., Lee, M., Strauss, R., & Bartek, J. (2018). High speed of fork progression induces DNA replication stress and genomic instability. *Nature*, *559*(7713), 279–284. https://doi.org/10.1038/s41586-018-0261-5

Mayle, R., Campbell, I. M., Beck, C. R., Yu, Y., Wilson, M., Shaw, C. A., Bjergbaek, L., Lupski, J. R., & Ira, G. (2015). Mus81 and converging forks limit the mutagenicity of replication fork breakage. *Science*, *349*(6249), 742–747. https://doi.org/10.1126/science.aaa8391

McAllister, K. A., Bennett, L. M., Houle, C. D., Ward, T., Malphurs, J., Collins, N. K., Cachafeiro, C., Haseman, J., Goulding, E. H., Bunch, D., Eddy, E. M., Davis, B. J., & Wiseman, R. W. (2002). Cancer Susceptibility of Mice with a Homozygous Deletion in the COOH-Terminal Domain of the Brca2 Gene1. *Cancer Research*, *62*(4), 990–994.

McClintock, B. (1942). The Fusion of Broken Ends of Chromosomes Following Nuclear Fusion. *Proceedings of the National Academy of Sciences*, *28*(11), 458–463. https://doi.org/10.1073/pnas.28.11.458

McKinley, K. L., & Cheeseman, I. M. (2014). Polo-like Kinase 1 Licenses CENP-A Deposition at Centromeres. *Cell*, *158*(2), 397–411. https://doi.org/10.1016/j.cell.2014.06.016

McKinley, K. L., & Cheeseman, I. M. (2016). The molecular basis for centromere identity and function. *Nature Reviews Molecular Cell Biology*, *17*(1), 16–29. https://doi.org/10.1038/nrm.2015.5

McNulty, S. M., Sullivan, L. L., & Sullivan, B. A. (2017). Human Centromeres Produce Chromosome-Specific and Array-Specific Alpha Satellite Transcripts that Are Complexed with CENP-A and CENP-C. *Developmental Cell*, *42*(3), 226-240.e6. https://doi.org/10.1016/j.devcel.2017.07.001

Mendiburo, M. J., Padeken, J., Fülöp, S., Schepers, A., & Heun, P. (2011). Drosophila CENH3 Is Sufficient for Centromere Formation. *Science*, *334*(6056), 686–690. https://doi.org/10.1126/science.1206880

Menzel, T., Nähse-Kumpf, V., Kousholt, A. N., Klein, D. K., Lund-Andersen, C., Lees, M., Johansen, J. V., Syljuåsen, R. G., & Sørensen, C. S. (2011). A genetic screen identifies BRCA2 and PALB2 as key regulators of G2 checkpoint maintenance. *EMBO Reports*, *12*(7), 705–712. https://doi.org/https://doi.org/10.1038/embor.2011.99

Michelini, F., Pitchiaya, S., Vitelli, V., Sharma, S., Gioia, U., Pessina, F., Cabrini, M., Wang, Y., Capozzo, I., Iannelli, F., Matti, V., Francia, S., Shivashankar, G. V, Walter, N. G., & d'Adda di Fagagna, F. (2017). Damage-induced lncRNAs control the DNA damage response through interaction with DDRNAs at individual double-strand breaks. *Nature Cell Biology*, *19*(12), 1400–1411. https://doi.org/10.1038/ncb3643

Mijic, S., Zellweger, R., Chappidi, N., Berti, M., Jacobs, K., Mutreja, K., Ursich, S., Ray Chaudhuri, A., Nussenzweig, A., Janscak, P., & Lopes, M. (2017). Replication fork reversal triggers fork degradation in BRCA2-defective cells. *Nature Communications*, *8*(1), 859. https://doi.org/10.1038/s41467-017-01164-5

Mikhailov, A., Cole, R. W., & Rieder, C. L. (2002). DNA Damage during Mitosis in Human Cells Delays the Metaphase/Anaphase Transition via the Spindle-Assembly Checkpoint. *Current Biology*, *12*(21), 1797–1806. https://doi.org/https://doi.org/10.1016/S0960-9822(02)01226-5

Mimitou, E. P., & Symington, L. S. (2008). Sae2, Exo1 and Sgs1 collaborate in DNA double-strand break processing. *Nature*, *455*(7214), 770–774. https://doi.org/10.1038/nature07312

Min, J., Wright, W. E., & Shay, J. W. (2017). Alternative Lengthening of Telomeres Mediated by Mitotic DNA Synthesis Engages Break-Induced Replication Processes. *Molecular and Cellular Biology*, *37*(20), e00226-17. https://doi.org/10.1128/MCB.00226-17

Minchell, N. E., Keszthelyi, A., & Baxter, J. (2020). Cohesin Causes Replicative DNA Damage by Trapping DNA Topological Stress. *Molecular Cell*, *78*(4), 739-751.e8. https://doi.org/10.1016/j.molcel.2020.03.013

Minocherhomji, S., Ying, S., Bjerregaard, V. A., Bursomanno, S., Aleliunaite, A., Wu, W., Mankouri, H. W., Shen, H., Liu, Y., & Hickson, I. D. (2015). Replication stress activates DNA repair synthesis in mitosis. *Nature*, *528*(7581), 286–290. https://doi.org/10.1038/nature16139

Mitelman, F., Johansson, B., & Mertens, F. (2008). *Mitelman Database of Chromosome Aberrations in Cancer*. Https://Mitelmandatabase.Isb-Cgc.Org.

Mitra, S., Gómez-Raja, J., Larriba, G., Dubey, D. D., & Sanyal, K. (2014). Rad51–Rad52 Mediated Maintenance of Centromeric Chromatin in Candida albicans. *PLOS Genetics*, *10*(4), e1004344. https://doi.org/10.1371/journal.pgen.1004344

Miyabe, I., Mizuno, K., Keszthelyi, A., Daigaku, Y., Skouteri, M., Mohebi, S., Kunkel, T. A., Murray, J. M., & Carr, A. M. (2015). Polymerase δ replicates both strands

after homologous recombination–dependent fork restart. *Nature Structural & Molecular Biology*, *22*(11), 932–938. https://doi.org/10.1038/nsmb.3100

Mondal, G., Rowley, M., Guidugli, L., Wu, J., Pankratz, V. S., & Couch, F. J. (2012). BRCA2 localization to the midbody by filamin A regulates cep55 signaling and completion of cytokinesis. *Developmental Cell*, *23*(1), 137–152. https://doi.org/10.1016/j.devcel.2012.05.008

Moran, E. C., Liu, L., Zasadzinska, E., Kestner, C. A., Sarkeshik, A., DeHoyos, H., I, J. R. Y. I. I., Foltz, D., & Stukenberg, P. T. (2021). Mitotic R-loops direct Aurora B kinase to maintain centromeric cohesion. *BioRxiv*, 2021.01.14.426738. https://doi.org/10.1101/2021.01.14.426738

Moree, B., Meyer, C. B., Fuller, C. J., & Straight, A. F. (2011). CENP-C recruits M18BP1 to centromeres to promote CENP-A chromatin assembly. *Journal of Cell Biology*, *194*(6), 855–871. https://doi.org/10.1083/jcb.201106079

Moudry, P., Watanabe, K., Wolanin, K. M., Bartkova, J., Wassing, I. E., Watanabe, S., Strauss, R., Troelsgaard Pedersen, R., Oestergaard, V. H., Lisby, M., Andújar-Sánchez, M., Maya-Mendoza, A., Esashi, F., Lukas, J., & Bartek, J. (2016). TOPBP1 regulates RAD51 phosphorylation and chromatin loading and determines PARP inhibitor sensitivity. *The Journal of Cell Biology*, *212*(3), 281–288. https://doi.org/10.1083/jcb.201507042

Mourón, S., Rodriguez-Acebes, S., Martínez-Jiménez, M. I., García-Gómez, S., Chocrón, S., Blanco, L., & Méndez, J. (2013). Repriming of DNA synthesis at stalled replication forks by human PrimPol. *Nature Structural & Molecular Biology*, *20*(12), 1383–1389. https://doi.org/10.1038/nsmb.2719

Moynahan, M. E., Pierce, A. J., & Jasin, M. (2001). BRCA2 Is Required for Homology-Directed Repair of Chromosomal Breaks. *Molecular Cell*, *7*(2), 263–272. https://doi.org/10.1016/S1097-2765(01)00174-5

Müller, S., & Almouzni, G. (2017). Chromatin dynamics during the cell cycle at centromeres. *Nature Reviews Genetics*, *18*(3), 192–208. https://doi.org/10.1038/nrg.2016.157

Muro, Y., Masumoto, H., Yoda, K., Nozaki, N., Ohashi, M., & Okazaki, T. (1992). Centromere protein B assembles human centromeric alpha-satellite DNA at the 17-bp sequence, CENP-B box. *Journal of Cell Biology*, *116*(3), 585–596. https://doi.org/10.1083/jcb.116.3.585

Murphy, A. K., Fitzgerald, M., Ro, T., Kim, J. H., Rabinowitsch, A. I., Chowdhury, D., Schildkraut, C. L., & Borowiec, J. A. (2014). Phosphorylated RPA recruits PALB2 to stalled DNA replication forks to facilitate fork recovery. *Journal of Cell Biology*, *206*(4), 493–507. https://doi.org/10.1083/jcb.201404111

Naim, V., Wilhelm, T., Debatisse, M., & Rosselli, F. (2013). ERCC1 and MUS81–EME1 promote sister chromatid separation by processing late replication intermediates at common fragile sites during mitosis. *Nature Cell Biology*, *15*(8), 1008–1015. https://doi.org/10.1038/ncb2793

Nakamura, K., Okamoto, A., Katou, Y., Yadani, C., Shitanda, T., Kaweeteerawat, C., Takahashi, T. S., Itoh, T., Shirahige, K., Masukata, H., & Nakagawa, T. (2008). Rad51 suppresses gross chromosomal rearrangement at centromere in

Schizosaccharomyces pombe. *The EMBO Journal*, *27*(22), 3036–3046. https://doi.org/10.1038/emboj.2008.215

Nakamura, K., Saredi, G., Becker, J. R., Foster, B. M., Nguyen, N. V, Beyer, T. E., Cesa, L. C., Faull, P. A., Lukauskas, S., Frimurer, T., Chapman, J. R., Bartke, T., & Groth, A. (2019). H4K20me0 recognition by BRCA1–BARD1 directs homologous recombination to sister chromatids. *Nature Cell Biology*, *21*(3), 311–318. https://doi.org/10.1038/s41556-019-0282-9

Nascakova, Z., Boleslavska, B., Urban, V., Oravetzova, A., Vlachova, E., Janscak, P., & Dobrovolna, J. (2021). RAD51 Inhibition Induces R-Loop Formation in Early G1 Phase of the Cell Cycle. *International Journal of Molecular Sciences*, *22*(7), 3740. https://doi.org/10.3390/ijms22073740

Natsume, T., Kiyomitsu, T., Saga, Y., & Kanemaki, M. T. (2016). Rapid Protein Depletion in Human Cells by Auxin-Inducible Degron Tagging with Short Homology Donors. *Cell Reports*, *15*(1), 210–218. https://doi.org/10.1016/j.celrep.2016.03.001

Nechemia-Arbely, Y., Miga, K. H., Shoshani, O., Aslanian, A., McMahon, M. A., Lee, A. Y., Fachinetti, D., Yates, J. R., Ren, B., & Cleveland, D. W. (2019). DNA replication acts as an error correction mechanism to maintain centromere identity by restricting CENP-A to centromeres. *Nature Cell Biology*, *21*(6), 743–754. https://doi.org/10.1038/s41556-019-0331-4

Niikura, Y., Kitagawa, R., Ogi, H., Abdulle, R., Pagala, V., & Kitagawa, K. (2015). CENP-A K124 Ubiquitylation Is Required for CENP-A Deposition at the Centromere. *Developmental Cell*, *32*(5), 589–603. https://doi.org/10.1016/j.devcel.2015.01.024

Nikkilä, J., Parplys, A. C., Pylkäs, K., Bose, M., Huo, Y., Borgmann, K., Rapakko, K., Nieminen, P., Xia, B., Pospiech, H., & Winqvist, R. (2013). Heterozygous mutations in PALB2 cause DNA replication and damage response defects. *Nature Communications*, *4*, 2578. https://doi.org/10.1038/ncomms3578

Nimonkar, A. V, Özsoy, A. Z., Genschel, J., Modrich, P., & Kowalczykowski, S. C. (2008). Human exonuclease 1 and BLM helicase interact to resect DNA and initiate DNA repair. *Proceedings of the National Academy of Sciences*, *105*(44), 16906–16911. https://doi.org/10.1073/pnas.0809380105

Nitiss, J. L. (2009). DNA topoisomerase II and its growing repertoire of biological functions. *Nature Reviews Cancer*, *9*(5), 327–337. https://doi.org/10.1038/nrc2608

Nurk, S., Koren, S., Rhie, A., Rautiainen, M., Bzikadze, A. V, Mikheenko, A., Vollger, M. R., Altemose, N., Uralsky, L., Gershman, A., Aganezov, S., Hoyt, S. J., Diekhans, M., Logsdon, G. A., Alonge, M., Antonarakis, S. E., Borchers, M., Bouffard, G. G., Brooks, S. Y., … Phillippy, A. M. (2022). The complete sequence of a human genome. *Science*, *376*(6588), 44–53. https://doi.org/10.1126/science.abj6987

O'Donnell, L., Panier, S., Wildenhain, J., Tkach, J. M., Al-Hakim, A., Landry, M.-C., Escribano-Diaz, C., Szilard, R. K., Young, J. T. F., Munro, M., Canny, M. D., Kolas, N. K., Zhang, W., Harding, S. M., Ylanko, J., Mendez, M., Mullin, M., Sun, T., Habermann, B., … Durocher, D. (2010). The MMS22L-TONSL Complex

Mediates Recovery from Replication Stress and Homologous Recombination. *Molecular Cell*, *40*(4), 619–631. https://doi.org/10.1016/j.molcel.2010.10.024

Ohzeki, J., Larionov, V., Earnshaw, W. C., & Masumoto, H. (2015). Genetic and epigenetic regulation of centromeres: a look at HAC formation. *Chromosome Research*, *23*(1), 87–103. https://doi.org/10.1007/s10577-015-9470-z

Ohzeki, J., Nakano, M., Okada, T., & Masumoto, H. (2002). CENP-B box is required for de novo centromere chromatin assembly on human alphoid DNA. *Journal of Cell Biology*, *159*(5), 765–775. https://doi.org/10.1083/jcb.200207112

Ohzeki, J., Otake, K., & Masumoto, H. (2020). Human artificial chromosome: Chromatin assembly mechanisms and CENP-B. *Experimental Cell Research*, *389*(2), 111900. https://doi.org/https://doi.org/10.1016/j.yexcr.2020.111900

Okada, T., Ohzeki, J., Nakano, M., Yoda, K., Brinkley, W. R., Larionov, V., & Masumoto, H. (2007). CENP-B Controls Centromere Formation Depending on the Chromatin Context. *Cell*, *131*(7), 1287–1300. https://doi.org/10.1016/j.cell.2007.10.045

Oliver, A. W., Swift, S., Lord, C. J., Ashworth, A., & Pearl, L. H. (2009). Structural basis for recruitment of BRCA2 by PALB2. *EMBO Reports*, *10*(9), 990–996. https://doi.org/https://doi.org/10.1038/embor.2009.126

Onaka, A. T., Toyofuku, N., Inoue, T., Okita, A. K., Sagawa, M., Su, J., Shitanda, T., Matsuyama, R., Zafar, F., Takahashi, T. S., Masukata, H., & Nakagawa, T. (2016). Rad51 and Rad54 promote noncrossover recombination between centromere repeats on the same chromatid to prevent isochromosome formation. *Nucleic Acids Research*, *44*(22), 10744–10757. https://doi.org/10.1093/nar/gkw874

Orthwein, A., Noordermeer, S. M., Wilson, M. D., Landry, S., Enchev, R. I., Sherker, A., Munro, M., Pinder, J., Salsman, J., Dellaire, G., Xia, B., Peter, M., & Durocher, D. (2015). A mechanism for the suppression of homologous recombination in G1 cells. *Nature*, *528*(7582), 422–426. https://doi.org/10.1038/nature16142

Otake, K., Ohzeki, J., Shono, N., Kugou, K., Okazaki, K., Nagase, T., Yamakawa, H., Kouprina, N., Larionov, V., Kimura, H., Earnshaw, W. C., & Masumoto, H. (2020). CENP-B creates alternative epigenetic chromatin states permissive for CENP-A or heterochromatin assembly. *Journal of Cell Science*, *133*(15), jcs243303. https://doi.org/10.1242/jcs.243303

Palmer, D. K., O'Day, K., Wener, M. H., Andrews, B. S., & Margolis, R. L. (1987). A 17-kD centromere protein (CENP-A) copurifies with nucleosome core particles and with histones. *Journal of Cell Biology*, *104*(4), 805–815. https://doi.org/10.1083/jcb.104.4.805

Panzarino, N. J., Krais, J. J., Cong, K., Peng, M., Mosqueda, M., Nayak, S. U., Bond, S. M., Calvo, J. A., Doshi, M. B., Bere, M., Ou, J., Deng, B., Zhu, L. J., Johnson, N., & Cantor, S. B. (2021). Replication Gaps Underlie BRCA Deficiency and Therapy Response. *Cancer Research*, *81*(5), 1388–1397. https://doi.org/10.1158/0008-5472.CAN-20-1602

Park, S. H., Kang, N., Song, E., Wie, M., Lee, E. A., Hwang, S., Lee, D., Ra, J. S., Park, I. B., Park, J., Kang, S., Park, J. H., Hohng, S., Lee, K., & Myung, K. (2019). ATAD5 promotes replication restart by regulating RAD51 and PCNA in response to replication stress. *Nature Communications*, *10*(1), 5718. https://doi.org/10.1038/s41467-019-13667-4

Park, Singh, T. R., Nassar, N., Zhang, F., Freund, M., Hanenberg, H., Meetei, A. R., & Andreassen, P. R. (2014). Breast cancer-associated missense mutants of the PALB2 WD40 domain, which directly binds RAD51C, RAD51 and BRCA2, disrupt DNA repair. *Oncogene*, *33*(40), 4803–4812. https://doi.org/10.1038/onc.2013.421

Patel, K. J., Yu, V. P. C. C., Lee, H., Corcoran, A., Thistlethwaite, F. C., Evans, M. J., Colledge, W. H., Friedman, L. S., Ponder, B. A. J., & Venkitaraman, A. R. (1998). Involvement of Brca2 in DNA Repair. *Molecular Cell*, *1*(3), 347–357. https://doi.org/10.1016/S1097-2765(00)80035-0

Pećina-Šlaus, N., Kafka, A., Salamon, I., & Bukovac, A. (2020). Mismatch Repair Pathway, Genome Stability and Cancer. *Frontiers in Molecular Biosciences*, *7*. https://www.frontiersin.org/articles/10.3389/fmolb.2020.00122

Pedersen, R. T., Kruse, T., Nilsson, J., Oestergaard, V. H., & Lisby, M. (2015). TopBP1 is required at mitosis to reduce transmission of DNA damage to G1 daughter cells. *Journal of Cell Biology*, *210*(4), 565–582. https://doi.org/10.1083/jcb.201502107

Pellegrini, L., Yu, D. S., Lo, T., Anand, S., Lee, M., Blundell, T. L., & Venkitaraman, A. R. (2002). Insights into DNA recombination from the structure of a RAD51–BRCA2 complex. *Nature*, *420*(6913), 287–293. https://doi.org/10.1038/nature01230

Perez-Castro, A. V, Shamanski, F. L., Meneses, J. J., Lovato, T. L., Vogel, K. G., Moyzis, R. K., & Pedersen, R. (1998). Centromeric Protein B Null Mice Are Viable with No Apparent Abnormalities. *Developmental Biology*, *201*(2), 135–143. https://doi.org/https://doi.org/10.1006/dbio.1998.9005

Pesenti, M. E., Weir, J. R., & Musacchio, A. (2016). Progress in the structural and functional characterization of kinetochores. *Current Opinion in Structural Biology*, *37*, 152–163. https://doi.org/https://doi.org/10.1016/j.sbi.2016.03.003

Petermann, E., Orta, M. L., Issaeva, N., Schultz, N., & Helleday, T. (2010). Hydroxyurea-stalled replication forks become progressively inactivated and require two different RAD51-mediated pathways for restart and repair. *Molecular Cell*, *37*(4), 492–502. https://doi.org/10.1016/j.molcel.2010.01.021

Piazza, A., Bordelet, H., Dumont, A., Thierry, A., Savocco, J., Girard, F., & Koszul, R. (2021). Cohesin regulates homology search during recombinational DNA repair. *Nature Cell Biology*, *23*(11), 1176–1186. https://doi.org/10.1038/s41556-021-00783-x

Piberger, A. L., Bowry, A., Kelly, R. D. W., Walker, A. K., González-Acosta, D., Bailey, L. J., Doherty, A. J., Méndez, J., Morris, J. R., Bryant, H. E., & Petermann, E. (2020). PrimPol-dependent single-stranded gap formation mediates homologous recombination at bulky DNA adducts. *Nature Communications*, *11*(1), 5863. https://doi.org/10.1038/s41467-020-19570-7

Piwko, W., Mlejnkova, L. J., Mutreja, K., Ranjha, L., Stafa, D., Smirnov, A., Brodersen, M. M. L., Zellweger, R., Sturzenegger, A., Janscak, P., Lopes, M., Peter, M., & Cejka, P. (2016). The MMS22L–TONSL heterodimer directly promotes RAD51-dependent recombination upon replication stress. *The EMBO Journal*, *35*(23), 2584–2601. https://doi.org/https://doi.org/10.15252/embj.201593132

Pommier, Y., Nussenzweig, A., Takeda, S., & Austin, C. (2022). Human topoisomerases and their roles in genome stability and organization. *Nature Reviews Molecular Cell Biology*, *23*(6), 407–427. https://doi.org/10.1038/s41580-022-00452-3

Promonet, A., Padioleau, I., Liu, Y., Sanz, L., Biernacka, A., Schmitz, A.-L., Skrzypczak, M., Sarrazin, A., Mettling, C., Rowicka, M., Ginalski, K., Chedin, F., Chen, C.-L., Lin, Y.-L., & Pasero, P. (2020). Topoisomerase 1 prevents replication stress at R-loop-enriched transcription termination sites. *Nature Communications*, *11*(1), 3940. https://doi.org/10.1038/s41467-020-17858-2

Quénet, D., & Dalal, Y. (2014). A long non-coding RNA is required for targeting centromeric protein A to the human centromere. *ELife*, *3*, e26016. https://doi.org/10.7554/eLife.03254

Quinet, A., Tirman, S., Jackson, J., Šviković, S., Lemaçon, D., Carvajal-Maldonado, D., González-Acosta, D., Vessoni, A. T., Cybulla, E., Wood, M., Tavis, S., Batista, L. F. Z., Méndez, J., Sale, J. E., & Vindigni, A. (2020). PRIMPOL-Mediated Adaptive Response Suppresses Replication Fork Reversal in BRCA-Deficient Cells. *Molecular Cell*, *77*(3), 461-474.e9. https://doi.org/10.1016/j.molcel.2019.10.008

Racca, C., Britton, S., Hédouin, S., Francastel, C., Calsou, P., & Larminat, F. (2021). BRCA1 prevents R-loop-associated centromeric instability. *Cell Death & Disease*, *12*(10), 896. https://doi.org/10.1038/s41419-021-04189-3

Raghunandan, M., Chaudhury, I., Kelich, S. L., Hanenberg, H., & Sobeck, A. (2015). FANCD2, FANCJ and BRCA2 cooperate to promote replication fork recovery independently of the Fanconi Anemia core complex. *Cell Cycle*, *14*(3), 342–353. https://doi.org/10.4161/15384101.2014.987614

Rajan, J. V., Wang, M., Marquis, S. T., & Chodosh, L. A. (1996). Brca2 is coordinately regulated with Brca1 during proliferation and differentiation in mammary epithelial cells. *Proceedings of the National Academy of Sciences*, *93*(23), 13078–13083. https://doi.org/10.1073/pnas.93.23.13078

Ramamoorthy, M., Tadokoro, T., Rybanska, I., Ghosh, A. K., Wersto, R., May, A., Kulikowicz, T., Sykora, P., Croteau, D. L., & Bohr, V. A. (2012). RECQL5 cooperates with Topoisomerase II alpha in DNA decatenation and cell cycle progression. *Nucleic Acids Research*, *40*(4), 1621–1635. https://doi.org/10.1093/nar/gkr844

Rattner, J. B., Hendzel, M. J., Furbee, C. S., Muller, M. T., & Bazett-Jones, D. P. (1996). Topoisomerase II alpha is associated with the mammalian centromere in a cell cycle- and species-specific manner and is required for proper centromere/kinetochore structure. *Journal of Cell Biology*, *134*(5), 1097–1107. https://doi.org/10.1083/jcb.134.5.1097

Ray Chaudhuri, A., Callen, E., Ding, X., Gogola, E., Duarte, A. A., Lee, J.-E., Wong, N., Lafarga, V., Calvo, J. A., Panzarino, N. J., John, S., Day, A., Crespo, A. V., Shen, B., Starnes, L. M., Ruiter, J. R. de, Daniel, J. A., Konstantinopoulos, P. A., Cortez, D., … Nussenzweig, A. (2016). Replication fork stability confers chemoresistance in BRCA-deficient cells. *Nature*, *535*(7612), 382–387. https://doi.org/10.1038/nature18325

Ray Chaudhuri, A., Hashimoto, Y., Herrador, R., Neelsen, K. J., Fachinetti, D., Bermejo, R., Cocito, A., Costanzo, V., & Lopes, M. (2012). Topoisomerase I poisoning results in PARP-mediated replication fork reversal. *Nature Structural & Molecular Biology*, *19*(4), 417–423. https://doi.org/10.1038/nsmb.2258

Rebbeck, T. R., Mitra, N., Wan, F., Sinilnikova, O. M., Healey, S., McGuffog, L., Mazoyer, S., Chenevix-Trench, G., Easton, D. F., Antoniou, A. C., Nathanson, K. L., & Consortium, and the C. (2015). Association of Type and Location of BRCA1 and BRCA2 Mutations With Risk of Breast and Ovarian Cancer. *JAMA*, *313*(13), 1347–1361. https://doi.org/10.1001/jama.2014.5985

Redington, J., Deveryshetty, J., Kanikkannan, L., Miller, I., & Korolev, S. (2021). Structural Insight into the Mechanism of PALB2 Interaction with MRG15. *Genes*, *12*(12), 2002. https://doi.org/10.3390/genes12122002

Reid, S., Schindler, D., Hanenberg, H., Barker, K., Hanks, S., Kalb, R., Neveling, K., Kelly, P., Seal, S., Freund, M., Wurm, M., Batish, S. D., Lach, F. P., Yetgin, S., Neitzel, H., Ariffin, H., Tischkowitz, M., Mathew, C. G., Auerbach, A. D., & Rahman, N. (2007). Biallelic mutations in PALB2 cause Fanconi anemia subtype FA-N and predispose to childhood cancer. *Nature Genetics*, *39*(2), 162–164. https://doi.org/10.1038/ng1947

Ribeiro, S. A., Vagnarelli, P., Dong, Y., Hori, T., McEwen, B. F., Fukagawa, T., Flors, C., & Earnshaw, W. C. (2010). A super-resolution map of the vertebrate kinetochore. *Proceedings of the National Academy of Sciences*, *107*(23), 10484–10489. https://doi.org/10.1073/pnas.1002325107

Richardson, C., & Jasin, M. (2000). Frequent chromosomal translocations induced by DNA double-strand breaks. *Nature*, *405*(6787), 697–700. https://doi.org/10.1038/35015097

Rief, N., & Löbrich, M. (2002). Efficient Rejoining of Radiation-induced DNA Double-strand Breaks in Centromeric DNA of Human Cells. *Journal of Biological Chemistry*, *277*(23), 20572–20582. https://doi.org/10.1074/jbc.M200265200

Rošić, S., Köhler, F., & Erhardt, S. (2014). Repetitive centromeric satellite RNA is essential for kinetochore formation and cell division. *Journal of Cell Biology*, *207*(3), 335–349. https://doi.org/10.1083/jcb.201404097

Roy, R., Chun, J., & Powell, S. N. (2012). BRCA1 and BRCA2: different roles in a common pathway of genome protection. *Nature Reviews Cancer*, *12*(1), 68–78. https://doi.org/10.1038/nrc3181

Ruis, P., & Boulton, S. J. (2021). The end protection problem—an unexpected twist in the tail. *Genes & Development*, *35*(1–2), 1–21. https://doi.org/10.1101/gad.344044.120

Saayman, X., Graham, E., Nathan, W. J., Nussenzweig, A., & Esashi, F. (2023). Centromeres as universal hotspots of DNA breakage, driving RAD51-mediated recombination during quiescence. *Molecular Cell*. https://doi.org/10.1016/j.molcel.2023.01.004

Saredi, G., Huang, H., Hammond, C. M., Alabert, C., Bekker-Jensen, S., Forne, I., Reverón-Gómez, N., Foster, B. M., Mlejnkova, L., Bartke, T., Cejka, P., Mailand, N., Imhof, A., Patel, D. J., & Groth, A. (2016). H4K20me0 marks post-replicative chromatin and recruits the TONSL–MMS22L DNA repair complex. *Nature*, *534*(7609), 714–718. https://doi.org/10.1038/nature18312

Sarlos, K., Biebricher, A., Petermann, E. J. G., Wuite, G. J. L., & Hickson, I. D. (2017). Knotty Problems during Mitosis: Mechanistic Insight into the Processing of Ultrafine DNA Bridges in Anaphase. *Cold Spring Harbor Symposia on Quantitative Biology*, *82*, 187–195. https://doi.org/10.1101/sqb.2017.82.033647

Sawai, T., Sasano, O., Tsuji, T., Nanashima, A., Yasutake, T., Kusano, H., Tagawa, Y., Nakagoe, T., & Ayabe, H. (1997). Numerical aberration of chromosome 17 is correlated with multiple primary cancer in colorectal carcinoma. *Nihon Shokakibyo Gakkai zasshi = The Japanese journal of gastro-enterology*, *94*(7), 464–468.

Schlacher, K., Christ, N., Siaud, N., Egashira, A., Wu, H., & Jasin, M. (2011). Double-Strand Break Repair-Independent Role for BRCA2 in Blocking Stalled Replication Fork Degradation by MRE11. *Cell*, *145*(4), 529–542. https://doi.org/10.1016/j.cell.2011.03.041

Schlacher, K., Wu, H., & Jasin, M. (2012). A distinct replication fork protection pathway connects Fanconi anemia tumor suppressors to RAD51-BRCA1/2. *Cancer Cell*, *22*(1), 106–116. https://doi.org/10.1016/j.ccr.2012.05.015

Scully, R., Panday, A., Elango, R., & Willis, N. A. (2019). DNA double-strand break repair-pathway choice in somatic mammalian cells. *Nature Reviews Molecular Cell Biology*, *20*(11), 698–714. https://doi.org/10.1038/s41580-019-0152-0

Sessa, G., Gómez-González, B., Silva, S., Pérez-Calero, C., Beaurepere, R., Barroso, S., Martineau, S., Martin, C., Ehlén, Å., Martínez, J. S., Lombard, B., Loew, D., Vagner, S., Aguilera, A., & Carreira, A. (2021). BRCA2 promotes DNA-RNA hybrid resolution by DDX5 helicase at DNA breaks to facilitate their repair. *The EMBO Journal*, *40*(7), e106018. https://doi.org/https://doi.org/10.15252/embj.2020106018

Sfeir, A., & Symington, L. S. (2015). Microhomology-Mediated End Joining: A Back-up Survival Mechanism or Dedicated Pathway? *Trends in Biochemical Sciences*, *40*(11), 701–714. https://doi.org/10.1016/j.tibs.2015.08.006

Shahid, T., Soroka, J., Kong, E. H., Malivert, L., McIlwraith, M. J., Pape, T., West, S. C., & Zhang, X. (2014). Structure and mechanism of action of the BRCA2 breast cancer tumor suppressor. *Nature Structural & Molecular Biology*, *21*(11), 962–968. https://doi.org/10.1038/nsmb.2899

Sharan, S. K., Morimatsu, M., Albrecht, U., Lim, D.-S., Regel, E., Dinh, C., Sands, A., Eichele, G., Hasty, P., & Bradley, A. (1997). Embryonic lethality and radiation hypersensitivity mediated by Rad51 in mice lacking Brca2. *Nature*, *386*(6627), 804–810. https://doi.org/10.1038/386804a0

Shivji, M. K. K., Renaudin, X., Williams, Ç. H., & Venkitaraman, A. R. (2018). BRCA2 Regulates Transcription Elongation by RNA Polymerase II to Prevent R-Loop Accumulation. *Cell Reports*, *22*(4), 1031–1039. https://doi.org/10.1016/j.celrep.2017.12.086

Shuaib, M., Ouararhni, K., Dimitrov, S., & Hamiche, A. (2010). HJURP binds CENP-A via a highly conserved N-terminal domain and mediates its deposition at centromeres. *Proceedings of the National Academy of Sciences*, *107*(4), 1349–1354. https://doi.org/10.1073/pnas.0913709107

Silva, M. C. C., Bodor, D. L., Stellfox, M. E., Martins, N. M. C., Hochegger, H., Foltz, D. R., & Jansen, L. E. T. (2012). Cdk Activity Couples Epigenetic Centromere Inheritance to Cell Cycle Progression. *Developmental Cell*, *22*(1), 52–63. https://doi.org/10.1016/j.devcel.2011.10.014

Simhadri, S., Vincelli, G., Huo, Y., Misenko, S., Foo, T. K., Ahlskog, J., Sørensen, C. S., Oakley, G. G., Ganesan, S., Bunting, S. F., & Xia, B. (2019). PALB2 connects BRCA1 and BRCA2 in the G2/M checkpoint response. *Oncogene*, *38*(10), 1585–1596. https://doi.org/10.1038/s41388-018-0535-2

Sollier, J., Stork, C. T., García-Rubio, M. L., Paulsen, R. D., Aguilera, A., & Cimprich, K. A. (2014). Transcription-Coupled Nucleotide Excision Repair Factors Promote R-Loop-Induced Genome Instability. *Molecular Cell*, *56*(6), 777–785. https://doi.org/10.1016/j.molcel.2014.10.020

Sonoda, E., Sasaki, M. S., Buerstedde, J.-M., Bezzubova, O., Shinohara, A., Ogawa, H., Takata, M., Yamaguchi-Iwai, Y., & Takeda, S. (1998). Rad51-deficient vertebrate cells accumulate chromosomal breaks prior to cell death. *The EMBO Journal*, *17*(2), 598–608. https://doi.org/https://doi.org/10.1093/emboj/17.2.598

Sopik, V., Phelan, C., Cybulski, C., & Narod, S. A. (2015). BRCA1 and BRCA2 mutations and the risk for colorectal cancer. *Clinical Genetics*, *87*(5), 411–418. https://doi.org/10.1111/cge.12497

Sotiriou, S. K., Kamileri, I., Lugli, N., Evangelou, K., Da-Ré, C., Huber, F., Padayachy, L., Tardy, S., Nicati, N. L., Barriot, S., Ochs, F., Lukas, C., Lukas, J., Gorgoulis, V. G., Scapozza, L., & Halazonetis, T. D. (2016). Mammalian RAD52 Functions in Break-Induced Replication Repair of Collapsed DNA Replication Forks. *Molecular Cell*, *64*(6), 1127–1134. https://doi.org/10.1016/j.molcel.2016.10.038

Spain, B. H., Larson, C. J., Shihabuddin, L. S., Gage, F. H., & Verma, I. M. (1999). Truncated BRCA2 is cytoplasmic: Implications for cancer-linked mutations. *Proceedings of the National Academy of Sciences*, *96*(24), 13920–13925. https://doi.org/10.1073/pnas.96.24.13920

Spies, M., & Fishel, R. (2015). Mismatch Repair during Homologous and Homeologous Recombination. *Cold Spring Harbor Perspectives in Biology*, *7*(3). https://doi.org/10.1101/cshperspect.a022657

Sriramachandran, A. M., Petrosino, G., Méndez-Lago, M., Schäfer, A. J., Batista-Nascimento, L. S., Zilio, N., & Ulrich, H. D. (2020). Genome-wide Nucleotide-Resolution Mapping of DNA Replication Patterns, Single-Strand Breaks, and Lesions by GLOE-Seq. *Molecular Cell*, *78*(5), 975-985.e7. https://doi.org/10.1016/j.molcel.2020.03.027

Stark, J. M., Hu, P., Pierce, A. J., Moynahan, M. E., Ellis, N., & Jasin, M. (2002). ATP hydrolysis by mammalian RAD51 has a key role during homology-directed DNA repair. *The Journal of Biological Chemistry*, *277*(23), 20185–20194. https://doi.org/10.1074/jbc.M112132200

Stark, J. M., & Jasin, M. (2003). Extensive Loss of Heterozygosity Is Suppressed during Homologous Repair of Chromosomal Breaks. *Molecular and Cellular Biology*, *23*, 733–743.

Stiff, T., O'Driscoll, M., Rief, N., Iwabuchi, K., Löbrich, M., & Jeggo, P. A. (2004). ATM and DNA-PK Function Redundantly to Phosphorylate H2AX after Exposure to Ionizing Radiation. *Cancer Research*, *64*(7), 2390–2396. https://doi.org/10.1158/0008-5472.CAN-03-3207

Subramanyam, S., Ismail, M., Bhattacharya, I., & Spies, M. (2016). Tyrosine phosphorylation stimulates activity of human RAD51 recombinase through altered nucleoprotein filament dynamics. *Proceedings of the National Academy of Sciences*, *113*(41), E6045–E6054. https://doi.org/10.1073/pnas.1604807113

Sullivan, Hechenberger, M., & Masri, K. (1994). Human CENP-A contains a histone H3 related histone fold domain that is required for targeting to the centromere. *Journal of Cell Biology*, *127*(3), 581–592. https://doi.org/10.1083/jcb.127.3.581

Sullivan, & Karpen, G. H. (2004). Centromeric chromatin exhibits a histone modification pattern that is distinct from both euchromatin and heterochromatin. *Nature Structural & Molecular Biology*, *11*(11), 1076–1083. https://doi.org/10.1038/nsmb845

Sumner, A. T. (1996). The distribution of topoisomerase II on mammalian chromosomes. *Chromosome Research*, *4*(1), 5–14. https://doi.org/10.1007/BF02254938

Suzuki, N., Nakano, M., Nozaki, N., Egashira, S., Okazaki, T., & Masumoto, H. (2004). CENP-B Interacts with CENP-C Domains Containing Mif2 Regions Responsible for Centromere Localization. *Journal of Biological Chemistry*, *279*(7), 5934–5946. https://doi.org/10.1074/jbc.M306477200

Swartz, S. Z., McKay, L. S., Su, K.-C., Bury, L., Padeganeh, A., Maddox, P. S., Knouse, K. A., & Cheeseman, I. M. (2019). Quiescent Cells Actively Replenish CENP-A Nucleosomes to Maintain Centromere Identity and Proliferative Potential. *Developmental Cell*, *51*(1), 35-48.e7. https://doi.org/10.1016/j.devcel.2019.07.016

Sy, Huen, M. S. Y., & Chen, J. (2009a). MRG15 Is a Novel PALB2-interacting Factor Involved in Homologous Recombination. *Journal of Biological Chemistry* , *284*(32), 21127–21131. https://doi.org/10.1074/jbc.C109.023937

Sy, Huen, M. S. Y., & Chen, J. (2009b). PALB2 is an integral component of the BRCA complex required for homologous recombination repair. *Proceedings of the National Academy of Sciences*, *106*(17), 7155–7160. https://doi.org/10.1073/pnas.0811159106

Symington, L. S. (2002). Role of RAD52 Epistasis Group Genes in Homologous Recombination and Double-Strand Break Repair. *Microbiology and Molecular*

Biology Reviews, *66*(4), 630–670. https://doi.org/10.1128/MMBR.66.4.630-670.2002

Taglialatela, A., Alvarez, S., Leuzzi, G., Sannino, V., Ranjha, L., Huang, J.-W., Madubata, C., Anand, R., Levy, B., Rabadan, R., Cejka, P., Costanzo, V., & Ciccia, A. (2017). Restoration of Replication Fork Stability in BRCA1- and BRCA2-Deficient Cells by Inactivation of SNF2-Family Fork Remodelers. *Molecular Cell*, *68*(2), 414-430.e8. https://doi.org/10.1016/j.molcel.2017.09.036

Takaoka, M., Saito, H., Takenaka, K., Miki, Y., & Nakanishi, A. (2014). BRCA2 Phosphorylated by PLK1 Moves to the Midbody to Regulate Cytokinesis Mediated by Nonmuscle Myosin IIC. *Cancer Research*, *74*(5), 1518 LP – 1528. https://doi.org/10.1158/0008-5472.CAN-13-0504

Takizawa, Y., Ho, C.-H., Tachiwana, H., Matsunami, H., Kobayashi, W., Suzuki, M., Arimura, Y., Hori, T., Fukagawa, T., Ohi, M. D., Wolf, M., & Kurumizaka, H. (2020). Cryo-EM Structures of Centromeric Tri-nucleosomes Containing a Central CENP-A Nucleosome. *Structure*, *28*(1), 44-53.e4. https://doi.org/10.1016/j.str.2019.10.016

Talbert, P. B., & Henikoff, S. (2010). Centromeres convert but don't cross. *PLoS Biology*, *8*(3), e1000326–e1000326. https://doi.org/10.1371/journal.pbio.1000326

Tan, S. L. W., Chadha, S., Liu, Y., Gabasova, E., Perera, D., Ahmed, K., Constantinou, S., Renaudin, X., Lee, M., Aebersold, R., & Venkitaraman, A. R. (2017). A Class of Environmental and Endogenous Toxins Induces BRCA2 Haploinsufficiency and Genome Instability. *Cell*, *169*(6), 1105-1118.e15. https://doi.org/10.1016/j.cell.2017.05.010

Tan-Wong, S. M., & Proudfoot, N. J. (2013). Rad51, friend or foe? *ELife*, *2*, e00914. https://doi.org/10.7554/eLife.00914

Thakur, J., Packiaraj, J., & Henikoff, S. (2021). Sequence, Chromatin and Evolution of Satellite DNA. *International Journal of Molecular Sciences*, *22*(9), 4309. https://doi.org/10.3390/ijms22094309

Tinline-Purvis, H., Savory, A. P., Cullen, J. K., Davé, A., Moss, J., Bridge, W. L., Marguerat, S., Bähler, J., Ragoussis, J., Mott, R., A Walker, C., & Humphrey, T. C. (2009). Failed gene conversion leads to extensive end processing and chromosomal rearrangements in fission yeast. *The EMBO Journal*, *28*(21), 3400–3412. https://doi.org/https://doi.org/10.1038/emboj.2009.265

Tirman, S., Quinet, A., Wood, M., Meroni, A., Cybulla, E., Jackson, J., Pegoraro, S., Simoneau, A., Zou, L., & Vindigni, A. (2021). Temporally distinct post-replicative repair mechanisms fill PRIMPOL-dependent ssDNA gaps in human cells. *Molecular Cell*, *81*(19), 4026-4040.e8. https://doi.org/https://doi.org/10.1016/j.molcel.2021.09.013

Tischkowitz, M., & Xia, B. (2010). PALB2/FANCN: Recombining Cancer and Fanconi Anemia. *Cancer Research*, *70*(19), 7353–7359. https://doi.org/10.1158/0008-5472.CAN-10-1012

Tiwari, A., Addis Jones, O., & Chan, K.-L. (2018). 53BP1 can limit sister-chromatid rupture and rearrangements driven by a distinct ultrafine DNA bridging-breakage

process. *Nature Communications*, *9*(1), 677. https://doi.org/10.1038/s41467-018-03098-y

Tombline, G., & Fishel, R. (2002). Biochemical Characterization of the Human RAD51 Protein: I. ATP HYDROLYSIS. *Journal of Biological Chemistry*, *277*(17), 14417–14425. https://doi.org/10.1074/jbc.M109915200

Tounekti, O., Kenani, A., Foray, N., Orlowski, S., & Mir, L. M. (2001). The ratio of single- to double-strand DNA breaks and their absolute values determine cell death pathway. *British Journal of Cancer*, *84*(9), 1272–1279. https://doi.org/10.1054/bjoc.2001.1786

Trier, I., Black, E. M., Joo, Y. K., & Kabeche, L. (2023). ATR protects centromere identity by promoting DAXX association with PML nuclear bodies. *Cell Reports*, *42*(5). https://doi.org/10.1016/j.celrep.2023.112495

Truong, L. N., Li, Y., Shi, L. Z., Hwang, P. Y.-H., He, J., Wang, H., Razavian, N., Berns, M. W., & Wu, X. (2013). Microhomology-mediated End Joining and Homologous Recombination share the initial end resection step to repair DNA double-strand breaks in mammalian cells. *Proceedings of the National Academy of Sciences*, *110*(19), 7720–7725. https://doi.org/10.1073/pnas.1213431110

Tsuzuki, T., Fujii, Y., Sakumi, K., Tominaga, Y., Nakao, K., Sekiguchi, M., Matsushiro, A., & Yoshimura, Y. (1996). Targeted disruption of the Rad51 gene leads to lethality in embryonic mice. *Proceedings of the National Academy of Sciences*, *93*(13), 6236–6240. https://doi.org/10.1073/pnas.93.13.6236

Tubbs, A., & Nussenzweig, A. (2017). Endogenous DNA Damage as a Source of Genomic Instability in Cancer. *Cell*, *168*(4), 644–656. https://doi.org/10.1016/j.cell.2017.01.002

Tuduri, S., Crabbé, L., Conti, C., Tourrière, H., Holtgreve-Grez, H., Jauch, A., Pantesco, V., De Vos, J., Thomas, A., Theillet, C., Pommier, Y., Tazi, J., Coquelle, A., & Pasero, P. (2009). Topoisomerase I suppresses genomic instability by preventing interference between replication and transcription. *Nature Cell Biology*, *11*(11), 1315–1324. https://doi.org/10.1038/ncb1984

Tutt, A., Bertwistle, D., Valentine, J., Gabriel, A., Swift, S., Ross, G., Griffin, C., Thacker, J., & Ashworth, A. (2001). Mutation in Brca2 stimulates error-prone homology-directed repair of DNA double-strand breaks occurring between repeated sequences. *The EMBO Journal*, *20*(17), 4704–4716. https://doi.org/https://doi.org/10.1093/emboj/20.17.4704

Uziel, T., Lerenthal, Y., Moyal, L., Andegeko, Y., Mittelman, L., & Shiloh, Y. (2003). Requirement of the MRN complex for ATM activation by DNA damage. *The EMBO Journal*, *22*(20), 5612–5621. https://doi.org/https://doi.org/10.1093/emboj/cdg541

Van Hooser, A. A., Ouspenski, I. I., Gregson, H. C., Starr, D. A., Yen, T. J., Goldberg, M. L., Yokomori, K., Earnshaw, W. C., Sullivan, K. F., & Brinkley, B. R. (2001). Specification of kinetochore-forming chromatin by the histone H3 variant CENP-A. *Journal of Cell Science*, *114*(19), 3529–3542. https://doi.org/10.1242/jcs.114.19.3529

van Vugt, M. A. T. M., Brás, A., & Medema, R. H. (2004). Polo-like Kinase-1 Controls Recovery from a G2 DNA Damage-Induced Arrest in Mammalian Cells. *Molecular Cell*, *15*(5), 799–811. https://doi.org/https://doi.org/10.1016/j.molcel.2004.07.015

Vilenchik, M. M., & Knudson, A. G. (2003). Endogenous DNA double-strand breaks: Production, fidelity of repair, and induction of cancer. *Proceedings of the National Academy of Sciences*, *100*(22), 12871–12876. https://doi.org/10.1073/pnas.2135498100

Vincenten, N., Kuhl, L.-M., Lam, I., Oke, A., Kerr, A. R. W., Hochwagen, A., Fung, J., Keeney, S., Vader, G., & Marston, A. L. (2015). The kinetochore prevents centromere-proximal crossover recombination during meiosis. *ELife*, *4*, e10850. https://doi.org/10.7554/eLife.10850

Voullaire, L. E., Slater, H. R., Petrovic, V., & Choo, K. H. (1993). A functional marker centromere with no detectable alpha-satellite, satellite III, or CENP-B protein: activation of a latent centromere? *American Journal of Human Genetics*, *52*(6), 1153–1163.

Vriend, L. E. M., & Krawczyk, P. M. (2017). Nick-initiated homologous recombination: Protecting the genome, one strand at a time. *DNA Repair*, *50*, 1–13. https://doi.org/https://doi.org/10.1016/j.dnarep.2016.12.005

Vujanovic, M., Krietsch, J., Raso, M. C., Terraneo, N., Zellweger, R., Schmid, J. A., Taglialatela, A., Huang, J.-W., Holland, C. L., Zwicky, K., Herrador, R., Jacobs, H., Cortez, D., Ciccia, A., Penengo, L., & Lopes, M. (2017). Replication Fork Slowing and Reversal upon DNA Damage Require PCNA Polyubiquitination and ZRANB3 DNA Translocase Activity. *Molecular Cell*, *67*(5), 882-890.e5. https://doi.org/10.1016/j.molcel.2017.08.010

Wang, Kim, T., Wagner, J. E., Conti, B. A., Lach, F. P., Huang, A. L., Molina, H., Sanborn, E. M., Zierhut, H., Cornes, B. K., Abhyankar, A., Sougnez, C., Gabriel, S. B., Auerbach, A. D., Kowalczykowski, S. C., & Smogorzewska, A. (2015). A Dominant Mutation in Human RAD51 Reveals Its Function in DNA Interstrand Crosslink Repair Independent of Homologous Recombination. *Molecular Cell*, *59*(3), 478–490. https://doi.org/10.1016/j.molcel.2015.07.009

Wang, Liu, X., Dou, Z., Chen, L., Jiang, H., Fu, C., Fu, G., Liu, D., Zhang, J., Zhu, T., Fang, J., Zang, J., Cheng, J., Teng, M., Ding, X., & Yao, X. (2014). Mitotic Regulator Mis18b Interacts with and Specifies the Centromeric Assembly of Molecular Chaperone Holliday Junction Recognition Protein (HJURP). *Journal of Biological Chemistry*, *289*(12), 8326–8336. https://doi.org/10.1074/jbc.M113.529958

Wang, Ma, B., Liu, X., Gao, G., Che, Z., Fan, M., Meng, S., Zhao, X., Sugimura, R., Cao, H., Zhou, Z., Xie, J., Lin, C., & Luo, Z. (2022). ZFP281-BRCA2 prevents R-loop accumulation during DNA replication. *Nature Communications*, *13*(1), 3493. https://doi.org/10.1038/s41467-022-31211-9

Wang, Mayer, B., Stemmann, O., & Nigg, E. A. (2010). Centromere DNA decatenation depends on cohesin removal and is required for mammalian cell division. *Journal of Cell Science*, *123*(5), 806–813. https://doi.org/10.1242/jcs.058255

Wang, Schwarzbraun, T., Speicher, M. R., & Nigg, E. A. (2008). Persistence of DNA threads in human anaphase cells suggests late completion of sister chromatid decatenation. *Chromosoma*, *117*(2), 123–135. https://doi.org/10.1007/s00412-007-0131-7

Ward, I. M., & Chen, J. (2001). Histone H2AX Is Phosphorylated in an ATR-dependent Manner in Response to Replicational Stress. *Journal of Biological Chemistry*, *276*(51), 47759–47762. https://doi.org/10.1074/jbc.C100569200

Waskom, M. (2021). seaborn: statistical data visualization. *Journal of Open Source Software*, *6*(60), 3021. https://doi.org/10.21105/joss.03021

Wassing, I. E., & Esashi, F. (2021). RAD51: Beyond the break. *Seminars in Cell & Developmental Biology*, *113*, 38–46. https://doi.org/https://doi.org/10.1016/j.semcdb.2020.08.010

Wassing, I. E., Graham, E., Saayman, X., Rampazzo, L., Ralf, C., Bassett, A., & Esashi, F. (2021). The RAD51 recombinase protects mitotic chromatin in human cells. *Nature Communications*, *12*(1), 5380. https://doi.org/10.1038/s41467-021-25643-y

Waszak, S. M., Northcott, P. A., Buchhalter, I., Robinson, G. W., Sutter, C., Groebner, S., Grund, K. B., Brugières, L., Jones, D. T. W., Pajtler, K. W., Morrissy, A. S., Kool, M., Sturm, D., Chavez, L., Ernst, A., Brabetz, S., Hain, M., Zichner, T., Segura-Wang, M., … Pfister, S. M. (2018). Spectrum and prevalence of genetic predisposition in medulloblastoma: a retrospective genetic study and prospective validation in a clinical trial cohort. *The Lancet Oncology*, *19*(6), 785–798. https://doi.org/10.1016/S1470-2045(18)30242-0

Williams, Lujan, S. A., & Kunkel, T. A. (2016). Processing ribonucleotides incorporated during eukaryotic DNA replication. *Nature Reviews Molecular Cell Biology*, *17*(6), 350–363. https://doi.org/10.1038/nrm.2016.37

Williams, Wilson, J. B., Clark, A. P., Mitson-Salazar, A. N., Bale, A. E., Jones, N. J., & Kupfer, G. M. (2010). Functional and Physical Interaction Between the Mismatch Repair and the FA-BRCA Pathways. *Blood*, *116*(21), 3370–3370. https://doi.org/10.1182/blood.V116.21.3370.3370

Wong, A. K. C., Pero, R., Ormonde, P. A., Tavtigian, S. V, & Bartel, P. L. (1997). RAD51 Interacts with the Evolutionarily Conserved BRC Motifs in the Human Breast Cancer Susceptibility Gene brca2. *Journal of Biological Chemistry* , *272*(51), 31941–31944. https://doi.org/10.1074/jbc.272.51.31941

Wooster, R., Bignell, G., Lancaster, J., Swift, S., Seal, S., Mangion, J., Collins, N., Gregory, S., Gumbs, C., Micklem, G., Barfoot, R., Hamoudi, R., Patel, S., Rices, C., Biggs, P., Hashim, Y., Smith, A., Connor, F., Arason, A., … Stratton, M. R. (1995). Identification of the breast cancer susceptibility gene BRCA2. *Nature*, *378*(6559), 789–792. https://doi.org/10.1038/378789a0

Wu, S., Zhou, J., Zhang, K., Chen, H., Luo, M., Lu, Y., Sun, Y., & Chen, Y. (2020). Molecular Mechanisms of PALB2 Function and Its Role in Breast Cancer Management. *Frontiers in Oncology*, *10*. https://www.frontiersin.org/articles/10.3389/fonc.2020.00301

Wyatt, H. D. M., Sarbajna, S., Matos, J., & West, S. C. (2013). Coordinated Actions of SLX1-SLX4 and MUS81-EME1 for Holliday Junction Resolution in Human Cells. *Molecular Cell*, *52*(2), 234–247. https://doi.org/10.1016/j.molcel.2013.08.035

Xia, B., Dorsman, J. C., Ameziane, N., de Vries, Y., Rooimans, M. A., Sheng, Q., Pals, G., Errami, A., Gluckman, E., Llera, J., Wang, W., Livingston, D. M., Joenje, H., & de Winter, J. P. (2007). Fanconi anemia is associated with a defect in the BRCA2 partner PALB2. *Nature Genetics*, *39*(2), 159–161. https://doi.org/10.1038/ng1942

Xia, B., Sheng, Q., Nakanishi, K., Ohashi, A., Wu, J., Christ, N., Liu, X., Jasin, M., Couch, F. J., & Livingston, D. M. (2006). Control of BRCA2 Cellular and Clinical Functions by a Nuclear Partner, PALB2. *Molecular Cell*, *22*(6), 719–729. https://doi.org/10.1016/j.molcel.2006.05.022

Xu, J., Zhao, L., Xu, Y., Zhao, W., Sung, P., & Wang, H.-W. (2017). Cryo-EM structures of human RAD51 recombinase filaments during catalysis of DNA-strand exchange. *Nature Structural & Molecular Biology*, *24*(1), 40–46. https://doi.org/10.1038/nsmb.3336

Yamagishi, A., Matsumoto, D., Kato, Y., Honda, Y., Morikawa, M., Iwata, F., Kobayashi, T., & Nakamura, C. (2019). Direct Delivery of Cas9-sgRNA Ribonucleoproteins into Cells Using a Nanoneedle Array. *Applied Sciences*, *9*(5), 965. https://doi.org/10.3390/app9050965

Yang, H., Jeffrey, P. D., Miller, J., Kinnucan, E., Sun, Y., Thomä, N. H., Zheng, N., Chen, P.-L., Lee, W.-H., & Pavletich, N. P. (2002). BRCA2 Function in DNA Binding and Recombination from a BRCA2-DSS1-ssDNA Structure. *Science*, *297*(5588), 1837–1848. https://doi.org/10.1126/science.297.5588.1837

Yano, K., Morotomi, K., Saito, H., Kato, M., Matsuo, F., & Miki, Y. (2000). Nuclear Localization Signals of the BRCA2 Protein. *Biochemical and Biophysical Research Communications*, *270*(1), 171–175. https://doi.org/https://doi.org/10.1006/bbrc.2000.2392

Yata, K., Bleuyard, J.-Y., Nakato, R., Ralf, C., Katou, Y., Schwab, R. A., Niedzwiedz, W., Shirahige, K., & Esashi, F. (2014). BRCA2 coordinates the activities of cell-cycle kinases to promote genome stability. *Cell Reports*, *7*(5), 1547–1559. https://doi.org/10.1016/j.celrep.2014.04.023

Yata, K., Lloyd, J., Maslen, S., Bleuyard, J.-Y., Skehel, M., Smerdon, S. J., & Esashi, F. (2012). Plk1 and CK2 Act in Concert to Regulate Rad51 during DNA Double Strand Break Repair. *Molecular Cell*, *45*(3), 371–383. https://doi.org/https://doi.org/10.1016/j.molcel.2011.12.028

Yesbolatova, A., Saito, Y., Kitamoto, N., Makino-Itou, H., Ajima, R., Nakano, R., Nakaoka, H., Fukui, K., Gamo, K., Tominari, Y., Takeuchi, H., Saga, Y., Hayashi, K., & Kanemaki, M. T. (2020). The auxin-inducible degron 2 technology provides sharp degradation control in yeast, mammalian cells, and mice. *Nature Communications*, *11*(1), 5701. https://doi.org/10.1038/s41467-020-19532-z

Yilmaz, D., Furst, A., Meaburn, K., Lezaja, A., Wen, Y., Altmeyer, M., Reina-San-Martin, B., & Soutoglou, E. (2021). Activation of homologous recombination in

G1 preserves centromeric integrity. *Nature*, *600*(7890), 748–753. https://doi.org/10.1038/s41586-021-04200-z

Yu, V. P. C. C., Koehler, M., Steinlein, C., Schmid, M., Hanakahi, L. A., van Gool, A. J., West, S. C., & Venkitaraman, A. R. (2000). Gross chromosomal rearrangements and genetic exchange between nonhomologous chromosomes following BRCA2 inactivation. *Genes & Development*, *14*(11), 1400–1406. https://doi.org/10.1101/gad.14.11.1400

Yuan, S.-S. F., Lee, S.-Y., Chen, G., Song, M., Tomlinson, G. E., & Lee, E. Y.-H. P. (1999). BRCA2 Is Required for Ionizing Radiation-induced Assembly of Rad51 Complex in Vivo1. *Cancer Research*, *59*(15), 3547–3551.

Zadorozhny, K., Sannino, V., Beláň, O., Mlčoušková, J., Špírek, M., Costanzo, V., & Krejčí, L. (2017). Fanconi-Anemia-Associated Mutations Destabilize RAD51 Filaments and Impair Replication Fork Protection. *Cell Reports*, *21*(2), 333–340. https://doi.org/10.1016/j.celrep.2017.09.062

Zafar, F., Okita, A. K., Onaka, A. T., Su, J., Katahira, Y., Nakayama, J., Takahashi, T. S., Masukata, H., & Nakagawa, T. (2017). Regulation of mitotic recombination between DNA repeats in centromeres. *Nucleic Acids Research*, *45*(19), 11222–11235. https://doi.org/10.1093/nar/gkx763

Zasadzińska, E., Huang, J., Bailey, A. O., Guo, L. Y., Lee, N. S., Srivastava, S., Wong, K. A., French, B. T., Black, B. E., & Foltz, D. R. (2018). Inheritance of CENP-A Nucleosomes during DNA Replication Requires HJURP. *Developmental Cell*, *47*(3), 348-362.e7. https://doi.org/10.1016/j.devcel.2018.09.003

Zeitlin, S. G., Baker, N. M., Chapados, B. R., Soutoglou, E., Wang, J. Y. J., Berns, M. W., & Cleveland, D. W. (2009). Double-strand DNA breaks recruit the centromeric histone CENP-A. *Proceedings of the National Academy of Sciences*, *106*(37), 15762–15767. https://doi.org/10.1073/pnas.0908233106

Zellweger, R., Dalcher, D., Mutreja, K., Berti, M., Schmid, J. A., Herrador, R., Vindigni, A., & Lopes, M. (2015). Rad51-mediated replication fork reversal is a global response to genotoxic treatments in human cells. *The Journal of Cell Biology*, *208*(5), 563–579. https://doi.org/10.1083/jcb.201406099

Zhang, Du, J., Sun, B., Dong, X., Xu, G., Zhou, J., Huang, Q., Liu, Q., Hao, Q., & Ding, J. (2006). Structure of human MRG15 chromo domain and its binding to Lys36-methylated histone H3. *Nucleic Acids Research*, *34*(22), 6621–6628. https://doi.org/10.1093/nar/gkl989

Zhang, Fan, Q., Ren, K., & Andreassen, P. R. (2009a). PALB2 Functionally Connects the Breast Cancer Susceptibility Proteins BRCA1 and BRCA2. *Molecular Cancer Research*, *7*(7), 1110 LP – 1118. https://doi.org/10.1158/1541-7786.MCR-09-0123

Zhang, Ma, J., Wu, J., Ye, L., Cai, H., Xia, B., & Yu, X. (2009b). PALB2 links BRCA1 and BRCA2 in the DNA-damage response. *Current Biology : CB*, *19*(6), 524–529. https://doi.org/10.1016/j.cub.2009.02.018

Zhang, Shi, J., Bian, C., & Yu, X. (2015). Poly(ADP-Ribose) Mediates the BRCA2-Dependent Early DNA Damage Response. *Cell Reports*, *13*(4), 678–689. https://doi.org/10.1016/j.celrep.2015.09.040

Zhao, Bacolla, A., Wang, G., & Vasquez, K. M. (2010). Non-B DNA structure-induced genetic instability and evolution. *Cellular and Molecular Life Sciences*, *67*(1), 43–62. https://doi.org/10.1007/s00018-009-0131-2

Zhao, Vaithiyalingam, S., San Filippo, J., Maranon, D. G., Jimenez-Sainz, J., Fontenay, G. V., Kwon, Y., Leung, S. G., Lu, L., Jensen, R. B., Chazin, W. J., Wiese, C., & Sung, P. (2015). Promotion of BRCA2-Dependent Homologous Recombination by DSS1 via RPA Targeting and DNA Mimicry. *Molecular Cell*, *59*(2), 176–187. https://doi.org/10.1016/j.molcel.2015.05.032

Zhu, Chung, W.-H., Shim, E. T., Lee, S. E., & Ira, G. (2008). Sgs1 Helicase and Two Nucleases Dna2 and Exo1 Resect DNA Double-Strand Break Ends. *Cell*, *134*(6), 981–994. https://doi.org/10.1016/j.cell.2008.08.037

Zhu, Y. (2022). Advances in CRISPR/Cas9. *BioMed Research International*, *2022*, 9978571. https://doi.org/10.1155/2022/9978571

Zimmer, J., Tacconi, E. M. C., Folio, C., Badie, S., Porru, M., Klare, K., Tumiati, M., Markkanen, E., Halder, S., Ryan, A., Jackson, S. P., Ramadan, K., Kuznetsov, S. G., Biroccio, A., Sale, J. E., & Tarsounas, M. (2016). Targeting BRCA1 and BRCA2 Deficiencies with G-Quadruplex-Interacting Compounds. *Molecular Cell*, *61*(3), 449–460. https://doi.org/10.1016/j.molcel.2015.12.004

Zimmermann, M., Murina, O., Reijns, M. A. M., Agathanggelou, A., Challis, R., Tarnauskaitė, Ž., Muir, M., Fluteau, A., Aregger, M., McEwan, A., Yuan, W., Clarke, M., Lambros, M. B., Paneesha, S., Moss, P., Chandrashekhar, M., Angers, S., Moffat, J., Brunton, V. G., … Durocher, D. (2018). CRISPR screens identify genomic ribonucleotides as a source of PARP-trapping lesions. *Nature*, *559*(7713), 285–289. https://doi.org/10.1038/s41586-018-0291-z

Zou, L., & Elledge, S. J. (2003). Sensing DNA Damage Through ATRIP Recognition of RPA-ssDNA Complexes. *Science*, *300*(5625), 1542–1548. https://doi.org/10.1126/science.1083430

Appendices

1. Automated foci counting and colocalisation analysis (FIJI macro)

This script was written by Isabel Wassing and modified for use by me.

1: Prepare images for analysis by organising them into different folders.

Step 1a: Prepare folder/subfolders.

DAPI, EdU, gH2AX, EdU_processed, gH2AX_processed

Output > EdU, gH2AX, object_EdU, object_gH2AX, roi_gH2AX, mask_EdU, mask_H2AX, mask_DAPI

Step 1b: Run macro: 'Processing_oib_files.ijm' to split .oib file into separate .tif images & process these images as appropriate (i.e. subtract background/despeckle).

```
//Define directory's containing images

Dir1 = getDir("Sample");

Dir2 = getDir("gH2AX");

Dir3 = getDir("EdU");

Dir5 = getDir("DAPI")

Dir6 = getDir("gH2AX_processed");

Dir7 = getDir("EdU_processed");

//Open images and save each channel into the relevant subfolder

function action(Dir1, filename1) {

run("Bio-Formats Importer", "open=' + Dir1 + list1[i] + color_mode=Grayscale
rois_import=[ROI manager] view=Hyperstack stack_order=XYCZT");

        run("Split Channels");

        filename1=getTitle();

        run("8-bit");

        saveAs ("Tiff", Dir2+filename1+"_gH2AX");

        //Image processing steps to remove background signal if necessary

        //run("Despeckle");

        //run("Subtract Background...", "rolling=5");

        //saveAs ("Tiff", Dir6+filename1+"gH2AX_processed");

        close();

        filename2=getTitle();

        run("8-bit");

        saveAs ("Tiff", Dir3+filename2+"_EdU");

        //Image processing steps to remove background signal if necessary
```

```
	//run("Despeckle");
	//run("Subtract Background...", "rolling=5");
	//saveAs ("Tiff", Dir7+filename2+"EdU_processed");
	close();
	filename3=getTitle();
	run("8-bit");
	saveAs ("Tiff", Dir5+filename3+"_DAPI");
	close();
	close("*");
}

list1 = getFileList(Dir1)
setBatchMode(true);
for (i = 0; i < list1.length; i++){
	action(Dir1, list1[i]);
	}
```

Step 1c: Copy ‘DAPI’ folder (e.g. name ‘DAPI_delete’). Prepare DAPI images in this folder by manually removing objects (Ctrl X) in the images that are not mitotic nuclei (e.g. debris, interphase nuclei etc.)

Step 1d: Run macro: ‘DAPI_mask.ijm’

```
// Choose appropriate threshold and briefly check them for each image (run macro on false).
// Choose threshold so that nuclei are not fragmented but make up one solid object.
Dir1 = getDir("DAPI_delete");
Dir2 = getDir("mask_DAPI");

function action(Dir1, filename1) {
	open(Dir1+filename1);
	run("8-bit");
	setAutoThreshold("Huang dark");
	setThreshold(60, 255);
	//run("Threshold...");
	//setThreshold(150, 255);
	setOption("BlackBackground", false);
```

```
        run("Convert to Mask");
        run("Dilate");
        run("Dilate");
        run("Fill Holes");
        run("Erode");
        run("Erode");
        //run("Watershed");
        saveAs ("Tiff", Dir2+filename1);
        close();
}

list1 = getFileList(Dir1)
setBatchMode(false);
for (i = 0; i < list1.length; i++){
action(Dir1, list1[i]);
}
```

Step 2: Detect foci

Step 2a: Use FindFoci GUI to find optimal parameters for foci detection for each of the channels (EdU, gH2AX). Do this based on 1-2 example images.

Notes: (1) Background method: Absolute (this avoids changing background levels based on overall intensity in the image). (2) Search method: Above background. (3) Peak Method: Absolute height. (4) Adjust other parameters for different experiments/antibodies used. (5) (Important for colocalization specifically). Check which parameters give the best mask image (e.g. Show mask = Fraction height above background = 0.5). Note, focus mask must be relatively accurate to get reliable foci overlap estimate later on. (6) Make sure that number of foci counted is reliable throughout images in folder → check a couple of representative images to make sure.

Step 2b: Save chosen parameters as a .txt file

Notes: .txt file should contain the following. Parameters to be changed per conditions are highlighted in bold.

background_method=Absolute, background_parameter=6, auto_threshold=Otsu statistics_mode=Both, search_method=[Above background], search_parameter=0.30 minimum_peak_height=[Absolute height], peak_parameter=6, minimum_size=2, minimum_above_saddle, sort_method=[Total intensity], maximum_peaks=10000, show_mask=[Fraction height above background], overlay_mask fraction_parameter=0.50, show_table, clear_table, mark_maxima, show_log_messages, results_directory=[], object_analysis, gaussian_blur=0.5, centre_method=[Max value (search image)], centre_parameter=2.

Step 2c: Use FindFoci Batch function to apply this to a batch (use .txt file as parameters file).

Save Output files into Output > EdU or gH2AX folders.

Step 2d: Sort .roi files from Output > EdU folder into Output > EdU_roi folder using

macro ‘sort_files_to_folder.ijm’.

```
Dir1 = getDir("EdU");
Dir3 = getDir("roi_EdU");

function action(Dir1, Dir3, filename1) {
        if (matches(filename1, ".*c1z0t1.roi*")) {
                open(Dir1 + filename1);
        saveAs (".roi", Dir3+filename1);
        close();
        }
}

list1 = getFileList(Dir1)
setBatchMode(true);
for (i = 0; i < list1.length; i++){
action(Dir1, Dir3, list1[i]);
}
```

Step 3: Count Foci.

Step 3a: Plot foci onto DAPI mask images.

Use FindFoci>Assign foci to objects plugin (Assign_foci_to_objects.ijm).

Save images to Output > ‘object_EdU’ folders etc.

```
// Macro copies assigned foci from EdU Image to thresholded DAPI Image.
Dir1 = getDir("roi_EdU");
Dir2 = getDir("mask_DAPI");
Dir3 = getDir("object_EdU");

function action(Dir1, Dir2, filename1, filename2) {
```

```
	open(Dir1 + filename1);
	open(Dir2 + filename2);
	run("Restore Selection");
	saveAs ("Tiff", Dir3+filename2);
	close("*");
	}
// Generates list of which object each foci is in. The objects are identified from top to bottom, left to right
list1 = getFileList(Dir1)
list2 = getFileList(Dir2)
setBatchMode(false);
for (i = 0; i < list1.length; i++){
action(Dir1, Dir2, list1[i], list2[i]);
}
```

Step 3b: Count foci plotted inside the objects (i.e. nuclei). Run macro ‘Count_roi’.

```
// Save Foci results file AND Foci distances file. Foci distances file will be useful if you continue on to analyse foci colocalization.
Dir1 = getDir("object_EdU");

function action(Dir1, filename) {
	open(Dir1 + filename);
run("Assign Foci to Objects", "foci=ROI radius=0 min_size=90 max_size=0 remove_small_objects show_distances");
close("*");
	}

list1 = getFileList(Dir1)
setBatchMode(true);
for (i = 0; i < list1.length; i++){
showProgress(i+1, list1.length);
action(Dir1, list1[i]);
}
```

Step 4: Colocalization

Step 4a: Run macro ‘Macro_colocalization_overlap.ijm’. Save as Excel sheet.

Notes: This macro uses Colocalization > Particle overlap plugin to get a measure of overlap between e.g. EdU and gH2AX.

Input used: Mask 1 (Mask of EdU foci – generated by FindFoci plugin); Image 1 (Image of EdU [processed] foci, unmasked); Mask 2 (Mask of H2AX foci – generated by FindFoci plugin)

Important Output: ID particle; Manders (= fraction of signal [EdU] which overlaps with gH2AX mask, value between 0-1)

The Particle Overlap Output lists the EdU foci detected and the degree to which they overlap with a masked gH2AX focus.

```
Dir1 = getDir("mask_EdU");
Dir2 = getDir("processed_EdU");
Dir3 = getDir("mask_gH2AX");
Dir4 = getDir("output");

function action(Dir1, Dir2, Dir3, Dir4, filename1, filename2, filename3) {
        open(Dir1 + filename1);
        name=getTitle();
        open(Dir2 + filename2);
        name2=getTitle();
        open(Dir3 + filename3);
        name3=getTitle();
        out = Dir4+name+".xls";
run("Particle Overlap", "particle_mask="+name+" particle_image="+name2+"
overlap_mask="+name3+" show_table file="+out);
        close("*");
}

list1 = getFileList(Dir1)
list2 = getFileList(Dir2)
list3 = getFileList(Dir3)
setBatchMode(false);
for (i = 0; i < list1.length; i++){
action(Dir1, Dir2, Dir3, Dir4, list1[i], list2[i], list3[i]);
```

}

Step 4b: Correlate particle ID (of colocalization output) to object (i.e. nucleus).

Copy data from ‘Assign Foci Distances’ Excel sheet of EdU foci into Particle overlap Excel sheet. ‘Assign Foci Distances’ lists all the EdU foci detected & the Object that the focus is found in. ‘Particle Overlap’ lists the EdU foci detected and the degree to which they overlap with a masked gH2AX focus. In this way, you can relate the two to find out how many of the overlapping EdU foci are found in a single object (i.e. nuclei), to find the number of overlapping EdU-gH2AX foci per mitotic cell.

Important: The foci ID given by ‘Assign Foci Distances’ is in the opposite order to those given by ‘Particle Overlap’. Flip the order in one of the columns manually to correctly be able to assign an object number to the colocalising particles.

Step 4c: Use VLOOKUP function in Excel to display the object associated with each particle ID – combining output of ‘Particle overlap’ and ‘Assign foci to object’.

This is the number of H2AX+ EdU foci

Can now calculate % of H2AX+ EdU foci

2. Automated microscopy analysis (FIJI macro)

The script was written by Xanita Saayman and modified for use by me.

// This macro should be saved as .java and run from within FIJI (ImageJ)

// This script was written to analyse two channels (C2 and C3), using C3 to create a box. As was done during IF analysis.

// Script can be modified to box each channel separately as done for cenFISH / telFISH analysis.

// Outputs: (1) boxes for each focus within each cell for each channel, which will be further processed. (2) DAPI and channel intensities per cell.

// Settings to define before start: (1) ‘prominence’ for foci selection, define manually before running macro. (2) Working directory to direct path to files of interest. (3) box size, defined manually.

// set the directory for image analysis

dir = getDir("…");

files = getFileList(dir)

// generate folders to store new files from downstream analysis

foci_intensity = dir+"foci_count"+File.separator;

File.makeDirectory(foci_intensity);

dapi_int = dir+"dapi_int"+File.separator;

```
File.makeDirectory(dapi_int);

foci_coloc_C2 = dir+"C2_foci_coloc"+File.separator;
File.makeDirectory(foci_coloc_C2);
med_focus_per_cell_C2 = dir+"C2_med_focus_per_cell"+File.separator;
File.makeDirectory(med_focus_per_cell_C2);
med_foci_images_C2 = dir+"C2_med_foci_images"+File.separator;
File.makeDirectory(med_foci_images_C2);

foci_coloc_C3 = dir+"C3_foci_coloc"+File.separator;
File.makeDirectory(foci_coloc_C3);
med_focus_per_cell_C3 = dir+"C3_med_focus_per_cell"+File.separator;
File.makeDirectory(med_focus_per_cell_C3);
med_foci_images_C3 = dir+"C3_med_foci_images"+File.separator;
File.makeDirectory(med_foci_images_C3);

final_summary = dir+"final_summary"+File.separator;
File.makeDirectory(final_summary);

//To exclude objects touching border of image
run("Options...", "iterations=1 count=1 pad");

//To display image regions of interest (ROI) information in the results table
setOption("Display Label", true);

for(f = 0; f < files.length; f++){
	if (endsWith(files[f], "/"))
		continue;
	name = files[f];
	if (File.exists(dir+"/C3_foci_coloc/"+name+"_C3_0_1.txt")) {
			print(files[f]+" has already been analyzed.");
			continue;
		}else{
			open(dir+files[f],"OK");
```

```
selectWindow(name);
run("Split Channels");
// define cell ROIs to analyse
selectWindow("C1-"+name);
run("Duplicate...", "title=dup");
selectWindow("dup");
run("8-bit");
run("Gaussian Blur...", "sigma=2 stack");
run("Auto Threshold", "method=Li white");
run("Convert to Mask");
run("Dilate");
run("Fill Holes");
run("Erode");
run("Watershed");
run("Analyze Particles...", "size=30-Infinity display
        exclude clear summarize add");
selectWindow("C2-"+name);
run("Grays");
// Manual inspection to verify accurate cell segmentation
waitForUser("Choose cells.");
run("Clear Results");
// measure number foci in each cell for each channel (C2 and C3)
nROIs = roiManager("count");
setBatchMode(true);
selectWindow("C2-"+name);
run("Grays");
// If background signal is high, run background subtraction
//run("Subtract Background...", "rolling=5");
for(x=0; x<nROIs;x++){
        roiManager("Select", x);
        run("Find Maxima...", "prominence=350 output=List");
        saveAs("Results", dir+"/foci_count/"+name+"-C2-"+x+".csv");
        run("Clear Results");
        }
```

```
selectWindow("C3-"+name);
// If background signal is high, run background subtraction
//run("Subtract Background...", "rolling=5");
for(x=0; x<nROIs;x++){
	roiManager("Select", x);
	run("Find Maxima...", "prominence=550 output=List");
	saveAs("Results", dir+"/foci_count/"+name+"-C3-"+x+".csv");
	run("Clear Results");
	}
// Export box surrounding foci within boxing channel e.g. C3 (or both with modification)
for(x=0; x<nROIs;x++){
	run("Clear Results");
	selectWindow("C1-"+name);
	roiManager("Select", x);
	run("Measure");
	saveAs("Results", dir+"/dapi_int/"+name+"-"+x+".csv");
	run("Clear Results");
	filestring=File.openAsString(dir+"/foci_count/"+name+"-C3-"+x+".csv"); // boxing channel
	xlines=split(filestring,"\n");
	for(i=1;i<xlines.length;i++){
		line=split(xlines[i],",");
		index=line[0];
		//defines the size of the box around the foci
		x_coord=parseInt(line[1])-6;
		y_coord=parseInt(line[2])-6;
		print(x_coord,y_coord);
		selectWindow("C3-"+name);
		//defines size of box
		makeRectangle(x_coord, y_coord, 12, 12);
		run("Duplicate...", "title="+name+"_"+i+" duplicate channels=3");
		selectWindow(name+"_"+i);
```

```
                saveAs("Text Image",
                dir+"/C3_foci_coloc/"+name+"_C3_"+x+"_"+i+".txt");

                close();

                //Project C3 box coordinates onto C2 images

                selectWindow("C2-"+name);

                makeRectangle(x_coord, y_coord, 12, 12);

                run("Duplicate...", "title="+name+"_"+i+" duplicate
                channels=2");

                selectWindow(name+"_"+i);

                saveAs("Text Image",
                dir+"/C3_foci_coloc/"+name+"_C2_"+x+"_"+i+".txt");

                close();

                }

        run("Clear Results");

        }

    run("Close All");

    }

    setBatchMode(false);

}
```

3. Downstream processing of microscopy data (Python)

The script was written by Xanita Saayman and modified for use by me.

analyse all foci boxes generated using a Macro java-based program (**appendix 1**).

these should be within subfolders i.e. C3_foci_coloc where the C3 denotes the boxing channel, and it should contain a matrix for each channel within each focus box.

this script will then generate an 'average' (actually, median) focus for each cell and save it under the 'med_focus_per_cell' subfolder.

importantly, np.nanmedian has to be used instead of np.median to prevent some anomalous data points from the image processing.

```
# import dependencies

import numpy as np

import seaborn as sns

import matplotlib.pyplot as plt

import pandas as pd

import os
```

```
# set the boxing channel and size
# box trimming can be done by changing the desired_size
channel = 'C3'
size = 12
desired_size=9

# input the following into terminal.
os.chdir(r"path")
cwd = os.getcwd()

list = os.listdir(cwd+'\\'+str(channel)+'_foci_coloc')
dapi_list=os.listdir(cwd+'\\dapi_int')

for file in os.listdir(cwd):
        if file.endswith('.oib'):
                treatment="_".join(file.split('_')[:-1])
                sample=file.split('.')[-2]
                # identify number of cells per sample
                dapi_sample_matching = [s for s in dapi_list if s.startswith(sample)]
                cell_num = max(int(x.split('-')[-1].split('.')[-2]) for x in
dapi_sample_matching)
                #
                sample_matching = [s for s in list if s.startswith(sample)]
                # parse through cells, identifying number of foci and parsing through foci
                for cell in range(0,cell_num+1):
                        #
                        cum_data_C2 = np.empty((size, size, 1))
                        cum_data_C3 = np.empty((size, size, 1))
                        #
                        cell_matching = [c for c in sample_matching if
                        c.startswith(file+'_'+str(channel)+'_'+str(cell)+'_')]
                        if len(cell_matching)==0:
                                print('Assigning '+str(sample)+' cell '+str(cell)+' with 0 due to
                                insufficient foci.')
```

```
        np.savetxt('./'+str(channel)+'_med_focus_per_cell/'+str(sample)+'_'+str(cell)+'_'+str
        (channel)+'_med_focus.txt',np.zeros((size,size)))
                                continue
                        else:
                                foci_num = max(int(x.split('.')[-2].split('_')[-1]) for x in
                                cell_matching)
                                foci_size_cell=pd.DataFrame(columns=['Sample','Cell','Foci',
                                'C2 Foci Size','C3 Foci Size','C4 Foci Size'])
                                # parse through all foci and generate heatmaps
                        for foci in range(1,foci_num+1):
                                data_C3 =
                                np.loadtxt('./'+str(channel)+'_foci_coloc/'+file+'_C3_'+str(cell)
                                +"_"+str(foci)+".txt")
                                if data_C3.shape==(size,size):
                                        cum_data_C3 = np.dstack((cum_data_C3, data_C3))
                                data_C2 =
                                np.loadtxt('./'+str(channel)+'_foci_coloc/'+file+'_C2_'+str(cell)
                                +"_"+str(foci)+".txt")
                                if data_C2.shape==(size,size):
                                        cum_data_C2 = np.dstack((cum_data_C2, data_C2))
                                #
np.savetxt('./'+str(channel)+'_med_focus_per_cell/'+str(sample)+'_'+str(cell)+'_C2_med_fo
cus.txt',np.nanmedian(cum_data_C2,axis=2))
np.savetxt('./'+str(channel)+'_med_focus_per_cell/'+str(sample)+'_'+str(cell)+'_C3_med_fo
cus.txt',np.nanmedian(cum_data_C3,axis=2))
        else:
                continue


# collect the cell data for each treatment and generate a heatmap for the 'average'
(actually, median) focus.
# a background subtraction step will be done on the cellular level.
# set the samples here, image names should begin with these strings:
txs = ['']
tx_list = os.listdir(cwd+'/'+str(channel)+'_med_focus_per_cell/')


def crop_center(array):
    y,x = array.shape
    startx = x//2-(desired_size//2)
```

```
    starty = y//2-(desired_size//2)
    return array[starty:starty+desired_size,startx:startx+desired_size]


for tx in txs:
        tx_sample_matching = [s for s in tx_list if s.startswith(tx) and "MPS1i" not in s]
        tx_num = len(tx_sample_matching)
        #
        data_C2_all = np.empty((desired_size, desired_size, 1))
        data_C2_all_BG_sub = np.empty((desired_size, desired_size, 1))
        #
        data_C3_all = np.empty((desired_size, desired_size, 1))
        data_C3_all_BG_sub = np.empty((desired_size, desired_size, 1))
        #
        foci_size_sample=pd.DataFrame(columns=['Sample','Cell','Foci','C2 Foci Size','C3
        Foci Size','C4 Foci Size'])
        #
        for file in tx_sample_matching:
                #
                if file.split('_')[-3]=='C2':
                        data_C2 =
                        crop_center(np.loadtxt('./'+str(channel)+'_med_focus_per_cell/'+file)
                        )
                        background_C2 =
                        np.nanmedian([np.nanmedian(data_C2[:1]),np.nanmedian(data_C2
                        [-1:]),np.nanmedian(data_C2[:,0]),np.nanmedian(data_C2[:,-1])])
                        net_data_C2 = data_C2 - background_C2
                        #
                        data_C2_all = np.dstack((data_C2_all, data_C2))
                        data_C2_all_BG_sub = np.dstack((data_C2_all_BG_sub,
                        net_data_C2))
                        #
                if file.split('_')[-3]=='C3':
                        data_C3 =
                        crop_center(np.loadtxt('./'+str(channel)+'_med_focus_per_cell/'+file)
                        )
                        background_C3 =
                        np.nanmedian([np.nanmedian(data_C3[:1]),np.nanmedian(data_C3
                        [-1:]),np.nanmedian(data_C3[:,0]),np.nanmedian(data_C3[:,-1])])
```

```
                    net_data_C3 = data_C3 - background_C3
                    #
                    data_C3_all = np.dstack((data_C3_all, data_C3))
                    data_C3_all_BG_sub = np.dstack((data_C3_all_BG_sub,
                    net_data_C3))
                    #
            #
            # plot each median focus, as well as background-subtracted focus
            #
            final_C2 = np.nanmedian(data_C2_all,axis=2)
            final_C2_BG_sub = np.nanmedian(data_C2_all_BG_sub,axis=2)
            #
            sns.heatmap(final_C2,vmin=0,vmax=1000)
            plt.savefig('./'+str(channel)+'_med_foci_images/'+tx+'_C2.pdf')
            plt.close()
            sns.heatmap(final_C2_BG_sub,vmin=0,vmax=1000)
            plt.savefig('./'+str(channel)+'_med_foci_images/'+tx+'_C2_BG_sub.pdf')
            plt.close()
            #
            final_C3 = np.nanmedian(data_C3_all,axis=2)
            final_C3_BG_sub = np.nanmedian(data_C3_all_BG_sub,axis=2)
            #
            sns.heatmap(final_C3,vmin=0,vmax=1000)
            plt.savefig('./'+str(channel)+'_med_foci_images/'+tx+'_C3.pdf')
            plt.close()
            sns.heatmap(final_C3_BG_sub,vmin=0,vmax=1000)
            plt.savefig('./'+str(channel)+'_med_foci_images/'+tx+'_C3_BG_sub.pdf')
            plt.close()
            #


# finally, collect all the data in a csv spreadsheet for plotting in prism and visualizing the
cell-cell variation in the average focus per cell, as well as the background-subtracted
focus per cell.

# of note, the background subtraction is done on a cellular level.

tx_list = os.listdir(cwd+'/'+str(channel)+'_med_focus_per_cell/')
```

```
data_all=pd.DataFrame(columns=['Sample','Cell','Channel','Raw Foci Size','BG-sub Foci Size'])


for tx in txs:
    tx_sample_matching = [s for s in tx_list if s.startswith(tx) and "MPS1i" not in s]
    tx_num = len(tx_sample_matching)
    #
    for file in tx_sample_matching:
        #
        # data collection depending on channel identity.
        #
        if file.split('_')[-3]=='C2':
            data_C2 =
            crop_center(np.loadtxt('./'+str(channel)+'_med_focus_per_cell/'+file)
            )
            background_C2 =
            np.nanmedian([np.nanmedian(data_C2[:1]),np.nanmedian(data_C2
            [-1:]),np.nanmedian(data_C2[:,0]),np.nanmedian(data_C2[:,-1])])
            final_data_C2 = data_C2 - background_C2
        if file.split('_')[-3]=='C3':
            data_C3 =
            crop_center(np.loadtxt('./'+str(channel)+'_med_focus_per_cell/'+file)
            )
            background_C3 =
            np.nanmedian([np.nanmedian(data_C3[:1]),np.nanmedian(data_C3
            [-1:]),np.nanmedian(data_C3[:,0]),np.nanmedian(data_C3[:,-1])])
            final_data_C3 = data_C3 - background_C3
        #
        # compile data into one table, depending on channel identity.
        #
        sample_data=pd.DataFrame(columns=['Sample','Cell','Channel','Raw Foci
        Size','BG-sub Foci Size'])
        #
        if file.split('_')[-3]=='C2':
            sample_data=sample_data.append({
                "Sample": tx+'_'+file.split('_')[-5],
                "Cell": file.split('_')[-4],
                "Channel": file.split('_')[-3],
```

```
                        "Raw Foci Size": sum(sum(data_C2)),
                        "BG-sub Foci Size": sum(sum(final_data_C2)),
                        }, ignore_index=True)
                #
                if file.split('_')[-3]=='C3':
                        sample_data=sample_data.append({
                                "Sample": tx+'_'+file.split('_')[-5],
                                "Cell": file.split('_')[-4],
                                "Channel": file.split('_')[-3],
                                "Raw Foci Size": sum(sum(data_C3)),
                                "BG-sub Foci Size": sum(sum(final_data_C3)),
                                }, ignore_index=True)
                #
                data_all = data_all.append(sample_data)

data_all.to_csv('./final_summary/signal_per_cell_'+str(channel)+'.csv')
```